

**FEDERAL UNIVERSITY OF RIO GRANDE DO SUL  
INSTITUTE OF CHEMISTRY BRAZIL**

**POSTGRADUATE PROGRAME IN CHEMISTRY**

**Title of Thesis**

“Catalytic Carbon Dioxide Transformation catalyzed  
by Ruthenium in Ionic Liquids”

Thesis

By

**MEHER ALI**

Submitted to PPGQ-UFRGS  
In partial fulfillment of the requirements for the degree of

DOCTOR OF CHEMISTRY

**June 2016**

Supervised by **Prof. Dr. Jairton Dupont**

Laboratory of Molecular Catalysis (LMC) PPGQ-UFRGSAv.  
Bento Gonçalves, 9500. Porto Alegre 91501-970 - RS - Brazil

## ABSTRACT

Catalytic CO<sub>2</sub> transformation signified a paradigm shift towards the fabrication of contemporary chemical energy. The abundance of CO<sub>2</sub> and the impending storage of fossil building blocks, has led to the proposal that CO<sub>2</sub> should be the C1-building block of the future. This doctoral thesis based on the development of an efficient homogeneous Ru-catalytic system in ionic liquids, and its exploitation for Ru-catalyzed carbonylations reactions with CO<sub>2</sub> as CO source. Primarily synthesized task-specific ionic Liquids for the generation of an active homogeneous Ru-catalytic system by reacting with Ru<sub>3</sub>(CO)<sub>12</sub> precursor. Then reaction was optimized for the Ru-catalyzed selective hydroformylation of alkenes with CO<sub>2</sub>, and also investigated the mechanistic insight (Chapter- 3). The reaction of *1-methyl-3-n-butyl-imidazolium chloride* [BMI•Cl], or *1-n-butyl-2,3-dimethyl imidazolium Chloride* [BMMI•Cl] with Ru<sub>3</sub>(CO)<sub>12</sub> generates Ru-hydride-carbonyl-carbene species *in-situ* that are efficient catalysts for Reverse Water Gas-Shift (RWGS) / hydroformylation / hydrogenation cascade reaction. The addition of H<sub>3</sub>PO<sub>4</sub> increases the catalytic activity of the first step (*i.e.*, the reduction of CO<sub>2</sub> to CO). Under optimized reaction conditions (120 °C and 60 bar CO<sub>2</sub>/H<sub>2</sub> (1:1) for 17 h), cyclohexene and 2,2-disubstituted alkenes were easily functionalized to alcohols *via* a sequential hydroformylation-carbonyl reduction by hydride transfer and protonolysis. These active Ru-hydride-carbonyl-carbene species further strongly catalyzed the selective hydroaminomethylation of alkenes, and N-formylation amines with CO<sub>2</sub> as CO source (Chapter-4). Addition of P(OEt)<sub>3</sub> and H<sub>3</sub>PO<sub>4</sub> substantially and selectively formed hydroaminomethylation of alkenes, and N-fomylation of amines, while N-methylation of amines was not observed. The *In-situ* generated Ru-hydride-cabonyl-carbene species are more efficient towards carbonylations of alkenes as compared to N-formylation of amines. Furthermore mechanistic studies revealed hydroaminomethylation of alkenes involve in a sequence of RWGSR / hydroformylation / reductive amination by hydrogenation of imines and enamines intermediates. Interestingly, in the presence of stable phosphine additives the same catalytic system promoted N-methylation of amines, and hydrogenation of alkenes. These findings of the CO<sub>2</sub> transformation provided a new and highly valuable opportunity to get advantage of abundant CO<sub>2</sub> as CO

source for important industrial carbonylation processes, such as for the production of fragrances, and useful chemicals. Furthermore, the thesis work included the synthesis of well-distributed Pd-NPs (ca. 3.7 nm) deposited onto active carbon by magnetron-sputtering process. Subsequently the catalytic performances were evaluated in the super hydrogenation of model of model substrates (i.e., nitrobenzene, 1,3-cyclohexadiene and cyclohexene) at 75°C under 4 bar dihydrogen (H<sub>2</sub>). The catalytic results revealed improved efficiencies in terms of activity and selectivity to those displayed by commercially available catalyst. Disproportion of 1,3-cyclohexadiene and cyclohexene were revealed also as active processes under reaction conditions.

## List of Publications

- (1) **Meher Ali**, A. Gual, G. Ebeling, J. Dupont, "Ru-catalysed hydroformylation of alkenes using CO<sub>2</sub> as the CO source in the presence of ionic liquids", *ChemCatChem*, **2014**, 6, 2224–2228 (7 JUL 2014). Keywords: Carbon dioxide, Hydroformylation, Ionic liquids, Reverse water gas shift and Ruthenium. DOI: 10.1002/cctc.201402226.
- (2) **Meher Ali**, A. Gual, G. Ebeling, J. Dupont, "Carbon dioxide transformation in imidazolium salts: hydroaminomethylation catalysed by Ru-complexes", *ChemSusChem*, **2016**. Keywords: Carbon dioxide, Hydroaminomethylation, Ionic liquids, Reverse water gas shift and Ruthenium. DOI: 10.1002/cssc.201600385.
- (3) **Meher Ali**, A. Gual, G. Ebeling, J. Dupont, "Carbon dioxide transformation in imidazolium salts: N-formylation catalysed by Ru-complexes", *XX*, **2016**, manuscript in preparation. Keywords: Carbon dioxide, N-formylation, Ionic liquids, Reverse water gas shift and Ruthenium.
- (4) **Meher Ali**, G. Abarca, D. Eberhardt, A. Gual, F. Bernardi, S. R. Teixeira, J. Dupont, "Superior Performance in Hydrogenation Reactions of Pd-NPs Deposited onto Activated Charcoal (AC) by Magnetron Sputtering", *Tetrahedron*, **2016**, manuscript is submitted. Keywords: Sputtering, Palladium, Nanoparticles, Hydrogenation, Disproportion.



## *ACKNOWLEDGEMENTS*

I would like to express my special appreciation and sincere gratitude to my advisor **Prof. Dr. Jairton Dupont**, an eminent scientist and pioneer of the Laboratory of Molecular Catalysis UFRGS, who gave me an opportunity to complete my Ph.D. among his prestigious research group. He always encouraged my research work and allowing me to grownup as a research scientist. His guidance on both my research skills as well as on my career has been priceless. I would also like to extend my sincere thanks to **Prof. Gunter**, and **Dr. Aitor**, they were extremely involved in my research projects during the experimental work and collecting data for my Ph.D. thesis. Further I will take this opportunity to express my especial thanks to **TWAS-CNPq** for awarded me a full-bright Ph.D. scholarship, provided research funding, and other financial supports.

I would like to express my deep sense of gratitude to Secretariat of Postgraduate Program Chemistry (**PPGQ**) **Prof. Paulo** and his technical staff for their proper guidance & facilitate me in partial fulfillment of the requirements for the Ph.D. degree. Extending my sincere gratitude to the faculty members of Laboratory of Molecular Catalysis, research fellows, and friends for your incredible support and hospitality during my peaceful stay in Federal University of Rio Grande Do Sul Brazil. I'm extremely thankful to my thesis evaluation jury members for their encouragements and appreciations with positive remarks.

A special thanks to my family, words cannot express how grateful I am to my parents, sisters, and brothers for all of the sacrifices that you've made on my behalf. Your prayer for me was what sustained me thus far.

Dr. Meher Ali

## Table of Contents

---

Abstract.....	II
List of Publications.....	IV
Acknowledgements.....	V
Table of Contents.....	VI
List of Symbols.....	X
List of Schemes.....	XII
List of Figures.....	XV
List of Tables.....	XVIII
<b>Chapter - 1 General Background.....</b>	<b>01</b>
1.1 Carbon Dioxide Fixation and Utilization.....	02
1.2 Catalytic reduction of carbon dioxide (CO <sub>2</sub> ).....	04
1.3 Rh / Ru-catalyzed hydroformylation of olefins with CO <sub>2</sub> as CO source. ....	07
1.4 Generation of NHC-Ru carbene catalysts.....	09
1.5 References .....	11
<b>Objectives.....</b>	<b>13</b>
<b>Chapter - 2 Task Specific Synthesis of Ionic Liquids &amp; CO<sub>2</sub>fixation.....</b>	<b>14</b>
2.1 Introduction.....	15
2.2 Synthesis and characterization of [BMI•X], [BMMI•X] ILs.....	16
2.3 Synthesis of 1-Methyl-3-butyl-(2- <sup>13</sup> C)-imidazolium chloride.....	18
2.4 Functionalization of imidazolium ILs.....	19
2.5 Synthesis of P-functionalized ionic liquids (PF-ILs).....	22
2.5.1 Synthesis of phosphine-modified imidazolium ILs.....	22
2.5.2 Synthesis of phosphite-modified imidazolium ILs.....	26
2.6 S-N-S Modified imidazolium IL.....	27
2.7 References.....	29

---

---

<b>Chapter - 3 Ru-catalysed Hydroformylation of Alkenes Using CO<sub>2</sub> as CO Source in the Presence of Ionic Liquids.....</b>	<b>31</b>
3.1 Introduction.....	32
3.2 Experimental.....	34
3.2.1 General experimental details.....	34
3.2.2 Experimental for catalysis.....	35
3.3 Results and discussion.....	36
3.3.1 Reaction optimization for the hydroformylation of cyclohexene.....	36
3.3.2 Hydroformylation of 1-hexene by optimizing IL/Ru ratio.....	38
3.3.3 Electronic and steric effects of P-donor ligands.....	39
3.3.4 Mechanistic study: generation of Ru-catalysts & reduction of CO <sub>2</sub> .....	42
3.3.4.1 NMR-mechanistic studies.....	42
3.3.4.2 Analysis of gas-phase of reactions.....	52
3.3.4.3 ESI-MS, and IR studies.....	53
3.3.5 Hydroformylation of versatile cyclic and terminal alkenes.....	57
3.4 Conclusions.....	58
3.5 References.....	59
<b>Chapter -4 Ruthenium Catalyzed Hydroaminomethylation / N-formylation with CO<sub>2</sub>/H<sub>2</sub> in Ionic Liquid Media, and Mechanistic Insights.....</b>	<b>62</b>
4.1 Introduction.....	63
4.2 Experimental.....	66
4.2.1 General considerations.....	66
4.2.2 N-formylation.....	66
4.2.3 Hydroaminomethylation.....	67
4.2.4 Reductive amination.....	68

---

---

4.3	Results and discussion.....	68
4.3.1	N-formylation/N-methylation of primary and secondary amines.....	68
4.3.2	N-formylation/N-methylation of aniline.....	71
4.3.3	Hydroaminomethylation of alkenes with CO <sub>2</sub> as CO source.....	76
4.3.4	Mechanistic insights for the hydroaminomethylation.....	80
4.3.4.1	Reductive amination.....	81
4.4	Conclusion.....	84
4,5	References.....	86

**Chapter -5 Liquid-phase Hydrogenation and Dehydrogenation Activities Via Pd-NPs Deposited onto Activated Carbon (AC) by Magnetron Sputtering.....**

5.1	Introduction.....	
5.2	Experimental section.....	91
5.2.1	General procedure.....	91
5.2.3	General procedure for the sputtering.....	91
5.2.4	General procedure for the hydrogenation tests.....	92
5.3	Results and Discussion.....	92
5.3.1	Sputtering deposition and characterization of Pd/C- NPs...	93
5.3.2	Catalytic activities.....	97
5.3.2.1	Catalytic activity of Pd/C-1 to Pd/C-5 for hydrogenation reactions...	97
5.3.2.2	Activity of Pd/C-1 catalyst on decreasing Ph-NO <sub>2</sub> /Pd ratio.....	100
5.3.2.3	Catalytic activity of Pd/C, and Pd/TiO <sub>2</sub> supported NPs.....	101
5.3.2.4	Pd-catalyzed disproportion of 1,3-cyclohexadiene .....	103
5.4	Conclusion.....	105
5.4	Experimental.....	106

**Chapter -6 GC, NMR Spectras of Compounds, & Reactions Mixtures... 110**

---

6.1	GC analysis and NMR spectras for Ru-catalyzed hydroformylation of alkenes by using CO <sub>2</sub> as CO source.....	111
6.2	GC, NMR Spectras for Ru-catalysed N-formylation of amines Using CO <sub>2</sub> as a CO source.....	121
6.3	GC, NMR spectras for Ru-catalysed hydroaminomethylation of alkenes using CO <sub>2</sub> as CO source.....	128
6.4	GC, NMR spectras for Ru-catalysed reductive aminations .....	139
6.5	GC-analysis for Pd-NPs catalyzed selective hydrogenation of 1,3 cyclohexadiene into cyclohexene.....	142
6.6	GC analysis for Pd-NPs catalyzed dehydrogenation-hydrogenation of 1,3-cyclohexadiene by enter-H <sub>2</sub> transfer mechanism.....	144

---

## List of Symbols

---

ABCN	1,1-azobis(cyclohexanecarbonitrile)
AIBN	Azobis(isobutyronitrile)
BMI•Cl	1-n-Butyl-3-methylimidazolium chloride
BMI•Br	1-n-Butyl-3-methylimidazolium bromide
BMI•I	1-n-Butyl-3-methylimidazolium iodide
BMMI•Cl	1-n-butyl-2,3-dimethyl imidazolium chloride
CCS	Carbon Capturing & Storage
<sup>13</sup> C-NMR	Carbon Nuclear Magnetic Resonances
[C2-bis(MMI)•Cl <sub>2</sub> ]	3,3'-(ethane-1,2-diyl)bis(1,2-dimethyl-1H-imidazol-3-ium) chloride
COSY	Correlation spectroscopy (Two-dimensional NMR)
Dppe	1,2-Bis(diphenylphosphino)ethane
PPh <sub>3</sub>	Triphenylphosphine
Dppm	1,1-Bis(diphenylphosphino)methane
Dppp	1,3-Bis(diphenylphosphino)propane
ESI-MS	Electron Spray Ionization Mass Spectroscopy
FID	Flame Ionization Detector
FILs	Functionalization of Ionic Liquids
GC	Gas Chromatography
GC-MS	Coupled Gas Chromatography-Mass Spectroscopy
GC-TCD	Gas Chromatograph with Thermal Conductivity Detector
HSQC	Heteronuclear Single Quantum Correlation (NMR spectroscopy)
<sup>1</sup> H-NMR	Proton Nuclear Magnetic Resonances
ILs	Ionic Liquids
Im.ILs	Imidazolium Ionic Liquids
IR	Infra Red Spectroscopy
MHz	Megahertz (International Standard symbol)
m/z	Mass-to-charge ratio
NHCs	N-heterocyclic Carbenes

---

---

NHCs-Ru	Ruthenium N-heterocyclic Carbenes
NTf2	Bis(trifluoromethylsulfonyl)imide
Pd-NPs	Palladium Nanoparticles
Ph-NO <sub>2</sub>	Nitrobenzene
Ppm	Parts per million (chemical shift unit)
PF-ILs	Phosphine / Phosphite Functionalized Ionic Liquids
<sup>31</sup> P-NMR	Phosphorus Nuclear Magnetic Resonances
Ru-H-CO-Cs	Ruthenium-hydride-carbonyl-carbenes
Ru	Ruthenium
REHATM	Reductive Enter Atoms Transfer Mechanism
RWGSR	Reverse Water Gas Shift Reaction
TEM	Transmission Electron Microscopy
TMS	Tetramethylsilane (internal standard for calibrating chemical shift for <sup>1</sup> H, <sup>13</sup> C and <sup>29</sup> Si NMR)
TON	Turnover Tumber of a Catalyst
TOF	Turnover Frequency = TON/Time of reaction
WGSR	Water Gas Shift Reaction
XPS	X-ray Photoelectron Spectroscopy
XRD	X Ray Diffraction

---

## List of Schemes

---

Scheme 1.1	Transition metal (M) catalysed Reduction of CO <sub>2</sub> into carbon monoxide (CO), and formate anion (HCOO <sup>-</sup> )	05
Scheme 1.2	Mechanism of the CO oxidation to CO <sub>2</sub> : (a) the amine oxide promoted carbonyl substitution, (b) and the Water-gas Shift Reaction.	06
Scheme 1.3	Catalytic hydroformylation of alkenes with CO <sub>2</sub> and CO in the presence of H <sub>2</sub> as a reducing agent.	07
Scheme 1.4	Schematic mechanism operating under hydroformylation conditions for the catalytic systems formed from the metallic precursors: (a) M <sup>(I)</sup> -X and (b) M <sup>(0)</sup> -□.	08
Scheme 1.5	Equilibrium between Rh-H and [Rh-(H <sub>2</sub> )] <sup>+</sup> species during Rh-catalysed hydroaminomethylation reaction using ionic liquids as solvent.	08
Scheme 1.6	Formation of carbenes by heat treatment of Ru <sub>3</sub> (CO) <sub>12</sub> in presence of imidazolium chloride salts.	09
Scheme 1.7	Formation of Ru-hydride complexes bearing abnormally bounded imidazolium carbenes.	09
Scheme 1.8	Reactivity of Ru-bis-carbene complexes, and Water-gas shift Reaction	10
Scheme 2.1	Synthesis of the -OH, -OMe, Cl, Br, -Si(OMe) <sub>3</sub> , -NH-functionalized imidazolium ionic liquids (FImILs).	20
Scheme 2.2	Two possible roots for the synthesis of the ionophilic phosphine-functionalized imidazolium ionic liquids.	24
Scheme 2.3	General-scheme for the synthesis of symmetrical mono-phosphites.	26
Scheme 2.4	Synthesis of the phosphite-functionalized imidazolium ILs.	27
Scheme 2.5	Synthesis of ionophilic ImIL-S-N-S-ImIL modified imidazolium IL	28
Scheme 3.1	Rh/Ru-catalysed hydroformylation of 1-alkenes by using mixture of CO/H <sub>2</sub> OR CO <sub>2</sub> /H <sub>2</sub> as C-1 feedstock	32
Scheme 3.2	Proposed mechanism for the cascade reactions RWGSR/	

---



---

	hydroformylation /hydrogenation catalyzed by situ generated of Ru-catalyst.	42
Scheme 3.3	Reported and possible Ru-carbenes species formed by heat treatment of Ru <sub>3</sub> (CO) <sub>12</sub> with imidazolium chloride salts.	43
Scheme 3.4a	<i>In-situ</i> generated Ru-catalytic species and reaction intermediates of RWGS reaction	56
Scheme 3.4b	Proposed reaction mechanism for the ru-catalyzed reductive conversion of CO <sub>2</sub> into CO by Reverse-Water-Gas-Shift reaction (RWGSR) promoted by H <sub>3</sub> PO <sub>4</sub>	57
Scheme 4.1	Possible pathways involved in the hydrogenation of carbon dioxide by [Ru-H] <sup>+</sup> catalytic active species.	64
Scheme 4.2	Hydroaminomylation of alkenes, N-formylation/N methylation of amines using CO <sub>2</sub> /H <sub>2</sub> as source of CO/H <sub>2</sub> syngas.	65
Scheme 4.3	Ru-catalyzed N-formylation/N-methylation of amines using CO <sub>2</sub> as a CO source in presence of ionic liquids [BMI•Cl] or [BMMI•Cl].	68
Scheme 4.4	Reaction optimization for the N-formylation of aniline.	71
Scheme 4.5	Ru-catalyzed hydrogenation of aromatic ring.	72
Scheme 4.6	Aniline resonance species, and its relationship with the product selectivity.	75
Scheme 4.7	Ru-catalysed Reaction mechanism for the N-formylation and N-methylation amines with CO <sub>2</sub> /H <sub>2</sub>	75
Scheme 4.8	Hydroaminomethylation/reductive amination of carvone catalyzed by [Ru <sub>3</sub> (CO) <sub>12</sub> ]/BMMI.Cl in the presence of H <sub>3</sub> PO <sub>4</sub> .	79
Scheme 4.9	Main steps involved in the hydroaminomethylation of alkenes by [Ru <sub>3</sub> (CO) <sub>12</sub> ]/IL catalytic system.	80
Scheme 4.10	Reductive amination of benzaldehyde with amines	81
Scheme 4.11	Reductive amination 2-furfuraldehyde (10 mmol), pyrrolidine (10.0 mmol)	82
Scheme 4.12	Catalytic tests for evaluating the ability of the Ru-hydroaminomethylation active species for catalysing: (b)	

---

---

	reduction of amides, and (c) hydroformylation-hydroaminomethylation of alkenes using dimethylformamide as a CO source, (d) reaction of morpholine with cyclohexene without CO <sub>2</sub> .	83
Scheme 4.13	Ru-catalyzed reaction mechanism for the hydroaminomethylation followed: (A) RWGSR, (B) Hydroformylation, (C) Reductive amination (hydrogenation of imines, & enamines).	84
Scheme 5.1	Pd/C-2, Pd/C-5 catalyzed disproportionation of 1,3-cyclohexadiene by reductive enter hydrogen transfer mechanism.	105

---

## List of Figures

---

Figure 1.1	Chemical Fixation of CO <sub>2</sub> into high-value chemicals, and various organic intermediates.	02
Figure 1.2	Schematic visual of energy profile for chemical fixation of CO <sub>2</sub> with energy-rich reactants.	03
Figure 1.3	Chemical transformations of carbon dioxide (CO <sub>2</sub> ) into Value-added Bulk and Fine Chemicals	05
Figure 2.1	<sup>31</sup> P-NMR spectrums of the P-modified imidazolium ILs 3, 4	26
Figure 3.1	Organic solvents and additives used in hydroformylation reactions.	34
Figure 3.2	Schematic diagram of Parr high pressure reactor (4590) used for the hydroformylation reactions.	35
Figure 3.3	Ru-catalysed hydroformylation of 1-hexene using CO <sub>2</sub> as a CO source. Reaction conditions: 1-hexene (20.0 mmol), Ru <sub>3</sub> (CO) <sub>12</sub> (0.1 mmol), 1-hexene / Ru = 64, 60 bar CO <sub>2</sub> /H <sub>2</sub> (1:1), 120 °C, 17 h;	38
Figure 3.4	<sup>31</sup> P-NMR analysis of Ru-catalyzed hydroformylation reaction mixture by using P(OEt) <sub>3</sub> as additive.	41
Figure 3.5	<sup>1</sup> H NMR (400 MHz, CDCl <sub>3</sub> ) spectra of Ru <sub>3</sub> (CO) <sub>12</sub> dissolved in BMI•Cl.	44
Figure 3.6	<sup>13</sup> C { <sup>1</sup> H} NMR (100 MHz, CDCl <sub>3</sub> ) and <sup>13</sup> C NMR (100 MHz, CDCl <sub>3</sub> ) spectra of Ru <sub>3</sub> (CO) <sub>12</sub> dissolved in BMI•Cl	46
Figure 3.7	<sup>1</sup> H NMR (400 MHz, CDCl <sub>3</sub> ) spectra of Ru <sub>3</sub> (CO) <sub>12</sub> dissolved in BMI•Cl under 1 bar Ar.	47
Figure 3.8	<sup>13</sup> C { <sup>1</sup> H} NMR (100 MHz, CDCl <sub>3</sub> ) spectra of Ru <sub>3</sub> (CO) <sub>12</sub> dissolved in BMI•Cl under 1 bar Ar.	48
Figure 3.9	<sup>1</sup> H NMR (400 MHz, CDCl <sub>3</sub> ) spectra of Ru <sub>3</sub> (CO) <sub>12</sub> dissolved in BMMI•Cl.	50
Figure 3.10	<sup>13</sup> C { <sup>1</sup> H} NMR (100 MHz, CDCl <sub>3</sub> ) spectra of Ru <sub>3</sub> (CO) <sub>12</sub> dissolved in BMMI•Cl.	51

---

---

Figure 3.11	GC-TCD-analysis spectrums of the gas phase during the reactions by adding additives $^{13}\text{CO}$ , $\text{H}_3\text{PO}_4$ , and $\text{P}(\text{OEt})_3$ .	52
Figure 3.12	ESI-MS <sup>+</sup> Analysis for the reaction mixture obtained by reacting $\text{Ru}_3(\text{CO})_{12}$ precursor with BMI•Cl (2 equiv. IL/Ru), 60 bar $\text{CO}_2/\text{H}_2$ (1:1).	53
Figure 3.13	ESI-MS <sup>-</sup> Analysis for the reaction mixture obtained by reacting $\text{Ru}_3(\text{CO})_{12}$ precursor with BMI•Cl (2 equiv. IL/Ru), 60 bar $\text{CO}_2/\text{H}_2$ (1:1).	54
Figure 3.14	[ESI-MS] <sup>+</sup> Analysis for the reaction mixture obtained by reacting $\text{Ru}_3(\text{CO})_{12}$ precursor with $^{13}\text{C}_2$ -labeled [BMI•Cl] (5 equiv. IL/Ru).	54
Figure 3.15	IR spectra of the species formed by reacting $\text{Ru}_3(\text{CO})_{12}$ with [BMI•Cl].	55
Figure 3.16	IR spectra of the species formed by reacting $\text{Ru}_3(\text{CO})_{12}$ with [BMMI•Cl].	56
Figure 3.17	Alkenes conversion and alcohol selectivity obtained from the Ru-catalysed hydroformylation of alkenes using $\text{CO}_2$ as a CO source.	58
Figure 4.1	Conversion of alkene (%) and amine selectivity (%) obtained in the Ru-catalysed hydroformylation of alkenes using $\text{CO}_2$ as a CO source.	79
Figure 5.1	Schematic representation of sputtering deposition chamber used for the immobilization of the transition M-NPs onto supporting materials.	90
Figure 5.2a	Deposition of Pd(0)-fcc nanoparticles on carbon using the magnetron-sputtering chamber developed by our group. Palladium content (wt. %) vs. deposition time (min).	94
Figure 5.2b	XRD pattern of Pd <sup>0</sup> /C-1 to 5 (Pd <sup>0</sup> = 0.15, 0.73, 1.31, 1.94, and 2.36 Wt%) deposited by sputtering on carbon(C 002) support.	95

---

Figure 5.3a	TEM images of Pd/C-1 Pd/C-5 NPs narrow distributed and deposited onto solid supports active carbon	95
Figure 5.3b	H <sub>2</sub> -chemisorptions analysis of Pd/C-2 Pd/C-5 NPs deposited onto solid supports active carbon.	96
Figure 5.4	Kinetic expression between % Conv. Vs Time (min), and TOF Vs TON relationship for the selective hydrogenation of nitrobenzene into aniline catalyzed by sputtered Pd/C-1 to Pd/C-5 catalysts and Pd/C-D under solvent-free liquid-phase condition	98
Figure 5.5	Kinetic between % Conv. Vs Time (min), and TOF Vs TON for the hydrogenation of cyclohexene catalyzed by sputtered Pd/C-1 to 5, Pd/SAB-15 and Pd/C-D, under solvent-free liquid-phase condition.	99
Figure 5.6	Kinetic expression between 0.73 Wt% Pd/C or TiO <sub>2</sub> supported NPs by using same Ph-NO <sub>2</sub> / Pd ratio of 13298	102
Figure 5.7	Pd/C-2 catalyzed reaction optimization for the disproportion of 1,3-cyclohexadiene by controlling the reaction time	103
Figure 5.8	Recycling activities of the Pd/C-2, Pd/C-5 for the disproportion of 1,3-cyclohexadiene.	106
Figure 6.1-6.20	GC-analysis, NMR spectrum for Ru-catalyzed hydroformylation of alkenes with CO <sub>2</sub> as CO source	111-120
Figure 6.21-6.34	GC, NMR spectrums for Ru-catalyzed N-formylation of amines using CO <sub>2</sub> as CO source.	121-127
Figure 6.35-6.56	GC, NMR spectrums for Ru-catalyzed hydroaminomethylation of amines using CO <sub>2</sub> as CO source	128-138
Figure 6.57-6.61	GC, NMR spectrums for Ru-catalyzed reductive amination of benzaldehyde.	139-141
Figure 6.62-6.65	GC analysis for Pd-NPs catalyzed selective hydrogenation of 1,3cyclohexadiene into cyclohexene	142-143
Figure 6.66	GC analysis for disproportion of 1,3cyclohexadiene.	144

## List of Tables

---

Table 2.1	Synthesis and characterization of [BMI•X], [BMMI•X] ionic liquids.	16
Table 2.2	Synthesis of the <sup>13</sup> C-labelled [BMI(2- <sup>13</sup> C)•Cl] ionic liquid.	19
Table 2.3	Characterization of functionalized ionic liquids (FILs).	21
Table 2.4	Characterization of vinalic, allylic and phosphie functionalizd ILs.	24
Table 3.1	Ru-catalysed hydroformylation of cyclohexene using CO <sub>2</sub> as a CO source.	37
Table 3.2	Ru-catalysed hydroformylation of cyclohexene using CO <sub>2</sub> as a CO source and monodentate or bidentate ligands with different electronic and steric properties.	40
Table 4.1	Ru-catalysed N-formylation of amines using CO <sub>2</sub> as a CO source in presence of ionic liquids [BMI•Cl] and [BMMI•Cl].	69
Table 4.2	Ru-catalysed N-formylation of aniline using CO <sub>2</sub> as a CO source.	73
Table 4.3	Ru-catalysed hydroaminomethylation of cyclohexene using CO <sub>2</sub> as a CO source	77
Table 5.1	Pd-nanocatalysts supported onto activated carbon (Pd-NPs/Cat.1 to Pd-NPs/Cat.5) prepared by magnetron-sputtering.	94
Table 5.2	Hydrogenation of aniline catalysed by Pd-nanocatalyst supported onto activated charcoal (Pd-NPs/C-1 to Pd-NPs/C-5) prepared by magnetron sputtering.	97
Table 5.3	Hydrogenation of cyclohexene catalysed by Pd-nanocatalyst supported onto activated charcoal (Pd-NPs/C-1 to Pd-NPs/C-5) prepared by magnetron sputtering.	100
Table 5.4	Hydrogenation of aniline catalysed by Pd-NPs/ C-1 prepared by magnetron sputtering.	101
Table 5.5	Comparative study between Pd/C-0.15, 0.73 wt%, and Pd/TiO <sub>2</sub> -0.15, 0.73 wt% NPs	102

---

---

Table 5.6	Pd-catalyzed catalyzed disproportionation of 1,3-cyclohexadiene activities by using 4 bar H <sub>2</sub> condition	104
Table 5.7	Pd-catalyzed catalyzed disproportionation of 1,3-cyclohexadiene activities under Ar condition.	105

---





## 1.1 Carbon Dioxide Fixation and Utilization

Chemical fixation and utilization of carbon dioxide ( $\text{CO}_2$ ) received enormous attentions of scientific community for the last couple of decades. Capturing and chemical transformation of  $\text{CO}_2$  has tremendous importance in both industrial and environmental perspectives. Today, attenuation of the increasing emission of  $\text{CO}_2$  in our atmosphere is an extensive and long-term global task for the world. However, the chemical fixation of  $\text{CO}_2$  is not certainly reducing  $\text{CO}_2$  concentration significantly. But the capturing and storage of  $\text{CO}_2$  has been paradigm shift towards the transformation of  $\text{CO}_2$  as renewable source of C1-feedstock for the fabrication of fuel products, and synthesis of important organic intermediates. These organic intermediates can further catalytically react with others high-energy organic molecules in the synthesis of useful fine and bulk chemicals (Figure-1.1).<sup>[1-4]</sup> Thus,  $\text{CO}_2$  gives access to high-value products from more ideal, nontoxic, and renewable-raw material. And it is an important development along with the replacement of conventional sources of C1-building-block carbon monoxide ( $\text{CO}$ ) due to its major disadvantage of high toxicity.<sup>[5-8]</sup>

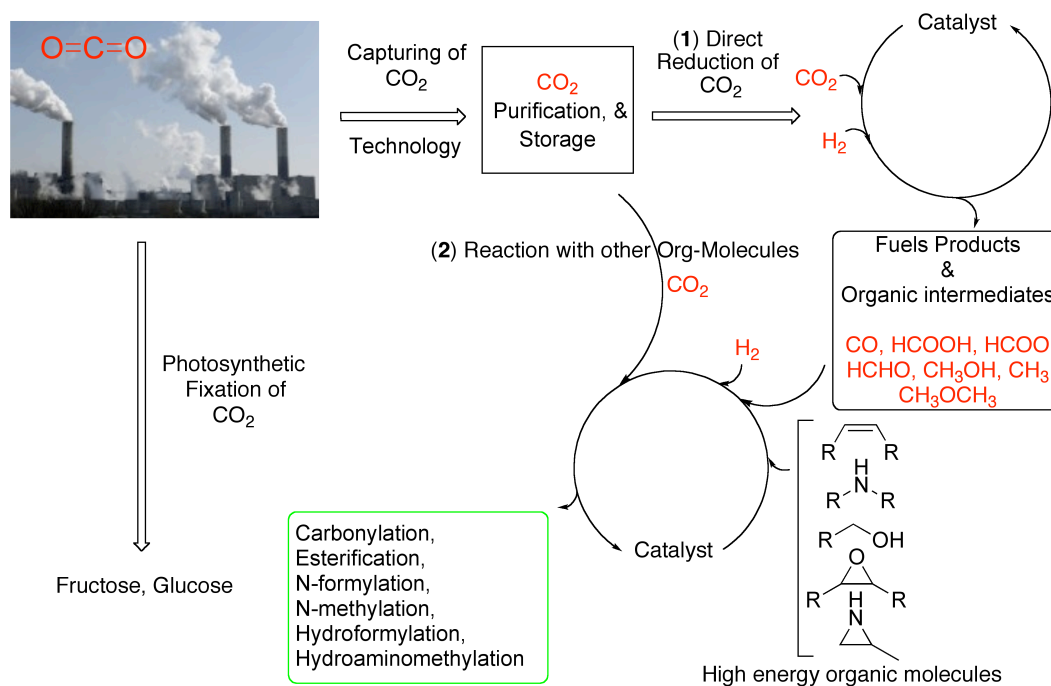


**Figure 1.1** Chemical Fixation of  $\text{CO}_2$  into high-value chemicals, and various organic intermediates. <sup>[1, 4]</sup>

Commercial utilization and recycling of CO<sub>2</sub> as a successful renewable C1-feedstock, is possible due to carbon capturing and storage (CCS) by the help of fairly well developed and robust technologies. CO<sub>2</sub> can be obtained from a range of large-scale sources, like most commonly as by-product in high purity from chemical industry and refineries. In the process, aqueous amine solutions are used for the washing of gas streams containing CO<sub>2</sub>, which subsequently released at elevated temperature.<sup>[9,10]</sup> Further more developed membranes,<sup>[11,12]</sup> less-expensive solid adsorbent materials, and ionic liquids are used for the separation of CO<sub>2</sub> from gas streams by adsorption / desorption process.<sup>[13, 14]</sup>

But still limitations are there for the efficient CCS and utilization of CO<sub>2</sub> as source of C1-building-block in future. However, the development of more efficient CO<sub>2</sub> absorbing materials and effective catalyst systems are extremely required for the significant fixation, and reduction of CO<sub>2</sub> into high-value fuels, and chemical products. Generally recycling of CO<sub>2</sub> as a C1-building-block can confront three major experimental and technological challenges for the industrial implementation of this concept, which is summarized in Figure-1.2. (1) “Identifying pathways and products” various chemical reactions that incorporated CO<sub>2</sub>,<sup>[1, 15]</sup> and many more can be visualized. However, further efforts are needed to discover new chemistry based on CO<sub>2</sub> molecule to identify the industrial relevant targeted transformations that can easily bring this promising research area into mainstream.

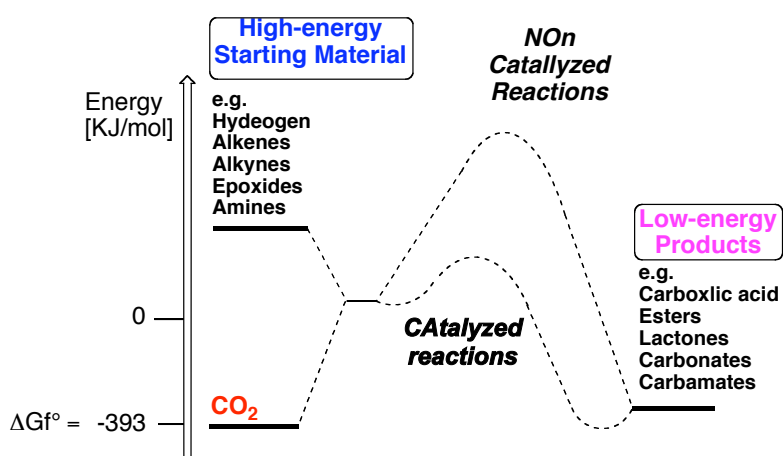


**Figure 1.2** Schematic visual of energy profile for chemical fixation of CO<sub>2</sub> reacting with other organic molecules.<sup>[1]</sup>

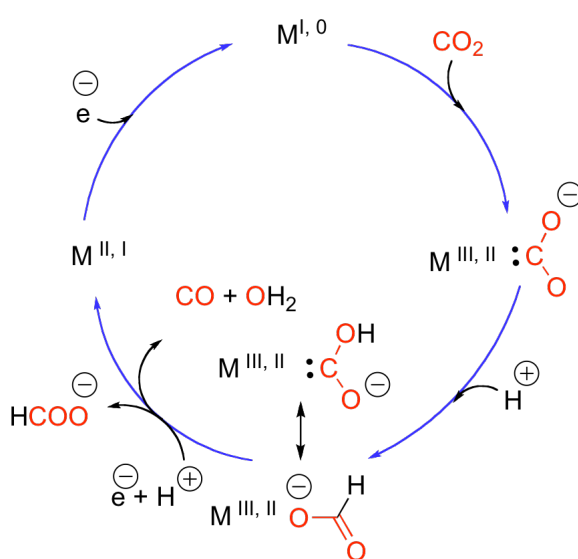
(2) “Understanding and development of new catalysts” is a major and core methodology for the successful recycling of CO<sub>2</sub>. It requires highly efficient, and abundant catalyst systems to accelerate the chemical reactions by CO<sub>2</sub> activation as C1-building block. In general, the catalytic conversion of CO<sub>2</sub> is brought about either by direct reduction into fuel products, and organic intermediates,<sup>[15-18]</sup> or it can react with other organic molecules to produce useful bulk chemicals.<sup>[19-24]</sup> (3) “Addressing energetic constraints” CO<sub>2</sub> is thermodynamically more stable molecule containing very low Gibbs free energy ( $\Delta G_f^\circ = -393$  KJ/mol, showed in Figure 1.2). Thus the activation of CO<sub>2</sub> is the major drawback for the chemical reactions under mild condition. Therefore, normally used high-energy substrates such as hydrogen, unsaturated compounds, strained cyclic molecules, and amines to drive the chemical reactions towards low energy products (Figure 1.2).<sup>[2, 5, 20, 22, 25]</sup>

Present efforts generated an effective, and abundant homogeneous Ru-catalyst system in the presence of imidazolium ionic liquids (ILs) for the utilization of CO<sub>2</sub> as source of C1-building block by reacting with versatile alkenes and amines. In this process Ru-hydride-carbonyl-carbene species formed (*in situ* by reaction of imidazolium ionic liquids with Ru<sub>3</sub>(CO)<sub>12</sub>), as efficient catalyst for the cascade of reactions of Reverse Water Gas Shift reaction, hydroformylation, hydroaminomethylation of alkenes, and N-formylation, N-methylation of amines by using CO<sub>2</sub> / H<sub>2</sub> as a source of CO.

## 1.2 Catalytic reduction of carbon dioxide (CO<sub>2</sub>)

The catalytic reductive conversion of CO<sub>2</sub> into fuel products and other organic intermediates (Figure 1.1) is an extremely significant matter of contemporary energy and environmental challenges.<sup>[17, 26, 27]</sup> Electro-catalytic reduction of CO<sub>2</sub> into formic acid has been extensively investigated and industrialized, but today low-oxidation-state transition metals (Rh, Pt, Ru, and Fe) precursors are recommended to promote homogeneous, or biphasic homogeneous catalysis for the reduction of CO<sub>2</sub> into fuel products.<sup>[17, 28-30]</sup> Kinetic studies for the formation of primary organic intermediates, specially, carbon monoxide (CO), and

formate anion ( $\text{HCOO}^-$ ) are more important among the huge number of catalysts that have been tested (Scheme 1.1). The proposed mechanisms for the catalytic reduction of  $\text{CO}_2$  indicates that  $\text{CO}_2$  easily coordinate with transition metals ( $\text{M}^{0,1}$ ) with low oxidation states<sup>[17, 28-30]</sup>. The ligation characteristics and electron density on the metal are essential parameters for the formation of two possible initial adducts of the  $\text{CO}_2$  ( $\text{CO}$  or  $\text{HCOO}^-$ ). But the acidic medium and electron transfer serve as two important tools in the mechanism. Initially stabilize the primary  $\text{CO}_2$  adduct and then it helps in the cleavage of the C-O bond leading to the formation of  $\text{CO}$  intermediate.<sup>[29, 31]</sup>

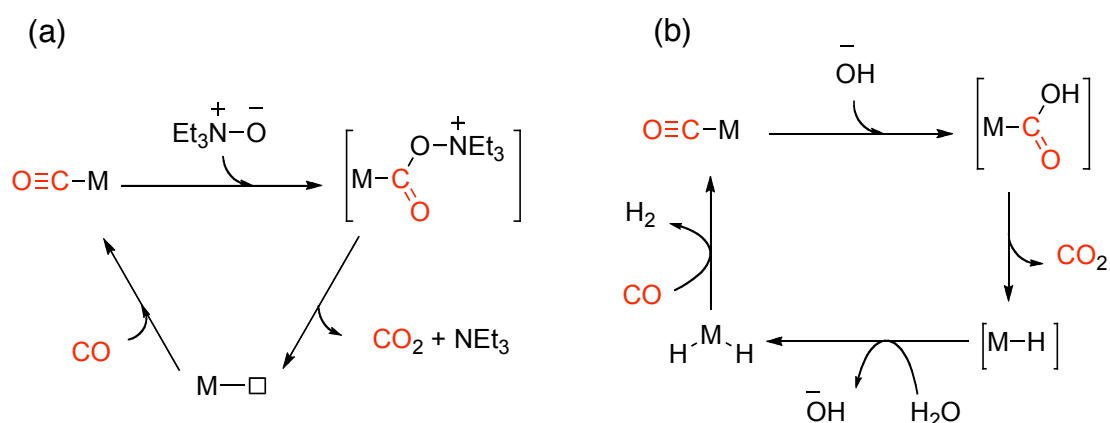


**Scheme 1.1** Transition metal (M) catalysed reduction of  $\text{CO}_2$  into carbon monoxide ( $\text{CO}$ ), and formate anion ( $\text{HCOO}^-$ ).

Water-gas Shift Reaction (WGS) process was extensively studied in the literature.<sup>[32]</sup> In general, two processes are described (see scheme 1.2): (a) the amine oxide promoted carbonyl substitution,<sup>[33-35]</sup> and (b) and the Water-gas Shift Reaction (WGS).<sup>[32]</sup> While, under the same catalysts systems Reverser Water-Gas Shift Reaction (RWGS) has also been investigated, that is responsible for the reduction of  $\text{CO}_2$  into  $\text{CO}$  molecule.



It is important to note that the oxidation of ligands (ca. P-donor ligands) can be accomplished if the reverse reaction so called “*amine oxide promoted carbonyl substitution*” is taken place during hydroformylation of alkenes using CO<sub>2</sub> as a CO source. The Reverse Water-gas Shift Reaction can be promoted with the courtesy of formation of a M-H species by reaction of the M-(H)<sub>2</sub> with H<sub>2</sub>O. These M-H species react with CO<sub>2</sub> thus forming the M-COOH, and eventually, further protonation allows the elimination of H<sub>2</sub>O by formation of M-CO species.

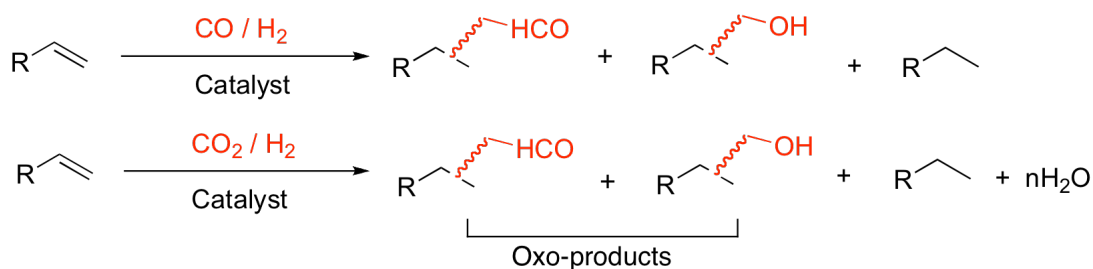


**Scheme 1.2** Mechanism of the CO oxidation to CO<sub>2</sub>: (a) the amine oxide promoted carbonyl substitution, (b) Water-gas Shift Reaction.

However, indirect production of methanol from CO<sub>2</sub> feedstock reveals that the Reverse Water-gas Shift Reaction (RWGSR) leads to the transformation of CO<sub>2</sub> into CO as reaction intermediate, which further hydrogenated into methanol. Commonly endothermic reactions are governed by “Lechatlier principle” require elevated temperatures, transition metal catalysts, and then reaction can be accelerated by increasing the pressure of H<sub>2</sub>, CO<sub>2</sub> feedstock.<sup>[4, 36]</sup> Reaction mechanism of the methanol formation from CO<sub>2</sub> has been extensively studied <sup>[15, 36]</sup>, but insights into this complex system having a long-standing challenge. Thus similarly, the reported studies for the reaction mechanism indicated two possible pathways for the transformation of CO<sub>2</sub> into methanol, (i) Formation of a formate species (HCOO<sup>-</sup>), as reaction intermediate, which subsequently reduced into methanol. While, (ii) reductive conversion of CO<sub>2</sub> into CO *via* the Reverse Water-gas Shift reaction, then hydrogenation of CO into methanol.<sup>[5, 15, 26, 27, 36, 37]</sup>

### 1.3 Rh / Ru- catalyzed hydroformylation of olefins with CO<sub>2</sub> as CO source.

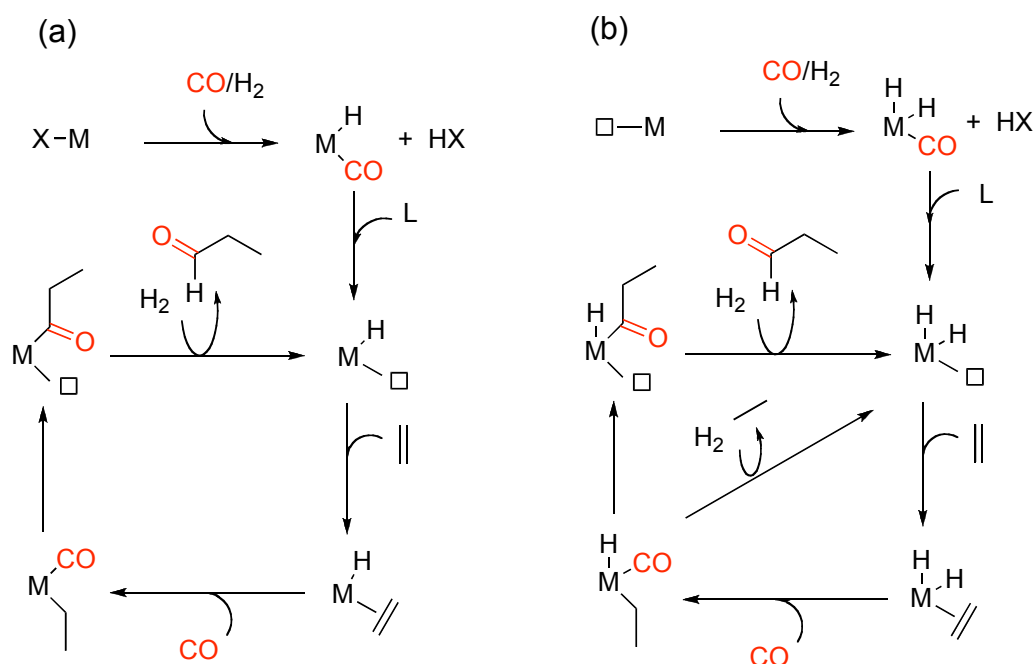
Rhodium (Rh) metal is the catalyst choice for the hydroformylation,<sup>[38-40]</sup> and hydroaminomethylation of alkenes by using both CO/H<sub>2</sub> and CO<sub>2</sub>/H<sub>2</sub> as C1-building block.<sup>[20]</sup> Various homogeneous Rh-centered catalysts have successfully been applied with several phosphine/phosphite ligands for the effective and regioselective hydroformylation, and hydroaminomethylation of alkenes.<sup>[20, 41, 42]</sup> But recently, the potential use of Ru as hydroformylation catalyst is of axis of interest since the use Rh is less abundant,<sup>[39, 43]</sup> and several Ru-mediated hydroformylation-hydrogenation,<sup>[41, 42, 43]</sup> hydroaminomethylation,<sup>[44]</sup> N-methylation and N-formylation methods have been developed. Ru-catalyzed hydroformylation of olefins generally accompanied with oxo-products (alcohol, aldehyde), and hydrogenation adduct (Scheme 1.3).



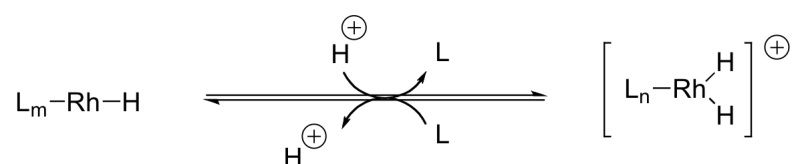
**Scheme 1.3** Catalytic hydroformylation of alkenes with CO<sub>2</sub> and CO in the presence of H<sub>2</sub> as a reducing agent.

The difference in selectivity can easily be understood if we look at the hydroformylation and hydrogenation mechanisms catalysed by Rh<sup>(I)</sup> and Ru<sup>(0)</sup> systems (Scheme 1.4). As Rh-H and the Ru-(H)<sub>2</sub> are the active catalytic species under hydroformylation conditions.<sup>[39, 43]</sup> However, it should be noted that the mechanism operated for the formation of M-(H)<sub>2</sub> assumed the homolytic cleavage of the H-H, while that for the formation of the M-H would be by intramolecular (ligands) or by intermolecular (external base) heterolysis of the H-H bond favored the formation of M-H species.<sup>[45-48]</sup> For instance, in the ruthenium catalyzed

hydrogenation of acids, cyclic carbonates, and CO<sub>2</sub> to alcohol happens with the formation of catalytically active cationic [Ru-H]<sup>+</sup> species. [49-51] [52] [53, 54]



**Scheme 1.4** Schematic mechanism operating under hydroformylation conditions for the catalytic systems formed from the metallic precursors: (a) M<sup>(I)</sup>-X and (b) M<sup>(0)</sup>-□.



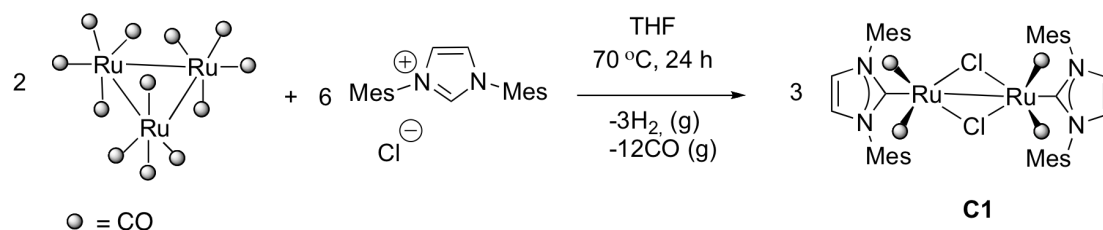
**Scheme 1.5** Equilibrium between Rh-H and [Rh-(H<sub>2</sub>)]<sup>+</sup> species during Rh-catalysed hydroaminomethylation reaction using ionic liquids as solvents.

The role of solvent or additives in the mechanism of Rh-catalysed hydroaminomethylation reaction using imidazolium ionic liquids as reaction media has been revealed earlier. Mechanistic studies proposed that the acidic protons of the imidazolium ring could shift the equilibrium between the Rh-H and [Rh-(H<sub>2</sub>)]<sup>+</sup> species, which is highly-active for the hydrogenation activities (Scheme 1.5).<sup>[48]</sup> This hypothesis was confirmed through observation of slower

hydrogenation rates in presence of 3-alkyl-1,2-dimethyl-imidazolium salts than in presence of 3-alkyl-1-methyl-imidazolium.

#### 1.4 Generation of NHC-Ru carbene catalysts with imidazolium ionic liquids.

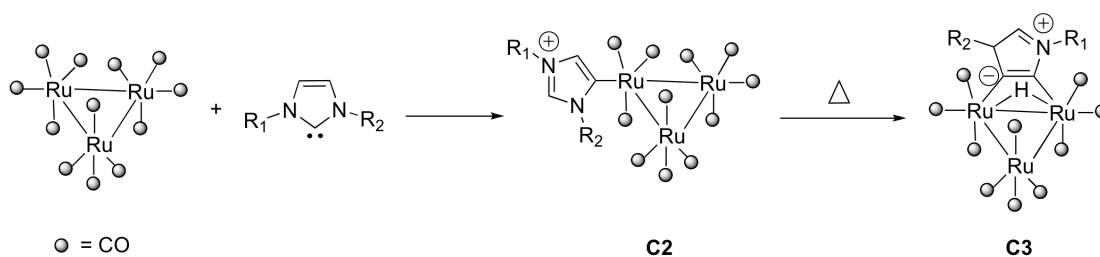
Coordination chemistry of N-heterocyclic carbenes (NHC)<sup>[55, 56]</sup> and fascinating catalytic properties of transition M-carbene complexes<sup>[57, 58]</sup> has lately driven interest for their use in synthesis. Ruthenium carbene chemistry has already stolen much-attentions with the synthesis of first and second generation of NHC-Ru catalysts for the alkenes metathesis. While, recently the *mono-* or *tri-*nuclear Ru-carbonyl clusters are commonly used for the generation of Ru-carbonyl-carbene species by their reaction with N-heterocyclic compounds or imidazolium ionic liquids.<sup>[59-62]</sup> Formation of Ru-carbene complexes through imidazolium ionic liquids has attracted significant interest towards the formation of Ru-hydride-carbonyl-carbene catalytic species during the reaction between imidazolium ionic liquids and Ru-precursors. These species would serve as active catalyst for the hydroformylation, and hydroaminomethylation of alkenes by using CO<sub>2</sub>.



**Scheme 1.6** Formation of carbenes by heat treatment of Ru<sub>3</sub>(CO)<sub>12</sub> with imidazolium chloride salts.

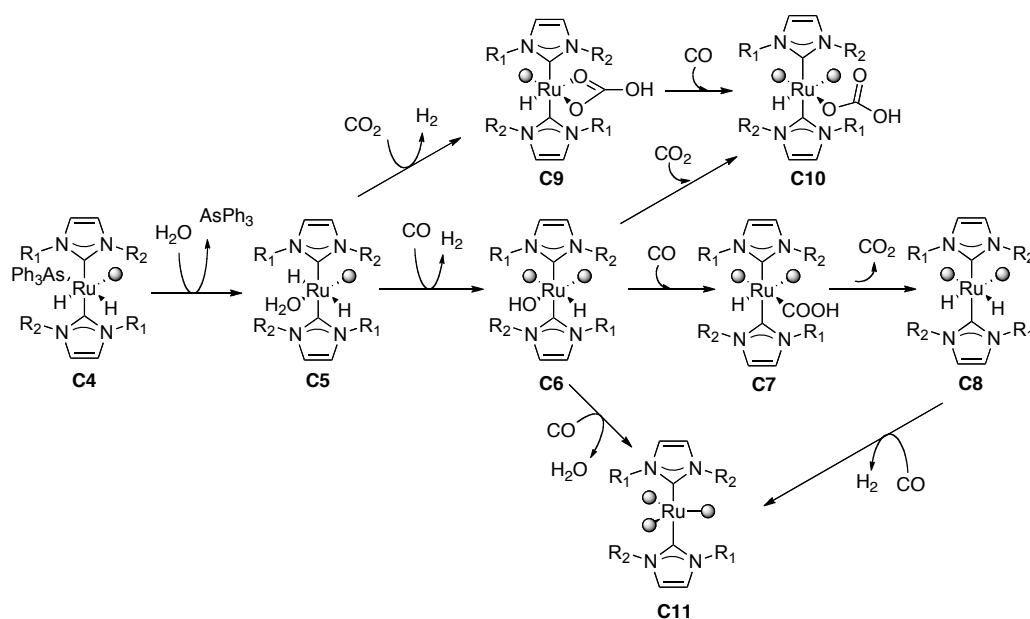
It has been previously reported the in-situ formation of carbene complex **C1** by the reaction of Ru<sub>3</sub>(CO)<sub>12</sub> with imidazolium chloride salt (Scheme 1.6).<sup>[63]</sup> furthermore it is also reported the formation of “abnormal carbene (C 4, 5)” of Ru-complexes (**C2-3**) by using N-substituted imidazole carbene (Scheme 1.7).<sup>[64]</sup>





**Scheme 1.7** Formation of Ru-hydride complexes bearing abnormally bounded imidazolium carbenes.

Currently the main focus is the synthesis of ionophilic phosphine functionalized imidazolium ionic liquids, and their coordination chemistry. P-functionalized imidazolium ionic liquids have already been studied to a significant extent for the formation of mononuclear and tri-nuclear Ru-carbonyl-carbenephosphine complexes.<sup>[59, 65, 66]</sup> Thus several Rh-carbene catalysts<sup>[67]</sup> have been successfully investigated for the hydroformylation, and hydroaminomethylation<sup>[68, 69]</sup> of alkenes, but recent studies are focused on the generation of Ru-hydride-carbonyls-carbenes or Ru-hydride-carbonyls-carbenes-phosphine species. These can offer selective hydroformylation, hydroaminomethylation of alkenes with hydrogenation product, and N-formylation, N-methylation of amines by CO<sub>2</sub> as source of CO involving Reverse Water-gas Shift reaction.



**Scheme 1.8** Reactivity of Ru-bis-carbene complexes and Water-gas Shift Reaction.

Whittlesey and co-workers studied the reactivity of similar ruthenium bis-carbene complexes (scheme 1.8) the water-gas shift ( $\text{CO} + \text{H}_2\text{O} \rightarrow \text{CO}_2 + \text{H}_2$ ).<sup>[70]</sup> Moreover, the application of ruthenium bis-carbene complexes as catalytic systems for the hydrogenation of olefins has been reported recently.<sup>[71] [72]</sup>

## 1.5 References

- [1] M. Peters, B. Kohler, W. Kuckshinrichs, W. Leitner, P. Markewitz, T. E. Muller, *ChemSusChem* **2011**, *4*, 1216.
- [2] T. Sakakura, J. C. Choi, H. Yasuda, *Chem. Rev.* **2007**, *107*, 2365.
- [3] C. Song, *Catalysis Today* **2006**, *115*, 2.
- [4] M. He, Y. Sun, B. Han, *Angew. Chem. Int. Ed.* **2013**, *52*, 2.
- [5] M. Cokoja, C. Bruckmeier, B. Rieger, W. A. Herrmann, F. E. Kuhn, *Angew. Chem. Int. Ed.* **2011**, *50*, 8510.
- [6] P. G. Jessop, T. Ikariya, R. Noyori, *Nature* **1994**, *368*, 231.
- [7] C. Federsel, R. Jackstell, M. Beller, *Angew. Chem. Int. Ed.* **2010**, *49*, 6254.
- [8] W. Leitner, *Angew. Chem. Int. Ed.* **1995**, *34*, 2207.
- [9] G. T. Rochelle, *Science* **2009**, *325*, 1652.
- [10] F. Barzagli, F. Mani, M. Peruzzinib, *Energy Environ. Sci.*, **2010**, *3*, 773.
- [11] Clem E. Powell, G. G. Qiao, *Journal of Membrane Science* **2006**, *279*, 1.
- [12] L. Zhao, E. Riensche, R. Menzer, L. Blum, D. Stolten, *Journal of Membrane Science* *325 (2008) 284–294* **2008**, *325*, 284.
- [13] S. Choi, J. H. Drese, C. W. Jones, *ChemSusChem* *2009*, *2*, 796 – 854 **2009**, *2*, 796.
- [14] A. L. Chaffee, G. P. Knowles, Z. Liang, J. Zhang, P. Xiao, P. A. Webley, *International Journal of Greenhouse Gas Control* *5 (2011) 1368* **2011**, *5*, 1368.
- [15] U. Rodemerck, M. Holena, E. Wagner, Q. Smejkal, A. Barkschat, M. Baerns, *Chemcatchem* **2013**, *5*, 1948.
- [16] T. Schaub, R. A. Paciello, *Angew. Chem. Int. Ed.* **2011**, *50*, 7278.
- [17] S. b. Bontemps, L. Vendier, S. Sabo-Etienne, *J. Am. Chem. Soc.* **2014**, *136*, 4419–4425.
- [18] S. N. Riduan, Y. Zhang, J. Y. Ying, *Angew. Chem.* **2009**, *121*, 3372
- [19] S. Bontemps, L. Vendier, S. Sabo-Etienne, *Angew. Chem. Int. Ed.* **2012**, *51*, 1671.
- [20] D. Crozet, M. Urrutigoity, P. Kalck, *Chemcatchem* **2011**, *3*, 1102.
- [21] X. Cui, Y. Zhang, Y. Deng, F. Shi, *Chem. Commun.*, **2014**, *50*, 189.
- [22] J. C. Anderson, R. B. Moreno, *Org. Biomol. Chem.* **2012**, *10*, 1334.
- [23] C. D. N. Gomes, O. Jacquet, C. Villiers, P. Thury, M. Ephritikhine, T. Cantat, *Angew. Chem. Int. Ed.* **2012**, *51*, 187
- [24] S. I. Fujita, S. Okamura, Y. Akiyama, M. Arai, *Int. J. Mol. Sci.* **2007**, *8*, 749.
- [25] D. J. Darensbourg, *Inorganic Chemistry* **2010**, *49*, 10765.
- [26] S. Wesselbaum, T. v. Stein, J. r. Klankermayer, W. Leitner, *Angew. Chem.* **2012**, *124*, 1617\_7620.
- [27] T. Schaub, R. A. Paciello, *Angew. Chem. Int. Ed.* **2011**, *50*, 7278
- [28] H. Ishida, K. Fujiki, T. Ohba, K. Ohkubo, K. Tanaka, T. Terada, T. Tanaka, *J. Chem. Soc., Dalton Trans.* **1990**.
- [29] C. Costentin, G. Passard, M. Robert, J.-M. Savéant, *Proc. Natl. Acad. Sci. U.S.A.* **2014**, *111*, 14990.
- [30] C. Costentin, G. Passard, M. Robert, J.-M. Savéant, *J. Am. Chem. Soc.* **2014**, *136*, 11821.
- [31] J.-M. Savéant, *Chem. Rev.* **2008**, *108*, 2348.

- [32] R. H. Crabtree, *The Organometallic Chemistry of the Transition Metals*, Wiley, **2011**.
- [33] J. K. Shen, Y. C. Gao, Q. Z. Shi, F. Basolo, *J. Organomet. Chem.* **1991**, *401*, 295.
- [34] J. K. Shen, Y. C. Gao, Q. Z. Shi, F. Basolo, *Organometallics* **1989**, *8*, 2144.
- [35] J. K. Shen, Y. L. Shi, Y. C. Gao, Q. Z. Shi, F. Basolo, *J. Am. Chem. Soc.* **1988**, *110*, 2414.
- [36] W. Wang, S. Wang, X. Ma, J. Gong, *Chem. Soc. Rev.* **2011**, *40*, 3703.
- [37] F. Liao, Y. Huang, J. Ge, W. Zheng, K. Tedsree, P. Collier, X. Hong, S. C. Tsang, *Angew. Chem.* **2011**, *123*, 2210
- [38] A. Gual, C. Godard, S. Castillon, C. Claver, *Tetrahedron-Asymmetry* **2010**, *21*, 1135.
- [39] J. C. Chadwick, R. Duchateau, Z. Freixa, P. W. N. M. van Leeuwen, *Homogeneous Catalysts*, Wiley, **2011**.
- [40] M. Haumann, A. Riisager, *Chem. Rev.* **2008**, *108*, 1474.
- [41] G. Liu, K. Huang, C. Cai, B. Cao, M. Chang, W. Wu, X. Zhang, *Chem. Eur. J.* **2011**, *17*, 14559.
- [42] S. Li, K. Huang, J. Zhang, W. Wu, X. Zhang, *Org. Lett.* **2013**, *15*, 3078.
- [43] P. W. N. M. van Leeuwen, *Homogeneous Catalysis: Understanding the Art*, Springer, **2004**.
- [44] L. Wu, I. Fleischer, R. Jackstell, M. Beller, *J. Am. Chem. Soc.* **2013**, *135*, 3989.
- [45] G. J. Kubas, *Chem. Rev.* **2007**, *107*, 4152.
- [46] D. Crozet, A. Gual, D. McKay, C. Dinoi, C. Godard, M. Urrutigoity, J. C. Daran, L. Maron, C. Claver, P. Kalck, *Chem. Eur. J.* **2012**, *18*, 7128.
- [47] D. Crozet, D. McKay, C. Bijani, A. Gual, C. Godard, C. Claver, L. Maron, M. Urrutigoity, P. Kalck, *Dalton Trans.* **2012**, *41*, 3369.
- [48] B. Hamers, P. S. Baeuerlein, C. Muller, D. Vogt, *Adv. Synth. Catal.* **2008**, *350*, 332.
- [49] F. M. Geilen, B. Engendahl, M. Holscher, J. Klankermayer, W. Leitner, *J. Am. Chem. Soc.* **2011**, *133*, 14349.
- [50] D. Spasyuk, S. Smith, D. G. Gusev, *Angew. Chem. Int. Ed.* **2013**, *52*, 2538.
- [51] D. Spasyuk, S. Smith, D. G. Gusev, *Angew. Chem. Int. Ed.* **2012**, *51*, 2772.
- [52] Z. Han, L. Rong, J. Wu, L. Zhang, Z. Wang, K. Ding, *Angew. Chem.* **2012**, *51*, 13041.
- [53] S. Wesselbaum, T. Vom Stein, J. Klankermayer, W. Leitner, *Angew. Chem. Int. Ed.* **2012**, *51*, 7499.
- [54] C. A. Huff, M. S. Sanford, *J. Am. Chem. Soc.* **2011**, *133*, 18122.
- [55] M. Melaimi, M. Soleihavoup, G. Bertrand, *Angew. Chem., Int. Ed.* **2010**.
- [56] M. Albrecht, *Science* **2009**, *326*, 532.
- [57] H. Clavier, K. Grela, A. Kirschning, M. Mauduit, S. P. Nolan, *Angew. Chem., Int. Ed.* **2007**, 6786.
- [58] O. Kaufhold, F. E. Hahn, *Angew. Chem., Int. Ed.* **2008**, 4057.
- [59] J. A. Cabeza, M. Damonte, P. G.-. Álvarez, A. R. Kennedy, E. Perez-Carreño, *Organometallics* **2011**, *30*, 826.
- [60] J. A. Cabeza, I. del Río, D. Miguel, E. Pérez-Carreño, M. G. Sánchez-Vega, *Organometallics* **2008**, *27*, 211.
- [61] C. E. Ellul, O. Saker, M. F. Mahon, D. C. Apperley, M. K. Whittlesey, *Organometallics* **2008**, *27*, 100.
- [62] C. Zhang, F. Luo, B. Cheng, B. Li, H. Song, S. Xu, B. Wang, *Dalton Trans.* **2009**, 7230.
- [63] M. I. Bruce, M. L. Cole, R. S. Fung, C. M. Forsyth, M. Hilder, P. C. Junk, K. Konstas, *Dalton Trans.* **2008**, 4118.
- [64] C. E. Ellul, M. F. Mahon, O. Saker, M. K. Whittlesey, *Angew. Chem. Int. Ed.* **2007**, *46*, 6343.
- [65] C. S. Consorti, G. L. P. Aydos, G. Ebeling, J. Dupont, *Org. Lett.* **2008**, *10*, 237.
- [66] C. S. Consorti, G. L. P. Aydos, G. Ebeling, J. Dupont, *Org. Lett.* **2008**, *19*, 237.
- [67] M. Ahmed, A. M. Seayad, R. Jackstell, M. Beller, *Angew. Chem. Int. Ed.* **2003**, *42*, 5615.
- [68] M. Ahmed, C. Buch, L. Routaboul, R. Jackstell, H. Klein, A. Spannenberg, M. Beller, *Chem. Eur. J.* **2007**, *13*, 1594.

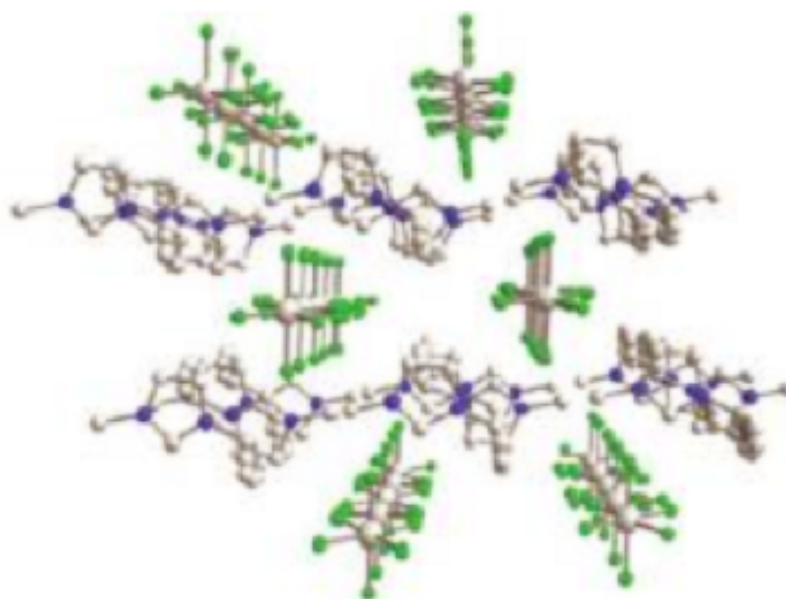
- [69] A. M. Seayad, K. Selvakumar, M. Ahmed, M. Beller, *Tetrahedron Lett.* **2003**, *44*, 1679.
- [70] R. F. R. Jazzar, S. A. Macgregor, M. F. Mahon, S. P. Richards, M. K. Whittlesey, *J. Am. Chem. Soc.* **2002**, *124*, 4944.
- [71] C. L. Lund, M. J. Sgro, R. Cariou, D. W. Stephan, *Organometallics* **2012**, *31*, 802.
- [72] C. Gandolfi, M. Heckenroth, A. Neels, G. Laurenczy, M. Albrecht, *Organometallics* **2009**, *28*, 5112.

## Objectives

- 1- Task specific synthesis of imidazolium ionic liquids for *in-situ* generation of Ru-catalytic systems for catalytic CO<sub>2</sub> transformation.
- 2- Development of a simple methodology for the generation of the biphasic-homogenous Ru-catalytic systems for the fixation of CO<sub>2</sub>, by solubilizing the Ru-precursors in the imidazolium ionic liquids.
- 3- Development of an efficient Ru-catalytic system for the selective hydroformylation of alkenes with CO<sub>2</sub> as CO source.
- 4- Development of an efficient phosphine free Ru-catalytic system for the hydroaminomethylation of alkenes with CO<sub>2</sub> as CO source.
- 5- Investigation for the Ru-catalysed N-formylation, & N-methylation of amines with CO<sub>2</sub>.
- 6- Generation of Ru-nanoparticle colloidal associated with the phosphine-functionalized ionic liquids with controlled size and shape for the CO<sub>2</sub> transformation.

## CHAPTER -2

### “Task Specific Synthesis of Ionic Liquids & CO<sub>2</sub> Fixation”



## 2.1 Introduction

Ionic liquids (ILs) are unique liquid electrolytes, and entirely composed of ions. A number of significant distinctive properties are attributed to ILs such as, negligible vapor pressure, high thermal stability and enormous chemistry.<sup>[1, 2]</sup> These promising electrolytes exhibit a wide spectrum of industrial and synthetic applications. Ionic liquids extensively are used as supporting material for the synthesis of M-NPs, as solvent in biphasic catalysis, in metal-extractions, fluid absorbents of gases, lubricants and baterias.<sup>[3]</sup> The most important property credited to ILs are their physico-chemical property, which can be easily modified by simple ions exchange process. Selection of anionic and cationic components allows the synthesis of ILs with required properties and custom functions.

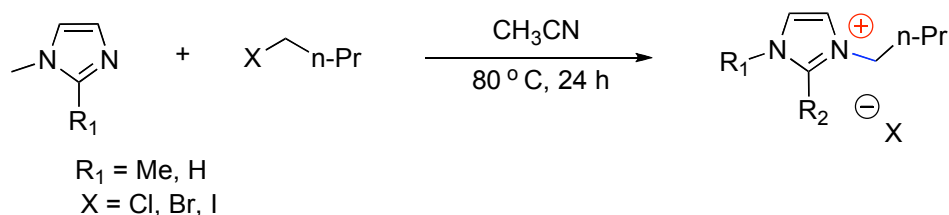
Moreover, recently ILs are attracting a significant attentions toward the solubility/absorption of carbon dioxide (CO<sub>2</sub>). However, ILs endorsed the fixation of CO<sub>2</sub> as a renewable source of C1-feedstock for the generation of contemporary energy (high-values chemicals, and fuel products), and separation of CO<sub>2</sub> from gas streams commercially. Brennecke and coworker (1999) reported first time the solubility of CO<sub>2</sub> in pyridinium and imidazolium ionic liquids (Im-ILs) indicated 0.72 mol fraction of CO<sub>2</sub> in [BMIM] [PF<sub>6</sub>] at 40 ° C, 93 bar.<sup>[4, 5]</sup> Later several studies revealed that appropriate counter anions (as [PF<sub>6</sub>]), <sup>[6-8]</sup> cationic ring, side chain, and task-specific functional groups are helping for the fixation of CO<sub>2</sub>.<sup>[9-11]</sup> C2 Substitution of imidazolium ring has thoroughly been discussed and documented the differences of solubility of CO<sub>2</sub> with Me-C2 or H-C2 substitutions. Recently our research group reported that [BMMI•pyrrolidine-2-carboxylate], and [BMMI•oxalate] have high-capacity of absorption of CO<sub>2</sub> among the several other ILs tested.<sup>[12]</sup> However, further modifications and task-specific functionalizations of Im-ILs could further improve the absorption of CO<sub>2</sub>. In the current study, we focused on the synthesis and functionalization of Im-ILs for the Ru-catalyzed hydroformylation, hydroaminomethylation of alkenes, and N-formylation, N-methylation of amines by using CO<sub>2</sub> as CO source. Ru-carbonyl precursors can easily react with simple Im-ILs, or P-functionalized (phosine, or phosphite) Im-ILs and generate an effective homogenous Ru-carbonyl-carbene or Ru-carbonyl-

carbene-phosphine containing catalytic species that render the reactions. Thus P-functionalized Im-ILs can also be used as supporting stabilizer for the synthesis of transition-metal nanostructures and NP-colloids.

## 2.2 Synthesis and characterization of [BMI•X], [BMMI•X] ILs.

Imidazolium molten salts such as, *1-n-butyl-3-methyl imidazole* [BMI•X], and *1-n-butyl-2,3-dimethyl imidazole* [BMMI•X] with halogens (X = Cl, Br, I) counter anions were synthesized by using well-developed experimental in our laboratory.<sup>[13, 14]</sup> In general, dry two-necked round-bottomed flask was equipped with a heating oil bath, charged with 1-eq. of freshly distilled N-methylimidazole or 1-2-dimethylimidazole, dry solvent acetonitrile, and 1 equiv of 1-halobutane. The reaction mixture was heated at 80 °C for 24 h, and then volatiles removed from reaction mixture under reduced pressure. Further ILs purified by simple solvent extraction and recrystallization processes. These imidazolium molten-salts have been studied for the Ru-catalyzed biphasic hydroformylation of cyclohexene. However, [BMI•X], and [BMMI•X] ILs indicated that chloride counter ion is better for the hydroformylation activity than the bromide or iodide counter ions (Chapter 3, Table 1, Entry 1-5).

**Table 2.1** Synthesis and characterization of [BMI•X], [BMMI•X] ionic liquids.

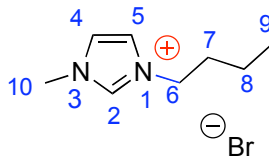


Ionic Liquids	Characterization
<b>[BMI•Cl]</b> 	<i>1-n-Butyl-3-methylimidazolium chloride</i> [BMI•Cl]: C <sub>8</sub> H <sub>15</sub> ClN <sub>2</sub> ; Molar mass: 174.67 g.mol <sup>-1</sup> ; Solid white (r temp). <sup>1</sup> H NMR <sup>[13, 14]</sup> (400 MHz, CDCl <sub>3</sub> ) δ ppm: 0.89 (t, J = 7.4 Hz, 3H, H9); 1.22-1.35 (m, 2H, H8); 1.82 (qp, J = 7.4 Hz, 2H, H7); 3.86 (s, 3H, H10); 4.17 (t, J = 7.2 Hz, 2H, H6); 7.40 (d, J = 2.0 Hz, 1H, H5); 7.45 (d, J = 2.0, 1H, H4), 10.21 (s, 1H, H2). <sup>13</sup> C-NMR (100 MHz, CDCl <sub>3</sub> ) δ ppm: 137.8 (C2);

---

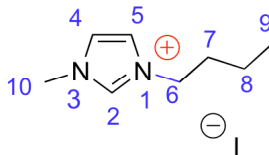
124.0 (C4); 122.3 (C5); 49.8 (NCH<sub>2</sub>); 36.6 (NCH<sub>3</sub>); 32.3 (C7); 19.6 (C8); 13.6 (C9). **D**<sub>25 °C</sub>: 1.086 g.mL<sup>-1</sup>.

**[BMI•Br]**



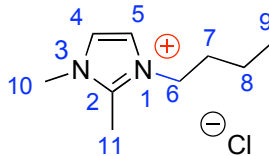
*1-n-Butyl-3-methylimidazolium bromide* [BMI•Br]: C<sub>8</sub>H<sub>15</sub>BrN<sub>2</sub>, Molar mass: 219.15 g mol<sup>-1</sup>, Yellow oil. **<sup>1</sup>H NMR**<sup>[13, 14]</sup> (400 MHz, CDCl<sub>3</sub>) δ ppm: 0.97 (t, 3H, H<sub>9</sub>); 1.35-1.46 (m, 2H, H<sub>8</sub>); 1.91-1.98 (m, 2H, H<sub>7</sub>); 4.16 (s, 3H, H<sub>10</sub>); 4.41 (t, *J* = 7.3 Hz, 2H, H<sub>6</sub>); 7.79 (t, *J* = 1,7 Hz, 1H, H<sub>5</sub>); 7.86 (t, *J* = 1,7 Hz, 1H, H<sub>4</sub>); 10.19 (s, 1H, H<sub>2</sub>). **<sup>13</sup>C NMR** (126 MHz, CDCl<sub>3</sub>) δ ppm: 137.8 (C<sub>2</sub>); 123.72 (C<sub>4</sub>); 122.15 (C<sub>5</sub>); 47.74 (C<sub>6</sub>); 36.61 (NCH<sub>3</sub>); 32.06 (C<sub>7</sub>); 19.33 (C<sub>8</sub>); 13.30 (C<sub>9</sub>). **D**<sub>25 °C</sub>: 1.101 g.mL<sup>-1</sup>.

**[BMI•I]**



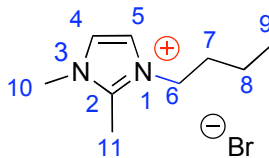
*1-n-Butyl-3-methylimidazolium Iodide* [BMI•I]: C<sub>8</sub>H<sub>15</sub>IN<sub>2</sub>, Molar mass: 266.12 g.mol<sup>-1</sup>, dark yellow oil. **<sup>1</sup>H-NMR**<sup>[13, 14]</sup> (400 MHz - CDCl<sub>3</sub>) δ ppm: 0.99 (t, *J* = 7,1Hz, 3H, H<sub>9</sub>); 1.33-1.52 (m, 2H, H<sub>8</sub>); 1.86- 2.03 (m, 2H, H<sub>7</sub>); 4.16 (s, 3H, H<sub>10</sub>); 4.40 (t, *J* = 7.2 Hz, 2H, H<sub>6</sub>); 7.73 (d, *J* = 1.5 Hz, 1H, H<sub>5</sub>); 7.77 (d, *J* = 1,5 Hz, 1H, H<sub>4</sub>); 9.81 (s, 1H, H<sub>2</sub>). **<sup>13</sup>C NMR** (126 MHz, CDCl<sub>3</sub>) δ ppm: 136.43 (C<sub>2</sub>); 123.80 (C<sub>4</sub>); 122.37 (C<sub>5</sub>); 49.80 (NCH<sub>2</sub>); 37.03 (NCH<sub>3</sub>); 32.02 (C<sub>7</sub>); 19.34 (C<sub>8</sub>); 13.41 CH<sub>3</sub> (C<sub>9</sub>). **D**<sub>25 °C</sub>: 1.372 g.mL<sup>-1</sup>.

**[BMMI•Cl]**



*1-n-butyl-2,3-dimethyl imidazolium chloride* [BMMI•Cl]: C<sub>9</sub>H<sub>17</sub>ClN<sub>2</sub>, Molar mass: 188.70 g mol<sup>-1</sup>, White solid, melting point (94.2 to 96.5 ° C). **<sup>1</sup>H-NMR**<sup>[13, 14]</sup> (500 MHz, CDCl<sub>3</sub>) δ ppm: 0.96 (t, 3H, *J* = 7.4 Hz, H<sub>9</sub>); 1.36 – 1.43 (m, 2H, H<sub>8</sub>); 1.78 – 1.84 (m, 2H, H<sub>7</sub>); 2.85 (s, 3H, H<sub>11</sub>); 4.07 (s, 3H, H<sub>10</sub>); 4.28 (t, 2H, *J* = 7.3, H<sub>6</sub>); 7.66 (d, 1H, *J* = 1.9 Hz, H<sub>5</sub>); 7.90 (d, 1H, *J* = 1.9 Hz, H<sub>4</sub>). **<sup>13</sup>C-NMR** (126 MHz, CDCl<sub>3</sub>) δ ppm: 10.1 (C<sub>11</sub>); 13.1 (C<sub>9</sub>); 19.1 (C<sub>8</sub>); 31.4 (C<sub>7</sub>); 35.5 (C<sub>10</sub>); 48.2 (C<sub>6</sub>); 121.0 (C<sub>5</sub>); 122.8 (C<sub>4</sub>), 143.0 (C<sub>2</sub>).

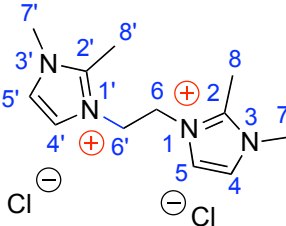
**[BMMI•Br]**



*1-n-butyl-2,3-dimethyl imidazolium bromide* [BMMI•Br]: Molar mass: 233. 15 g.mol<sup>-1</sup>, Solid yellow. **<sup>1</sup>H RMN**<sup>[14]</sup> (400 MHz, CDCl<sub>3</sub>) δ ppm: 0,96 (t, 3H, *J* = 7,4 Hz, H<sub>9</sub>); 1,38 – 1,43 (m, 2H, H<sub>8</sub>); 1,80 – 1,84 (m, 2H, H<sub>7</sub>); 2,84 (s, 3H, H<sub>11</sub>); 4,05 (s, 3H, H<sub>10</sub>); 4,25 (t, 2H, *J* = 7,4 Hz, H<sub>6</sub>); 7,59 (d, 1H, *J* = 1,9 Hz, H<sub>5</sub>); 7,79 (d, 1H, *J* = 1,9 Hz, H<sub>4</sub>). **<sup>13</sup>C NMR** (126 MHz, CDCl<sub>3</sub>) δ ppm 10,7 (C<sub>11</sub>); 13,3 (C<sub>9</sub>); 19,3 (C<sub>8</sub>); 31,6 (C<sub>7</sub>); 36,0 (C<sub>10</sub>); 48,5 (C<sub>6</sub>); 121,1 (C<sub>5</sub>); 122,8 (C<sub>4</sub>); 143,4 (C<sub>2</sub>).

---



<b>[C2-bis(MMI)•Cl<sub>2</sub>]</b>	<i>3,3'-(ethane-1,2-diyl)bis(1,2-dimethyl-1H-imidazol-3-ium) chloride</i>
	<p>[C2-bis(MMI)•Cl<sub>2</sub>]: Synthesized by using 1:2 mol ratio between 1,2-dichloroethane (0.1 mol), and 1,2-dimethylimidazole (0.2 mol) refluxed yielded 97 % white solide, C<sub>13</sub>H<sub>22</sub>Cl<sub>2</sub>N<sub>4</sub>, Molar mass: 305.25 g.mol<sup>-1</sup>. <sup>1</sup>H RMN<sup>[14]</sup> (400 MHz, D<sub>2</sub>O) δ ppm: 2,84 (s, 6H, H8,8'); 4,05 (s, 6H, H7,7'); 4,25 (t, 4H, J = 7,4 Hz, H6,6'); 7,59 (dd, 2H, J = 1,9 Hz, H5, 5'); 7,79 (dd, 2H, J = 1,9 Hz, H4, 4'). <sup>13</sup>C NMR (126 MHz, D<sub>2</sub>O) δ ppm: 11,0 (C8, 8'); 37,0 (C7,7'); 48,5 (C6, 6'); 121,5 (C5, 5'); 122,9 (C4,4'); 157,4 (C2).</p>

## 2.3 Synthesis of 1-Methyl-3-butyl-(2-<sup>13</sup>C)-imidazolium chloride

<sup>13</sup>C<sub>2</sub>-labelled imidazolium ionic liquid was especially synthesized for the <sup>13</sup>C-NMR kinetic studies (See Chap-3, Figure 3.6) in order to characterize the NHC-Ru carbene species formed *in-situ* by reaction of [BMI•Cl] or [BMI•Cl] with Ru<sub>3</sub>(CO)<sub>12</sub> precursor during hydroformylation of alkenes using CO<sub>2</sub> as CO source. Synthesis of [BMI(2-<sup>13</sup>C)•Cl] IL was completed in two steps reaction.

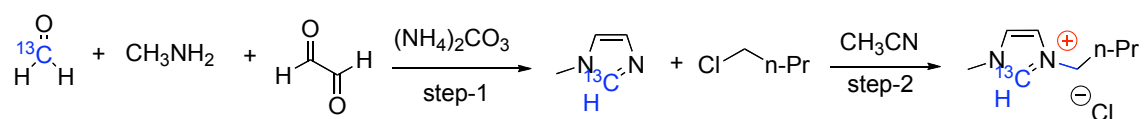
### *First step: Synthesis of 1-Methyl-(2-<sup>13</sup>C)-imidazole*

The following procedure was followed from reference 4. To a 50 mL round-bottomed flask, added <sup>13</sup>C-paraformaldehyde (2.00 g, 66.6 mmol). The flask was cooled using an ice/water bath, followed by addition of methylamine (aqueous 40%, 5.17 g, 66.6 mmol) and ammonium carbonate (3.20 g, 33.3 mmol). Then glyoxal (aqueous 40%, 9.67 g, 66.6 mmol) was added drop wise. After this later addition, the ice bath was removed and the reaction mixture was stirred at room temperature for 2 days. Volatiles were removed under reduced pressure and the brown viscous residue was distilled, giving 1-methyl-(2-<sup>13</sup>C)-imidazole (3.13 g, 57% yield) as a colourless liquid (b.p. 60°C/4 mmHg). <sup>1</sup>H NMR (60 MHz, acetone-d<sub>6</sub>) δ: 7.43 (d, 1H, J<sup>1</sup><sub>H-<sup>13</sup>C</sub> = 205 Hz, arom. H); 7.14-6.84 (m, 2H, arom. H); 3.70 (d, 3H, J<sup>1</sup><sub>H-<sup>13</sup>C</sub> = 3.4 Hz, NCH<sub>3</sub>)

### *Second step: 1-Methyl-3-butyl-(2-<sup>13</sup>C)-imidazolium chloride synthesis.*

1-Methyl-(2-<sup>13</sup>C)-imidazole (3.13 g, 37.7 mmol) was added to 1-chlorobutane (10.0 g, 108 mmol) and the resulting solution was heated at reflux temperature (~80°C) with vigorous stirring for 36 h. The excess 1-chlorobutane was decanted from the viscous crude imidazolium salt and this was mixed with hot acetone (5 mL), followed by the addition of sufficient methanol to ensure a clear solution. The desired 1-methyl-3-butyl-(2-<sup>13</sup>C)-imidazolium chloride crystallized (room temperature and then refrigerator) as pale amber crystals, which were collected and dried under reduced pressure (3.70 g, 56% yield).

**Table 2.2** Synthesis of the <sup>13</sup>C-labelled [BMI(2-<sup>13</sup>C)•Cl] ionic liquid.



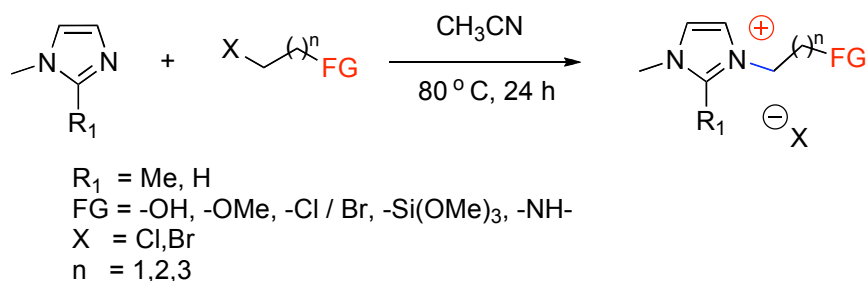
IL	Characterization
<p><b>[BMI(2-<sup>13</sup>C)•Cl]</b></p>	<p>1-methyl-3-butyl-(2-<sup>13</sup>C)-imidazolium chloride [BMI(2-<sup>13</sup>C)•Cl], C<sub>8</sub>H<sub>15</sub>ClN<sub>2</sub>, Molar mass: 174.67 g.mol<sup>-1</sup>, pale amber crystals. <sup>1</sup>H NMR (400 MHz, acetonitrile-d<sub>3</sub>) δ: 9.74 (br d, 1H, <i>J</i><sup>1H-<sup>13</sup>C</sup> = 221 Hz, arom. H); 7.58-7.52 (m, 2H, arom. H), 4.24 (dt, 2H, <i>J</i><sub>H-H</sub> = 7.2 Hz and <i>J</i><sup>1H-<sup>13</sup>C</sup> = 4.4 Hz, NCH<sub>2</sub>); 3.92 (d, 3H, <i>J</i><sup>1H-<sup>13</sup>C</sup> = 4.0 Hz, NCH<sub>3</sub>); 1.84 (q, 2H, <i>J</i><sub>H-H</sub> = 7.2 Hz, CH<sub>2</sub>); 1.33 (h, 2H, <i>J</i><sub>H-H</sub> = 7.2 Hz, CH<sub>2</sub>); 0.93 (t, 3H, <i>J</i><sub>H-H</sub> = 7.2 Hz, CH<sub>3</sub>). <sup>13</sup>C NMR (100 MHz, acetonitrile-d<sub>3</sub>) δ: 137.17 (C2, <sup>13</sup>C enriched); 123.47 (d, <i>J</i><sup>13C-<sup>13</sup>C</sup> = 2.5 Hz, C4); 122.13 (d, <i>J</i><sup>13C-<sup>13</sup>C</sup> = 2.5 Hz, C5); 49.03 (d, <i>J</i><sup>13C-<sup>13</sup>C</sup> = 2.5 Hz, NCH<sub>2</sub>); 35.73 (d, <i>J</i><sup>13C-<sup>13</sup>C</sup> = 3.2 Hz, NCH<sub>3</sub>); 31.68 (C7); 18.96 (C8); 12.72 (CH<sub>3</sub>).</p>

## 2.4 Functionalization of the imidazolium ILs.

Numerous functionalized ionic liquids (F.ILs) have already been explored by assimilation of various functional groups (FG) as a part of cation or anion of ILs. Integration of organic FG can produce task-specific chemical and physical capabilities of ILs. Imidazolium ionic liquids (Im.ILs) are capable of achieving

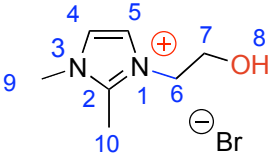
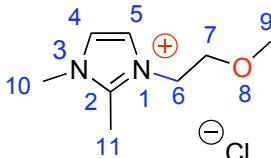
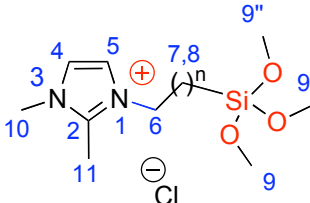
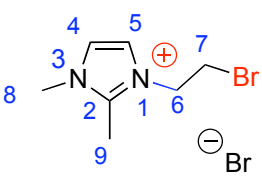
specific tasks includes; catalyst immobilization, liquid supported organic reactions,<sup>[15]</sup> CO<sub>2</sub> capturing from gas streams<sup>[16]</sup>, metal extraction from aqueous solutions, construction of *nano*-assemblies and ion conduction.<sup>[17]</sup> However, still synthesis of task-specific ionic liquids remains a lot to explore. In fact, design and synthesis of novel functionalized Im-ILs for the task specific activities will be extended with nearly limitless possibilities. The functionalized ionic liquids have already founded their applications in many areas such as, homogeneous catalysis, nanostructures materials, and surface modification of solid supports. Especially, N, S, and P-functionalized (P = phosphines, phosphites) Im-ILs are sharply promoting the homogeneous catalysis by generating catalytic and regioselective active species.<sup>[18-22]</sup>

On the other hand, various task-specific organic functional groups such as -C=C, -OH, -OMe, -X (Cl, Br), -Si(OMe)<sub>3</sub>, -RNHR, -SR, S-N-S, and P-modified imidazolium ionic liquids have been synthesized during this study. Later were extensively used for the generation of transition M-based homogenous or heterogeneous catalysts. However the hydroxyl, ether, silylether, and, halogen functionalized Im-ILs were synthesized by using reported experimental.<sup>[13, 14, 23]</sup> The synthesis commonly involved one-step nucleophilic substitution reaction between imidazole moiety and corresponding functionalized substrates (Scheme 2.3, Table 2.3). While -NH-, S-N-S, and P-modified Im-ILs were synthesized by optimizing the developed experimental in our research group (Scheme 2.4-2.7). Functionalized Im-ILs were characterized by <sup>1</sup>H, and <sup>13</sup>C NMR studies by matching with reported data.



**Scheme 2.1** Synthesis of the -OH, -OMe, Cl, Br, -Si(OMe)<sub>3</sub>, -NH- functionalized imidazolium ionic liquids (F-Im-ILs).

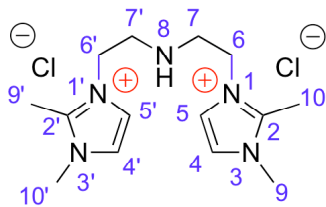
**Table 2.3** Characterization of the functionalized ionic liquids (F-ILs).

F-ILs	Characterization
<b>[C2-OHMMI•Br]</b> 	<i>3-(2-hydroxyethyl)-1,2-dimethyl-1H-imidazol-3-ium bromide</i> Molecular F: C <sub>7</sub> H <sub>13</sub> BrN <sub>2</sub> O, Molar mass: 221.09 g.mol <sup>-1</sup> , Brown solid, melting point (85.5 to 87.7 ° C). <sup>1</sup> H NMR <sup>[23, 24]</sup> (500 MHz, CD <sub>3</sub> OD) δ ppm: 2.7 (s, 3H, H10); 3.88 (s, 3H, H9); 3.90 (t, 2H, J = 5,0 Hz, H6); 4.31 (t, 2H, J = 5,0 Hz, H7); 7.53 (d, 1H, J = 1,4 Hz, H4); 7.57 (d, 1H, J = 1,4 Hz, H5). <sup>13</sup> C NMR (126 MHz, CD <sub>3</sub> OD) δ ppm: 10.1 (C10); 35.6 (C9); 51.9 (C6); 61,4 (C7); 122.5 (C5); 123.5 (C4); 146.6 (C2).
<b>[C2-Ome-MMI•Cl]</b> 	<i>3-(2-methoxyethyl)-1,2-dimethyl-1H-imidazol-3-ium chloride</i> Molecular F: C <sub>8</sub> H <sub>15</sub> ClN <sub>2</sub> O, Molar mass: 190.67 g mol <sup>-1</sup> , white solid, melting point (70 ° C). <sup>1</sup> H NMR <sup>[23, 24]</sup> (500 MHz, CD <sub>3</sub> OD) δ ppm: 2.5 (s, 3H, H11); 3.30 (s, 3H, H9); 3.68 (s, 3H, H10); 3.69 (t, 2H, J = 5,0 Hz, H7); 4.19 (t, 2H, J = 5,0 Hz, H6); 7.21 (d, 1H, J = 1,4 Hz, H4); 7.25 (d, 1H, J = 1,4 Hz, H5). <sup>13</sup> C NMR (126 MHz, CD <sub>3</sub> OD) δ ppm: 8.9 (C11); 34.6 (C10); 47.5 (C6); 58.3 (C9); 69.9 (C7); 120.8 (C5); 122.2 (C4); 146.6 (C2).
<b>[C3-Si(OMe)<sub>3</sub>MMI•Cl]</b> 	<i>1,2-dimethyl-3-(3-(trimethoxysilyl)propyl)-1H-imidazol-3-ium chloride</i> , Molecular F: C <sub>11</sub> H <sub>23</sub> ClN <sub>2</sub> O <sub>3</sub> Si, Molar mass: 294.85 g mol <sup>-1</sup> , Brown highly viscous oil. <sup>1</sup> H NM (500 MHz, CD <sub>3</sub> OD) δ ppm: 0.6 (t, 2H, H8); 1.5 (m, 2H, H7); 2.7 (s, 3H, H11); 3.2 (s, 9H, H9-9'') 3.68 (s, 3H, H10); 3.90 (t, 2H, J = 5,0 Hz); 4.61 (t, 2H, J = 5,0 Hz); 7.53 (d, 1H, J = 1,4 Hz, H4); 7.57 (d, 1H, J = 1,4 Hz, H5). <sup>13</sup> C NMR (126 MHz, CD <sub>3</sub> OD) δ ppm: 10-11 (C7, 8, 11); 35.6 (C10); 48.0 (C9-9''); 51.9 (C6); 122.5 (C5); 123.5 (C4); 146.6 (C2).
<b>[C2-BrMMI•Br]</b> 	<i>3-(2-bromoethyl)-1,2-dimethyl-1H-imidazol-3-ium bromide</i> Molecular F: C <sub>7</sub> H <sub>12</sub> Br <sub>2</sub> N <sub>2</sub> , Molar mass: 283.99 g mol <sup>-1</sup> , white solid, <sup>1</sup> H NMR (500 MHz, CD <sub>3</sub> OD) δ ppm: 2.45 (t, 2H, J = 5,0 Hz H7); 2.60 (s, 3H, H9); 3.78 (s, 3H, H8); 4.61 (t, 2H, J = 5,0 Hz); 7.23 (d, 1H, J = 1,4 Hz, H4); 7.27 (d, 1H, J = 1,4 Hz, H5). <sup>13</sup> C NMR (100 MHz, CD <sub>3</sub> OD) δ ppm: 9.45 (C9); 30.11 (C7), 34.91 (C8); 49.01 (C6); 120.38 (C5); 122.45 (C4); 144.31 (C2).

---

**[-C2-NH-C2-(MMI•Cl)<sub>2</sub>]** 3,3'-(2,2'-azanediylbis(ethane-2,1-diyl))bis(1,2-dimethyl-1H-imidazol-3-ium) chloride, Molecular F: C<sub>14</sub>H<sub>25</sub>Cl<sub>2</sub>N<sub>5</sub>, Molar mass: 334.29 g mol<sup>-1</sup>, Synthesis: bis(dichloroethyl) ammonium chloride salt (0.1 mol, Synthesis see in Scheme 2.7, T3) dissolved in 10 mL solution of 0.15 molar KOH, heated for 15 min at 100 °C, and extracted the bis(dichloroethyl)amine using 10x3 mL CH<sub>2</sub>Cl<sub>2</sub>, removed the solvent and added 1,2-dimethylimidazole (0.2 mol), and 15 mL EtOH and stirred at 80 °C over night, yielded 98% white solid. <sup>1</sup>H NMR<sup>[23, 24]</sup> (500 MHz, CD<sub>3</sub>OD) δ ppm: 2.5 (s, 3H, H<sub>9,9'</sub>); 3.63 (s, 3H, H<sub>10, 10'</sub>); 3.30 (t, 4H, H<sub>7, 7'</sub>); 3.63 (s, 3H, H<sub>10, 10'</sub>); 4.31 (t, 4H, *J* = 5,0 Hz, H<sub>6,6'</sub>); 7.23 (d, 2H, *J* = 1,4 Hz, H<sub>4,4'</sub>); 7.27 (d, 1H, *J* = 1,4 Hz, H<sub>5,5'</sub>). <sup>13</sup>C NMR (126 MHz, CD<sub>3</sub>OD) δ ppm: 9.05 (C<sub>10, 10'</sub>); 35.6 (C<sub>9,9'</sub>); 45-46 (C<sub>7,7'</sub>) 47.9 (C<sub>6,6'</sub>); 120.75 (C<sub>5</sub>); 122.85 (C<sub>4</sub>); 145.6 (C<sub>2</sub>).

---



## 2.5 Synthesis of P-functionalized ionic liquids (PF-ILs)

Task specific phosphine / phosphite ligands already contributed significant role in the field of homogeneous catalysis. Interestingly the regioselective P-functionalized Rh / Ru based homogeneous catalysts systems have been recently investigated for the hydroformylation, hydroaminomethylation of alkenes,<sup>[25-27]</sup> and N-methylation of a mines,<sup>[28]</sup> by using CO/H<sub>2</sub> as C1 building block. However, synthesis of P-functionalized (phosphine / phosphite) ionic liquids (PFILs) fascinated task-specific significant interest due to their potential to bind with soft and hard metals *via* phosphorus, and NHC-carbene of imidazolium ring.<sup>[29]</sup> Several symmetrically substituted trialkyl and triaryl mono-phosphines/phosphite ligands have extensively been used in homogeneous catalysis, while their electronic and steric properties can be tuned by varying the R-substitutions.

### 2.5.1 Synthesis of phosphine-modified ILs

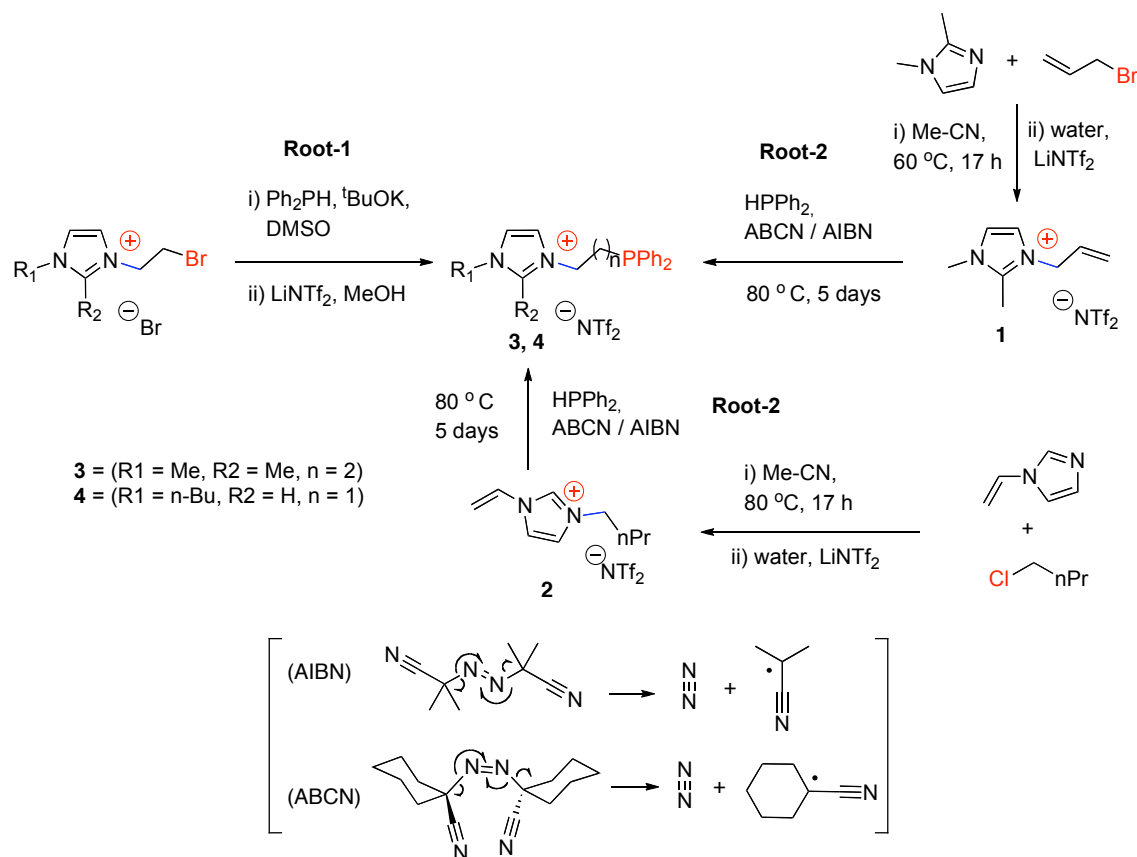
Phosphine ligands are widely used for the generation of several significant and task-specific transition metal complexes, nanoparticle, and nanoparticle-

colloidal.<sup>[30-32]</sup> Ionophilic phosphine-functionalized ionic liquids (IPFILs) received considerable attentions for their applications in the field of molecular catalysis for the last decade. Few Ru/Rh-carbene-phosphine catalytic species have been reported by reacting phosphine-functionalized Im-ILs with Ru /Rh-carbonyl precursors.<sup>[30, 33]</sup> Synthesis of PFILs is challenging due-to oxidation of phosphine reagents. Mainly two protocols have usually been applied in the synthesis of phosphine-modified imidazolium ILs (Scheme 2.4, root-1, 2). Single-step C-P bond formation between allylic or vinylic substituted imidazolium ILs (**1**, **2**), and secondary phosphine reagent (HPR<sub>2</sub>),<sup>[29]</sup> was reported by our group (Scheme 2.4, root-2). The reaction actually driven by radical-mechanism catalyzed by 1,1-azobis(cyclohexanecarbonitrile) (ABCN), or azobisisobutyronitrile (AIBN) as appropriate radical initiators (Scheme 2.4 root-2).<sup>[29, 32, 34]</sup> Radical addition of secondary phosphines (HPPh<sub>2</sub>) to the allyl imidazolium salt **1**<sup>[29, 30]</sup> and vinyl imidazolium salt **2**<sup>[29, 30]</sup> is straight forward, and almost quantitative conversions are attained with the mild radical initiator azobis(isobutyronitrile) (AIBN).

Phosphine-modified ILs **3** and **4** (Scheme 2.4) have been synthesized by optimizing the methodology given in the supporting information of references.<sup>[29, 30]</sup> Generally synthesis was carried out by using (2 mmol) of 1-allyl-2,3-dimethyl-imidazolium NTf<sub>2</sub> (**1**), or 1-vinyl-3-butyl-imidazolium NTf<sub>2</sub> (**2**), with (3 mmol) of secondary phosphine (HPPh<sub>2</sub>), then added appropriate radical initiator AIBN (0.05 mmol) in a dry box. The mixture was stirred at 70 °C for 48h - 3 days; during the reaction additional AIBN (0.23 – 0.30 mmol) was added in the reaction mixture. P-modified ionic liquid **3** and **4** were isolated as colorless oils in 94% and 88% yields, respectively.

Optimized single-step method (Scheme 2.4, root-2) has several advantages over others reported so far such as, base-catalyzed addition of primary or secondary phosphines to 1-vinylimidazole,<sup>[35, 36]</sup> alkylation of imidazoles with bromoalkyl (diphenylphosphine) oxide followed by phosphine reduction<sup>[37]</sup> in 4-steps, or nucleophilic substitution using bromo-alkyl-1-methylimidazolium salts in the presence of organic bases <sup>[18, 30, 33]</sup> (Scheme 2.4, root-1). Synthetic PFILs (**3**, **4**)

were characterized by  $^{31}\text{P}$ ,  $^1\text{H}$ , and  $^{13}\text{C}$  NMR studies by matching reported data.<sup>[29, 30]</sup>

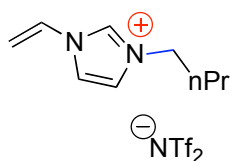


**Scheme 2.2** Two possible routes for the synthesis of the ionophilic phosphine-functionalized imidazolium ionic liquids.

**Table 2.4** Characterization of vinylic, allylic and phosphines functionalized ILs.

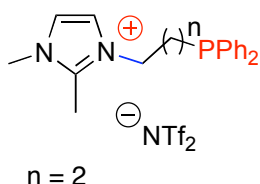
P-F.ILs	Characterization
	<p><b>[1]</b> <i>1-allyl-2,3-dimethyl-imidazolium NTf2 (1)</i> yellowish oil; yield: 20.0 g (92%); ESI/MS(+): <math>m/z</math> 137.08 [<math>[\text{C}_8\text{H}_{13}\text{N}_2]^+</math>]; Molecular F: <math>\text{C}_{10}\text{H}_{13}\text{F}_6\text{N}_3\text{O}_4\text{S}_2</math>; <b><math>^1\text{H}</math> NMR</b> (400 MHz, <math>\text{DMSO}-d_6</math>) <math>\delta</math> ppm 7.63 and 7.58 (d, <math>J_3 = 1.9</math> Hz, H4 and H5), 5.96 (m, <math>\text{NCH}_2\text{CH}=\text{CH}_2</math>), 5.29 (d, <math>J_3 = 10.4</math> Hz, <math>\text{NCH}_2\text{CH}=\text{CH}_2</math>), 5.13 (d, <math>J_3 = 17.1</math> Hz, <math>\text{NCH}_2\text{CH}=\text{CH}_2</math>), 4.80 (d, <math>J_3 = 5.4</math> Hz, <math>\text{NCH}_2\text{CH}=\text{CH}_2</math>), 3.75 (s, <math>\text{NCH}_3</math>), 2.53 (s, <math>\text{CCH}_3</math>). <b><math>^{13}\text{C}</math> NMR</b><sup>[38]</sup> (100 MHz, <math>\text{DMSO}-d_6</math>) <math>\delta</math> ppm 144.5 (s, C2), 131.5 (s, <math>\text{NCH}_2\text{CH}=\text{CH}_2</math>), 122.4 and 121.0 (s, C4 and C5), 119.4 (q, <math>J_{\text{CF}} = 321.9</math> Hz, <math>\text{NTf}_2^-</math>), 118.8 (s, <math>\text{NCH}_2\text{CH}=\text{CH}_2</math>), 49.6 (s, <math>\text{NCH}_2\text{CH}=\text{CH}_2</math>), 34.7 (s, <math>\text{NCH}_3</math>), 9.1 (s, <math>\text{CCH}_3</math>).</p>

[2]



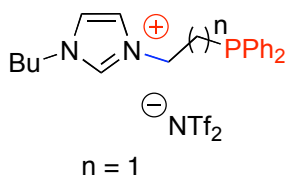
1-vinyl-3-butyl-imidazolium NTf<sub>2</sub> (**2**) yellowish oil; yield: (88%), ESI/MS(+): m/z 151.12 ([C<sub>9</sub>H<sub>15</sub>N<sub>2</sub>]<sup>+</sup>, 100%). Molecular F: C<sub>11</sub>H<sub>15</sub>F<sub>6</sub>N<sub>3</sub>O<sub>4</sub>S<sub>2</sub>; <sup>1</sup>H NMR (400 MHz, DMSO-d<sub>6</sub>) δ ppm 9.46 (s, H<sub>2</sub>), 8.19 and 7.92 (s, H<sub>4</sub> and H<sub>5</sub>), 7.27 (dd, J<sub>3</sub> = 15.6 Hz, J<sub>2</sub> = 8.7 Hz, NCH=CH<sub>2</sub>), 5.94 (dd, J<sub>3</sub> = 15.6 Hz, J<sub>2</sub> = 2.3 Hz, NCH=CH<sub>2</sub>), 5.42 (dd, J<sub>3</sub> = 8.7 Hz, J<sub>2</sub> = 2.3 Hz, NCH=CH<sub>2</sub>), 4.19 (t, J<sub>3</sub> = 7.22 Hz, NCH<sub>2</sub>), 1.91-1.69 (m, NCH<sub>2</sub>CH<sub>2</sub>), 1.41-1.19 (m, NCH<sub>2</sub>CH<sub>2</sub>CH<sub>2</sub>), 0.91 (t, J<sub>3</sub> = 7.39 Hz, CH<sub>3</sub>). <sup>13</sup>C NMR<sup>[38]</sup> (100 MHz, DMSO-d<sub>6</sub>) δ ppm 135.2 (s, C<sub>2</sub>), 128.8 (s, NCH=CH<sub>2</sub>), 123.2 and 119.1 (s, C<sub>4</sub> and C<sub>5</sub>), 119.4 (q, J<sub>CF</sub> = 321.9 Hz, NTf<sub>2</sub><sup>-</sup>), 108.5 (s, NCH=CH<sub>2</sub>), 48.9 (s, NCH<sub>2</sub>), 31.0 (s, NCH<sub>2</sub>CH<sub>2</sub>), 18.7 (s, NCH<sub>2</sub>CH<sub>2</sub>CH<sub>2</sub>), 13.2 (s, CH<sub>3</sub>).

[3]



Viscous liquid; 1.32g (94%), ESI/MS(+): m/z [C<sub>20</sub>H<sub>24</sub>N<sub>2</sub>P]<sup>+</sup> 323.1679: <sup>1</sup>H NMR (400 MHz, DMSO-d<sub>6</sub>) δ ppm 7.69 and 7.60 (s, H<sub>4</sub> and H<sub>5</sub>), 7.48-7.30 (m, 10H, 2Ph), 4.21 (t, J<sub>3</sub> = 6.9 Hz, 2H, NCH<sub>2</sub>CH<sub>2</sub>), 3.73 (s, 3H, NCH<sub>3</sub>), 2.54 (s, 3H, CCH<sub>3</sub>), 2.11 (m, 2H, CH<sub>2</sub>CH<sub>2</sub>P). <sup>13</sup>C NMR (100 MHz, DMSO-d<sub>6</sub>) δ ppm 144.2 (s, CCH<sub>3</sub>), 137.7 (d, J = 13.3 Hz, 2C ipso-Ph), 132.3 (d, J<sub>2, CP</sub> = 18.6 Hz, 4C o-Ph), 128.7 (s, 2C p-Ph), 128.5 (d, J<sub>3, CP</sub> = 6.6 Hz, 4C m-Ph), 122.2 and 120.7 (s, C<sub>4</sub> and C<sub>5</sub>), 119.4 (q, J<sub>CF</sub> = 322.3, NTf<sub>2</sub><sup>-</sup>), 48.0 (d, J<sub>3, CP</sub> = 14.9 Hz, NCH<sub>2</sub>CH<sub>2</sub>), 34.5 (s, NCH<sub>3</sub>), 25.9 (d, J = 18.2 Hz, CH<sub>2</sub>CH<sub>2</sub>P), 22.8 (d, J<sub>2, CP</sub> = 11.7 Hz, NCH<sub>2</sub>CH<sub>2</sub>), 9.1 (s, CCH<sub>3</sub>). <sup>31</sup>P NMR (121 MHz, DMSO-d<sub>6</sub>) δ ppm -16.4 (s).

[4]



Yields a viscous oil; 1.27 g (88%), ESI/MS(+): m/z [C<sub>21</sub>H<sub>26</sub>N<sub>2</sub>P]<sup>+</sup> 337.1831; <sup>1</sup>H NMR (300 MHz, DMSO-d<sub>6</sub>) δ ppm 9.21 (s, H<sub>2</sub>), 7.83 and 7.72 (2d, J<sub>3</sub> = 1.4 Hz, H<sub>4</sub> and H<sub>5</sub>), 7.58-7.27 (m, 10H, 2Ph), 4.30 (m, 2H, NCH<sub>2</sub>CH<sub>2</sub>P), 4.10 (t, J<sub>3</sub> = 7.0 Hz, 2H, NCH<sub>2</sub>CH<sub>2</sub>CH<sub>2</sub>CH<sub>3</sub>), 2.73 (m, 2H, NCH<sub>2</sub>CH<sub>2</sub>P), 1.73 (m, 2H, NCH<sub>2</sub>CH<sub>2</sub>CH<sub>2</sub>CH<sub>3</sub>), 1.24 (m, 2H, NCH<sub>2</sub>CH<sub>2</sub>CH<sub>2</sub>CH<sub>3</sub>), 0.90 (t, J<sub>3</sub> = 7.2 Hz, 3H, NCH<sub>2</sub>CH<sub>2</sub>CH<sub>2</sub>CH<sub>3</sub>). <sup>13</sup>C NMR (75 MHz, DMSO-d<sub>6</sub>) δ ppm 136.6 (d, J = 12.2 Hz, 2C ipso-Ph), 135.9 (s, NCHN), 132.3 (d, J<sub>2, CP</sub> = 19.3 Hz, 4C o-Ph), 129.0 (s, 2C p-Ph), 128.6 (d, J<sub>3, CP</sub> = 6.9 Hz, 4C m-Ph), 122.3 and 122.2 (2s, C<sub>4</sub> and C<sub>5</sub>), 119.4 (q, J<sub>CF</sub> = 321.8 Hz, NTf<sub>2</sub><sup>-</sup>), 48.4 (s, 1C, NCH<sub>2</sub>CH<sub>2</sub>CH<sub>2</sub>CH<sub>3</sub>), 46.6 (d, J<sub>2, CP</sub> = 25.6 Hz, NCH<sub>2</sub>CH<sub>2</sub>P), 31.2 (s, 1C, NCH<sub>2</sub>CH<sub>2</sub>CH<sub>2</sub>CH<sub>3</sub>), 27.1 (d, J<sub>CP</sub> = 13.7 Hz, NCH<sub>2</sub>CH<sub>2</sub>P), 18.6



(s,1C, NCH<sub>2</sub>CH<sub>2</sub>CH<sub>2</sub>CH<sub>3</sub>), 13.2 (s,1C, N NCH<sub>2</sub>CH<sub>2</sub>CH<sub>2</sub>CH<sub>3</sub>). <sup>31</sup>P  
 NMR (121 MHz, DMSO-d<sub>6</sub>) δ ppm -21.4 (s).

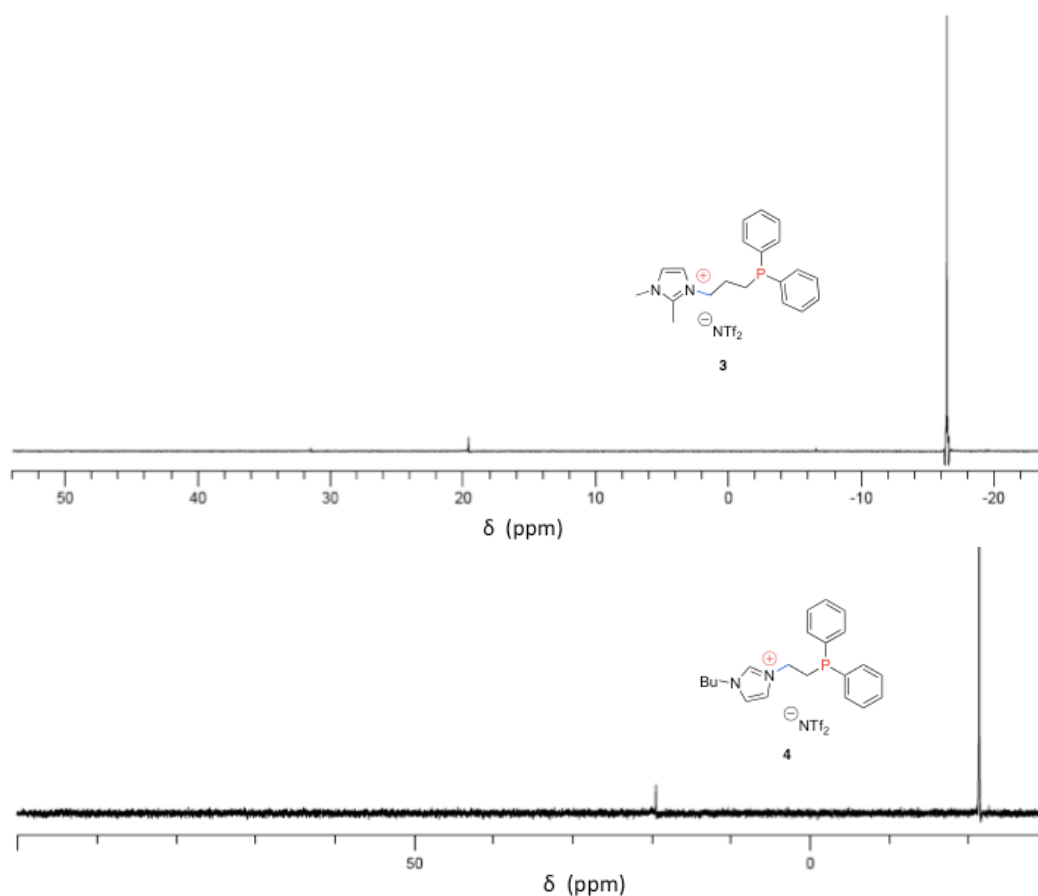
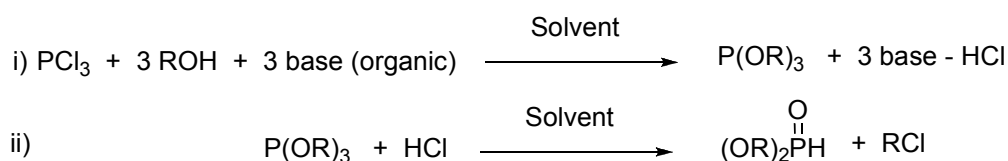


**Figure 2.1** <sup>31</sup>P-NMR spectrums of the P-modified imidazolium ILs **3**, **4**.

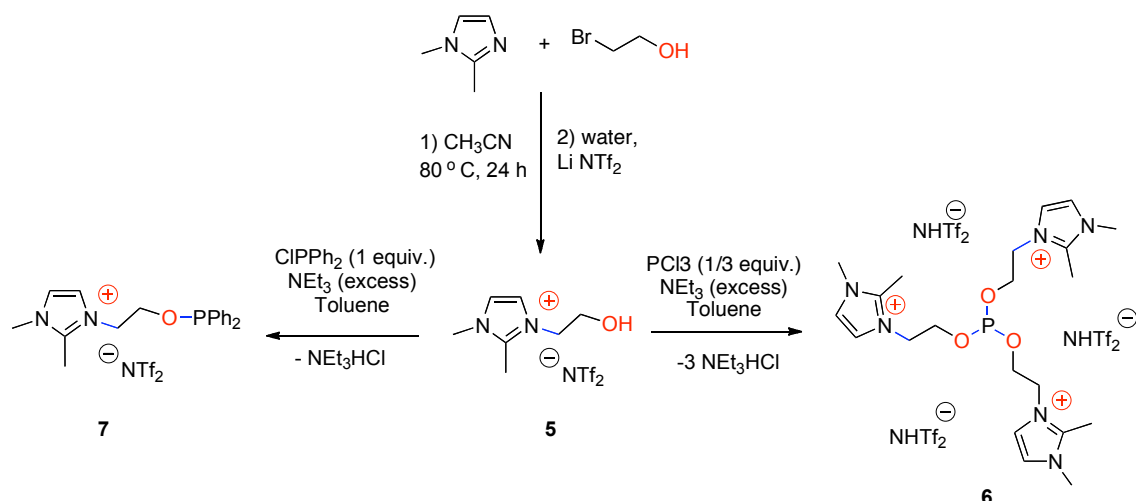
### 2.5.2 Synthesis of phosphite-modified imidazolium IL

Phosphites also have affluent coordination chemistry, they are strong  $\pi$  acceptors and form stable complexes with electron-rich transition metals. Recent inspection indicated that anti-bonding  $\sigma^*$  orbital of phosphorus to oxygen acting as  $\pi$  acceptor orbital on phosphorus. Phosphites are less prone to oxidation than phosphines but can decompose by hydrolysis. General synthetic way of phosphites is given in scheme-2.3.



**Scheme 2.3** General-scheme for the synthesis of symmetrical mono-phosphite Ls.

Symmetrically substituted monophosphites can readily be prepared by reacting alcohol with phosphorus trichloride ( $\text{PCl}_3$ ) in the presence of base (i, Scheme 4.5). Base trapping the generated HCl, which can further react with phosphite (ii, Scheme 2.3). However, phosphite-modified imidazolium ILs **6**, **7** have been synthesized by using the same experimental under inert conditions.<sup>[39, 40]</sup> Hydroxyl-functionalized IL (**5**) easily reacts with phosphorylating reagents in the presence of base ( $\text{NEt}_3$ ), and toluene as solvent. Reaction mixture was stirred for 3-4 hours. Generated,  $\text{Et}_3\text{NHCl}$  salt during the process was washed out by using 15 mL water from the reaction mixture. The organic phase of reaction dried, and removed the volatiles, and solvent under reduced pressure. Formation of phosphite modified ILs **6**, **7** was conformed by  $^{31}\text{P}$  NMR analysis.



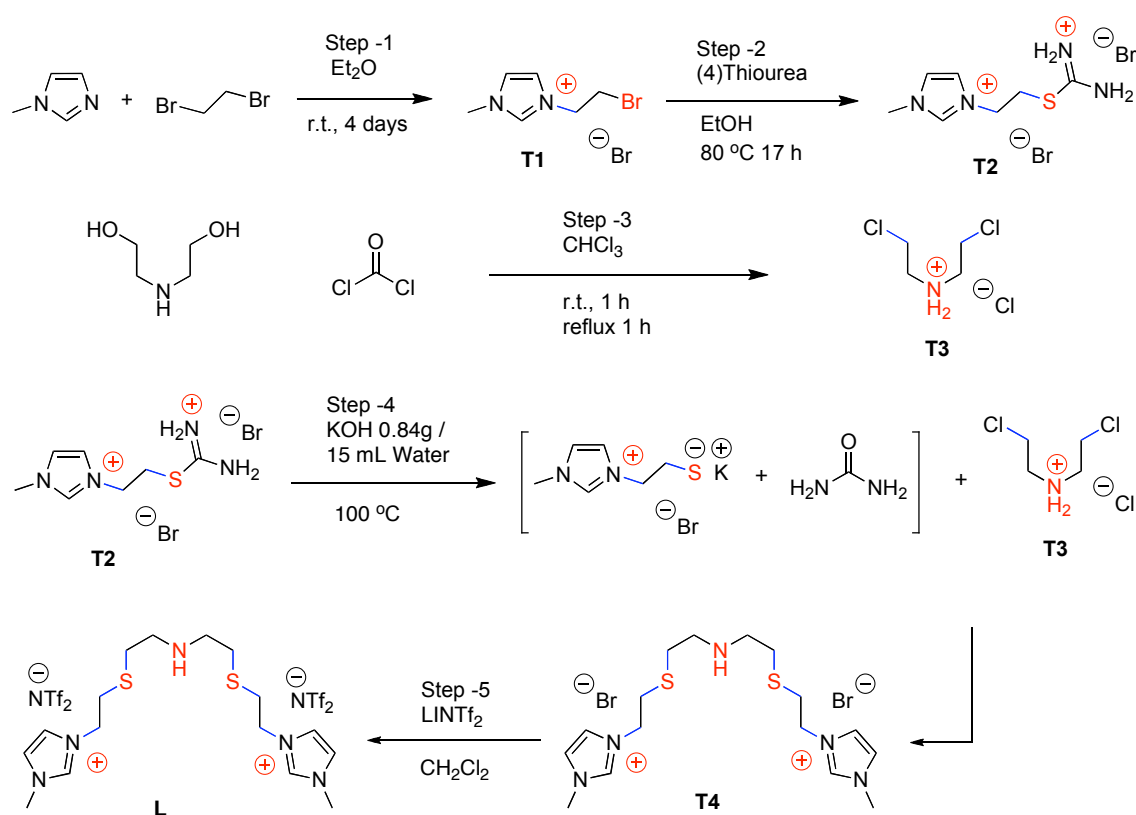
**Scheme-2.4** Synthesis of the phosphite-functionalized imidazolium ILs.

## 2.6 S-N-S Modified imidazolium IL

S S-N-S-functionalized ligand recently reported as better replacement of the phosphines for the Ru-catalyzed reduction of ester into alcohol.<sup>[21, 22]</sup> New S-N-S modified imidazolium IL was synthesized by exploiting new protocol. Synthesis of the targeted S-N-S modified ionic liquid is completed with in 5 steps.

**Step-1:** Preparation of *3-(2-bromoethyl)-1-methyl-1H-imidazol-3-ium bromide (T1)*, used 250 mL of round bottom flask, charged with 1-methylimidazole 8.0 mL (100 mmol), 1,2-dibromoethane 50.0 mL (580 mmol), and 50 mL  $\text{Et}_2\text{O}$  solvent. The reaction was stirred at room temperature for 4 days, a white solid **T1**

was formed which was washed, and filtered out by 30 mL Et<sub>2</sub>O solvent. **Step-2:** synthesis of **T2** by using salt **T1** 4.30 g (15.9 mmol), and thiourea 1.21 g (15.9 mmol), and added 30 mL ethanol as solvent. Reaction mixture was stirred and heated at 80°C for 17 h, cool down the reaction mixture at room temperature white solid 3-(2-(amino(iminio)methylthio)ethyl)-1-methyl-1H-imidazol-3-ium bromide (**T2**) was formed washed, and filtered the salt by ethanol and dried it, a white solid (yield 75%) was obtained. <sup>1</sup>HNMR (400 MHz, DMSO -D<sub>6</sub>) δ = 3.72 (t, 2H, J = 6.81 Hz) 3.81 (s, 3H); 4.48 (t, 2H, J = 6.81 Hz); 7.75 (d, 1H, J = 2 Hz); 7.73 (d, 1H, J = 2 Hz), 9.23 (s, 4H). <sup>13</sup>CNMR (100 MHz, DMSO-d<sub>6</sub>) δ = 10,15; 35.40; 46.85; 121.89; 122.80; 145.42, 168.96. While in **step-3:** Synthesized the bis(dichloroethyl)ammonium chloride salt (**T3**), 250 mL round bottom flask was charged with thiophosgene 55.6 ml (768 mmol), 45 mL chloroform, and added 2,2-azanediyldiethanol drop wise, over the period of 2.5 h at 0°C, and left the solution for 1h at room temperature, then refluxed the reaction mixture for 1h, pure salt **T3** as white solid was obtained by washing with chloroform and dried it.



**Scheme 2.5** Synthesis of inophilic ImIL-S-N-S-ImIL modified imidazolium IL.

**Step-4:** A solution of salt **T2** 2.077 g (6.0 mmol), and KOH 0.84 g (15 mmol), in 15 mL of water was heated in a schlenk flask at 100°C for 15 min. Reaction solution was cooled down at room temperature then added *bis(dichloroethyl)amonium chloride* (**T3**) 0.536 g (3.0 mmol), and heated at 100°C for 20-25 min. Further in step-5: same reaction solution involved for the counter anion exchange with LiNTf<sub>2</sub> (4.02 g, (14 mmol), extracted Ligand **L** with ethyl acetate (3x15 mL), dried the extracted solution by using MgSO<sub>4</sub> and the solvent was removed under vacuum pressure. Colorless viscous liquid yield 85%, HRMS: M<sup>+</sup> = 915.6927. <sup>1</sup>HNMR (400 MHz, CD<sub>3</sub>CN) δ = 2.84 (t, 4H, J = 6.8 Hz); 2.98 (t, 4H, J = 6.8 Hz); 3.24 (t, 4H, J = 6.8 Hz); 3.87 (s, 6H); 4.34 (t, 4H, J = 6.8 Hz); 7.39 (s, 2H); 7.45 (s, 2H), 8.49 (s, 2H). <sup>13</sup>CNMR (100 MHz, DMSO-d<sub>6</sub>) δ = 27.77; 31.69; 37.08; 47.85; 49,5 4; 124.86; 137.31. Anion: 116.19; 119.58; 123.58 and 125.75 (q, CF<sub>3</sub>, J = 319 Hz).

## 2.6 References

- [1] J. Dupont, R. F. d. Souza, P. A. Z. Suarez, *Chem. Rev.* **2002**, *102*, 3667–3692.
- [2] P. Wasserscheid, W. Keim, *Angewandte Chemie-International Edition* **2000**, *39*, 3773.
- [3] R. D. Rogers, K. R. Seddon, *Science* **2003**, *302*, 792.
- [4] L. A. Blanchard, D. Hancu, E. J. Beckman, J. F. Brennecke, *Nature* **1999**, 28.
- [5] X. Zhang, X. Zhang, H. Dong, Z. Zhao, S. Zhang, Y. Huan, *Energy & Environmental Science* **2012**, *5*, 6688.
- [6] J. Jacquemin, P. Husson, V. Majer, M. F., C. Gomes, *Solution Chem* **2007**, *36*, 967.
- [7] J. Huang, T. R  ther, *Australian Journal of Chemistry* **2009**, *62*, 298.
- [8] Mitsuhiro, Kanakubo, , Tatsuya, Umecky, Yusuke Hiejima, Takafumi Aizawa, Hiroshi Nanjo, Y. Kameda, , *J.Phys. Chem. Letters B*, **2005**, *109*.
- [9] L. A. Blanchard, Z. Gu, J. F. Brennecke, *J. Phys. Chem.* **2001**, *105*, 2437.
- [10] Dean Camper, Jason E. Bara, Douglas L. Gin, R. D. Noble, *Ind. Eng. Chem. Res.* **2008**, *47*, 8496.
- [11] Elena Torralba-Calleja, James Skinner, D. Guti  rrez-Tauste, *Journal of Chemistry* **2013**, *1*.
- [12] M. C. Corvo<sup>1</sup>, Jo  o Sardinha, Teresa Casimiro, Graciane Marin, Marcus Seferin, Sandra Einloft, Sonia C. Menezes, Jairton Dupont, Eurico J. Cabrita, *ChemSusChem* **2015**, *8*, 1935.
- [13] J. Dupont, P. A. Z. Suarez, C. S. Consorti, R. F. deSouza, *Organic Synthesis* **2002**, *79*, 236.
- [14] M. Zanatta, *Universidade Federal do Rio Grande do Sul (Porto Alegre)* **2014**.
- [15] S. Zhang, K. Dokko, M. Watanabe, *Chem. Sci.* **2015**, *6*, 3684.
- [16] E. D. Bates, R. D. Mayton, I. Ntai, J. J. H. Davis, *J. Am. Chem. Soc.* **2002**, *124*, 926.
- [17] S.-g. Lee, *Chem. Commun.* **2006**, 1049.
- [18] J. A. Vicente, A. Mlonka, H. Q. Gunaratne, M. Swadzba-Kwasny, P. Nockemann, *Chem. Commun.* **2012**, *48*, 6115.

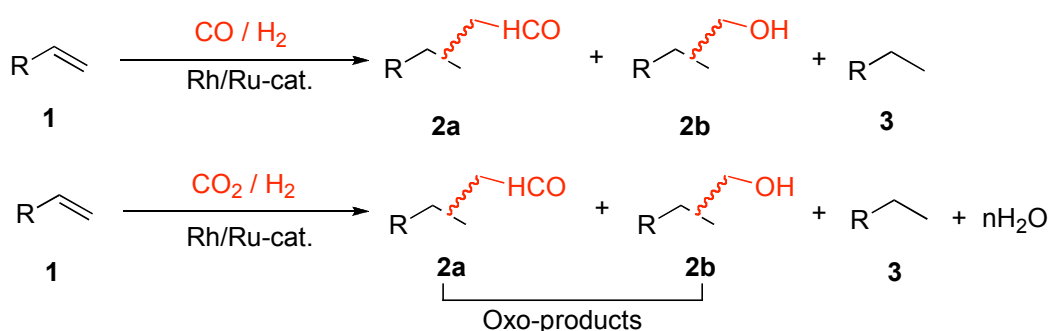
- [19] I. Abdellah, C. Lepetit, Y. Canac, C. Duhayon, R. Chauvin, *Chem. Eur. J.* **2010**, *16*, 13095.
- [20] L. D. Field, B. A. Messerle, K. Q. Vuong, P. Turner, *Organometallics* **2005**, *27*, 4243.
- [21] D. Spasyuk, S. Smith, D. G. Gusev, *Angew. Chem. Int. Ed.* **2012**, *51*, 2772.
- [22] D. Spasyuk, S. Smith, D. G. Gusev, *Angew. Chem. Int. Ed.* **2013**, *52*, 1.
- [23] Luís C. Branco, João N. Rosa, Joaquim J. Moura Ramos, C. A. M. Afonso, *Chem. Eur. J.* **2002**, *8*, 3671.
- [24] X. He, T. H. Chan, *Tetrahedron* **2006**, *62*, 3389.
- [25] L. Wu, I. Fleischer, R. Jackstell, M. Beller, *J. Am. Chem. Soc.* **2013**, *135*, 3989–3996.
- [26] Xiao-Feng Wu, Xianjie Fang, Lipeng Wu, Ralf Jackstell, Helfried Neumann, M. Beller, *Acc. Chem. Res.* **2014**, *47*, 1041–1053.
- [27] Jola Pospech, I. Fleischer, R. Franke, S. Buchholz, M. Beller, *Angew. Chem. Int. Ed.* **2013**, *52*.
- [28] K. Beydoun, T. Vom Stein, J. Klankermayer, W. Leitner, *Angew. Chem. Int. Ed.* **2013**, *52*, DOI: 10.1002/anie.201304656.
- [29] C. S. Consorti, G. L. P. Aydos, G. Ebeling, J. Dupont, *Org. Lett.* **2008**, *10*, 237.
- [30] J. A. Cabeza, M. Damonte, P. G.-. Álvarez, A. R. Kennedy, E. Pérez-Carreño, *Organometallics* **2011**, *30*, 826.
- [31] C. Zhang, F. Luo, B. Cheng, B. Li, H. Song, S. Xua, B. Wang, *Dalton Trans.* **2009**.
- [32] K. L. Luska, A. Moores, *Adv. Synth. Catal.* **2011**, *353*, 3167.
- [33] L. D. Field, B. A. Messerle, K. Q. Vuong, P. Turner, *Organometallics* **2005**, *24*, 4241.
- [34] C. S. Consorti, G. L. P. Aydos, G. Ebeling, J. Dupont, *Org. Lett.* **2008**, *10*, 237.
- [35] K. W. Kottsieper, O. Stelzer, P. Wasserscheid, *J. Mol. Catal. A-Chem.* **2001**, *175*, 285.
- [36] J. Passays, T. Ayad, V. Ratovelomanana-Vidal, A.-C. Gaumont, P. Jubault, E. Leclerc, *Tetrahedron: Asymmetry* **2011**, *22*, 562.
- [37] N. Tsoureas, A. A. Danopoulos, A. A. D. Tulloch, M. E. Light, *Organometallics* **2003**, *22*, 4750.
- [38] Y. J. Kim, R. S. Varma, *J. Org. Chem.* **2005**, *70*, 7882.
- [39] K. N. Gavrilov, S. E. Lyubimov, O. G. Bondarev, M. G. Maksimova, S. V. Zheglov, P. V. Petrovskii, V. A. Davankov, M. T. Reetz, *Adv. Synth. Catal.* **2007**, *349*, 609.
- [40] X. He, T. H. Chan, *Tetrahedron* **2006**, *62*, 3389.

## **CHAPTER -3**

### **“Ru-catalysed Hydroformylation of Alkenes Using CO<sub>2</sub> as CO Source in Presence of Ionic Liquids”**

### 3.1 Introduction

Synthetic point of view hydroformylation of alkenes is a one-carbon chain elongation reaction by addition of carbon monoxide, hydrogen across the  $\pi$ -system of alkenes, and produced oxo-products (aldehyde, alcohol).<sup>[1, 2]</sup> Carbon dioxide sequestration and use as feedstock in industrial processes are major challenges in the development of alternative greener and sustainable processes.<sup>[3]</sup> Indeed, several catalytic processes are under investigation, and include the incorporation of  $\text{CO}_2$  via addition to epoxides to generate organic carbonates, diols, and polycarbonates using either organic and/or metal-based catalysts.<sup>[4]</sup> However, the substitution of carbon monoxide (CO) by carbon dioxide ( $\text{CO}_2$ ) in carbonylation reactions<sup>[5-8]</sup> may allow for new applications with broader use for this important and abundant, but slowly-reactive substrate. Indeed, at the industrial scale, the hydroformylation<sup>[1, 2]</sup> of alkenes is one of the most important applications of homogeneous catalysis, with over 9 million tons of so-called oxo-products, such as aldehydes and alcohols are produced each year.<sup>[9]</sup>



**Scheme 3.1** Rh/Ru-catalysed hydroformylation of 1-alkenes by using mixture of  $\text{CO}/\text{H}_2$  OR  $\text{CO}_2/\text{H}_2$  as C-1 feedstock.

Rh-modified systems are the catalysts of choice for this reaction since they are highly active and selective to the formation of aldehydes,<sup>[1, 2]</sup> as well as, for cascade reactions involving hydroformylation-Witting,<sup>[10]</sup> hydroaminomethylation sequences<sup>[11, 12]</sup> and hydroformylation-cyclization reactions<sup>[13-16]</sup>. Other metals, such as Pt and Ru, have been much less studied due to their high hydrogenation activity, which resulted in the formation of large amounts of alkanes as by-products.<sup>[17-20]</sup> However, the use of Rh-Ru bimetallic systems is of interest for the production of alcohols by hydroformylation hydrogenation sequences.<sup>[21-25]</sup> These

difference in selectivity could be easily understood if we look for the hydroformylation and hydrogenation mechanisms catalysed by Rh(I) and Ru(0) systems, since the active catalytic species under hydroformylation conditions are the Rh-H and the Ru-(H)<sub>2</sub> species.<sup>[1, 2, 9, 26]</sup> The accepted mechanism for the formation of M-(H)<sub>2</sub> is the homolytic cleavage of the H-H, since the formation of the M-H occur either by intramolecular (ligands) or by intermolecular (external base) heterolysis of the H-H bond, which favours the formation of M-H species.<sup>[12, 27, 28]</sup> For instance, in the Ru-catalysed hydrogenation of acids, cyclic carbonates and CO<sub>2</sub> to alcohol is described the formation of catalytically active cationic [Ru-H]<sup>+</sup> species.<sup>[29-34]</sup> The effect of the solvent is important since it was proposed that for the Rh-catalysed hydroaminomethylation reaction using imidazolium ILs as the reaction media, the acid protons of the imidazolium ring could shift the equilibrium between Rh-H and [Rh-(H)<sub>2</sub>]<sup>+</sup> to the formation of the hydrogenation catalytically active [Rh-(H)<sub>2</sub>]<sup>+</sup> species.<sup>[28]</sup> This hypothesis was confirmed by the observation that the presence of 3-alkyl-1,2-dimethyl-imidazolium salts slowed hydrogenation rates.

The potential use of Ru as a hydroformylation catalyst is of interest since Rh is much less abundant,<sup>[1, 2, 9]</sup> and several Ru-catalysed processes involving hydroformylation-hydrogenation<sup>[21-25]</sup> and hydroaminomethylation<sup>[17]</sup> were recently developed. However, a much more interesting system is that which can catalyse cascade reactions (i.e. CO<sub>2</sub> reduction to CO, hydroformylation, and hydrogenation sequence to produce alcohols of high added value). There are reports that this process is viable when either Ru-based systems with LiCl salts dissolved in N-methyl-pyrrolidone (Figure 3.1) <sup>[35-37]</sup> or in a biphasic imidazolium ILs/toluene <sup>[38-41]</sup> (Figure 3.1) was used. Advances in this area revealed that when the Ru-catalysed hydroformylation of 1-hexene (using CO<sub>2</sub> as the CO source) was carried out using 1-butyl-3-methyl-imidazolium chloride salts [BMI•Cl]<sup>[42]</sup> (30 equiv. IL/ equiv. Ru) as the solvent and a mixture 1:1 of 1-butyl-3-methyl-imidazolium chloride [BMI•Cl] (15 equiv. IL/equiv. Ru) and 1-butyl-3-methyl-imidazolium bis(trifluoromethyl sulfonyl)imide [BMI•NTf<sub>2</sub>] (15 equiv. IL/equiv. Ru), alcohol yields of up to 51% and 82%, respectively, were achieved.<sup>[39]</sup> Recent reports also described the use of LiCl-benzyl triethyl ammonium chloride (BTAC; Figure 3.1) salts in the Ru-catalysed hydroaminomethylation of cyclopentene with



morpholine, resulting in product yields of up to 98% after 5 days of reaction at 160 °C.<sup>[43]</sup> Here, we report the Ru-catalysed hydroformylation of alkenes using CO<sub>2</sub> as a CO source in the presence of [BMI•Cl] and 3-*n*-butyl-1,2-dimethyl imidazolium chloride salts [BMMI•Cl]. The involvement of Ru-carbene complexes as the catalytic active species was revealed by NMR experiments using labelled <sup>13</sup>C compounds (CO, CO<sub>2</sub> and <sup>13</sup>C-2-BMI•Cl) in the reactions promoted by Ru<sub>3</sub>(CO)<sub>12</sub> in the presence of [BMI•Cl]. Finally, the use of acid additives, such as H<sub>3</sub>PO<sub>4</sub>, improved both the catalytic activity and selectivity.

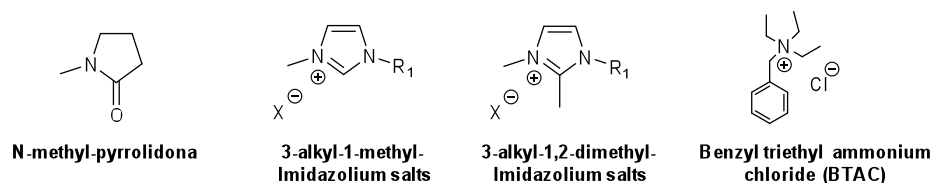


**Figure 3.1** Organic solvents and additives used in hydroformylation reactions.

## 3.2 Experimental

### 3.2.1 General experimental details

All syntheses were performed using standard Schlenk techniques under argon atmosphere. Solvents were purified by standard procedure.<sup>[1]</sup> RuCl<sub>3</sub>·*n*H<sub>2</sub>O and [RuCl<sub>2</sub>(COD)]<sub>*n*</sub> were purchased from Sigma-Aldrich, and Ru<sub>3</sub>(CO)<sub>12</sub> was purchased from Johnson & Matthey. Cyclohexene and 1-hexene were purchased from Sigma-Aldrich. PPh<sub>3</sub>, P(OEt)<sub>3</sub>, diphenylphosphine methane (dppm), diphenylphosphine ethane (dppe) and diphenylphosphine propane (dppp) were purchased from Sigma-Aldrich. Xantphos was prepared following reported procedures.<sup>[2]</sup> Imidazolium ionic liquids were prepared following reported procedures.<sup>[3]</sup> H<sub>2</sub> (> 99.999%) and CO<sub>2</sub> (> 99.999%) were purchased from White-Martins Ltd Brasil. GC analyses were run with an Agilent GC System 6820. GC-MS analyses were run with a Shimadzu QP50 (EI = 70 eV). GC-TCD analyses were run with an Agilent Micro GC System 3000A. <sup>1</sup>H, <sup>13</sup>C, COSY and HSQC NMR analysis were performed on a Varian 400 MHz at the CNANO/UFRGS using CDCl<sub>3</sub> as a solvent. Chemical shifts (ppm) are given relative to TMS in <sup>1</sup>H NMR and CDCl<sub>3</sub> in <sup>13</sup>C-NMR. Signals were assigned as s (singlet), d (doublet), t (triplet), dd (doublet of

doublet), m (multiplet) and br. s (broad singlet). ESI-MS(+) experiment were performed on a Q-ToF (Micromass) mass spectrometer. The ESI-MS mass spectra were acquired using an ESI capillary voltage of 3 kV and a cone voltage of 10 V. The sample (10  $\mu\text{L}$  aliquots) of reaction mixture added to 1 mL of methanol. Introduction was performed using a syringe pump set to 5  $\mu\text{L min}^{-1}$ .

### 3.2.2 Experimental for catalysis

We used a common procedure for the hydroformylation of alkenes using  $\text{CO}_2$  as a CO source. In a typical experiment, 20.0 mmol of the corresponding substrate was added to a 100 mL reactor vessel (Parr Micro-reactor 4590, see figure 3.2) containing the corresponding Ru precursor (Substrate/Ru = 64) and the imidazolium ionic liquid.

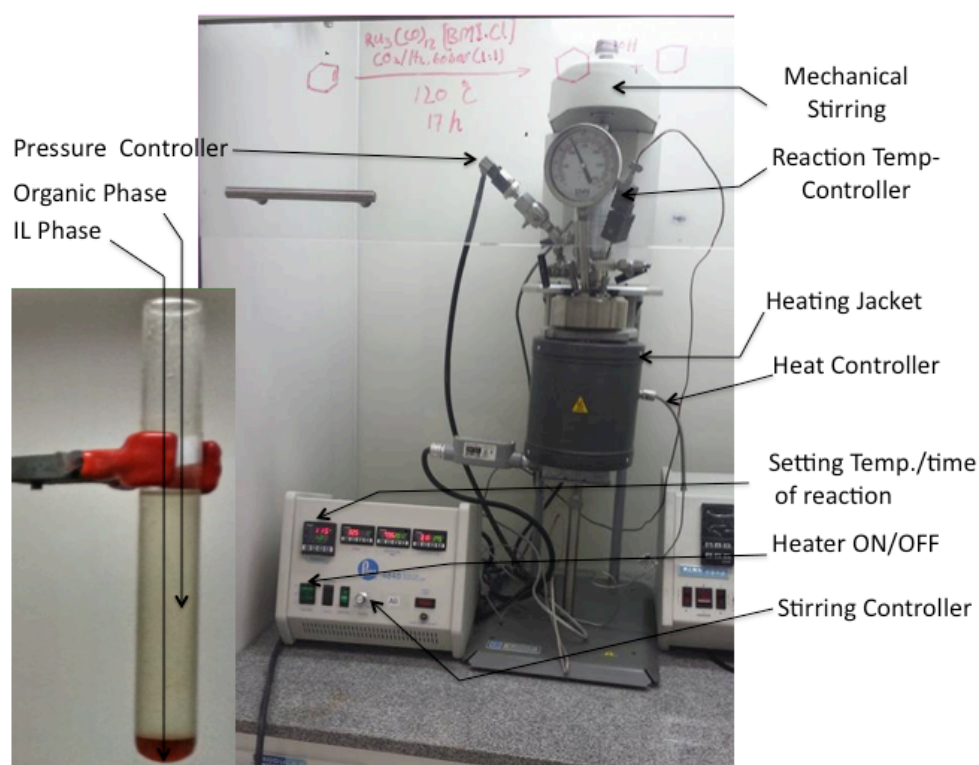


**Figure 3.2** Schematic diagram of Parr high-pressure reactor (4590) used for the hydroformylation reactions.

Then, the reactor was pressurised with  $\text{CO}_2/\text{H}_2$  and warmed to the desired reaction temperature for 17 h. After that, the reactor was cooled and the reaction

products were extracted with Et<sub>2</sub>O (3 x 15 mL). The reaction products were determined by GC-MS analysis (DB-17, T injector = 250 °C, P = 15 psi, and T programme = 10 min at 40 °C, 10 °C min<sup>-1</sup> until 250 °C, and 10 min at 250 °C), and the conversion, selectivity, and yield was quantified by GC-FID analysis (DB-17, 30 m x 0.250 mm, T injector = 250 °C, T detector = 250 °C, P = 15 psi, and T programme = 10 min at 40 °C, 10 °C min<sup>-1</sup> until 250 °C, and 10 min at 250 °C) using n-heptane as the internal standard. The gas phase composition was determined by GC-TCD analysis (PLOT-U, T injector = 90 °C, P = 20 psi, and T programme = 5 min at 70 °C). The volatiles are removed under vacuum from the organic phase of reactions mixture, then carried-out NMR-analysis (see chp-6) of these reaction mixtures (dried) of all reactions by using CD<sub>3</sub>Cl solvent.

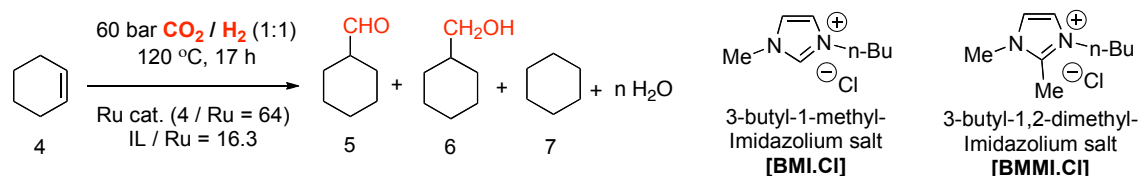
### 3.3 Results and Discussion

#### 3.3.1 Reaction optimization for the hydroformylation of cyclohexene

Effect of Ru-metallic precursors on the catalytic performance was investigated by performing the hydroformylation of cyclohexene using RuCl<sub>3</sub>·nH<sub>2</sub>O, [RuCl<sub>2</sub>(COD)]<sub>n</sub>, and Ru<sub>3</sub>(CO)<sub>12</sub> as catalytic precursors in the presence of [BMI•Cl] ILs (16.3 equiv. of IL/equiv. of Ru) under 60 bar CO<sub>2</sub>/H<sub>2</sub> (1:1) at 120 °C for 17 h (Entries 1–3, Table 3.1). Under these reaction conditions, the ruthenium precursors RuCl<sub>3</sub>·nH<sub>2</sub>O and [RuCl<sub>2</sub>(COD)]<sub>n</sub> exclusively formed hexane, with conversions of up to 99% and 90%, respectively (Entries 1 and 2, Table 3.1). In contrast, Ru<sub>3</sub>(CO)<sub>12</sub> revealed conversions up to 96% with oxo-product selectivity up to 83%, and alcohol selectivity in the oxo-product fraction was up to 94 % (Entry 3, Table 3.1). The effect of the IL counter-ion was studied by carrying out the reactions in presence of 3-butyl-1-methyl-imidazolium bromide [BMI•Br] and iodide [BMI•I]. They yielded similar alcohol selectivities in the oxo-product fraction, but with lower conversions and much lower oxo-product selectivities (less than 31%), thus confirming the key role of chlorides (Entries 3 *versus* 4 and 5, Table 3.1). Interestingly, an improvement in the oxo-product selectivity (up to 98%) with similar alcohol selectivities in the oxo-product fraction, but with much lower conversions (lower than 51%), was achieved using 3-butyl-1,2-dimethyl-

imidazolium chloride [BMMI•Cl] IL (Entries 3 *versus* 6, Table 3.1). This behavior can be explained if we assume the presence of an equilibrium between the M-(H)<sub>2</sub> and M-H species, as was proposed for the hydroaminomethylation.<sup>[28]</sup>

**Table 3.1** Ru-catalysed hydroformylation of cyclohexene using CO<sub>2</sub> as a CO source.<sup>[a,b]</sup>



Entry	Precursor	IL	Additive <sup>[c]</sup>	Conv.	Sel. 5+6	Sel. 6/5+6
1	RuCl <sub>3</sub> ·nH <sub>2</sub> O	[BMI•Cl]	-	> 99	-	-
2	[RuCl <sub>2</sub> (COD)] <sub>n</sub>	[BMI•Cl]	-	90	-	-
3	Ru <sub>3</sub> (CO) <sub>12</sub>	[BMI•Cl]	-	96	83	94
4	Ru <sub>3</sub> (CO) <sub>12</sub>	[BMI•Br]	-	78	31	96
5	Ru <sub>3</sub> (CO) <sub>12</sub>	[BMI•I]	-	71	31	94
6	Ru <sub>3</sub> (CO) <sub>12</sub>	[BMMI•Cl]	-	51	98	93
7	Ru <sub>3</sub> (CO) <sub>12</sub> <sup>[d]</sup>	[BMI•Cl]	-	86	98	96
8	Ru <sub>3</sub> (CO) <sub>12</sub> <sup>[e]</sup>	[BMI•Cl]	-	6.8	91	85
9	Ru <sub>3</sub> (CO) <sub>12</sub>	[BMI•Cl]	P(OEt) <sub>3</sub>	92	82	93
10	Ru <sub>3</sub> (CO) <sub>12</sub>	[BMMI•Cl]	P(OEt) <sub>3</sub>	93	93	93
11	Ru <sub>3</sub> (CO) <sub>12</sub>	[BMI•Cl]	H <sub>3</sub> PO <sub>4</sub>	85	95	99
12	Ru <sub>3</sub> (CO) <sub>12</sub>	[BMMI•Cl]	H <sub>3</sub> PO <sub>4</sub>	>99	97	98

[a] Reaction conditions: cyclohexene (20.0 mmol), ionic liquid (5.1 mmol), cyclohexene/Ru = 64, IL/Ru = 16.3, 60 bar CO<sub>2</sub>/H<sub>2</sub> (1:1), 120 °C, 17 h. [b] Conversion and selectivity (%) as determined by GC-MS and GC-FID. [c] Additive/Ru = 3.0. [d] Using CO instead of CO<sub>2</sub>. [e] Using only H<sub>2</sub> (30 bar).

Note that similar catalytic activity and selectivity is obtained in the hydroformylation of cyclohexene using CO instead of CO<sub>2</sub> catalyzed by [BMI•Cl]/Ru<sub>3</sub>(CO)<sub>12</sub> (entry 7, Table 3.1). The hydrogenation (30 bar) of

cyclohexene by the catalytic mixture [BMI•Cl]/Ru<sub>3</sub>(CO)<sub>12</sub> is only marginal (less than 1%) in absence of CO<sub>2</sub> (entry 8, Table 3.1). It is worth to mention that in this hydrogenation reaction the amount of oxo-products is almost the same expected for the total consumption of CO present on catalyst precursor (6.2%). Therefore it indicated, the presence of CO<sub>2</sub> is necessary to induce the formation of catalytic active species for the C=C hydrogenation and/or it could increase the solubility of the alkenes into the IL catalytic phase for the mass transfer reaction in bi-phasic system.

### 3.3.2 Hydroformylation of 1-hexene by optimizing IL/Ru ratio

The effect of the [BMI•Cl]/Ru molar ratio was studied by carrying out the Ru-catalysed hydroformylation of 1-hexene (a substrate with high hydrogenating tendency) using CO<sub>2</sub> as a CO source (Figure 3.3).

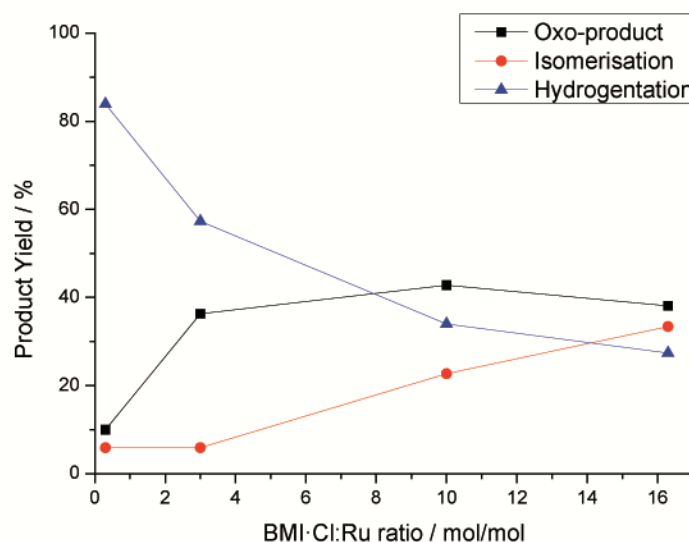
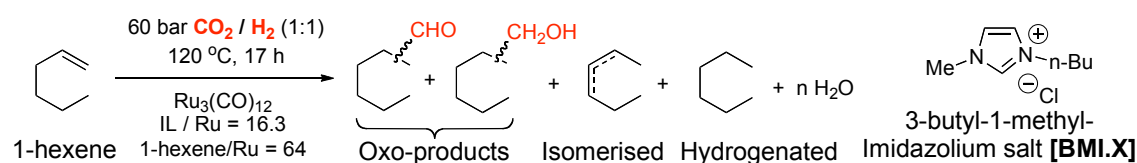


**Figure 3.3** Ru-catalysed hydroformylation of 1-hexene using CO<sub>2</sub> as a CO source. Reaction conditions: 1-hexene (20.0 mmol), Ru<sub>3</sub>(CO)<sub>12</sub> (0.1 mmol), 1-hexene / Ru = 64, 60 bar CO<sub>2</sub>/H<sub>2</sub> (1:1), 120 °C, 17 h;

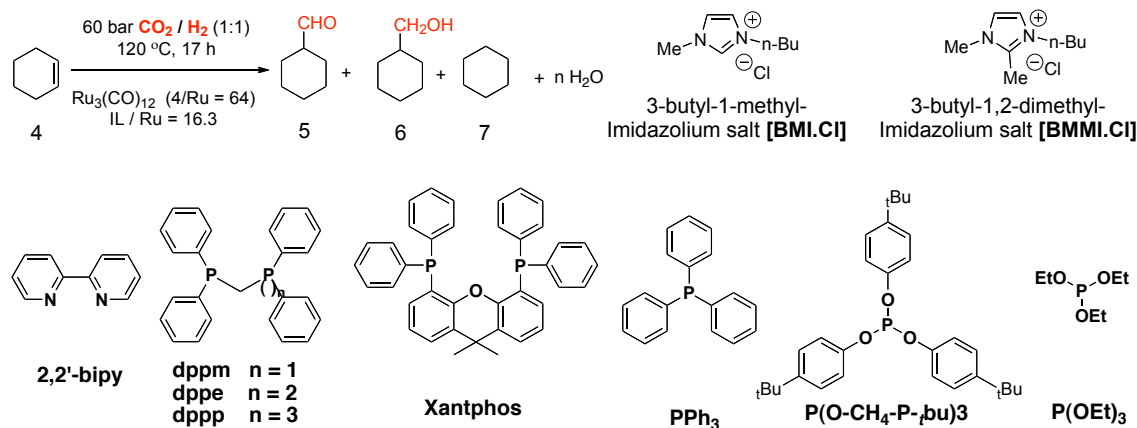
It was found that the oxo-product yield drastically increased when the [BMI•Cl]/Ru molar ratio was raised from 0.3 to 3.0, whereas [BMI•Cl]/Ru molar ratio of 16.3 were found optimal for reducing the undesired hydrogenation of the alkene. Furthermore, reaction was optimized by increasing the ratio (5:1) of CO<sub>2</sub>/H<sub>2</sub>, but it revealed no big difference in the selectivity of the oxo-products.

### 3.3.3 Electronic and steric-effects of P-donor ligands

The effect of using P-ligands as additives on the Ru-catalytic performance was also explored. The use of monodentate and bidentate phosphine ligands as additives resulted in much lower conversion and higher hydrogenation product yields (see Table 3.2). The monodentate and bidentate ligands with different electronic and steric properties was tested in presence of [BMI•Cl] ionic liquid. Its resulted lower cyclohexene conversion, oxo-product selectivity and alcohol selectivity (Entries 2 - 7, Table 3.2). This effect is more drastic for 2,2'-bipy and bidentate phosphine with a bite angles which favoured their coordination in *cis*-positions (Entries 2 - 5, Table 3.2). This behaviour could be related to the higher chelating effect of these ligands with the ruthenium catalytic active species. In contrast, Xantphos displayed higher conversion, oxo-product selectivity and alcohol selectivity than the others bidentate ligands used in this study (Entry 6, Table 3.2). This behaviour could be attributed to its larger bite angle, which could lead to the formation of less stable chelating complexes thus acting as a monodentate ligand.<sup>[44-46]</sup> This hypothesis was checked by carrying out the reaction in presence of monodentate phosphines such as triphenylphosphine (Entry 7, Table 3.2). Therefore by using monophosphite ligands showed higher conversion, and oxo-product selectivities with similar alcohol selectivities than those achieved using PPh<sub>3</sub> were achieved (Entry 9 Table 3.1 *versus* Entry 7, Table 3.2). In particular, no appreciable effect in the conversion and product selectivity was observed when P(OEt)<sub>3</sub> was used as the additive in the presence of [BMI•Cl] (Entries 3 *versus* 9, Table 3.1). The effect of the ligand/Ruthenium ratio was studied in case of P(OEt)<sub>3</sub> by using 1.0, 6.0, and 12.0 equiv. L/equiv. Ru (Entries 8-10, Table 3.2) compared with the 3.0 equiv. L/equiv. Ru (Entry 9, Table 3.1). Here

observed the similar selectivities with lower conversions were achieved as the L/Ru ratio was increased (Entries 8-10, Table 3.2).

**Table 3.2** Ru-catalysed hydroformylation of cyclohexene using CO<sub>2</sub> as a CO source and monodentate or bidentate ligands with different electronic and steric properties.



E <sup>[a,b]</sup>	Ionic Liquid	Ligands	Conv./ %	Oxo-product Sel./ %	Sel. 6/ %
1	[BMI·Cl]	-	98	63	98
2	[BMI·Cl]	2,2'-bipy	12	46	63
3	[BMI·Cl]	Dppm	11	59	74
4	[BMI·Cl]	Dppe	27	39	85
5	[BMI·Cl]	Dppp	22	20	53
6	[BMI·Cl]	Xantphos	61	65	85
7	[BMI·Cl]	PPh <sub>3</sub>	69	50	94
8 <sup>[c]</sup>	[BMI·Cl]	P(OEt) <sub>3</sub>	75	86	97
9 <sup>[d]</sup>	[BMI·Cl]	P(OEt) <sub>3</sub>	69	80	96
10 <sup>[e]</sup>	[BMI·Cl]	P(OEt) <sub>3</sub>	18	75	96
11	[BMMI·Cl]	P(O-C <sub>6</sub> H <sub>4</sub> -p-tBu) <sub>3</sub>	69	87	95
12	[BMMI·Cl]	P(O-C <sub>6</sub> H <sub>4</sub> -p-tBu) <sub>3</sub>	79	96	89

[a] Reaction conditions: Cyclohexene (20.0 mmol), ionic liquid (5.1 mmol), Ru<sub>3</sub>(CO)<sub>12</sub> (0.1 mmol), Cyclohexene / Ru = 64, IL/Ru = 16.3, 60 bar CO<sub>2</sub>/H<sub>2</sub> (1:1), 120 °C, 17 h, bidentate ligand (1.0 equiv. L/equiv. Ru) or monodentate ligand (3.0 equiv. L/equiv. Ru). [b]

Conversion and selectivity determined by GC-MS and GC-FID. [c] 1.0 equiv. L/ equiv. Ru. [d] 6.0 equiv. L/ equiv. Ru. [e] 12.0 equiv. L/ equiv. Ru.

Therefore in the presence of [BMMI•Cl], much higher conversions (up to 93%) with similar products selectivity were obtained (Entries 6 *versus* 10, Table 3.1). surprisingly,  $^{31}\text{P}$ -NMR studies of the reaction mixture was carried-out with  $\text{P}(\text{OEt})_3$  additive indicated that the  $\text{P}(\text{OEt})_3$  completely hydrolyzed into  $\text{H}_3\text{PO}_4$  during the reaction under same reaction conditions (see Figure 3.4). It could be due to formation of  $\text{H}_2\text{O}$  molecules during the reduction of  $\text{CO}_2$  into  $\text{CO}$  by Reverse Water-gas Shift Reaction (RWGSR). Spectra showed only  $\text{H}_3\text{PO}_4$  signal at 0.0 ppm, others expecting signals were not revealed for the phosphite  $\text{P}(\text{OEt})_3$  ligand / phosphite-Ru, or oxidized species. It is previously reported that the posphites can easily hydrolyzed instead of oxidized.

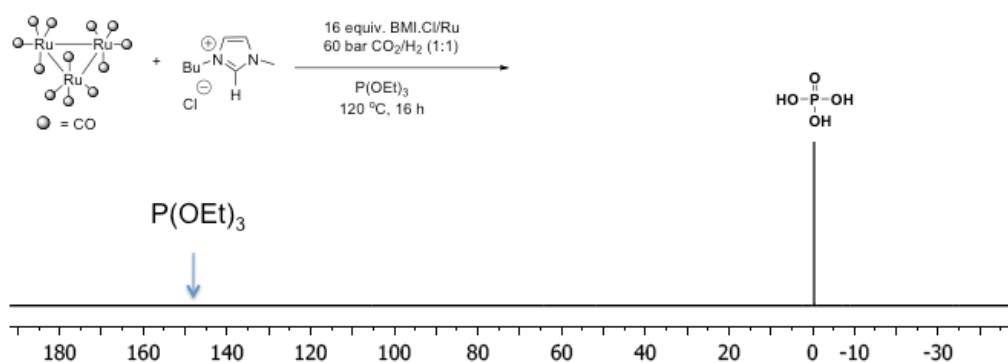
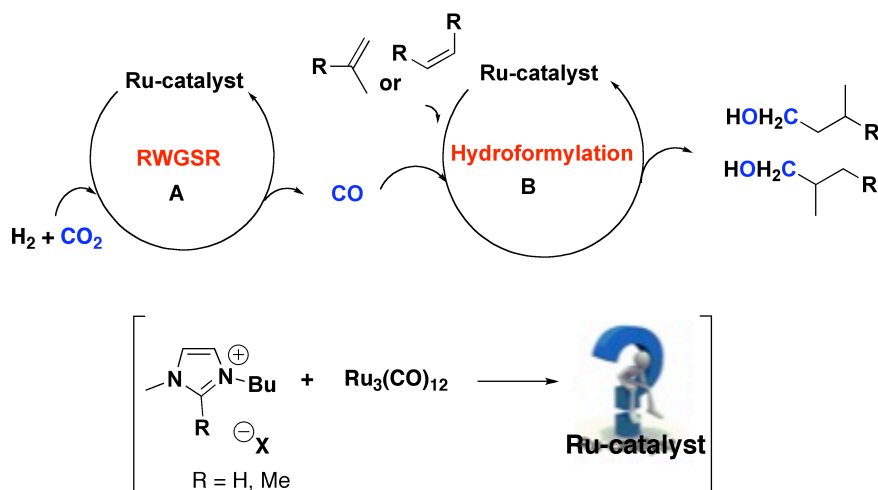


**Figure 3.4**  $^{31}\text{P}$ -NMR analysis of Ru-catalyzed hydroformylation reaction mixture by using  $\text{P}(\text{OEt})_3$  as additive.

Therefore, further experiments were carried out by adding  $\text{H}_3\text{PO}_4$  instead of  $\text{P}(\text{OEt})_3$ , which resulted in an improvement in oxo-product selectivity and alcohol selectivity in the oxo-product fraction (Entries 9 and 10 *versus* 11 and 12, Table 3.1) in both cases. The acid likely facilitates the hydride transfer and protonolysis, which is key step for the addition of hydrogen to carboxylate group.<sup>[29]</sup> Therefore, speculated the generation of *in-situ* Ru-hydride-carbonyl-carbene catalytic active species by reacting  $\text{Ru}_3(\text{CO})_{12}$  with [BMI•Cl] or [BMMI•Cl] ILs. These active Ru-hydride-carbonyl-carbene species (Ru-catalyst) initially probed reduction of  $\text{CO}_2$  into  $\text{CO}$ ,  $\text{H}_2\text{O}$  by Reverse Water-Gas Shift Reaction (RWGSR).





**Scheme 3.2** Proposed mechanism for the cascade reactions RWGSR/ hydroformylation/hydrogenation catalyzed by Ru-catalyst.

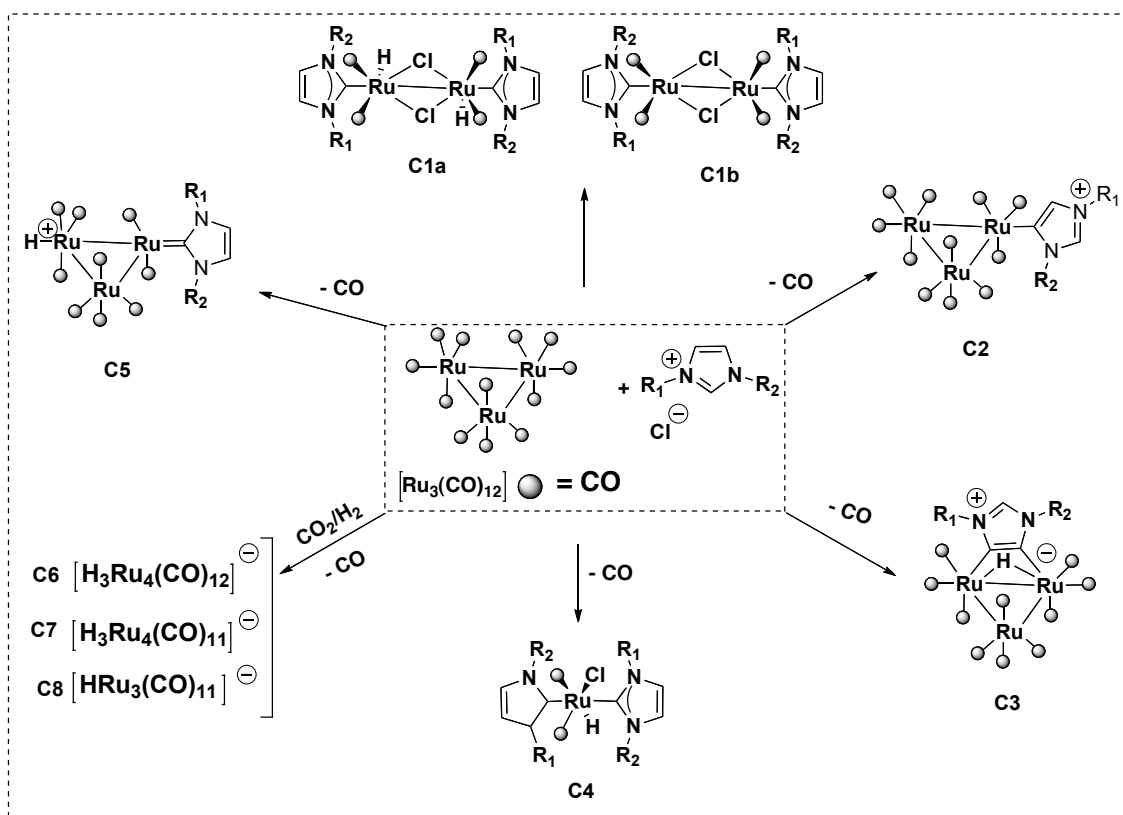
While in the second-step probed hydroformylation of alkenes by addition of CO across the  $\pi$ -bond, and produced aldehyde as initial hydroformylation product by hydride transfer. Then further aldehyde reduced into alcohol by hydride transfer and protonolysis in the final step (Scheme 3.2). Generated active Ru-catalytic species, and reaction intermediates during the hydroformylation reaction have been characterized and identified by performing various  $^{13}\text{C}$ -labeled,  $^1\text{H}$ -NMR, ESI-MS, and IR mechanistic studies. Furthermore, the gaseous phase of the reactions were also analyzed by GC-TCD to fined-out the reduction of  $\text{CO}_2$  into CO by involving RWGS reaction.

### 3.3.4 Mechanistic study: generation of Ru-catalyst & reduction of $\text{CO}_2$

#### 3.3.4.1 NMR-mechanistic studies

Various possible  $^{13}\text{C}$ -labeled,  $^{31}\text{P}$ , and  $^1\text{H}$ -NMR mechanistic studies were carried out to characterize the active Ru-catalytic species, and reaction intermediates generated during the hydroformylation of alkenes with  $\text{CO}_2/\text{H}_2$ . Previous reports were supported the formation of Ru-hydride-carbonyl-carbene  $[\text{H}_n\text{Ru}_n(\text{CO})_n\text{BMI}/\text{BMMI}]$  species by dissolving the  $\text{Ru}_3(\text{CO})_{12}$  precursor into ionic liquids  $[\text{BMI}\cdot\text{Cl}]$ , or  $[\text{BMMI}\cdot\text{Cl}]$  in the presence of 60 bar  $\text{CO}_2/\text{H}_2$  (1:1). Because it is

known that the Ru-carbene complexes formed by heat treatment of  $\text{Ru}_3(\text{CO})_{12}$  in the presence of imidazolium chloride salts (Scheme 1.6-1.7, Chapter-1).<sup>[47]</sup>



**Scheme 3.3** Reported and possible Ru-carbenes species formed by heat treatment of  $\text{Ru}_3(\text{CO})_{12}$  with imidazolium chloride salts. and generation of tri, tetra-nuclear Ru-hydride-carbonyls species in the presence of  $\text{CO}_2/\text{H}_2$  gas.

However characterized *in-situ* generated Ru-hydride-carbonyl-(normal, or abnormal)-carbene species. Here, we described the complementary experiments carried out in order to investigate the nature and structure of the species formed by dissolving  $\text{Ru}_3(\text{CO})_{12}$  either in the  $\text{BMI}\cdot\text{Cl}$  or  $\text{BMMI}\cdot\text{Cl}$ . Various NMR experiments were carried out under inert condition or by using mixture of  $\text{CO}_2/\text{H}_2$ . Initially,  $\text{Ru}_3(\text{CO})_{12}$  was dissolved in  $\text{BMI}\cdot\text{Cl}$  and this mixture was exposed to 60 bar  $\text{CO}_2/\text{H}_2$  (1:1) and warmed at  $120^\circ\text{C}$  during 16 h.  $^1\text{H}$  NMR spectrum of this solution displayed two main signals at the hydride region at  $\delta - 17.6$  and  $- 19.8$

ppm together with some other small signals at the hydride region  $\delta$  – 12.2, – 12.3, and – 13.2 ppm (Figures 3.5).

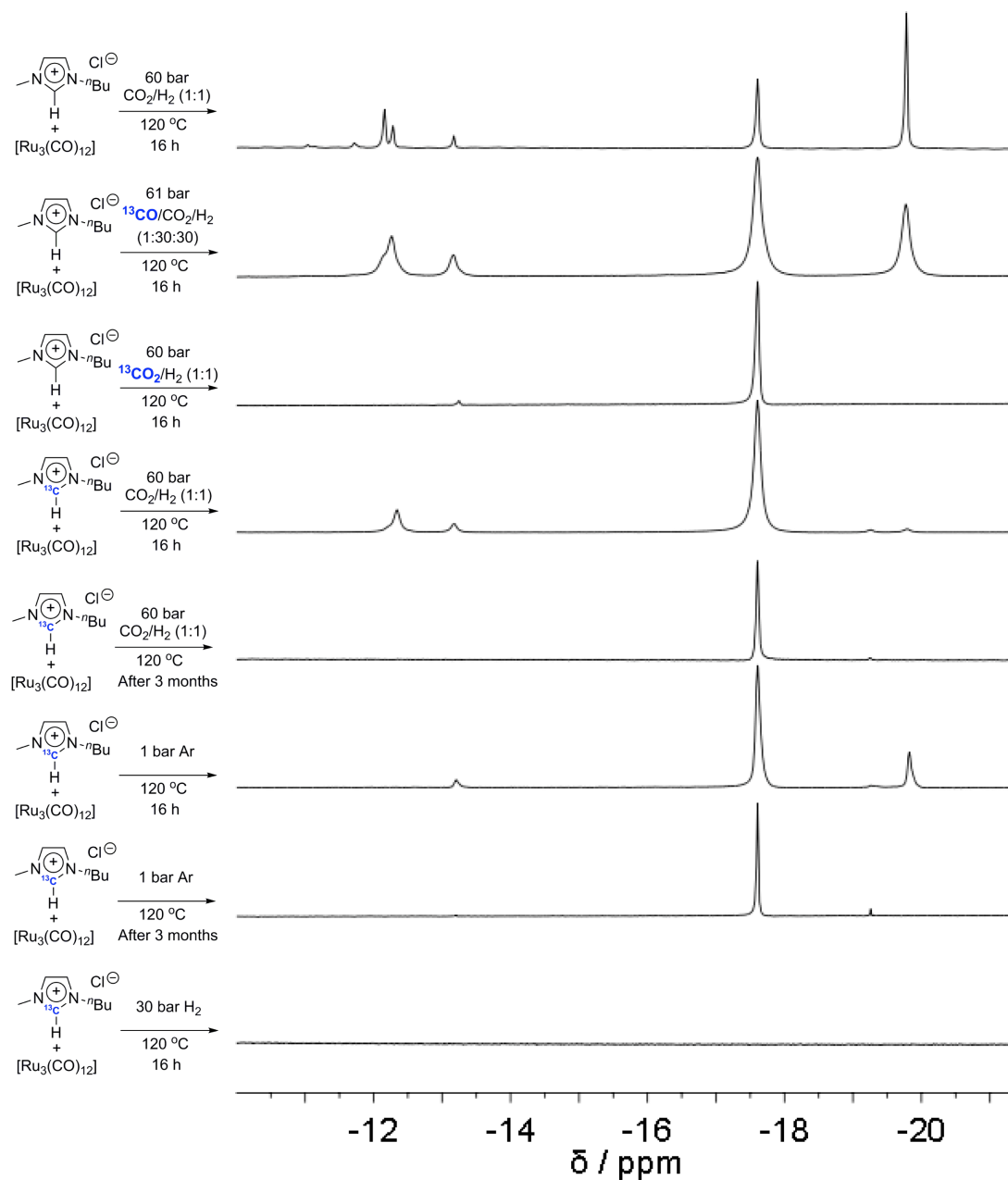


**Figure 3.5**  $^1\text{H}$  NMR (400 MHz,  $\text{CDCl}_3$ ) spectra of  $\text{Ru}_3(\text{CO})_{12}$  dissolved in BMI·Cl.

$^{13}\text{C}$   $\{^1\text{H}\}$  NMR spectrum of this solution revealed the presence of signals attributed to carbenes ( $\delta$  160.7 ppm) and carbonyls ( $\delta$  190-200 ppm) coordinated to Ru (Figure 3.6). This suggested the formation of Ru–hydride–carbonyl–carbene complexes under carbonylation conditions (i.e.,  $\text{CO}_2/\text{H}_2$  atmosphere). The formation of a Ru–hydride–NHC–carbene species (could be **C2-5**, NHC–Ru carbene

complex, Schemes 3.3).[48-50] These complexes are probable a result of the oxidative addition of a C-H imidazolium bond to the Ru<sup>0</sup> centre, similar to that reported for Ni and Pd.[51] Thus by heat treatment under CO<sub>2</sub>/H<sub>2</sub> could also favour the formation of carbene complexes (C4) by reaction of imidazolium carboxylate with the ruthenium complexes.[52-54]

The Ru<sub>3</sub>(CO)<sub>12</sub>/BMI•Cl mixture was exposed to 60 bar <sup>13</sup>CO<sub>2</sub>/H<sub>2</sub> (30:30) and warmed at 120°C during 16 h. <sup>1</sup>H NMR displayed exclusively the hydride signal at δ – 17.6 ppm, whereas <sup>13</sup>C {<sup>1</sup>H} NMR spectrum of this solution revealed enhancement of the Ru-carbonyl signals as well signals at 63 ppm, 121 ppm and 160 ppm (Figure 3.6). The signal at 63 ppm was attributed to <sup>13</sup>CH<sub>2</sub>OH<sup>13</sup>CH<sub>2</sub>OH (ethyleneglycol) formed by hydrogenation of the in-situ generated <sup>13</sup>CO. The signal at 121 ppm was attributed to <sup>13</sup>CO<sub>2</sub> dissolved in BMI•Cl. The signal at 63 ppm corresponds to <sup>13</sup>CH<sub>2</sub>OH<sup>13</sup>CH<sub>2</sub>OH (ethyleneglycol) and the signal at 160 ppm corresponds to H<sup>13</sup>COOH. These attributions were confirmed by the fact that these signals appeared in <sup>13</sup>C NMR as a triplet (coupling of one carbon with two protons in the <sup>13</sup>CH<sub>2</sub>OH<sup>13</sup>CH<sub>2</sub>OH) and a doublet (coupling of one carbon with one proton in the H<sup>13</sup>COOH), respectively. The Ru<sub>3</sub>(CO)<sub>12</sub>/BMI•Cl mixture was exposed to 61 bar <sup>13</sup>CO/CO<sub>2</sub>/H<sub>2</sub> (1:30:30) and warmed at 120°C during 16 h. <sup>1</sup>H NMR displayed similar signals with a sharper profile (Figure 3.5), whereas <sup>13</sup>C {<sup>1</sup>H} NMR spectrum of this solution revealed no enhancement of the Ru-carbonyl signals (Figure 3.6). Note that under enriched <sup>13</sup>CO atmosphere and if there is no CO production via RWGS, it is expected the enhancement of the Ru-carbonyl signals. Therefore, this observation indicates that RWGS is active process under these conditions. Interestingly, the enhancement of a signal at 63 ppm in the <sup>13</sup>C {<sup>1</sup>H} NMR spectrum suggested the formation of <sup>13</sup>CH<sub>2</sub>OH<sup>13</sup>CH<sub>2</sub>OH (ethyleneglycol) by hydrogenation of the <sup>13</sup>CO. Therefore, we conclude that the formed species by dissolving Ru<sub>3</sub>(CO)<sub>12</sub> in BMI•Cl catalysed the RWGS as well as the hydrogenation of CO<sub>2</sub> to HCOOH and CO to <sup>13</sup>CH<sub>2</sub>OH<sup>13</sup>CH<sub>2</sub>OH.

To corroborate that the signal observed in the <sup>13</sup>C{<sup>1</sup>H} NMR spectrum at 160.7 ppm is due to the formation of a NHC carbene and not to HCOOH, Ru<sub>3</sub>(CO)<sub>12</sub> was dissolved with <sup>13</sup>C-labelled BMI•Cl and the mixture was exposed to 60 bar

CO<sub>2</sub>/H<sub>2</sub> (30:30) at 120°C during 16 h. <sup>1</sup>H NMR displayed exclusively the hydride signal at δ – 17.6 ppm (Figure SI1), whereas <sup>13</sup>C {<sup>1</sup>H} NMR spectrum of this solution revealed enhancement of the signal at 160.7 ppm (Figure 3.6). We corroborated that this signal at 160.7 ppm corresponds to carbene and not to HCOOH by comparing the signal observed in the <sup>13</sup>C{<sup>1</sup>H} NMR spectra for the HCOOH dissolved in BMI•Cl, and the fact that this signal is a singlet in <sup>13</sup>C NMR. Therefore, we conclude that carbenes were formed by dissolving Ru<sub>3</sub>(CO)<sub>12</sub> in BMI•Cl and treatment under CO<sub>2</sub>/H<sub>2</sub> atmosphere at temperatures as low as 120°C.

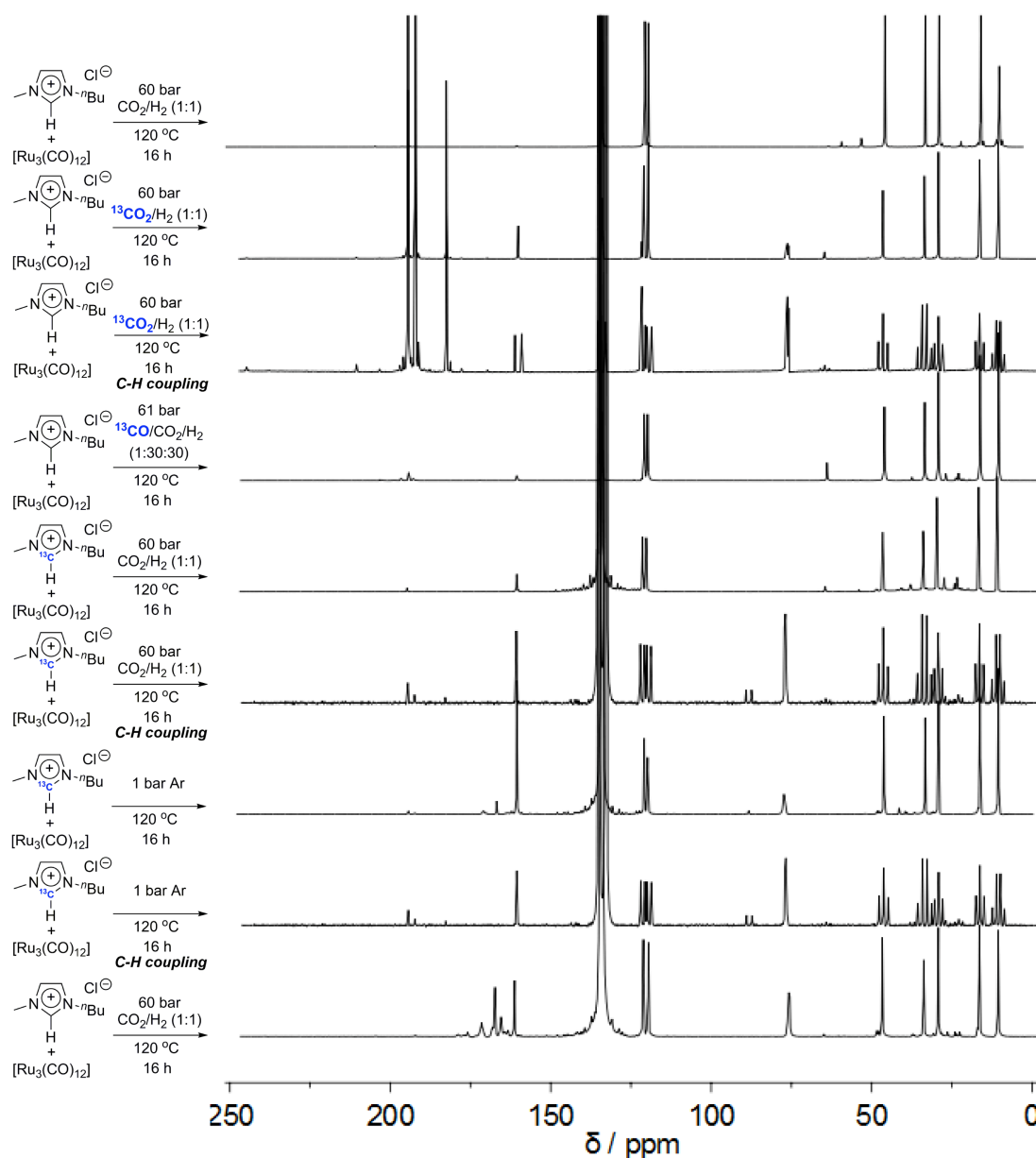


**Figure 3.6:** <sup>13</sup>C {<sup>1</sup>H} NMR (100 MHz, CDCl<sub>3</sub>) and <sup>13</sup>C NMR (100 MHz, CDCl<sub>3</sub>) spectra of Ru<sub>3</sub>(CO)<sub>12</sub> dissolved in BMI•Cl.

$\text{Ru}_3(\text{CO})_{12}$  was dissolved with  $^{13}\text{C}$ -labelled BMI•Cl and the mixture was exposed to inert atmosphere (1 bar Ar) at  $120^\circ\text{C}$  during 16 h.  $^1\text{H}$  NMR spectrum of this solution displayed also the two main signals at the hydride region at  $\delta - 17.6$  and  $- 19.8$  ppm (Figure 3.5), whereas  $^{13}\text{C}$   $\{^1\text{H}\}$  NMR spectrum of this solution revealed also the presence of the carbonyl and carbene signals with an enhancement of the Ru-carbene signal (Figure 3.6). Therefore, we conclude that carbenes were formed also by dissolving  $\text{Ru}_3(\text{CO})_{12}$  in BMI•Cl and treatment under inert atmosphere at temperatures as low as  $120^\circ\text{C}$ . It should be remarked that the stability of the formed complexes was evaluated by keeping these solutions in the sealed NMR tubes under inert atmosphere, and performing  $^1\text{H}$  NMR after 3 months and no noticeable variations of the signals were observed.

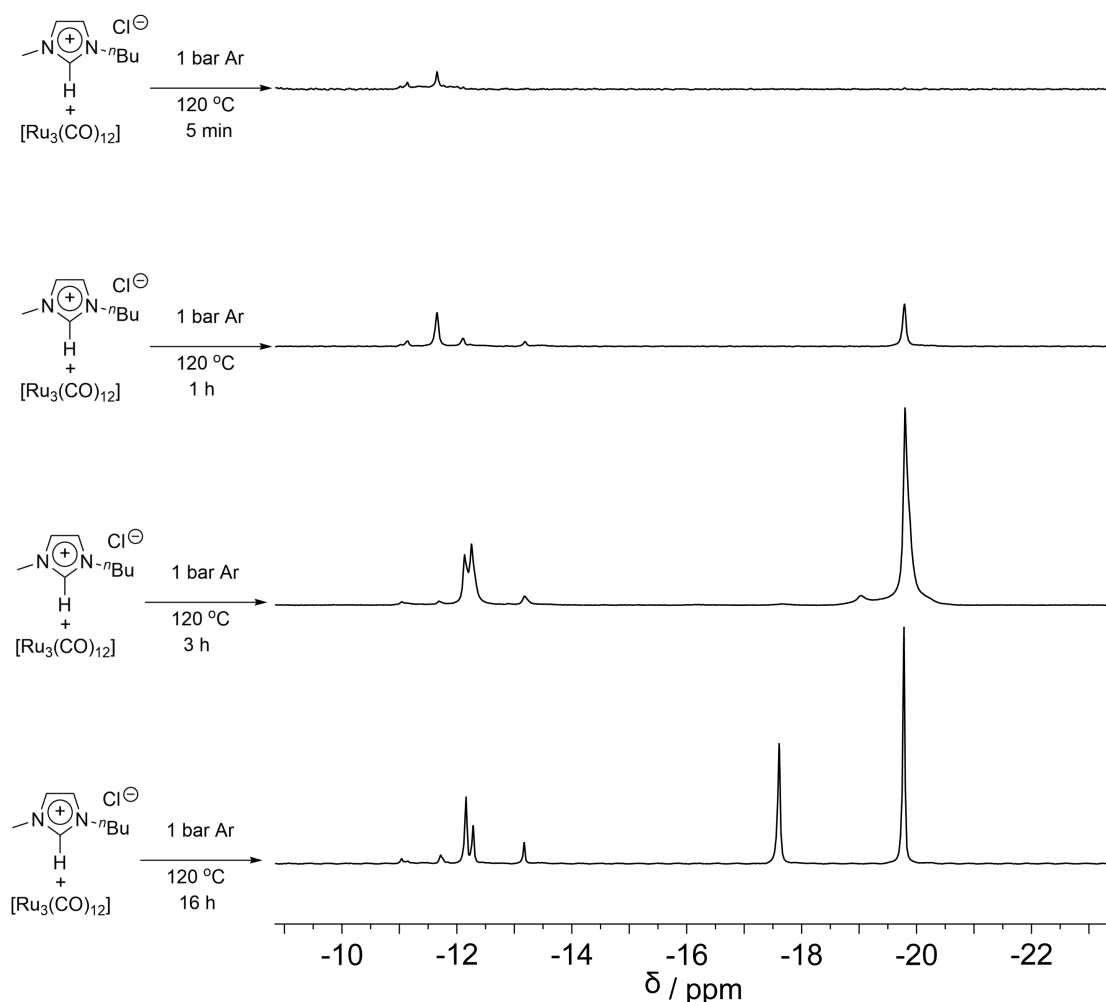


**Figure 3.7:**  $^1\text{H}$  NMR (400 MHz,  $\text{CDCl}_3$ ) spectra of  $\text{Ru}_3(\text{CO})_{12}$  dissolved in BMI•Cl under 1 bar Ar.

$\text{Ru}_3(\text{CO})_{12}$  was dissolved with  $^{13}\text{C}$ -labelled BMI•Cl and the mixture was exposed to  $\text{H}_2$  atmosphere (30 bar) at  $120^\circ\text{C}$  during 16 h.  $^1\text{H}$  NMR spectrum of this solution revealed no hydride signals and  $^{13}\text{C}$   $\{^1\text{H}\}$  NMR spectrum displayed no Ru-carbonyl and a complex mixture of signals between 160-170 ppm (Figure 3.6). These observations suggested the decomposition of the Ru-carbonyl complex and probably the formation of metal particles by heat treatment under  $\text{H}_2$  atmosphere.

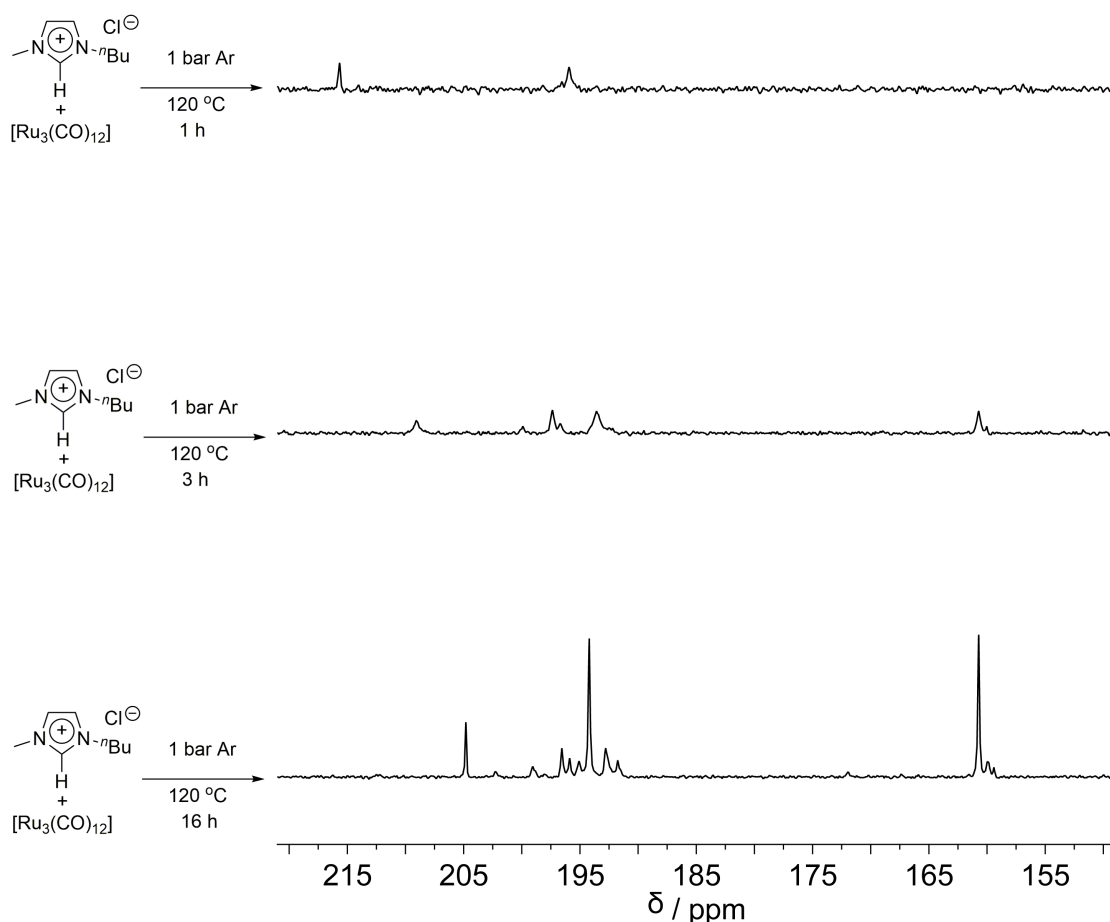


**Figure 3.8:**  $^{13}\text{C}$   $\{^1\text{H}\}$  NMR (100 MHz,  $\text{CDCl}_3$ ) spectra of  $\text{Ru}_3(\text{CO})_{12}$  dissolved in BMI•Cl under 1 bar Ar.

In order to address the nature of the distinct species formed,  $\text{Ru}_3(\text{CO})_{12}$  was dissolved in BMI•Cl and this mixture was exposed inert atmosphere at  $120^\circ\text{C}$  during 5 min, 1 h, 3 h and 16 h.  $^1\text{H}$  NMR spectrum in the hydride region of this solution after 5 min displayed only small signals at  $\delta - 12.3$  ppm (Figure 3.7). After 1 h and 3 h,  $^1\text{H}$  NMR spectra in the hydride region of this solution displayed a fast growing of the signal at  $\delta - 19.3$  ppm (Figure 3.7). Finally,  $^1\text{H}$  NMR spectra in

the hydride region of this solution after 16 h displayed two signals at  $\delta - 17.6$  and  $- 19.8$  ppm (Figure 3.7). It should be noted that the appearance of this hydride signals was accompanied by the appearance of new signals in the  $^{13}\text{C}\{^1\text{H}\}$  NMR attributed to Ru-hydride-carbonyl-carbene species (Figure 3.8).

Interestingly, some groups reported that the  $\text{RuHCl}(\text{CO})(\text{NHC})(\text{PPh}_3)$  complexes effectively catalyzed the hydrogenation of cyclic olefins and isomerisation of terminal olefins.<sup>[58, 59][60, 61]</sup> This could explain the higher cyclohexane selectivity obtained in our study when phosphines additives were used (Table 3.2) during the hydroformylation of cyclohexene, and the formation of internal hexenes by isomerisation of 1-hexenes (Figure 3.3). Interestingly ruthenium bis-carbene complexes (**C4**) also reported as a active catalyst for the hydrogenation of olefins.<sup>[62] [63]</sup> Ru-abnormal carbene complexes have been previously reported in the literature,<sup>[64]</sup> isomerisation of the imidazolium carboxylate to abnormal position at higher temperatures.<sup>[65]</sup> Formation of metal-abnormal-carbene complexes with imidazolium ILS<sup>[53, 54]</sup> and recently reported trinuclear Ru-hydride-carbene complexes bearing abnormally bounded with C4, C5 of imidazolium ring (Scheme 1.7, Chapter-1).<sup>[66]</sup>

Similarly,  $\text{Ru}_3(\text{CO})_{12}$  was dissolved in  $\text{BMMI}\cdot\text{Cl}$  and this mixture was exposed to either inert atmosphere or  $\text{CO}_2/\text{H}_2$  atmosphere at  $120^\circ\text{C}$ . In the  $^1\text{H}$  NMR and  $^{13}\text{C}\{^1\text{H}\}$  NMR spectra, similar behaviour to those observed with  $\text{BMI}\cdot\text{Cl}$  were recorded (Figure 3.9 and 3.10). It should be noted that in these  $^1\text{H}$  NMR spectra is also initially observed the appearance of the hydrides at  $\delta - 11$  to  $- 13$  and  $- 19.4$  ppm, and the further appearance of the hydride at  $- 17.6$  ppm. Additionally, after 1 week, the reversible transformation of the hydride at  $- 17.6$  ppm to those at  $\delta - 11$  to  $- 13$  and  $- 19.4$  ppm was evidenced.

Additionally, NMR spectra were recorded after heat treatment under  $\text{CO}_2/\text{H}_2$  atmosphere of the mixture of  $\text{Ru}_3(\text{CO})_{12}$ ,  $\text{BMMI}\cdot\text{Cl}$  and  $\text{P}(\text{OEt})_3$  (3 equiv./equiv of Ru). In the  $^1\text{H}$  NMR and  $^{13}\text{C}\{^1\text{H}\}$  NMR spectra, this mixture displayed similar signals to those observed with the other mixtures but with a distinct proportion of the signals, thus suggesting a ligand modification of the Ru-



complex, although this ligand effect is only apparent because when the  $^{31}\text{P}$  NMR was recorded only the signal of  $\text{H}_3\text{PO}_4$  was observed (Figure 3.4), and additionally, the results of the catalytic experiments using either  $\text{P}(\text{OEt})_3$  or  $\text{H}_3\text{PO}_4$  are very similar.

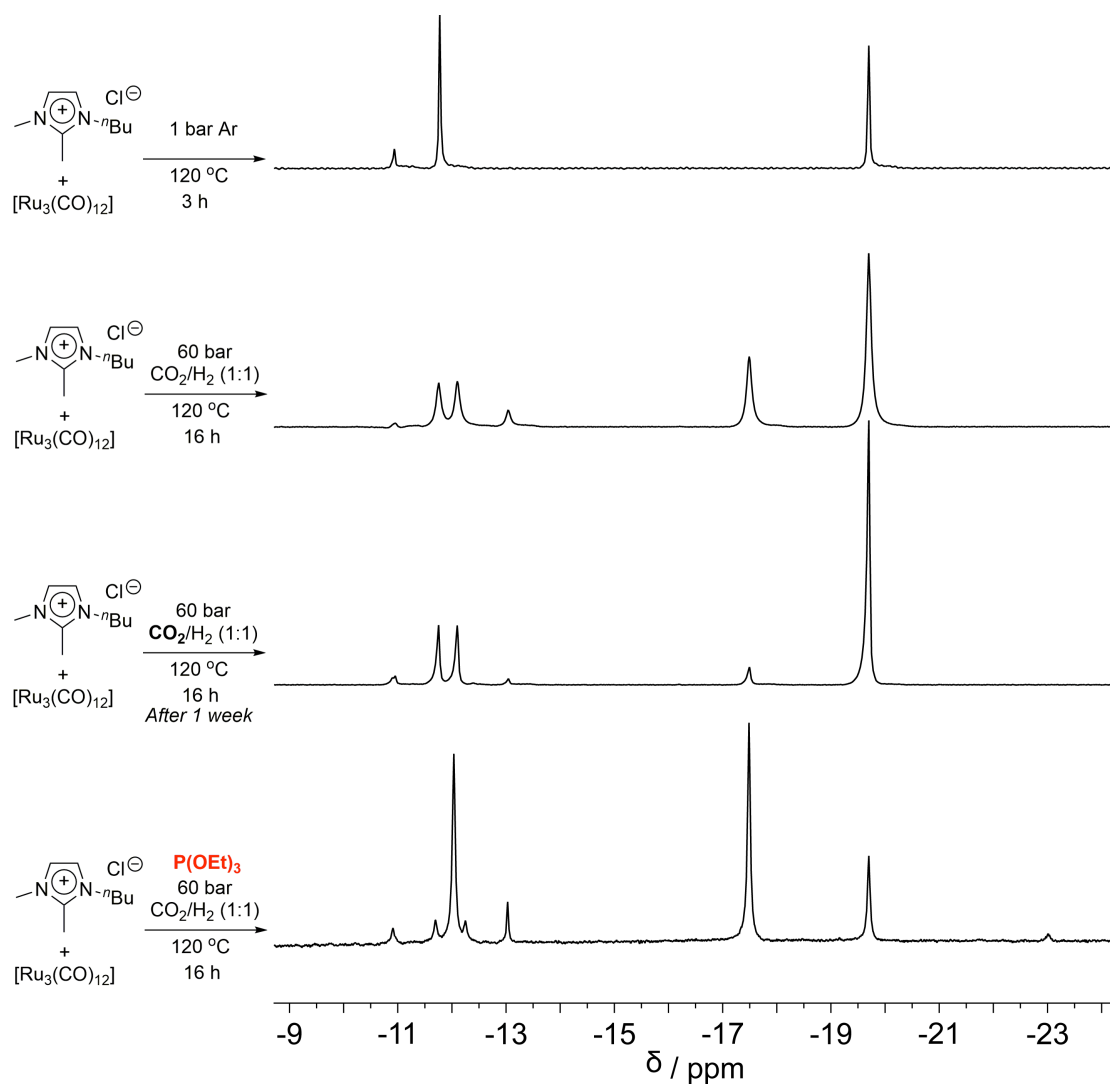


**Figure 3.9:**  $^1\text{H}$  NMR (400 MHz,  $\text{CDCl}_3$ ) spectra of  $\text{Ru}_3(\text{CO})_{12}$  dissolved in  $\text{BMMI}\cdot\text{Cl}$ .

Therefore, similar catalytic species with different proportion ratios were formed by dissolving  $\text{Ru}_3(\text{CO})_{12}$  in  $\text{BMI}\cdot\text{Cl}$  and in  $\text{BMMI}\cdot\text{Cl}$ , and the addition of  $\text{P}(\text{OEt})_3$  produced also a variation in the proportion of these species, thus modifying the catalytic activity and selectivity for carbonylation (i.e., hydroformylation or hydroaminomethylation) reactions using  $\text{CO}_2$  as a CO source.

The NMR studies also evidenced the formation of CO and HCOOH via RWGS and hydrogenation of CO<sub>2</sub>, respectively.

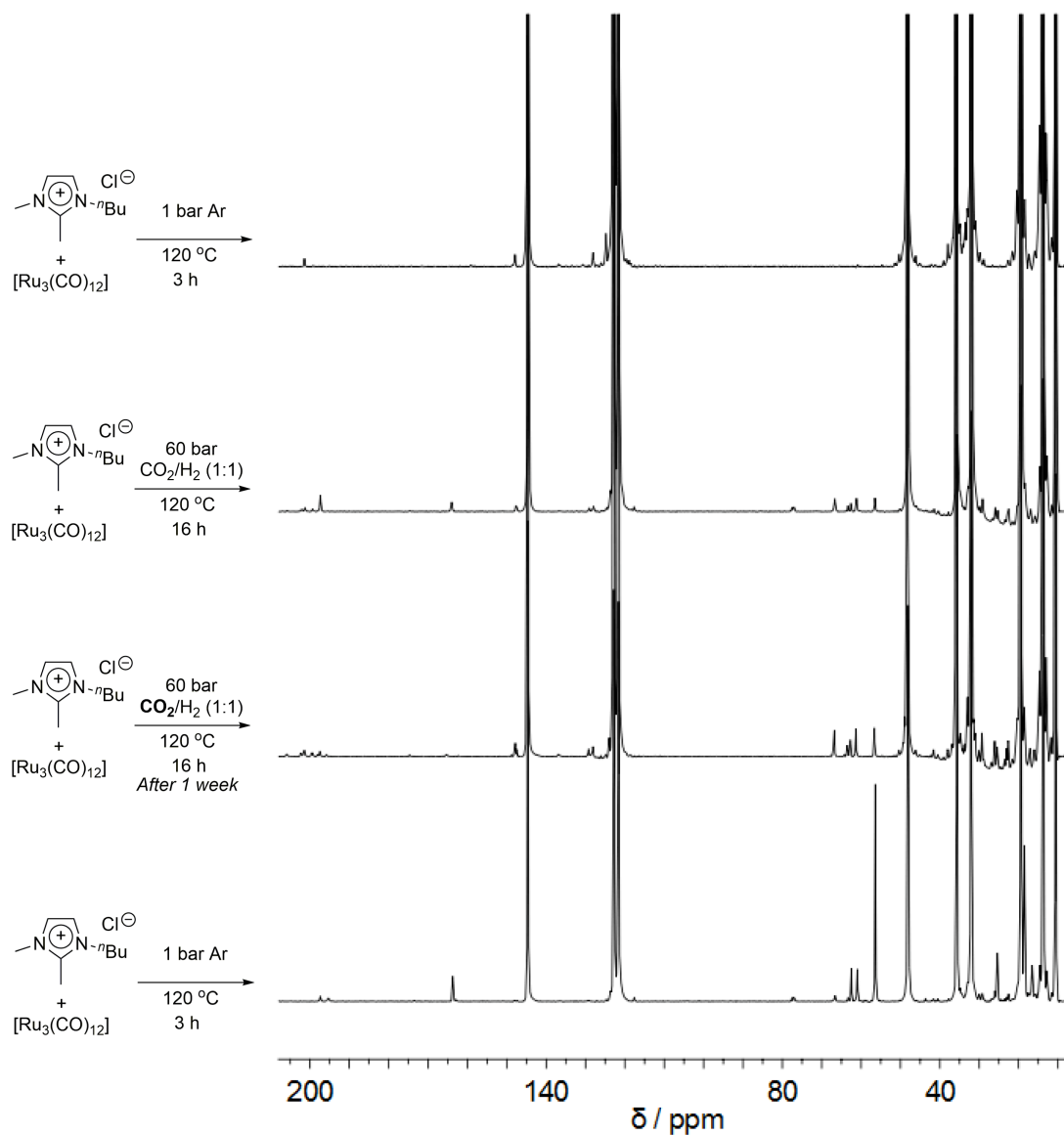


**Figure 3.10:** <sup>13</sup>C {<sup>1</sup>H} NMR (100 MHz, CDCl<sub>3</sub>) spectra of Ru<sub>3</sub>(CO)<sub>12</sub> dissolved in BMMI·Cl.

Thus, NMR mechanistic studies revealed the formation of Ru-hydride-carbonyl-carbene multifunctional species *in situ* by reaction of Ru<sub>3</sub>(CO)<sub>12</sub> with [BMI·Cl] or [BMMI·Cl]. Which strongly promoted the RWGSR/hydroformylation/hydrogenation reactions in the presence of P(OEt)<sub>3</sub> and H<sub>3</sub>PO<sub>4</sub>, because, the <sup>31</sup>P-NMR revealed fully hydrolysis of the triethyl phosphite into H<sub>3</sub>PO<sub>4</sub>, the fact which was corroborated by observing a signal at 0 ppm in the <sup>31</sup>P NMR (Figure 3.4).

Phosphites are more prone to be hydrolyzed than oxidized (fact was not observing a signal at 10 ppm in the  $^{31}\text{P}$  NMR) when they are dissolved in ionic liquids. Thus the positive effect of  $\text{P}(\text{OEt})_3$  in the hydroformylation speculated to be not caused by their coordination to the metal center. But it promoted RWGSR ( $\text{CO}_2$  into  $\text{CO}$ ) by hydrolyzed into phosphoric acid. Note that in the reduction of  $\text{CO}_2$  to  $\text{CH}_3\text{OH}$ , alcohols (ca.  $\text{MeOH}$  and  $\text{EtOH}$ ) were used as additives just for promoting the formation of a carbonate and their further reduction.<sup>[33]</sup>

### 3.3.4.2 Analysis of gas-phase of reactions

During the hydroformylation of alkenes gas-phase of reactions constantly analyzed. The GC-TCD-FID analysis indicated the presence of  $\text{CO}$  together with  $\text{CO}_2$  and  $\text{H}_2$  gases in all reactions. But hereby given the data of contemporary analysis of the following three significant and characteristic reactions (Figure 3.11). Experiments for the analysis carried out by using of  $^{13}\text{C}$ , or triethyl phosphite or phosphoric acid as additives for hydroformylation of cyclohexene with  $\text{CO}_2$  as  $\text{CO}$  source

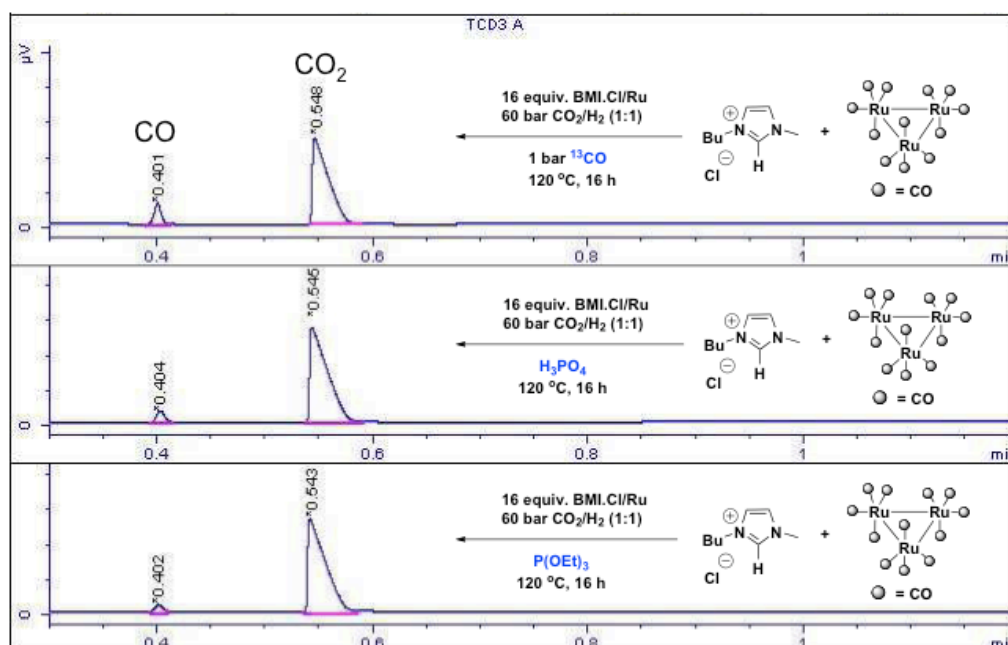


**Figure 3.11** GC-TCD-analysis spectrums of the gas phase during the reactions by adding additives  $^{13}\text{C}$ ,  $\text{H}_3\text{PO}_4$ , and  $\text{P}(\text{OEt})_3$ .

### 3.3.4.3 ESI-MS, and IR studies

Generation of mononuclear, bi, and tri-nuclear Ru-hydride-carbonyl-carbene complexes **C1** to **C5** (Scheme 3.3), by reacting  $\text{Ru}_3(\text{CO})_{12}$  with  $[\text{BMI}\cdot\text{Cl}]$  has been already reported. Laterally Ken-ichi Tominaga (2004) reported an ESI-MS data for the formation of  $[\text{H}_3\text{Ru}_4(\text{CO})_{12}]^-$  ( $m/z = 744$ ), and  $[\text{HRu}_3(\text{CO})_{10}]^-$  ( $m/z = 598$ ) species by using  $\text{Ru}_3(\text{CO})_{12}$  precursor during the hydrofomylation of alkenes in the presence of  $\text{CO}_2/\text{H}_2$  gas. Then M.-L. Kontkanen (2009) also reported the tetra, tri-nuclear Ru-hydride-carbonyl species (**C6-C8**, Scheme 3.3).

Prominently here investigated an  $[\text{ESI-MS}]^{\cdot+}$  analysis for the reaction mixture formed by reacting  $\text{Ru}_3(\text{CO})_{12}$  with 2 equiv. of  $[\text{BMI}\cdot\text{Cl}]/\text{Ru}$  in the presence of  $\text{CO}_2/\text{H}_2(1:1 \text{ 60 bar})$ .  $[\text{ESI-MS}]^+$  analysis indicated the formation of tri-nuclear Ru-hydride-carbonyl-carbene species, and relevant reaction intermediates during the reaction:  $[\text{HRu}_3(\text{CO})_{11}]^+$ ,  $[\text{HRu}_3(\text{CO})_{10}\text{BMI}]^+$   $[\text{HRu}_3(\text{CO})_9(\text{CO}_2\text{H})\text{BMI}]^+$ ,  $[\text{HRu}_3(\text{CO})_8(\text{HCO}_2)\text{BMI}]^+$  (Figure 3.12).

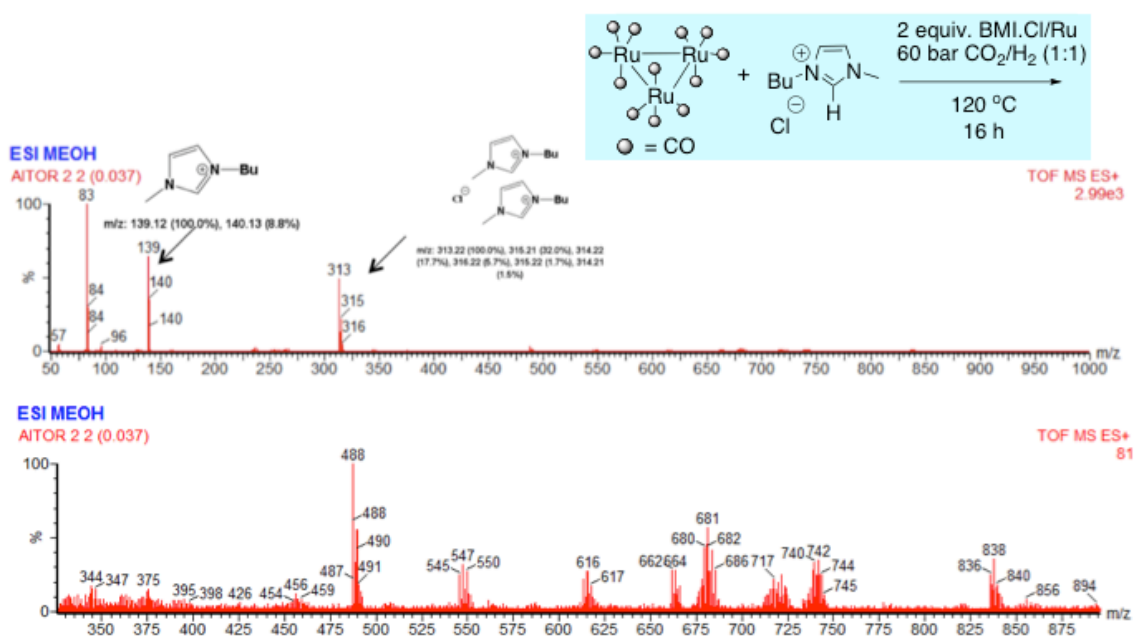


**Figure 3.12** ESI-MS<sup>+</sup> Analysis for the reaction mixture obtained by reacting  $\text{Ru}_3(\text{CO})_{12}$  precursor with  $[\text{BMI}\cdot\text{Cl}]$  (2 equiv. IL/Ru), 60 bar  $\text{CO}_2/\text{H}_2$  (1:1), reaction condition: 120°C, for 16-17 h.

While, the [ESI-MS]<sup>-</sup> analysis of same reaction mixture revealed signals at  $m/z = 715, 687, 659$  for the formation of tetra-nuclear Ru-hydride-carbonyl species  $[\text{H}_3\text{Ru}_4(\text{CO})_{11}]^-$ ,  $[\text{H}_3\text{Ru}_4(\text{CO})_{10}]^-$ , and  $[\text{H}_3\text{Ru}_4(\text{CO})_9]^-$  (Figure 3.13). Generated tetra, and tri-nuclear Ru-species were identified either by positive or negative ESI-MS analysis with accurate masses and isotopic distribution of species. Interestingly as increased the amount of IL ([BMI•Cl]/Ru 2 to 10, 16 equiv.), tri-nuclear Ru-hydride-carbonyl-carbene  $[\text{HRu}_3(\text{CO})_n\text{BMI}]^+$  species were dominantly formed as compared to  $[\text{H}_3\text{Ru}_4(\text{CO})_n]^-$ , species by using  $\text{CO}_2/\text{H}_2$  (1:1 60 bar). However, further performed the [ESI-MS]<sup>+</sup> analysis by using <sup>13</sup>C<sub>2</sub>-labeled 5 equiv. [BMI•Cl]/Ru without using  $\text{CO}_2/\text{H}_2$  gas under same reaction condition (Figures 3.14).

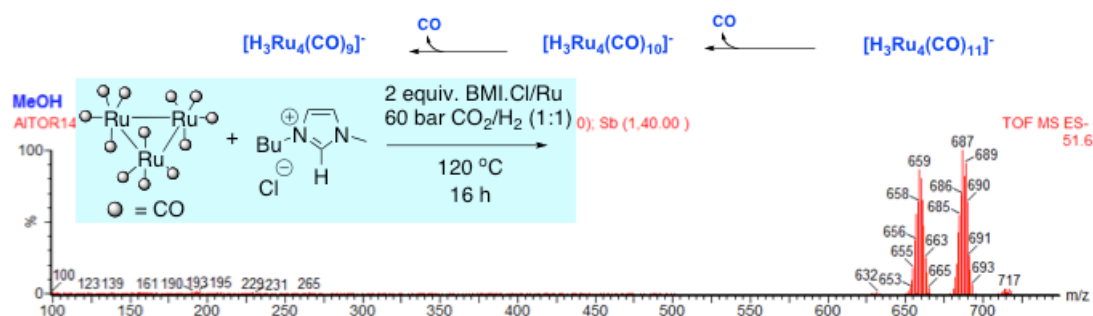


**Figure 3.13** ESI-MS<sup>-</sup> Analysis for the reaction mixture obtained by reacting  $\text{Ru}_3(\text{CO})_{12}$  precursor with BMI•Cl (2 equiv. IL/Ru), 60 bar  $\text{CO}_2/\text{H}_2$  (1:1), reaction condition: 120°C, for 16-17 h.

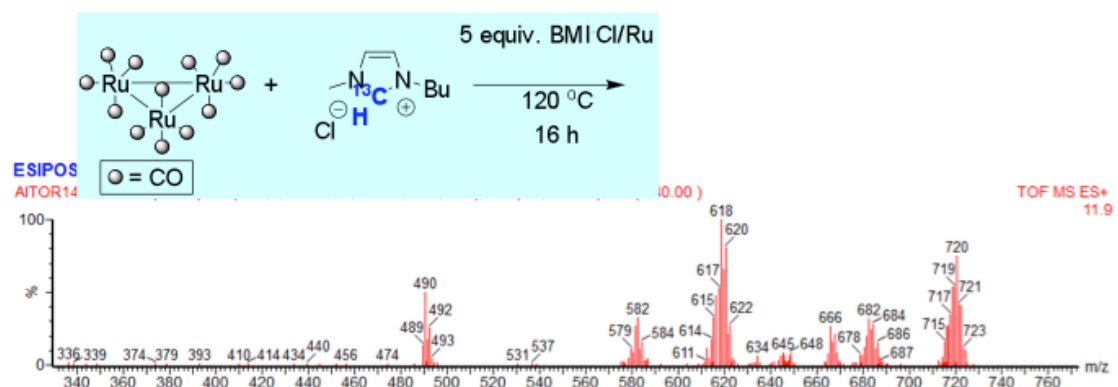


**Figure 3.14** [ESI-MS]<sup>+</sup> Analysis for the reaction mixture obtained by reacting  $\text{Ru}_3(\text{CO})_{12}$  precursor with <sup>13</sup>C<sub>2</sub>-labeled [BMI•Cl] (5 equiv. IL/Ru), reaction condition: 120°C, for 16-17 h.

[ESI-MS]<sup>+</sup> analysis of reaction mixture (obtained using 5 equiv. of <sup>13</sup>C<sub>2</sub>-labeled IL [BMI•Cl] without using CO<sub>2</sub>/H<sub>2</sub> gas) revealed the formation of [HRu<sub>3</sub>(CO)<sub>11</sub>]<sup>+</sup>, [HRu<sub>3</sub>(CO)<sub>10</sub>BMI]<sup>+</sup> species. While intermediates species [HRu<sub>3</sub>(CO)<sub>n</sub>(CO<sub>2</sub>H)BMI] of RWGSR were not appeared in the absence of CO<sub>2</sub>/H<sub>2</sub> gases (Figure 3.12). Further [ESI-MS]<sup>-</sup> analysis of same reaction also indicted no signals for the formation [H<sub>3</sub>Ru<sub>4</sub>(CO)<sub>n</sub>]<sup>-</sup> species in the absence of CO<sub>2</sub>/H<sub>2</sub>. Thus it is conformed the [H<sub>3</sub>Ru<sub>4</sub>(CO)<sub>n</sub>]<sup>-</sup> species only can formed in the presence of CO<sub>2</sub>/H<sub>2</sub> gas pressure by using low concentration of ILs. While, with High Equiv. IL/Ru ratio, reaction preferentially generated stable tri-nuclear Ru-hydride-carbonyl-carbene [HRu<sub>3</sub>(CO)<sub>n</sub>BMI]<sup>+</sup> species instead of using CO<sub>2</sub>/H<sub>2</sub> high pressure.

Further IR-analysis of the reaction mixtures also revealed the formation of Ru-hydride-carbonyl-carbene species by reacting Ru<sub>3</sub>(CO)<sub>12</sub> with [BMI•Cl], and [BMMI•Cl] ILs. IR-analysis of the species formed by reacting Ru<sub>3</sub>(CO)<sub>12</sub> with [BMI•Cl] or [BMMI•Cl] (Figure 3.15, 3.16), indicated the formation of Ru/HNC-carbenes at C4, C5 position. And also revealed decreasing of the significant band of Ru<sub>3</sub>(CO)<sub>12</sub> CO = 2059 cm<sup>-1</sup>, further indicated the additional bands of [HRu<sub>3</sub>(CO)<sub>10</sub>BMI, or BMMI]<sup>+</sup> CO = 1952, 2005 cm<sup>-1</sup> by reaction with CO<sub>2</sub>.

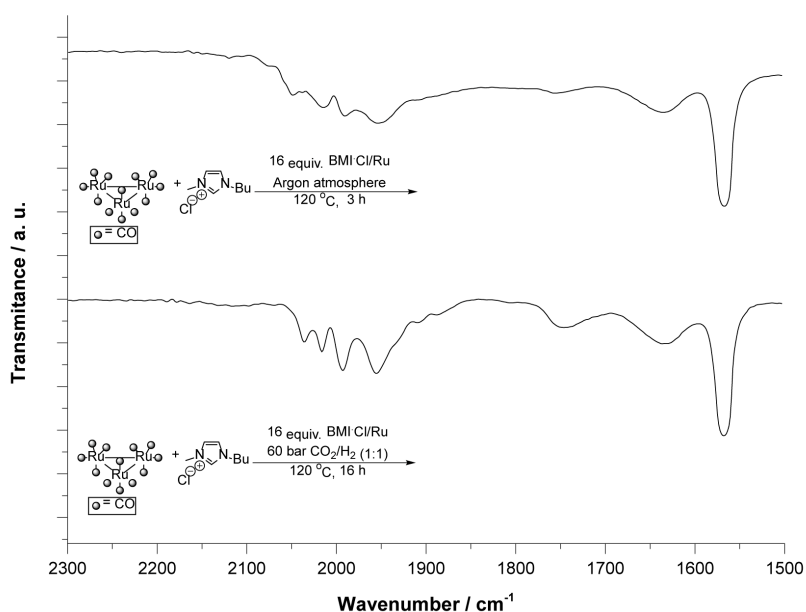


**Figure 3.15** IR spectra of the species formed by reacting Ru<sub>3</sub>(CO)<sub>12</sub> with BMI•Cl.

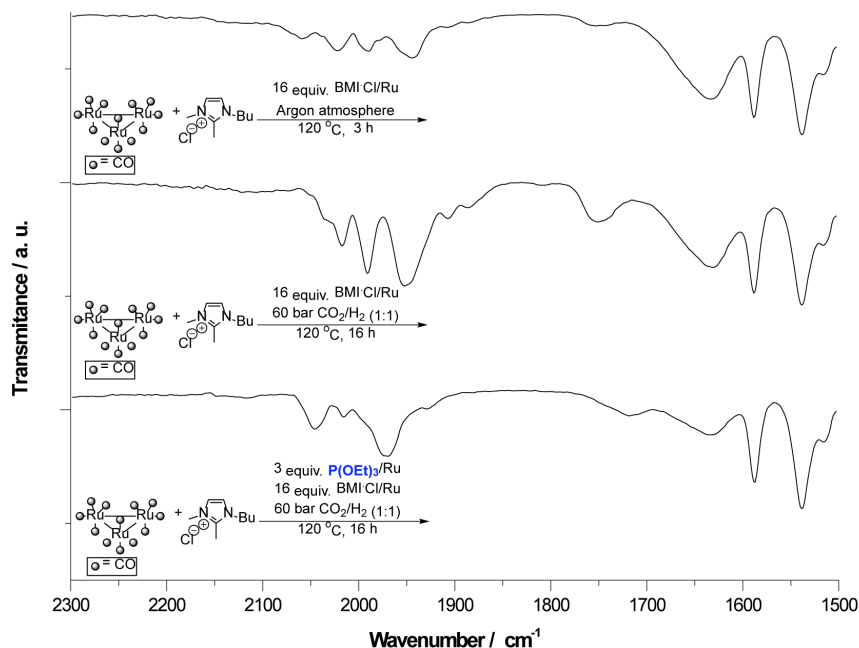
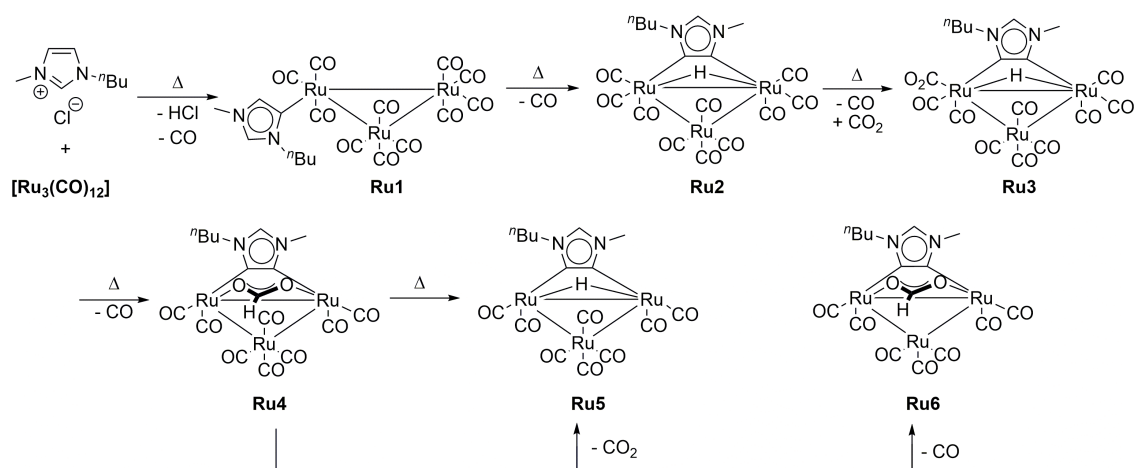
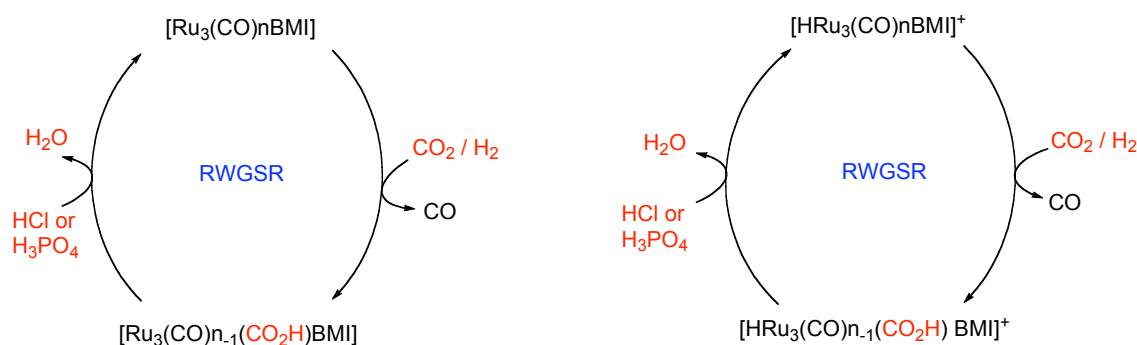


**Figure 3.16** IR spectra of the species formed by reacting  $\text{Ru}_3(\text{CO})_{12}$  with  $\text{BMMI}\cdot\text{Cl}$ .

Conclusion of mechanistic studies indicted the generation of possible Ru-hydride-carbonyl-carbene species (Ru1-Ru3) by reacting  $\text{Ru}_3(\text{CO})_{12}$  with  $[\text{BMMI}\cdot\text{Cl}]$   $[\text{BMMI}\cdot\text{Cl}]$ , and also indicated the formation of RWGSR intermediates (Ru4-Ru6) on by using mixture of  $\text{CO}_2/\text{H}_2$ , (60 bar 1:1).



**Scheme 3.4a** *In-situ* generated Ru-catalytic species and reaction intermediates of RWGS reaction.



**Scheme 3.4b** Proposed reaction mechanism for the Ru-catalyzed reductive conversion of  $\text{CO}_2$  into  $\text{CO}$  by Reverse-Water-Gas-Shift reaction (RWGSR) promoted by  $\text{H}_3\text{PO}_4$ .

Generated multifunctional Ru-catalysts initially strongly promoted the reductive conversion of  $\text{CO}_2$  into  $\text{CO}$  and water by Reverse Water-Gas Shift Reaction (Scheme 3.4b). The addition of  $\text{H}_3\text{PO}_4$  as additive strongly accelerated the RWGS reaction by providing an acidic proton during the reaction. Then the active catalytic species promoted the hydroformylation of alkenes by addition of  $\text{CO}$ , and reduction of carbonyl by hydride transfer and protonolysis mechanism.

### 3.3.5 Hydroformylation of versatile cyclic and terminal alkenes

Under optimized reaction conditions, cyclic disubstituted alkenes (cyclooctene and norbornene), cyclic disubstituted dienes (1,5-cyclooctadiene), cyclic disubstituted conjugated dienes (1,3-cyclooctadiene) and 2,2-disubstituted alkenes (methylstyrene, (R)-(+)-limonene and Carvone) were easily hydroformylated, thus leading to the alcohols with moderate-to-high conversions (74% to > 99%) and selectivities (69% to 93%) (Figure 3.17). Whereas, too hindered alkenes such as 2-methyl-2-butene, displayed low conversions (25%) with selectivities up to 90%. Mono-substituted alkyl substituted alkenes, such as 1-hexene, gave full conversions, with the production of internal hexenes (selectivity up to 43%), hexanes (selectivity up to 19%), and heptanols (selectivity up to 38%).



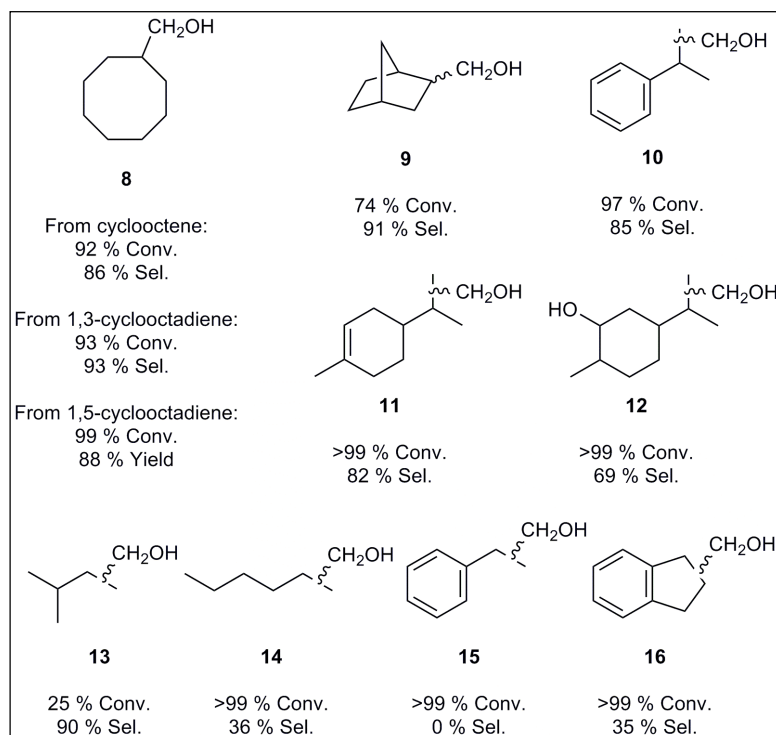


**Figure 3.17** Alkene conversion and alcohol selectivity obtained from the Ru-catalysed hydroformylation of alkenes using CO<sub>2</sub> as a CO source. Reaction conditions: alkenes (20.0 mmol), [BMMI•Cl] (5.1 mmol), 2,2'-disubstituted alkene /Ru = 64, IL/Ru = 16.3, H<sub>3</sub>PO<sub>4</sub>/ Ru = 3.0, 60 bar CO<sub>2</sub>/H<sub>2</sub> (1:1), and 120 °C for 17 h.

Whereas, substrates bearing alkenes conjugated with aromatic groups (styrene and indene) gave full conversions with high-hydrogenated product selectively. This behavior was ascribed to the relatively faster hydrogenation rate of the C=C bond of these type of substrates (terminal alkyl-substituted alkenes and substrates with alkenes conjugated to aromatic groups) when compared to the other two processes (reverse water gas shift and hydroformylation). However, the NMR characterization, and GC-analyzed spectras of all compounds, and reactions mixture are given in Chapter-6 (Figure 6.1-to 6.20)

### 3.4 Conclusions

In conclusion, Ru-hydride-carbonyl-carbene species formed in situ by reaction of [BMMI•Cl] or [BMMI•Cl] with Ru<sub>3</sub>(CO)<sub>12</sub> precursor. These Ru-species are

efficient catalyst for the cascade reactions of Reverse Water Gas-Shift, hydroformylation of alkenes, and hydrogenation using CO<sub>2</sub>. The reductive conversion of CO<sub>2</sub> to CO is facilitated by the addition of H<sub>3</sub>PO<sub>4</sub>, and disubstituted alkenes are easily functionalised to alcohols through sequential hydroformylation-carbonyl reduction by hydride transfer and protonolysis mechanism. All these findings open a new window of opportunity to use abundant and cheap CO<sub>2</sub> as a source of CO for important industrial carbonylation processes, such as the production of fragrances.<sup>[67]</sup>

## 2.6 References

- [1] J. C. Chadwick, R. Duchateau, Z. Freixa, P. W. N. M. van Leeuwen, *Homogeneous Catalysts*, Wiley, **2011**.
- [2] P. W. N. M. van Leeuwen, *Homogeneous Catalysis: Understanding the Art*, Springer, **2004**.
- [3] G. Centi, E. A. Quadrelli, S. Perathoner, *Energy & Environmental Science* **2013**, *6*, 1711.
- [4] E. A. Quadrelli, G. Centi, J. L. Duplan, S. Perathoner, *Chemsuschem* **2011**, *4*, 1194.
- [5] U. Rodemerck, M. Holena, E. Wagner, Q. Smejkal, A. Barkschat, M. Baerns, *Chemcatchem* **2013**, *5*, 1948.
- [6] M. Peters, B. Kohler, W. Kuckshinrichs, W. Leitner, P. Markewitz, T. E. Muller, *ChemSusChem* **2011**, *4*, 1216.
- [7] M. Cokoja, C. Bruckmeier, B. Rieger, W. A. Herrmann, F. E. Kuhn, *Angew. Chem. Int. Ed.* **2011**, *50*, 8510.
- [8] C. Federsel, R. Jackstell, M. Beller, *Angew. Chem. Int. Ed.* **2010**, *49*, 6254.
- [9] K. Weissermel, H. J. Arpe, *Industrial Organic Chemistry*, Wiley-VCH GmbH & Company KGaA, **2003**.
- [10] G. W. Wong, C. R. Landis, *Angew. Chem. Int. Ed.* **2013**, *52*, 1564.
- [11] D. Crozet, A. Gual, D. McKay, C. Dinoi, C. Godard, M. Urrutigoity, J. C. Daran, L. Maron, C. Claver, P. Kalck, *Chem. Eur. J.* **2012**, *18*, 7128.
- [12] D. Crozet, D. McKay, C. Bijani, A. Gual, C. Godard, C. Claver, L. Maron, M. Urrutigoity, P. Kalck, *Dalton Trans.* **2012**, *41*, 3369.
- [13] M. Alhaffar, R. Suleiman, B. El Ali, *Catal. Commun.* **2010**, *11*, 778.
- [14] E. Airiau, C. Chemin, N. Girard, G. Lonzi, A. Mann, E. Petricci, J. Salvadori, M. Taddei, *Synthesis-Stuttgart* **2010**, 2901.
- [15] P. S. Bauerlein, I. A. Gonzalez, J. J. Weemers, M. Lutz, A. L. Spek, D. Vogt, C. Muller, *Chem. Commun.* **2009**, 4944.
- [16] T. O. Vieira, H. Alper, *Org. Lett.* **2008**, *10*, 485.
- [17] L. Wu, I. Fleischer, R. Jackstell, M. Beller, *J. Am. Chem. Soc.* **2013**, *135*, 3989.
- [18] B. Deb, B. J. Borah, B. J. Sarmah, B. Das, D. K. Dutta, *Inorg. Chem. Commun.* **2009**, *12*, 868.
- [19] M. A. Moreno, M. Haukka, A. Turunen, T. A. Pakkanen, *J. Mol. Catal. A* **2005**, *240*, 7.
- [20] L. Avila, T. A. Pakkanen, T. T. Pakkanen, O. Krause, *J. Mol. Catal.* **1992**, *73*, 325.
- [21] K. Takahashi, M. Yamashita, Y. Tanaka, K. Nozaki, *Angew. Chem. Int. Ed.* **2012**, *51*, 4383.
- [22] K. Takahashi, M. Yamashita, K. Nozaki, *J. Am. Chem. Soc.* **2012**, *134*, 18746.

- [23] K. Takahashi, M. Yamashita, T. Ichihara, K. Nakano, K. Nozaki, *Angew. Chem. Int. Ed.* **2010**, *49*, 4488.
- [24] C. P. Casey, *Chemcatchem* **2010**, *2*, 1209.
- [25] J. Zakzeski, H. R. Lee, Y. L. Leung, A. T. Bell, *Appl. Catal. A* **2010**, *374*, 201.
- [26] G. Wilkinson, F. G. A. Stone, E. W. Abel, *Comprehensive organometallic chemistry: the synthesis, reactions, and structures of organometallic compounds*, Pergamon Press, **1982**.
- [27] G. J. Kubas, *Chem. Rev.* **2007**, *107*, 4152.
- [28] B. Hamers, P. S. Baeuerlein, C. Muller, D. Vogt, *Adv. Synth. Catal.* **2008**, *350*, 332.
- [29] F. M. Geilen, B. Engendahl, M. Holscher, J. Klankermayer, W. Leitner, *J. Am. Chem. Soc.* **2011**, *133*, 14349.
- [30] D. Spasyuk, S. Smith, D. G. Gusev, *Angew. Chem. Int. Ed.* **2013**, *52*, 2538.
- [31] D. Spasyuk, S. Smith, D. G. Gusev, *Angew. Chem. Int. Ed.* **2012**, *51*, 2772.
- [32] Z. Han, L. Rong, J. Wu, L. Zhang, Z. Wang, K. Ding, *Angew. Chem.* **2012**, *51*, 13041.
- [33] S. Wesselbaum, T. Vom Stein, J. Klankermayer, W. Leitner, *Angew. Chem. Int. Ed.* **2012**, *51*, 7499.
- [34] C. A. Huff, M. S. Sanford, *J. Am. Chem. Soc.* **2011**, *133*, 18122.
- [35] K. Tominaga, Y. Sasaki, *J. Mol. Catal. A* **2004**, *220*, 159.
- [36] S. Jääskeläinen, M. Haukka, *Appl. Catal. A* **2003**, *247*, 95.
- [37] K. Tominaga, Y. Sasaki, *Catal. Commun.* **2000**, *1*, 1.
- [38] M.-L. Kontkanen, L. Oresmaa, M. A. Moreno, J. Janis, E. Laurila, M. Haukka, *Appl. Catal., A* **2009**, *365*, 130.
- [39] K. Tominaga, *Catal. Today* **2006**, *115*, 70.
- [40] K. Tominaga, Y. Sasaki, *Chem. Lett.* **2004**, *33*, 14.
- [41] K. I. Tominaga, Y. Sasaki, *Stud. Surf. Sci. Catal.* **2004**, *153*, 227.
- [42] H. Arakawa, M. Aresta, J. N. Armor, M. A. Barteau, E. J. Beckman, A. T. Bell, J. E. Bercaw, C. Creutz, E. Dinjus, D. A. Dixon, K. Domen, D. L. DuBois, J. Eckert, E. Fujita, D. H. Gibson, W. A. Goddard, D. W. Goodman, J. Keller, G. J. Kubas, H. H. Kung, J. E. Lyons, L. E. Manzer, T. J. Marks, K. Morokuma, K. M. Nicholas, R. Periana, L. Que, J. Rostrup-Nielson, W. M. Sachtler, L. D. Schmidt, A. Sen, G. A. Somorjai, P. C. Stair, B. R. Stults, W. Tumas, *Chem. Rev.* **2001**, *101*, 953.
- [43] V. K. Srivastava, P. Eilbracht, *Catal. Commun.* **2009**, *10*, 1791.
- [44] A. Wu, B. O. Patrick, B. R. James, *Inorg. Chem. Commun.* **2012**, *24*, 11.
- [45] A. E. Ledger, M. F. Mahon, M. K. Whittlesey, J. M. Williams, *Dalton Trans.* **2009**, 6941.
- [46] A. E. Ledger, P. A. Slatford, J. P. Lowe, M. F. Mahon, M. K. Whittlesey, J. M. Williams, *Dalton Trans.* **2009**, 716.
- [47] M. I. Bruce, M. L. Cole, R. S. Fung, C. M. Forsyth, M. Hilder, P. C. Junk, K. Konstas, *Dalton Trans.* **2008**, 4118.
- [48] W. A. Herrmann, M. Elison, J. Fischer, C. Köcher, G. R. J. Artus, *Chemistry (Weinheim an der Bergstrasse, Germany)* **1996**, *2*, 772.
- [49] C. E. Ellul, M. F. Mahon, O. Saker, M. K. Whittlesey, *Angewandte Chemie International Edition* **2007**, *46*, 6343.
- [50] J. A. Cabeza, I. del Río, D. Miguel, M. G. Sánchez-Vega, *Chemical Communications* **2005**, 3956.
- [51] N. D. Clement, K. J. Cavell, C. Jones, C. J. Elsevier, *Angewandte Chemie-International Edition* **2004**, *43*, 1277.
- [52] M. Besnard, M. I. Cabaco, F. V. Chavez, N. Pinaud, P. J. Sebastiao, J. A. Coutinho, Y. Danten, *Chem. Commun.* **2012**, *48*, 1245.
- [53] A. M. Voutchkova, M. Feliz, E. Clot, O. Eisenstein, R. H. Crabtree, *J. Am. Chem. Soc.* **2007**, *129*, 12834.
- [54] A. M. Voutchkova, L. N. Appelhans, A. R. Chianese, R. H. Crabtree, *J. Am. Chem. Soc.* **2005**, *127*, 17624.

- [55] R. F. R. Jazzar, S. A. Macgregor, M. F. Mahon, S. P. Richards, M. K. Whittlesey, *J. Am. Chem. Soc.* **2002**, *124*, 4944.
- [56] R. H. Crabtree, *Coordination Chemistry Reviews* **2013**, *257*, 755.
- [57] H. Lebel, M. K. Janes, A. B. Charette, S. P. Nolan, *Journal Of The American Chemical Society* **2004**, *126*, 5046.
- [58] H. M. Lee, D. C. Smith, Z. J. He, E. D. Stevens, C. S. Yi, S. P. Nolan, *Organometallics* **2001**, *20*, 794.
- [59] U. L. Dharmasena, H. M. Foucault, E. N. dos Santos, D. E. Fogg, S. P. Nolan, *Organometallics* **2005**, *24*, 1056.
- [60] Z. Strassberger, M. Mooijman, E. Ruijter, A. H. Alberts, A. G. Maldonado, R. V. Orru, G. Rothenberg, *Adv. Synth. Catal.* **2010**, *352*, 2201.
- [61] Z. Strassberger, M. Mooijman, E. Ruijter, A. H. Alberts, C. de Graaff, R. V. A. Orru, G. Rothenberg, *Appl. Organomet. Chem.* **2009**, *24*, 142.
- [62] C. L. Lund, M. J. Sgro, R. Cariou, D. W. Stephan, *Organometallics* **2012**, *31*, 802.
- [63] C. Gandolfi, M. Heckenroth, A. Neels, G. Laurency, M. Albrecht, *Organometallics* **2009**, *28*, 5112.
- [64] A. Prades, M. Viciano, M. Samáu, E. Peris, *Organometallics* **2008**, *27*, 4254.
- [65] M. Smiglak, J. D. Holbrey, S. T. Griffin, W. M. Reichert, R. P. Swatloski, A. R. Katritzky, H. F. Yang, D. Z. Zhang, K. Kirichenko, R. D. Rogers, *Green Chem.* **2007**, *9*, 90.
- [66] C. E. Ellul, M. F. Mahon, O. Saker, M. K. Whittlesey, *Angew. Chem. Int. Ed.* **2007**, *46*, 6343.
- [67] E. V. Gusevskaya, J. Jiménez-Pinto, A. Börner, *ChemCatChem* **2014**, *6*, 382.

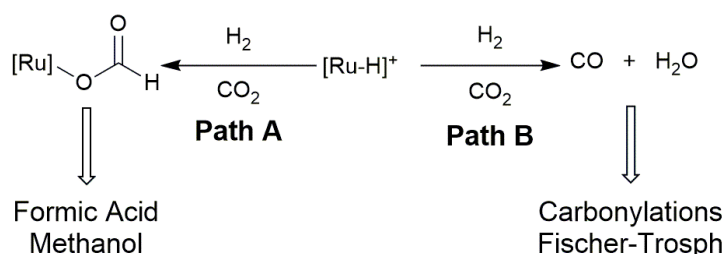
## **CHAPTER-4**

### **“Ruthenium Catalyzed Hydroaminomethylation, N-formylation with CO<sub>2</sub> in Ionic Liquid Media, and Mechanistic Insights”**

## 4.1 Introduction

Global warming, caused by man-made emission of greenhouse gases is threatening our climate. A main contributing factor is the large emission of CO<sub>2</sub> that accompanies the growing energy sector, which is still largely dependent on burning of fossil fuels. The abundance of CO<sub>2</sub> and the impending storage of fossil building blocks, has led to the proposal that CO<sub>2</sub> should be the C1-building block of the future. Ru-catalyzed carbonylations with CO<sub>2</sub> is receiving tremendous attention by the scientific community during the last decades. Concerning classical carbonylation processes (those in which CO is used as carbonylation reagent), Ru-catalytic systems displayed successful results in cascade reactions involving carbonylation steps, such as hydroformylation-hydrogenation [1-5] and hydroaminomethylation. [6] However, the major advantage of Ru-catalysts is their ability to reduce CO<sub>2</sub> into CO, and water by Reverse Water Gas Shift reaction (RWGS) during carbonylation reactions. [7-10] This concept opened new applications with broader uses of this greener, renewable ubiquitous CO<sub>2</sub> source as C1-feedstock without logistic problems, but act as slowly reactive substrate. [11, 12] Indeed, at the industrial scale, carbonylations (ca. hydroformylation of alkenes) [13, 14] reactions are the most important applications of homogeneous catalysis, with over 9 million tons of so-called oxo-products are produced each year. [15] There are reports that carbonylations of alkenes using CO<sub>2</sub> as a CO source is a viable process when either Ru-based systems with LiCl salts dissolved in N-methyl-pyrrolidone (Chapter 3.1, Figure 3.1) [16-18] or in a biphasic imidazolium ILs/toluene [19-22] (Figure 4.1) was used. Advances in this area revealed the Ru-catalysed hydroformylation of 1-hexene (using CO<sub>2</sub> as the CO source) by using 1-butyl-3-methyl-imidazolium chloride salts [BMI•Cl] [23] and 1-butyl-3-methyl-imidazolium bis(trifluoromethyl sulfonyl)imide [BMI•NTf<sub>2</sub>] (15 equiv. IL/equiv. Ru), alcohol yields of up to 51% and 82%, respectively were achieved. [20] In the Ru-catalyzed carbonylations, it has been proposed that the first step of the reaction involves in the presence of cationic ruthenium-hydrido ([Ru-H]<sup>+</sup>) complexes and the addition of a proton source usually significantly improve the catalytic activity. These [Ru-H]<sup>+</sup> species can follow two paths: (a) formation of the reactive metal-formate intermediate (Scheme 4.1, path A) or (b) reduction to CO (Scheme 4.1, RWGS, Path

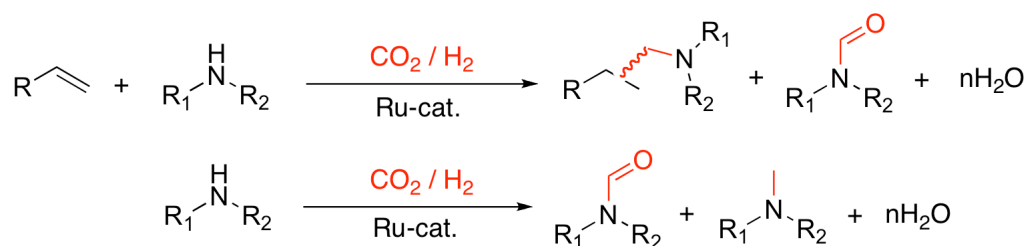
B). In other words, by controlling the reactivity of  $[\text{Ru-H}]^+$  species the incorporation can either use the formate intermediate to produce, for example, formic acid or methanol, or the RWGS to generate carbonylation products or Fischer-Tropsch products. More recently, we studied the Ru-catalysed hydroformylation of alkenes using  $\text{CO}_2$  as a CO source in the presence of  $[\text{BMI}\cdot\text{Cl}]$  and 3-*n*-butyl-1,2-dimethyl imidazolium chloride salts  $[\text{BMMI}\cdot\text{Cl}]$  (Chapter 2) under similar conditions to those previously reported in the literature (1.5% mol Ru, 60 bar,  $\text{CO}_2/\text{H}_2 = 1:1$ ,  $120^\circ\text{C}$ , 17 h). <sup>[24]</sup> NMR experiments using labelled  $^{13}\text{C}$  compounds ( $\text{CO}$ ,  $\text{CO}_2$  and  $^{13}\text{C}$ -2-BMI $\cdot\text{Cl}$ ), and ESI-MS mechanistic studies revealed the involvement of Ru-hydride-carbonyl-carbene complexes as active catalytic species for the RWGS reaction.



**Scheme 4.1** Possible pathways involved in the hydrogenation of carbon dioxide by  $[\text{Ru-H}]^+$  catalytic active species.

We also observed that the use of phosphines (ca.  $\text{PPh}_3$ ) and diphosphines (dppm, dppe, dppp, and Xantphos) as metal modifiers resulted in poor selectivities to the formation of carbonylation products with high selectivity to the hydrogenation of the alkenes. In contrast, monophosphites ( $\text{P}(\text{OEt})_3$ ) provided an improvement of both the catalytic activity and selectivity. However,  $^{31}\text{P}$  NMR experiments revealed that this apparent ligand effect was caused by the formation of  $\text{H}_3\text{PO}_4$  under reaction conditions (Chapter 3, Figure 3.3). Other research groups also observed the beneficial effect in terms of activity and selectivity by using of phosphite ligands as additives. The reactions promoted by  $\text{Ru}_3(\text{CO})_{12}$  (1.5% Ru, 60 bar  $\text{CO}_2/\text{H}_2 = 1:1$ ,  $130^\circ\text{C}$ , 24 h) in the presence of LiCl salts dissolved in N-methylpyrrolidone. <sup>[25]</sup> But the highest TONs were obtained in our previous study by using  $\text{H}_3\text{PO}_4$  and 1.5% mol Ru after shorter reaction times (ca. 17 h, chapter 3,

Table 1). Apart from hydroformylation, the use of LiCl-benzyl triethyl ammonium chloride (BTAC; Figure 4.1) salts as additives in the Ru-catalysed hydroaminomethylation of cyclopentene with morpholine using CO<sub>2</sub> as a CO source, the product yield was up to 98% after long reaction periods (5 days), under the harsh reaction conditions (160 °C and 80 bar) but using a large amount of metal (6% mol. of Ru).<sup>[26]</sup> But the active Ru-hydride-carbonyl-carbene species strongly promoted the Reverse Water Gas Shift reaction (RWGS), *in situ* generation of syngas (CO/H<sub>2</sub>) by using CO<sub>2</sub>/H<sub>2</sub> as greener source of C1-feedstock. The reaction was accelerated by adding H<sub>3</sub>PO<sub>4</sub> as additive for the conversion of CO<sub>2</sub> into CO source. The catalytic species simultaneously further sponsored the hydroformylation-hydrogenation by hydride transfer and protonolysis.<sup>[24]</sup> Thus the phosphines-free, well-developed simple Ru-catalytic system turned our attention toward the hydroaminomethylation of alkenes, and N-formylation of amines with CO<sub>2</sub> as C1-feedstock under the same reaction condition (Scheme 4.2).



**Scheme 4.2** Hydroaminomethylation of alkenes, N-formylation/N-methylation of amines using CO<sub>2</sub>/H<sub>2</sub> as source of CO/H<sub>2</sub> syngas.

First, investigated the selective hydroaminomethylation of alkenes, and N-formylation of amines with CO<sub>2</sub> as CO source in the presence of H<sub>3</sub>PO<sub>4</sub>. Then the same Ru-catalytic system probed for the N-formylation Vs N-methylation of aniline by using of mono or bi-dentate phosphines additives. Further investigated the mechanistic pathways for the hydroaminomethylation of alkenes by testing the activity of Ru-catalyst comparatively, and competitively (reductive amination, reduction of amide, and reaction between amines and alkenes) under the same reaction condition. Hydroaminomethylation could involve in sequence of Reverse Water Gas Shift (RWGS) reaction / hydroformylation of alkenes/and then reductive amination.



## 4.2- Experimental

### 4.2.1- General considerations:

Reagents and solvents were purified when required by following standard procedures [W. L. F. Armarego, D. D. Perrin, Purification of Laboratory Chemicals, Oxford (UK), 4th ed., Butterworth-Heinemann, 1997]. The imidazolium ionic liquids (1-butyl-3-methyl-imidazolium chloride [BMI•Cl] and 1-butyl-2,3-dimethyl-imidazolium chloride [BMMI•Cl]) were prepared by using the well-developed experimental in our laboratory (see Chapter 2). The ruthenium precursor triruthenium dodecarbonyl ( $\text{Ru}_3(\text{CO})_{12}$ ) was purchased from Johnson & Mathey.  $\text{H}_2$  (> 99.999%) and  $\text{CO}_2$  (> 99.999%) were purchased from White-Martins Ltd Brasil. Additives/ P-ligands, such as triethyl phosphite ( $\text{P}(\text{OEt})_3$ ), phosphoric acid ( $\text{H}_3\text{PO}_4$ ), and phosphines ( $\text{PPh}_3$ ), diphenylphosphine-methane (dppm), diphenylphosphine-ethane (dppe), diphenylphosphine-propane (dppp) and Xanthphos (Xanth.) were purchased from Sigma-Aldrich. Amines (morpholine, pyrrolidine, butylamine, aniline, and diethylamine), alkenes (Cyclohexene, 1-hexene, 1-octene, 1,5-cyclooctadiene, 1,3-cyclooctadiene,  $\alpha$ -methylstyrene, limonene, norbornene, styrene, (*R*)-(+)-Limonene and (*R*)-(-)-Carvone and aldehydes (Benzaldehyde and furfural) were purchased from Sigma-Aldrich. GC-FID analyses were run with an Agilent GC System 6820 (column DB-17; T injector = 250 °C; P=103 kPa; T program =10 min at 40 °C, 10°C/min until 250 °C, then 10 min at 250 °C). GC-MS analyses were run with a Shimadzu GC System QP50 (column DB-17; T injector = 250 °C; P=103 kPa; T program =10 min at 40 °C, 10°C/min until 250 °C, then 10 min at 250 °C; EI = 70 eV).  $^1\text{H}$ ,  $^{13}\text{C}$ , COSY and HSQC NMR analysis were performed on a Varian 400 MHz at the CNANO/UFRGS using  $\text{CDCl}_3$  as a solvent. Chemical shifts (ppm) are given relative to TMS in  $^1\text{H}$  NMR and  $\text{CDCl}_3$  in  $^{13}\text{C}$  NMR. Signals were assigned as s (singlet), d (doublet), t (triplet), dd (doublet of doublet), m (multiplet) and br. s (broad singlet).

### 4.2.2- N-formylation:

In a typical experiment, the corresponding amine (20.0 mmol) was added to a 100 mL reactor vessel (Parr Micro-reactor 4590, see Chapter 3, Figure 3.16)

containing the  $\text{Ru}_3(\text{CO})_{12}$  precursor (0.5 mol %) and the imidazolium IL. Then added 3 equiv. mol of common additive  $\text{P}(\text{OEt})_3$ ,  $\text{H}_3\text{PO}_4$  as reaction promoter for the N-formylation reaction. While in case of reaction optimization for the aniline N-formylation / N-methylation added 3 equiv. mol of various phosphines ( $\text{PPh}_3$ ), diphenylphosphine-methane (dppm), diphenylphosphine-ethane (dppe), diphenylphosphine-propane (dppp) and Xanthphos (Xanth.) in the reactor. The reactor was pressurized with 60 bar  $\text{CO}_2/\text{H}_2$  (1:1) and warmed to the desired reaction temperature 120-140°C for 17-24 h. The reactor was cooled down, depressurized, and the products were extracted with  $\text{CH}_2\text{Cl}_2$  (3 x 15 mL). The products were determined by GC, GC-MS-FID, and NMR analysis. The conversion of substrate, and selectivity of products were quantified by GC-FID analysis by using *n*-heptane as the internal standard. Then removed volatiles from the reaction mixture of organic phase and characterized by NMR analysis. GC, and NMR spectrums of the all N-formylated compounds are given in Chapte-6 (Figures 6.21-6.34).

#### 4.2.3- Hydroaminomethylation:

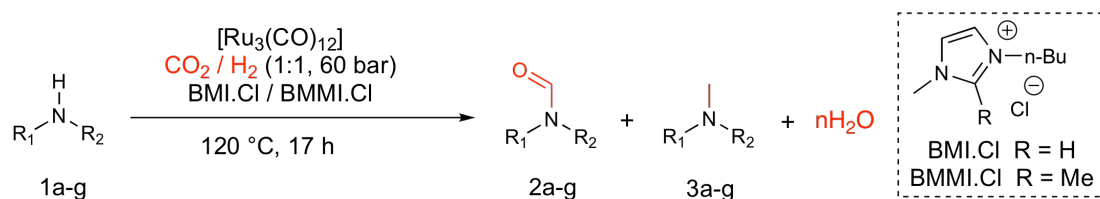
Hydroaminomethylation experiments were carried out by adding the corresponding 20.0 mmol of alkenes, and 20.0 mmol of amines in a 100 mL reactor vessel (Same Parr Micro-reactor 4590) containing the  $\text{Ru}_3(\text{CO})_{12}$  precursor (0.5 mol %) and the imidazolium IL/Ru (16.3 equiv.). Then added 3 equiv. mol additives/Ru such as  $\text{P}(\text{OEt})_3$ , or  $\text{H}_3\text{PO}_4$ . The reactor was pressurized with 60 bar  $\text{CO}_2/\text{H}_2$  (1:1), and warmed at 120 °C for 24 h. Cool down the reactor, and depressurized. Then organic-phase of reactions extracted with EtOAc (3 x 15 mL). The products were determined, and quantified by GC-MS, GC-FID analysis. The conversion of substrates, and selectivity, and yield of compounds were determined by GC-FID analysis by using *n*-heptane as the internal standard. Then the dried reactions mixtures were characterized by  $^1\text{H}$ ,  $^{13}\text{C}$  NMR studies after removed the volatiles under reduced pressure. The relevant GC, and NMR spectrums of the all hydroaminomethylation reactions are given as supporting information in Chapter-6, (Figures 6.35-6.56).

#### 4.2.4- Reductive amination:

Generally the reductive amination reactions were carried-out by adding corresponding aldehyde (20.0 mmol) and amine (20.0 mmol) in a 100 mL reactor vessel (Same reactor) containing the  $\text{Ru}_3(\text{CO})_{12}$  precursor (0.75 mol %) and the imidazolium IL (2.5 mol%), 3 equiv  $\text{H}_3\text{PO}_4/\text{Ru}$ . In case of reactions with benzaldehyde, and amines (aniline, morpholine) reactor was pressurized either with the mixture of  $\text{CO}_2/\text{H}_2$  (1:1, 60 bar), or only  $\text{H}_2$  (20 bar), while in the case of reductive amination of 2-furfuraldehyde with pyrrolidine reactor was pressurized with 20 bar  $\text{H}_2$ . Reactions were warmed at 120 for 17 h. Then cooled down and depressurized the reactor. Organic phase or reactions mixtures were extracted with  $\text{CH}_2\text{Cl}_2$  (3 x 15 mL). The products were characterized and determined by NMR and GC-MS analysis. Conversion, selectivity, and yields were quantified by GC-FID analysis by using *n*-heptane as the internal standard. All GC, NMR spectrums of the hydroaminomethylation reactions, and (Chap-6, Figures 6.57-6.62).

### 4.3- Results and Discussion

#### 4.3.1- N-formylation/N-methylation of amines:

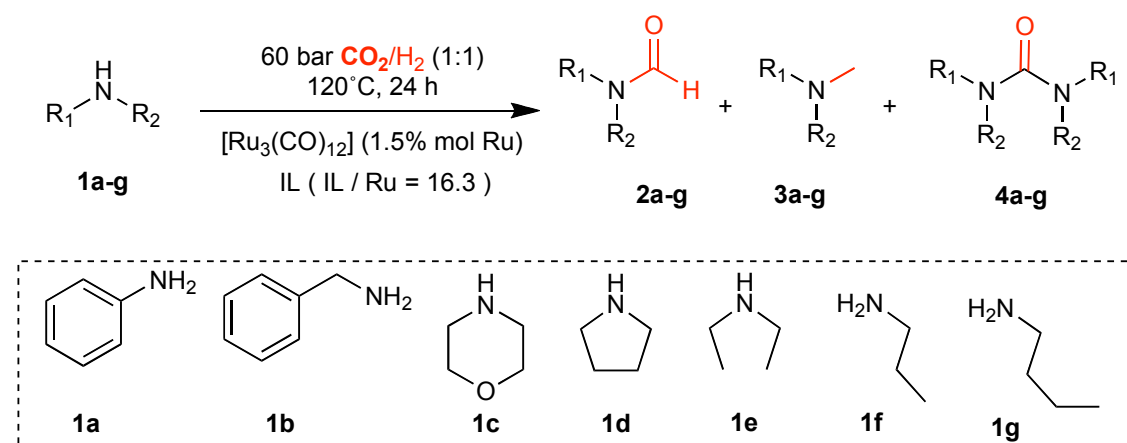


**Scheme 4.3** Ru-catalyzed N-formylation/N-methylation of amines using  $\text{CO}_2$  as a CO source in the presence of ionic liquids [BMI•Cl] or [BMMI•Cl].

As a general procedure for the N-formylations reactions: the corresponding amine was mixed with a solution of the catalytic precursor  $\text{Ru}_3(\text{CO})_{12}$  (0.5 mmol%) in the appropriate imidazolium salts ([BMMI.Cl] or [BMI.Cl]). The reactions were carried out at 120 °C under 60 bar  $\text{CO}_2/\text{H}_2$  (1:1) for 17 h. Summarized the obtained

results for the Ru-catalysed phosphine free N-formylation or N-methylation of various amines (**1a-g**, in Table 4.1) under the optimised reaction condition.

**Table 4.1** Ru-catalysed N-formylation of amines using CO<sub>2</sub> as a CO source in the presence of ionic liquids [BMI•Cl] and [BMMI•Cl]



E.[a,b]	1	IL	Add.[c]	Conv. 1/%	Sel. 2/%	Sel. 3/%	Sel. 4/%
1	1c	[BMI•Cl]	-	65	>99	0	0
2	1c	[BMMI•Cl]	-	21	>99	0	0
3	1c	[BMI•Cl]	P(OEt) <sub>3</sub>	98	>99	0	0
4	1c	[BMMI•Cl]	P(OEt) <sub>3</sub>	95	>99	0	0
5	1c	[BMI•Cl]	H <sub>3</sub> PO <sub>4</sub>	99	>99	0	0
6	1c	[BMMI•Cl]	H <sub>3</sub> PO <sub>4</sub>	97	>99	0	0
7 <sup>[d]</sup>	1c	[BMMI•Cl]	H <sub>3</sub> PO <sub>4</sub>	98	>99	0	0
8 <sup>[d]</sup>	1c	[BMMI•Cl]	H <sub>3</sub> PO <sub>4</sub>	95	>99	0	0
9	1d	[BMMI•Cl]	H <sub>3</sub> PO <sub>4</sub>	99	>99	0	0
10	1e	[BMMI•Cl]	H <sub>3</sub> PO <sub>4</sub>	94	>99	0	0
11	1f	[BMMI•Cl]	H <sub>3</sub> PO <sub>4</sub>	93	85	0	15
12	1g	[BMMI•Cl]	H <sub>3</sub> PO <sub>4</sub>	87	87	0	13
13	1b	[BMMI•Cl]	H <sub>3</sub> PO <sub>4</sub>	89	86	0	14
14	1a	[BMMI•Cl]	H <sub>3</sub> PO <sub>4</sub>	22	0	0	>99

[a] Reaction conditions: **1a-g** (20.0 mmol), ionic liquid (IL, 5.1 mmol), 0.5% mol of [Ru<sub>3</sub>(CO)<sub>12</sub>] (1.5 mol % Ru), 60 bar CO<sub>2</sub>/H<sub>2</sub> (1:1), 120 °C, 17 h. [b] Conversion of **1a-g** and selectivity of products determined by GC-MS and GC FID analysis by using *n*-heptane as internal standard. [c] Additive/Ru = 3.0; [d] 60 bar CO<sub>2</sub>/H<sub>2</sub> (1:5).

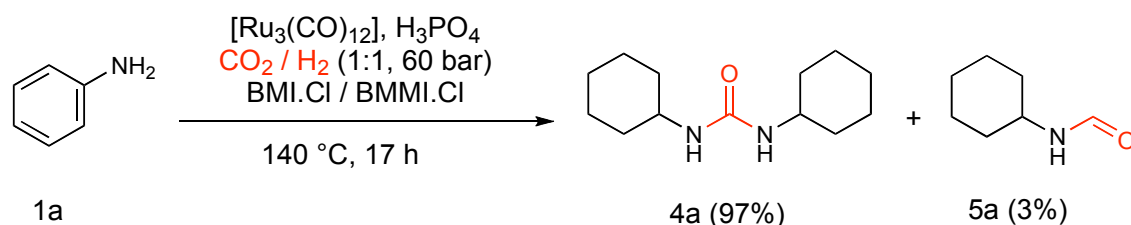
Morpholine (**1c**) was used as model substrate, and investigated the effect of additives by comparing the obtained results in the presence or absence of triethoxyphosphite [P(OEt)<sub>3</sub>], or phosphoric acid (H<sub>3</sub>PO<sub>4</sub>) (Entries 1-6, Table 4.1). The results demonstrated the formation of only *N*-formylated product (Sel. **2c** up to > 99%), and no *N*-methylation product (**3c**) is observed even in the presence of a large excess of hydrogen (H<sub>2</sub>/CO<sub>2</sub> = 5: 1, Entries 7-8, Table 4.1). This is a clear indication that our catalytic system does not catalyses the hydrogenation of the formamides as it promoted by other Ru-phosphine modified catalysts.<sup>[27, 28]</sup> Selectively *N*-formylated products **2c-2e** were exclusively formed when secondary amines (**1c-e**) were reacted with CO<sub>2</sub> as CO source (Entries 8-10, Table 4.1). But in the case of *n*-propyl (**1f**), *n*-butyl (**1g**) and benzyl amine (**1b**), indicated moderate-to-high conversions (ca. 87-93%) of the primary amine with high *N*-formylated product (**2b, 2f** and **2g** Sel. = 85-87%, Entries 11-13, Table 4.1) selectivity together with minor amounts of the corresponding urea (**4b, 4f**, and **4g** Sel. = 13-15%).

However, primary amines, and aniline undergoes further transformation to produce urea adducts (4a-b, 4f-g). Which, probably results from the reaction of unreacted primary amines with their corresponding *N*-formamides. It indicated that the primary amines, and aniline is less active toward *N*-formylation with CO<sub>2</sub> than secondary amines because of having less nucleophilicity/basicity comparatively. Thus in conclusion, the generated phosphine-free Ru-catalytic species are inactive for the further reduction of *N*-formamides/urea into corresponding *N*-methyl/*NN*-methylene products. All the reaction selectively formed *N*-formamines, no *N*-methylation product is detected during the *N*-formylation of various amine in the presence of P(OEt)<sub>3</sub>, and H<sub>3</sub>PO<sub>4</sub>. Conversions of reactions, and selectivity of products were determined GC-MS, GC FID analysis of the organic phase by using *n*-heptane as internal standard. Organic phase from the crude reactions mixtures were obtained by extraction with (3x5 mL, AcOEt) solvent. Then the *N*-formylated, and urea products were characterized by <sup>1</sup>H and <sup>13</sup>C NMR analysis after removal of the volatiles from reaction mixtures under reduced pressure. The NMR, and GC spectrums of all compounds are given in Chapter-6, Figures 6.21-6.34.

But In the case of aniline (**1a**), under the same reaction condition: revealed low conversion (22 %), and significantly indicated a unique product 1,3-dicyclohexylurea was selectively formed (**4a** Sel. = 99 %, Entries 14, Table 4.1). It indicated aromaticity of the aniline loss during the reaction, and selectively produced 1,3-dicyclohexylurea (**4a**). Uniqueness, and low conversion of aniline reaction turned our attention for the further optimization of reaction condition.

### 4.3.2- N-formylation / N-methylation of aniline

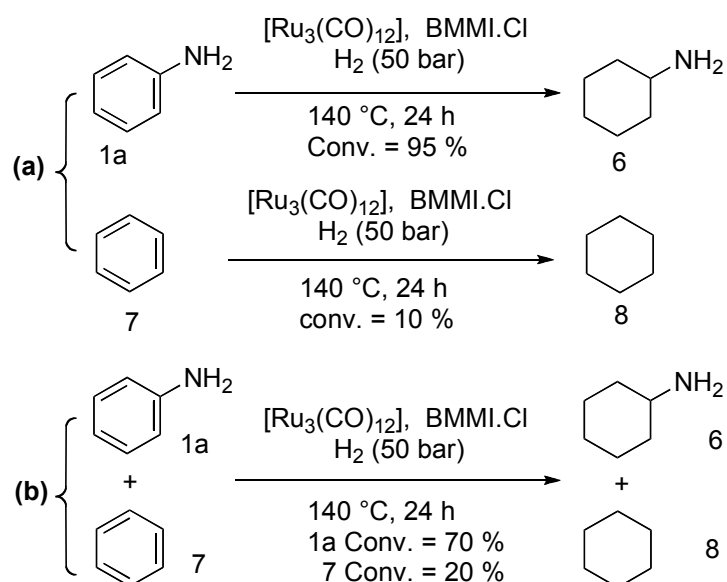
Initially, reaction was optimized for the N-formylation Vs N-methylation of aniline at 140 °C, by using P(OEt)<sub>3</sub> and H<sub>3</sub>PO<sub>4</sub> additives (Table 4.2). The N-formylation of aniline under the optimized reactions condition (Entries 1-6, Table 4.2) revealed surprisingly the main product in all cases was 1,3-dicyclohexylurea (**4a**) (Sel. up to = 99%), and also a drastic increase in the catalytic activity was achieved by using P(OEt)<sub>3</sub> and H<sub>3</sub>PO<sub>4</sub> as additives (Table 4.2). But interestingly during the reactions by using P(OEt)<sub>3</sub> and H<sub>3</sub>PO<sub>4</sub> as additives, traces of N-methylation of aniline was also detected at 140 °C (**3a** Sel. =1%, Entries 3-6, Table 4.2)



**Scheme 4.4** N/formylation of aniline by increasing temperature. Reaction conditions: aniline (20.0 mmol), BMMI.Cl/BMI.Cl (5.1 mmol), Ru<sub>3</sub>(CO)<sub>12</sub> (1.5 mol%), 60 bar CO<sub>2</sub>/H<sub>2</sub> (1:1), H<sub>3</sub>PO<sub>4</sub>, (4.5 mol%), 140 °C, 17 h.

High selectivity of 1,3-dicyclohexylurea (**4a**) as a main product with aniline reaction under the optimized condition: indicated that the Ru-catalytic species initially reduced aniline into cyclohexylamine (**6**), which led into formation of 1,3-dicyclohexylurea. Aromaticity of aniline loss due to presence of ring activating

group, or can be Ru-clusters or colloidal of Ru-nanoparticles were probably formed, since these species were well-known as the catalytic active specie for the hydrogenation of the aromatic ring instead of the carbonyl group. Indeed, it is known that the preferential reduction of arene rings in front of carbonyl groups (urea function) is catalyzed by metal nanoparticles rather than by monometallic complexes.<sup>[29, 30]</sup> However under the similar reaction conditions: the ability of Ru-catalyst was evaluated for the hydrogenation of aromatic rings (Scheme 4.5 a, b). (a) Indicating hydrogenation of aniline (20 mmol) into cyclohexylamine (Conv. = 95 %), and benzene (20 mmol) into cyclohexane (Conv. = 10 %, Scheme 4.5 a) by using 50 bar H<sub>2</sub> gas. While in case of (b) catalyst was tested by using a mixture of aniline and benzene (1:1, 40 mmol), indicated increases in the conversion of benzene (**1a** Conv. = 70 %, **7** Conv. = 20 %, Scheme 4.5 b).

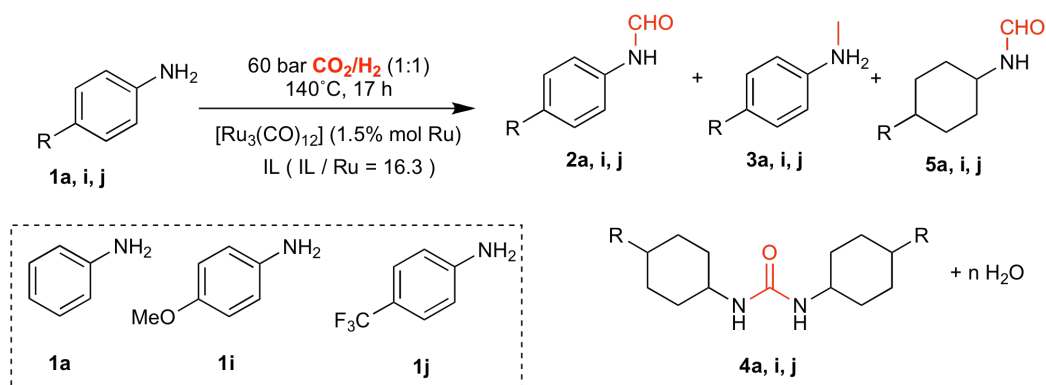


**Scheme 4.5** Ru-catalyzed hydrogenation of aniline, and benzene: (a) single substrate reactions by using 20 mmol of each one, (b) mixture of **1a,7** (1:1, 40 mmol), Reaction condition: [Ru<sub>3</sub>(CO)<sub>12</sub>] (1.5 mol%), BMMI.Cl (15.1 mmol), and H<sub>3</sub>PO<sub>4</sub> (4.5 mol%) 50 bar H<sub>2</sub>, 140 °C, 24 h.

Further the same reaction was repeated in the presence of 60 bar CO<sub>2</sub>/H<sub>2</sub> (1:1) under same reaction condition, which used for the N-formation of aniline. Benzene partially hydrogenated (Conv. = 4-5%), while aniline (Conv. = 60 %)

produced a mixture of corresponding N-formylation products: N-cyclohexylformamide (14%), 1,3-dicyclohexaneurea (85%), N-methylaniline (1-2%).

**Table 4.2** Ru-catalysed N-formylation of aniline using CO<sub>2</sub> as a CO source.<sup>[a,b]</sup>



E.	1	IL	Add. [c]	Conv.	Sel. 2	Sel. 3	Sel. 5	Sel. 4
1	1a	[BMI·Cl]	-	35	0	0	0	>99
2	1a	[BMMI·Cl]	-	30	0	0	0	>99
3	1a	[BMI·Cl]	P(OEt) <sub>3</sub>	95	0	1	2	97
4	1a	[BMMI·Cl]	P(OEt) <sub>3</sub>	93	0	1	1	98
5	1a	[BMI·Cl]	H <sub>3</sub> PO <sub>4</sub>	97	0	1	2	97
6	1a	[BMMI·Cl]	H <sub>3</sub> PO <sub>4</sub>	96	0	1	1	98
7	1a	[BMMI·Cl]	PPh <sub>3</sub>	15	0	23	57	20
8	1a	[BMMI·Cl]	Dppm	18	0	22	55	23
9	1a	[BMMI·Cl]	Dppe	7	0	>99	0	0
10	1a	[BMMI·Cl]	Dppp	16	0	>99	0	0
11	1a	[BMMI·Cl]	Xanth.	27	0	>99	0	0
12	1i	[BMMI·Cl]	H <sub>3</sub> PO <sub>4</sub>	>99	15	48	7	30
13	1j	[BMMI·Cl]	H <sub>3</sub> PO <sub>4</sub>	>99	0	0	7	93

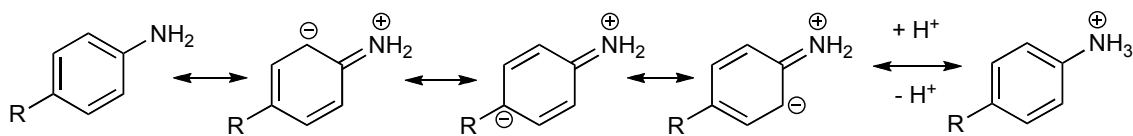
[a] Reaction condition: amine (20.0 mmol), ionic liquid (5.1 mmol), [Ru<sub>3</sub>(CO)<sub>12</sub>] (1.5 mol % Ru), 60 bar CO<sub>2</sub>/H<sub>2</sub> (1:1), 140 °C, 17 h; [b] %: Conversion and selectivity products determined by GC-MS and GC-FID analysis by using *n*-heptane as internal standard; [c] Additive/Ru = 3.0 equiv. L / equiv. Ru ; [d] 120°C.



Consequently, N-formylation Vs N-methylation reaction of aniline further extensively investigated by using other phosphines additives, such as triphenylphosphine (**PPh<sub>3</sub>**), diphenylphosphine-methane (**dppm**), diphenylphosphine-ethane (**dppe**), diphenylphosphine-propane (**dppp**) and Xanthphos (**Xanth.**) (Entries 7-11, Table 4.2). PPh<sub>3</sub> and dppm produced very similar results in terms of activity (22-23 % of Conv.) and product selectivity (in these cases, the major compound is **5a**). The very similar results between PPh<sub>3</sub> and dppm were attributed to the possibility that dppm was coordinated as a monodentate ligand. For the case of diphenylphosphine-ethane (**dppe**), diphenylphosphine-propane (**dppp**) and Xanthphos (**Xanth.**), the activity of the catalytic system increased with the size of the bite angle, whereas full selectivities to the formation of N-methylation compound (**3a**) were observed. Thus it indicated in the presence stable phosphine ligands the generated Ru-carbonyl-carbene-phosphine species promote the reduction of N-formamide (**2a**) into N-methylation product (**3a**).

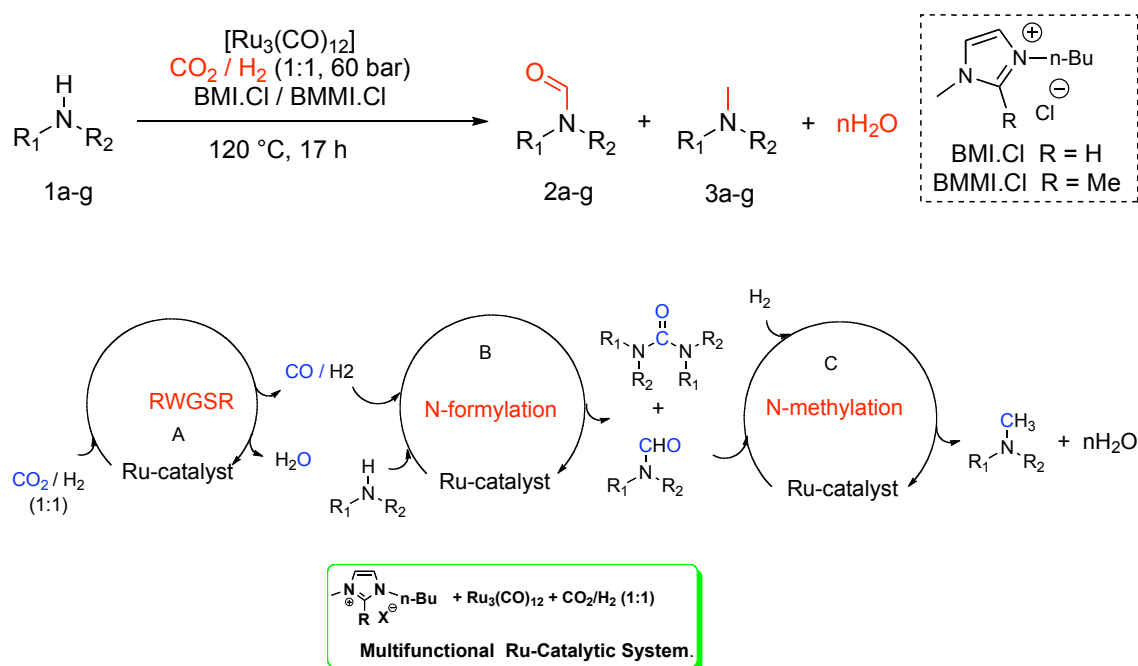
It is reported that the Ru-complexes mainly associated with triphos also catalyze the reductive methylation of imines,<sup>[31]</sup> amines<sup>[32]</sup> and C-H bonds<sup>[33]</sup>, as well as, the reduction of CO<sub>2</sub> to methanol.<sup>[34]</sup> Apparently, in the later cases there is the involvement of [Ru-H]<sup>+</sup> species and the activation of CO<sub>2</sub> follows similar paths (hydride transfer and protonolysis) proposed for the reduction of carboxylate groups.<sup>[35]</sup> Probably, ligands with larger bite-angles favoured the formation of [Ru-H]<sup>+</sup> species, and thus increased the catalytic activity to the formation of N-methylation products. Finally, in order to confirm the effect of the basicity of the amine in its tendency to form the N-formylation or N-methylation products, p-anisidine (**1i**) (pKa = 5.3) and p-trifluoromethyl-aniline (**1j**) (pKa = 3.5) results were compared to those obtained using aniline (**1a**) (pKa = 4.6). The lone pair of electrons on the nitrogen of aniline are conjugated to the  $\pi$ -electrons of the aromatic ring and are therefore it represented the following resonating sequences (see Scheme 4.6). Thus the expected tendency that anilines with electron-withdrawing groups produced larger amounts of compounds with the hydrogenated aromatic ring (compounds **4j** and **5j**), while anilines with electron-donating groups was selectivity formed N-methylation/formylation of aniline and

revealed low selectivity of ring hydrogenated products (Entries 6, 12 and 13, Table 4.2)



**Scheme 4.6** Aniline resonance species, and its relationship with the product selectivity.

So, *in-situ* generated Ru-hydride-carbonyl-carbene species could be promoted the N-formylation and N-methylation of amines with CO<sub>2</sub> (Scheme 4.7) in sequences of RWGSR/N-formylation/reduction of amide into amines by hydride transfer and protonolysis mechanism.



**Scheme-4.7** Ru-catalysed Reaction mechanism for the N-formylation and N-methylation amines with CO<sub>2</sub>/H<sub>2</sub>

### 4.3.3- Hydroaminomethylation of alkenes with CO<sub>2</sub> as CO source

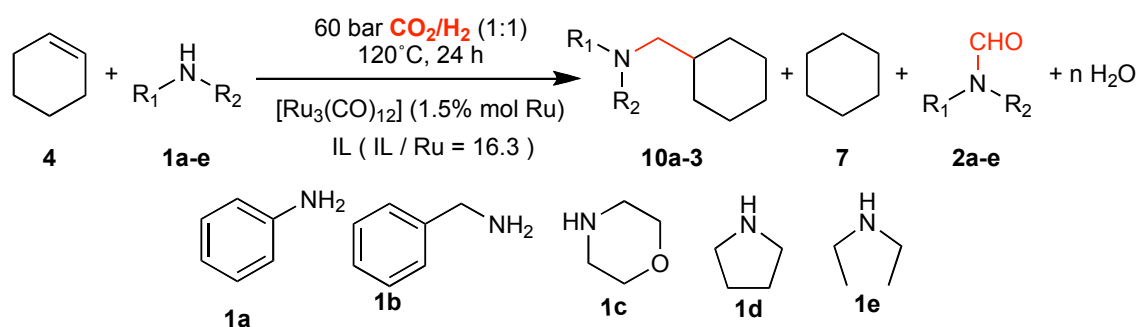
Most importantly, further the same Ru-catalytic system was extensively investigated for the hydroaminomethylation of alkenes with CO<sub>2</sub> as a CO source under the hydroformylation, and N-formylation reaction condition. Experiments were carried-out by dissolving [Ru<sub>3</sub>(CO)<sub>12</sub>] precursor in the 3-*n*-butyl-1-methyl imidazolium chloride salts [BMI•Cl] or 3-*n*-butyl-1,2-dimethyl imidazolium chloride salts [BMMI•Cl] ILs, under similar condition previously reported for the hydroformylation using CO<sub>2</sub> as a CO (1.5% mol Ru, 60 bar, CO<sub>2</sub>/H<sub>2</sub> = 1:1, 120°C, 17 h, Chapter 3).<sup>[24]</sup> It should be noted that our reaction conditions are milder than those reported in the literature,<sup>[26]</sup> and the amount of metal is also much lower. Furthermore, the activity of this Ru-catalytic system in the reductive amination, and *N*-formylation reactions was corroborated under same reaction condition.

The hydroaminomethylation of cyclohexene (**4**) with aniline (**1a**) was carried out using CO<sub>2</sub> as a CO source (entries 1-6, Table 4.3) using the same reaction conditions developed earlier for the hydroformylation of alkenes with CO<sub>2</sub>.<sup>[24]</sup> Cyclohexene conversions up to 99% after 17 h and selectivity up to 98% for product (**10**) were achieved. In all cases *N*-formylation (**2**) by-products were also observed indicating that both paths (A and B, Scheme 4.1) are operative under these reaction conditions. However, the RWGS pathway is predominant since the system is much selective to hydroaminomethylation reaction rather than *N*-formylation ones.

The use of the additive H<sub>3</sub>PO<sub>4</sub> or P(OEt)<sub>3</sub> (that undergoes hydrolysis to yield acids, under the reaction conditions used) produce an increase of the selectivity in the hydroaminoaminations products (**10**). This behaviour is similar to that previously described in the Ru-catalysed hydroformylation using CO<sub>2</sub> as a CO source and it was attributed to the fact that the acid likely facilitates hydride transfer and protonolysis, which are key steps for the addition of hydrogen to carboxylate groups.<sup>[24]</sup> The beneficial effect of protic additives in the hydroaminomethylation results was also previously ascribed to an increase in the imine hydrogenation activity. This is another indication that reaction proceeds

through RWGS, hydroformylation, imine-enamine formation and reduction (see below).

**Table 4.3** Ru-catalysed hydroaminomethylation of cyclohexene using CO<sub>2</sub> as a CO source.<sup>[a,b]</sup>



E.	1	IL	Add. <sup>[c]</sup>	Conv.	Sel.10	Sel.8	Yield 2
1	1a	[BMI·Cl]	-	79	66	34	13
2	1a	[BMMI·Cl]	-	68	49	51	2
3	1a	[BMI·Cl]	P(OEt) <sub>3</sub>	82	84	16	8
4	1a	[BMMI·Cl]	P(OEt) <sub>3</sub>	98	98	2	4
5	1a	[BMI·Cl]	H <sub>3</sub> PO <sub>4</sub>	96	95	5	8
6	1a	[BMMI·Cl]	H <sub>3</sub> PO <sub>4</sub>	99	98	2	3
7	1b	[BMMI·Cl]	H <sub>3</sub> PO <sub>4</sub>	27	57	43	85
8	1c	[BMMI·Cl]	H <sub>3</sub> PO <sub>4</sub>	57	65	35	32
9	1d	[BMMI·Cl]	H <sub>3</sub> PO <sub>4</sub>	84	88	12	17
10	1e	BMMI·Cl	H <sub>3</sub> PO <sub>4</sub>	36	64	36	16

[a] Reaction conditions: cyclohexene (20.0 mmol), **1a-d** (20.0 mmol), ionic liquid (5.1 mmol), [Ru<sub>3</sub>(CO)<sub>12</sub>] (1.5 mol % Ru), 60 bar CO<sub>2</sub>/H<sub>2</sub> (1:1), 120 °C, 24 h. [b] Conversion of **9** (%), yield of **2** (%) and selectivity (%) determined by GC-MS and GC-FID, [c] Additive/Ru = 3.0.

Other amines with distinct steric and electronic properties, such as benzylamine (**1b**), morpholine (**1c**), pyrrolidine (**1d**) and diethylamine (**1e**), were also evaluated in the hydroaminomethylation of cyclohexene (entries 7–10, Table

4.3). It should be noted that these results revealed that the *N*-formylation of the amines is a competitive process to the carbonylation of the alkenes, and thus higher *N*-formylation yields (**2**) reduced the selectivity to carbonylation products (**10**).

Our reported procedure is more efficient in terms of activity and productivity than those reported earlier for Ru-catalysed hydroaminomethylation of alkenes with secondary alkylic amines employing LiCl-benzyl triethyl ammonium chloride (BTAC) salts as additives, large amount of metal (6% mol. of Ru) under harsh reaction conditions (160 °C and 80 bar) and long reaction periods (5 days).<sup>[26]</sup> Furthermore, in general, the main drawback of the hydroaminomethylation reaction is that for primary amines the selectivity generally is low because of over-alkylation occurred.<sup>[41]</sup> Our catalytic system provided the formation of secondary amines from primary amines (**1a** and **1b**) with no formation of over-alkylated amine. This selectivity is probably due to the removing of the less soluble secondary amine from the catalyst containing IL phase. Nucleophilicity basicity and steric properties of amines could also play an important role in the selectivity of hydroaminomethylation and *N*-formylation products. Aniline with lowest nucleophilicity, basicity indicated highest activity in hydroaminomethylation (**10a** > 95%, Entry 4-6, Table 4.3), and least active toward *N*-formylation process (Entry 14, Table 4.1).

Furthermore, various cyclic and terminal alkenes were investigated for the hydroaminomethylation with CO<sub>2</sub> as CO source by using aniline as a choice of amine (see Figure 4.1). Under optimized reaction conditions, mono-substituted alkyl substituted alkenes, such as 1-hexene, 1-octene gave full conversion, with the production of the corresponding amines (**11a,b**) in high selectivities (selectivity up to 96%). Much lower selectivities in heptanols were previously obtained in the Ru-catalysed hydroformylation of 1-hexenes (Chap-3, Figure 3.2) under similar reaction conditions. Monosubstituted alkenes conjugated with aromatic groups (styrene) gave full conversions with high-hydrogenated product selectivity and low selectivity in the hydroaminomethylation product (**12**). This behavior was ascribed to the relatively faster hydrogenation rate of the C=C bond of these type of substrates (terminal alkyl-substituted alkenes and substrates with alkenes

conjugated to aromatic groups) when compared to the other two processes (reverse water gas shift and hydroformylation).

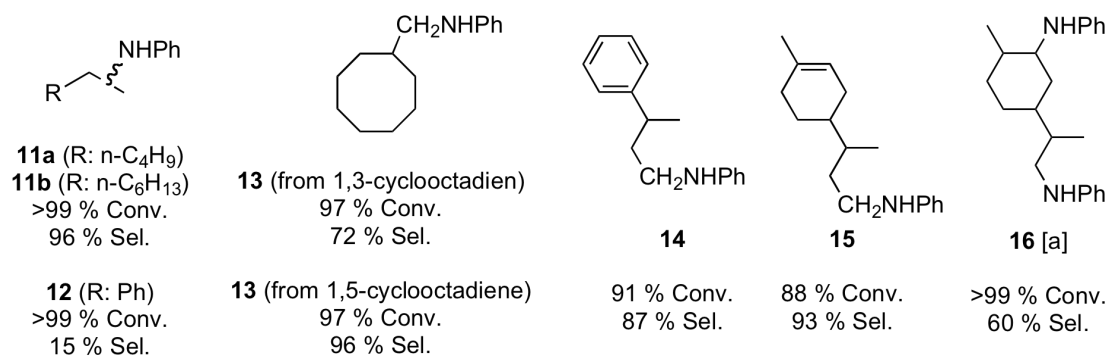
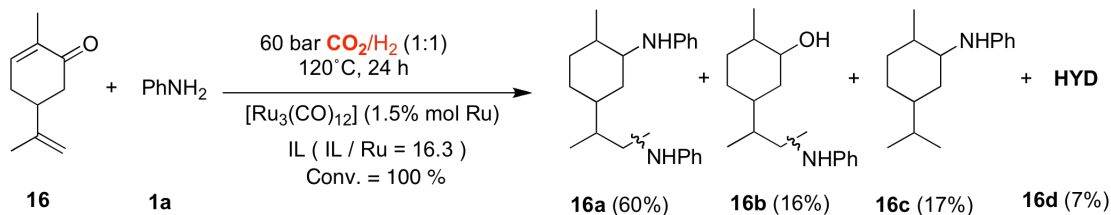


**Figure 4.1** Conversion of alkene (%) and amine selectivity (%) obtained in the Ru-catalysed hydroformylation of alkenes using CO<sub>2</sub> as a CO source. Reaction conditions: alkene (20.0 mmol), **1a** (21.5 mmol), ionic liquid (5.1 mmol), [Ru<sub>3</sub>(CO)<sub>12</sub>] (1.5 mol % Ru), H<sub>3</sub>PO<sub>4</sub>/ Ru = 3.0, 60 bar CO<sub>2</sub>/H<sub>2</sub> (1:1), 120 °C, 36 h. [a] **1a** (40.0 mmol).



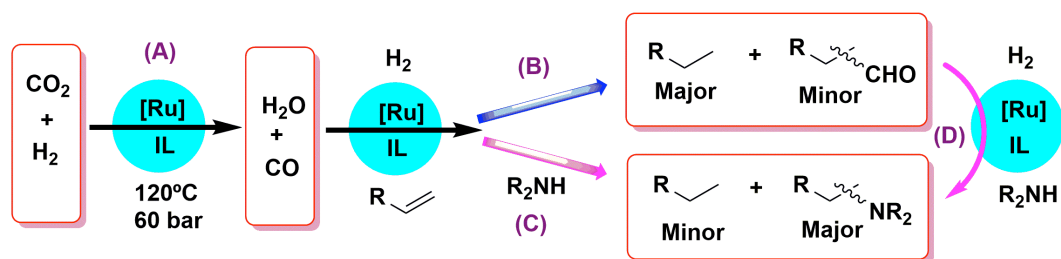
**Scheme 4.8** Hydroaminomethylation/reductive amination of carvone, Reaction conditions: Carvone (20.0 mmol), aniline (40.0 mmol), BMMI.Cl (5.1 mmol), Ru (1.5 mol%), H<sub>3</sub>PO<sub>4</sub> (4.3 mol %); 120 °C, 24 h, **HYD**= carvone hydrogenated products;

Cyclic disubstituted dienes (1,5-cyclooctadiene), cyclic disubstituted conjugated dienes (1,3-cyclooctadiene) and 2,2-disubstituted alkenes (methylstyrene, (R)-(+)-limonene and carvone) were easily hydroaminomethylated, thus leading to the amines **13-16** with moderate-to-high conversions (88% to >99%) and selectivities (60% to 96%). It should be remarked the special case of Carvone, which contained a carbonyl function which was transformed into corresponding amine **16a** by following a reductive

amination step. For this reason, the hydroaminomethylation of carvone was conducted using a carvone: aniline ratio of 1:2 under same reaction condition (Scheme 4.8). It revealed, that this catalyst is also active for the reductive amination. GC, NMR-spectrums of reactions are given in chap-6 (Figures 6.35-56).

#### 4.3.4- Mechanistic insights for the hydroaminomethylation

Reverse Water Gas Shift (RWGS) reaction is responsible for the reduction of CO<sub>2</sub> into CO, and water. The reaction commonly occurs during the carbonylation, N-formylation, urea synthesis, N-methylation, and alcohol formation by using of CO<sub>2</sub>/H<sub>2</sub> mixture. [36] Conventional catalysts required high temperature to promote the RWGS reaction, it is strongly endothermic ( $\Delta H_{298\text{ K}} = 41.2\text{ KJ/mol}$ ). But recent efforts are bringing effective homogeneous noble metal catalysts (such as, Pt, Ru, and Rh) and reaction promoters based in ionic additives (such as Li-salts, ILs, Chapter 3, Figure 3.1). Our previous study revealed that the Ru-hydride-cabene complex is active species for the RWGS reaction (Reduction of CO<sub>2</sub> into CO, and water) during hydroformylation of alkenes in the presence of phosphoric acid. [24] But no studies were reported for the Ru-catalyzed hydroaminomethylation of alkenes with CO<sub>2</sub> as a CO source. It was expected that this reaction (by comparison with the hydroaminomethylation using CO) followed the sequence of RWGS /carbonylation, /and reductive amination of the aldehyde formed during hydroformylating step in the presence of amine. [6]

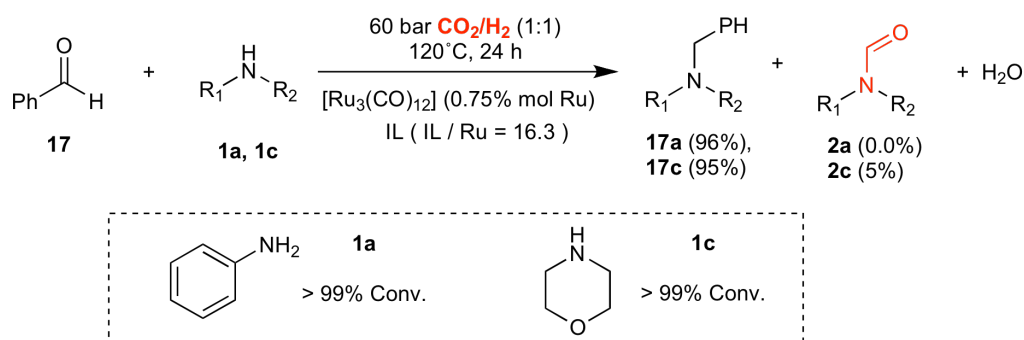


**Scheme 4.9** Main steps involved in the hydroaminomethylation of alkenes by [Ru<sub>3</sub>(CO)<sub>12</sub>]/IL catalytic system.

However further investigated the mechanistic insights, conducting various experiments comparatively and competitively by using the same Ru-catalyst (Scheme 4.10-4.12), under similar reaction condition, which commonly used for the hydroaminomethylation of alkenes.

#### 4.3.4.1 Reductive amination of aldehydes with amines

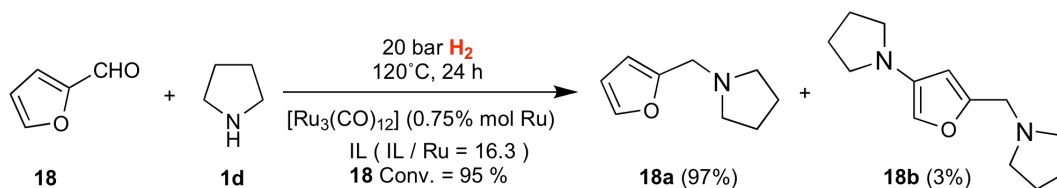
Ru-catalyzed reductive amination was investigated using benzaldehyde as model substrate with morpholine and aniline under same reaction condition (Scheme 4.8, 4.9) by using CO<sub>2</sub>/H<sub>2</sub> (1:1, 60 bar). The aim of study was find-out the reductive amination between initial oxo-product (aldehyde) of hydroformylation of alkenes with corresponding amines during hydroaminomethylation process. However the catalyst was tested for the reductive amination reaction by using benzaldehyde (10 mmol) with either 10 mmol of aniline or morpholine (Scheme 4.8). Results indicated high activity (Conv. > 99%), and selectivity of reductive amination products (**17a** = 96%, **17c** = 95%). Interestingly reaction with morpholine revealed N-fomylated side product (**2c** = 5%) in the presence of CO<sub>2</sub>/H<sub>2</sub> (1:1, 60 bar), and also traces of imines, and enamines intermediates were detected during GC, GC-MS analysis.



**Scheme 4.10** Reductive amination of benzaldehyde, reaction conditions: benzaldehyde (10 mmol), amines (10 mmol), BMMI.Cl (2.6 mmol), Ru<sub>3</sub>(CO)<sub>12</sub> (0.75 mol%), H<sub>3</sub>PO<sub>4</sub> (2.2 mol %); 60 bar CO<sub>2</sub>/H<sub>2</sub>(1:1), 120 °C, 24 h.



Then the same reactions were repeated by using only H<sub>2</sub> (20 bar) instead of using mixture of CO<sub>2</sub>/H<sub>2</sub> (1:1, 60 bar), reactions revealed > 99 % of reductive amination products. It indicated, Ru-catalyst highly promoting the reductive amination during hydroaminomethylation reaction. In the process hydrogenation of imines, and enamines intermediates led into corresponding secondary or tertiary amines.

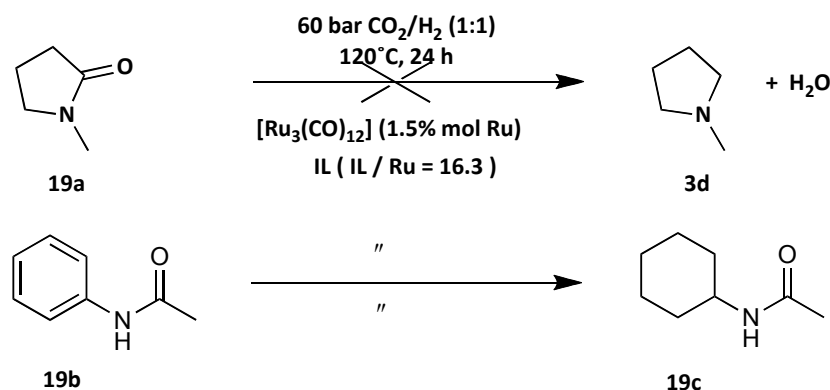


**Scheme 4.11** Reductive amination 2-furfuraldehyde (10 mmol), pyrrolidine (10.0 mmol), BMMI.Cl (2.6 mmol), alkene/Ru=67 (0.75 mol%), H<sub>3</sub>PO<sub>4</sub> (2.2 mol %); 120 °C, 24 h.

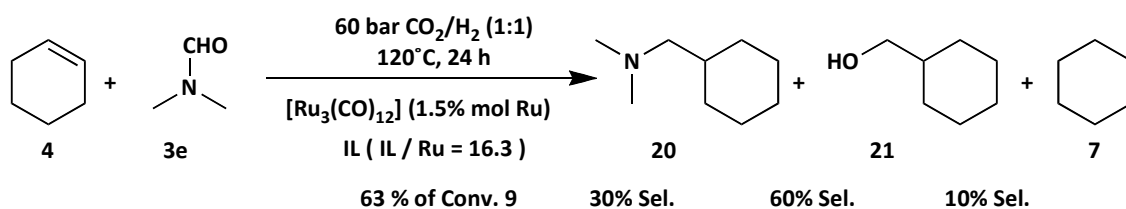
Finally, this new experimental applied for the reductive amination of furfural aldehyde with pyrrolidine (Scheme 4.11). Reaction indicated 1-(furan-2-ylmethyl) pyrrolidine as main product (**18a** Sel. = 92%) with compound **18b** (Sel. = 3-4 %). Amine **18a** is one of the most promising candidates for the generation of ionic liquids from renewable sources that may be used in biorefineries. This compound was earlier prepared from the treatment of the furfural with diethylamine and sodium triacetoxyborohydride in 1,2-dichloroethane follow by a two-step acid/base workup to provide the desired tertiary amine. However it has been conformed that the Ru-Hydride-carbonyl-carbene species are extremely active for the reductive amination reaction. Further more experiments B-D competitively investigated for the development of hydroaminomethylation reaction mechanism (Scheme 4.12).

(B) Indicated catalyst is inactivity for the reduction of amide (**19** was used as a model amide), also during N-formylation of various amines (Table 4.1) no N-methylation was detected. Thus the involvement of amides in the reaction mechanism was excluded,

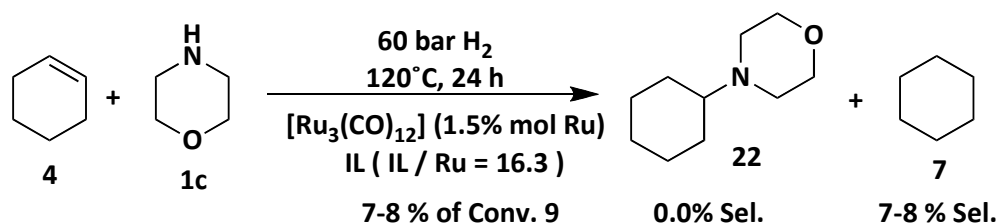
**(B) Reduction of amides under hydroaminomethylation conditions:**



**(C) Reaction of dimethylformamide with cyclohexene under hydroaminomethylation conditions:**



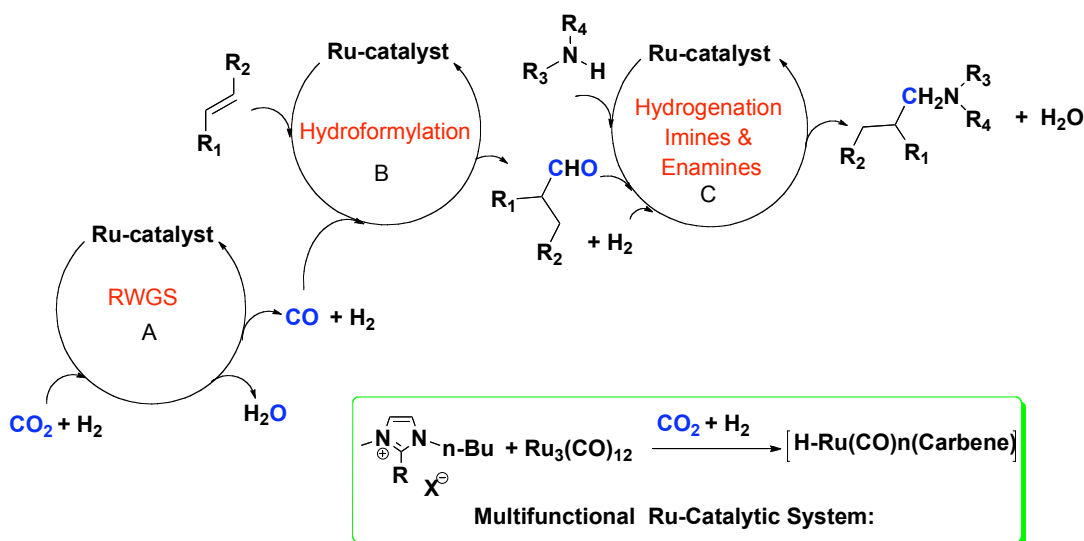
**(D) Reaction of morpholine with cyclohexene under hydroaminomethylation conditions without using CO<sub>2</sub>:**



**Scheme 4.12** Catalytic tests for evaluating the ability of the Ru-hydroaminomethylation active species for catalysing: (b) reduction of amides, and (c) hydroformylation-hydroaminomethylation of alkenes using dimethylformamide as a CO source, (d) reaction of morpholine with cyclohexene without CO<sub>2</sub>.

(C) Moderate activity in the hydroformylation-hydroaminomethylation of alkenes using dimethylformamides (**3e**) as a CO source, and thus the involvement of formamides in the reaction mechanism was excluded, and (D) no C-N bond forming reaction between cyclohexene (**9**) and morpholine (**1c**), and thus the

involvement reductive amination of alkenes in the reaction mechanism was excluded. [37]



**Scheme 4.13** Ru-catalyzed reaction mechanism for the hydroaminomethylation followed: (A) RWGSR, (B) Hydroformylation, (C) Reductive amination (hydrogenation of imines, & enamines).

However, all the supporting studies indicated that hydroaminomethylation reaction involved in sequence of RWGSR/ hydroformylation/reductive amination by hydrogenation of imines or enamine intermediates (involving hydride transfer and protonolysis). Traces of imines, and enamines were detected by GC, GC-MS analysis of hydroaminomethylation reactions mixtures, and also during reductive amination of benzaldehyde with aniline, morpholine. Thus on the bases of the above mechanistic studies, we proposed a reaction mechanism for Ru-catalyzed hydroaminomethylation of alkenes (Scheme 4.13).

#### 4.4- Conclusion

In conclusion, the use of  $P(OEt)_3$  and  $H_3PO_4$  as additive for the Ru-catalysed hydroaminomethylation of alkenes using  $CO_2$  as a CO source produced an improvement in both the catalytic activity and the product selectivity to amines. Analysis of the probable reaction pathways for the hydroaminomethylation

revealed that the Ru-catalytic system is able to catalyse with efficiency the carbonylation of alkenes and the reductive amination. Whereas, using dimethylformamide as a CO source distinct reaction kinetics were observed, and the reduction of amides is not accomplished by our catalytic system. Additionally, when aniline (amine which displayed the highest hydroaminomethylation product selectivity) was reacted under hydroaminomethylation conditions without the presence of the alkene (N-formylation conditions) displayed low reactivity with high selectivity to the formation of ureas. Therefore, these experiments excluded the involvement of the following reactions in the reaction mechanism of the hydroaminomethylation: (a) N-formylation of amines, and N-formylamines as a reagent for the carbonylation of alkenes, (b) formation of amides and reduction to amines. Series of amines less basic than aniline were studied under N-formylation conditions, and thus confirmed that amines and alkenes were in competition during the carbonylation process. Secondary amines with higher basicity than aniline were N-formylated with moderate-to-high yields, however the formation of ureas as a by-product was observed for aniline and other related primary amines. Thus, the obtained data suggested that the selectivity for the hydroaminomethylation/N-formylation product is ruled by the ratio of rates of carbonylation of alkenes/amines. The product distribution in the N-formylation of aniline (model substrate) was highly affected by the nature of the additive: (a) in absence of P-donor ligands, urea is exclusively formed; (b) in presence of monodentate P-donor ligands, N-formylation and N-methylation products selectivity is increased, and (ii) in presence bidentate P-donor ligands, full selectivity to the N-methylation products with increasing activity with the size of the bite angle was observed. These behaviour was ascribed to the favoured formation of  $[Ru-H]^+$  species when bidentate ligands with large bite angles were used. Research details described are expected to contribute to develop new processes involving the use of  $CO_2$  as an abundant, cheap, with no-logistic problems ( $CO_2$  is ubiquitous in the atmosphere) and green source of CO for important industrial carbonylation processes, for instance for the production of fragrances. [38]

## 4.5- References:

- [1] K. Takahashi, M. Yamashita, Y. Tanaka, K. Nozaki, *Angew. Chem. Int. Ed.* **2012**, *51*, 4383.
- [2] K. Takahashi, M. Yamashita, K. Nozaki, *J. Am. Chem. Soc.* **2012**, *134*, 18746.
- [3] K. Takahashi, M. Yamashita, T. Ichihara, K. Nakano, K. Nozaki, *Angew. Chem. Int. Ed.* **2010**, *49*, 4488.
- [4] C. P. Casey, *Chemcatchem* **2010**, *2*, 1209.
- [5] J. Zakzeski, H. R. Lee, Y. L. Leung, A. T. Bell, *Appl. Catal. A* **2010**, *374*, 201.
- [6] L. Wu, I. Fleischer, R. Jackstell, M. Beller, *J. Am. Chem. Soc.* **2013**, *135*, 3989.
- [7] U. Rodemerck, M. Holena, E. Wagner, Q. Smejkal, A. Barkschat, M. Baerns, *Chemcatchem* **2013**, *5*, 1948.
- [8] M. Peters, B. Kohler, W. Kuckshinrichs, W. Leitner, P. Markewitz, T. E. Muller, *ChemSusChem* **2011**, *4*, 1216.
- [9] M. Cokoja, C. Bruckmeier, B. Rieger, W. A. Herrmann, F. E. Kuhn, *Angew. Chem. Int. Ed.* **2011**, *50*, 8510.
- [10] C. Federsel, R. Jackstell, M. Beller, *Angew. Chem. Int. Ed.* **2010**, *49*, 6254.
- [11] G. Centi, E. A. Quadrelli, S. Perathoner, *Energy & Environmental Science* **2013**, *6*, 1711.
- [12] Q. Liu, L. Wu, R. Jackstell, M. Beller, *Nat. Commun.* **2015**, *6*.
- [13] J. C. Chadwick, R. Duchateau, Z. Freixa, P. W. N. M. van Leeuwen, *Homogeneous Catalysts*, Wiley, **2011**.
- [14] P. W. N. M. van Leeuwen, *Homogeneous Catalysis: Understanding the Art*, Springer, **2004**.
- [15] K. Weissermel, H. J. Arpe, *Industrial Organic Chemistry*, Wiley-VCH GmbH & Company KGaA, **2003**.
- [16] K. Tominaga, Y. Sasaki, *J. Mol. Catal. A* **2004**, *220*, 159.
- [17] S. Jääskeläinen, M. Haukka, *Appl. Catal. A* **2003**, *247*, 95.
- [18] K. Tominaga, Y. Sasaki, *Catal. Commun.* **2000**, *1*, 1.
- [19] M.-L. Kontkanen, L. Oresmaa, M. A. Moreno, J. Janis, E. Laurila, M. Haukka, *Appl. Catal., A* **2009**, *365*, 130.
- [20] K. Tominaga, *Catal. Today* **2006**, *115*, 70.
- [21] K. Tominaga, Y. Sasaki, *Chem. Lett.* **2004**, *33*, 14.
- [22] K. I. Tominaga, Y. Sasaki, *Stud. Surf. Sci. Catal.* **2004**, *153*, 227.
- [23] H. Arakawa, M. Aresta, J. N. Armor, M. A. Barteau, E. J. Beckman, A. T. Bell, J. E. Bercaw, C. Creutz, E. Dinjus, D. A. Dixon, K. Domen, D. L. DuBois, J. Eckert, E. Fujita, D. H. Gibson, W. A. Goddard, D. W. Goodman, J. Keller, G. J. Kubas, H. H. Kung, J. E. Lyons, L. E. Manzer, T. J. Marks, K. Morokuma, K. M. Nicholas, R. Periana, L. Que, J. Rostrup-Nielson, W. M. Sachtler, L. D. Schmidt, A. Sen, G. A. Somorjai, P. C. Stair, B. R. Stults, W. Tumas, *Chem. Rev.* **2001**, *101*, 953.
- [24] M. Ali, A. Gual, G. Ebeling, J. Dupont, *ChemCatChem* **2014**, *6*, 2224.
- [25] Q. Liu, L. P. Wu, I. Fleischer, D. Selent, R. Franke, R. Jackstell, M. Beller, *Chemistry-a European Journal* **2014**, *20*, 6888.
- [26] V. K. Srivastava, P. Eilbracht, *Catal. Commun.* **2009**, *10*, 1791.
- [27] J. Coetzee, D. L. Dodds, J. Klankermayer, S. Brosinski, W. Leitner, A. M. Slawin, D. J. Cole-Hamilton, *Chem. Eur. J.* **2013**, *19*, 11039.
- [28] A. A. Nunez Magro, G. R. Eastham, D. J. Cole-Hamilton, *Chem. Commun.* **2007**, 3154.
- [29] G. S. Fonseca, J. D. Scholten, J. Dupont, *Synlett* **2004**, 1525.
- [30] D. Gonzalez-Galvez, P. Lara, O. Rivada-Wheelaghan, S. Conejero, B. Chaudret, K. Philippot, P. van Leeuwen, *Catalysis Science & Technology* **2013**, *3*, 99.
- [31] K. Beydoun, G. Ghattas, K. Thenert, J. Klankermayer, W. Leitner, *Angewandte Chemie-International Edition* **2014**, *53*, 11010.
- [32] K. Beydoun, T. vom Stein, J. Klankermayer, W. Leitner, *Angewandte Chemie-International Edition* **2013**, *52*, 9554.

- [33] Y. H. Li, T. Yan, K. Junge, M. Beller, *Angewandte Chemie-International Edition* **2014**, *53*, 10476.
- [34] S. Wesselbaum, T. Vom Stein, J. Klankermayer, W. Leitner, *Angew. Chem. Int. Ed.* **2012**, *51*, 7499.
- [35] F. M. A. Geilen, B. Engendahl, M. Holscher, J. Klankermayer, W. Leitner, *Journal of the American Chemical Society* **2011**, *133*, 14349.
- [36] W. Wang, S. Wang, X. Ma, J. Gong, *Chem. Soc. Rev.* **2011**, *40*, 3703.
- [37] Y. Wan, M. Alterman, M. Larhed, A. Hallberg, *J. Org. Chem.* **2002**, *67*, 6232.
- [38] E. V. Gusevskaya, J. Jiménez-Pinto, A. Börner, *ChemCatChem* **2014**, *6*, 382.

## **CHAPTER-5**

**“Liquid-phase Hydrogenation and Dehydrogenation Activities via Pd-NPs Deposited onto Activated Carbon (AC) by Magnetron Sputtering.”**

## 5.1 Introduction

Palladium nanostructures (Pd-NPs) are extensively applied in remarkable organic transformation involving dihydrogen.<sup>[1-4]</sup> The efficient industrial implementation of this catalytic processes requires the use of modern synthetic methodologies which allow the precise control over the physical (i.e., size and shape) and chemical (i.e., well-defined composition) properties of this nanostructures.<sup>[5]</sup> Conventionally, the most extensively extended approach consist in the chemical reduction of metallic salts under non-sustainable conditions (i.e., hazardous reducing agents and generation of large amount of residues).<sup>[6-10]</sup>

Among the recently developed alternative processes, the magnetron-sputtering technique is receiving increasing attention as the most sustainable method to generate efficient metal nanoestructures.<sup>[11-14]</sup> During the process, the collision of the accelerated ions of the in-situ generated plasma with the highly purity metallic targets produced the ejection of a sputtering beam consisting in metal atoms and small clusters. The stabilization of metal nanoparticles (M-NPs) occurs when the incident sputtering beam is is directed onto the appropriate solid support or low vapor pressure liquid supports.<sup>[14,15]</sup>

Among the advantages of this technique, the most important are the atomic efficiency of the process and the faster generation-isolation of small and well dispersed nanostructures of high purity.<sup>[16-24]</sup> Recently, our group has developed a new sputtering chamber, which allowed the constant mixing of the solid support, and thus, the distribution of the metallic nanoparticles in all the support spatial planes.<sup>[24,25]</sup> We recently demonstrated that the Pd-NPs generated by magnetron-sputtering are small and uniformly distributed are more accessible to the reagents because deposited onto the most external layers is favoured when highly porous supports (i.e., SiO<sub>2</sub>) were used. This behavior is probably because of limitations in the diffusion of the metal atoms and clusters through support pores.<sup>[26]</sup> To date, the effect of time of sputtering on the chemical and physical properties of the formed Pd-NPs deposited onto solid has not been reported.

Here, the use of the magnetron-sputtering approach for the deposition of Pd-NPs onto a commercially available Activated charcoal is reported. Carbon based



support were evaluated selected due to its wide variety of applications.<sup>[27]</sup> The study of the effect of the deposition time revealed the linear dependence of the deposition time with the final metal content and the formation of small (ca. 3.7 nm) and uniformly distributed Pd-NPs onto the solid supports. H<sub>2</sub>-chemisorption measurement revealed a decrease of the metal dispersion when the deposition time was increased.

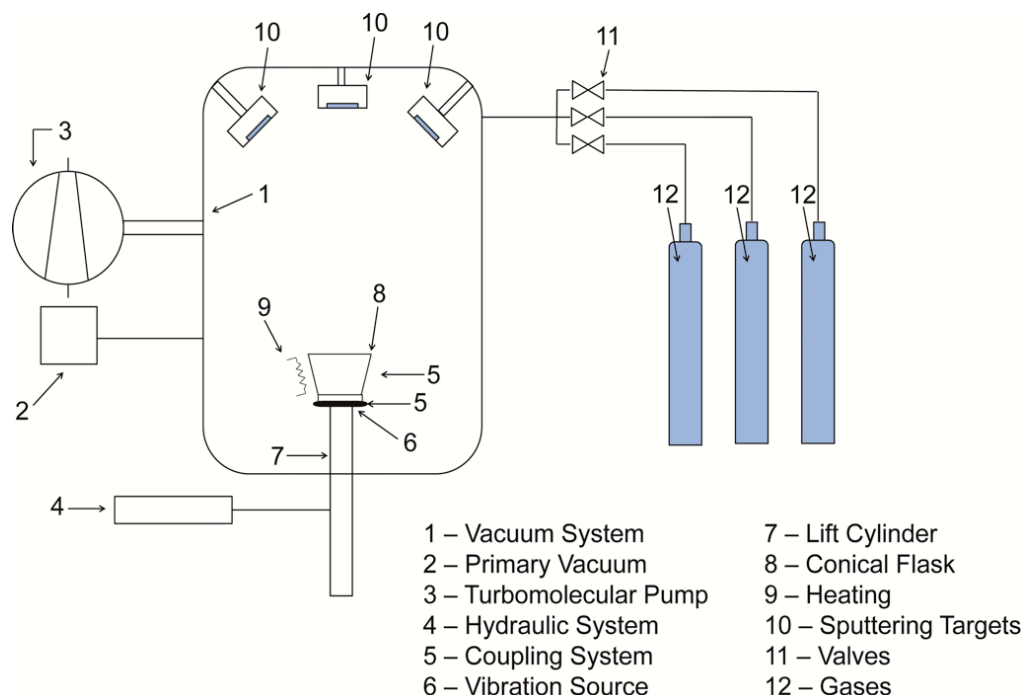


**Figure 5.1** Schematic representation of sputtering deposition chamber used for the immobilization of the transition M-NPs onto supporting materials.<sup>[24,25]</sup>

The Pd-NPs catalytic performances were evaluated in the reduction of model substrates (i.e., nitrobenzene, 1,3-cyclohexadiene and cyclohexene) at 75°C under 4 bar dihydrogen (H<sub>2</sub>). The catalytic results revealed improved efficiencies in terms of activity and selectivity to those displayed by commercially available catalyst. Disproportion of 1,3-cyclohexadiene and cyclohexene were revealed also as active processes under reaction conditions.

## 5.2 Experimental section

### 5.2.1 General procedures:

All syntheses were performed using standard Schlenk techniques under argon atmosphere. Chemicals were purchased from Sigma-Aldrich and purified by standard procedures.  $^{[32]}$  H<sub>2</sub> (> 99.999%), N<sub>2</sub> (> 99.999%) and Ar (> 99.999%) were purchased from White-Martins. Pd-targets were ICP-OES analysis for the determination of the Pd content were carried out after sample digestion by using the Thermo Scientific™ iCAP™ 7400. ICP-OES analyser X-ray diffraction (XRD) experiments were performed by using a Philips X'Pert MPD diffractometer with Bragg-Brentano geometry using a graphite curved-crystal with the Cu K $\alpha$  X-ray radiation (1.5406 Å). The TEM imaging experiments were performed on a JEOL – JEM 1200ExII, operating at an accelerating voltage of 200 kV. Size histograms of the Pd-nanoparticles were obtained by measuring at least 300 particles. H<sub>2</sub>-chemisorption analysis for the determination of the metal dispersion and metallic surface were carried out on ASAP 2020 surface area and porosimetry analyzer and using of 30 mg of each Pd-catalysts.

### 5.2.2 General procedure for the sputtering:

As a general procedure, activated charcoal (100 mg) was loaded in a conical Al flask and placed inside the vacuum chamber. The chamber was closed and evacuated to a base pressure of  $4 \times 10^{-7}$  mbar vacuum for 4 h. Then, the chamber was placed under  $4 \times 10^{-3}$  mbar of Ar at room temperature (298 K). The Pd-NPs/C-1 to Pd-NPs/C-5 catalysts were obtained by sputtering of Pd-targets (99.99%) at power of 50 W during 0.5, 2.5, 5.0, 7.5 and 12.0 min, respectively. The support was continuously homogenized by revolving the Al flask at a frequency of 23 Hz during the time of sputtering. After that, the chamber was vented with Ar, and the Pd-NPs/C catalysts were recovered and stored under Ar for their further characterization and application.

### 5.2.3 General procedure for the hydrogenation test:

As a general procedure, the substrate (1.12 g of aniline, 0.81 g of cyclohexene or 0.79 g of 1,3-cyclohexadiene) was added to a Fischer-Porter reactor containing the appropriate amount of Pd/C catalyst (10 mg). After that, the reactor was pressurized and maintained at constant pressure of 4 bar of H<sub>2</sub> and warmed the desired temperature (90°C for nitrobenzene and 75°C for cyclohexene and 1,3-cyclohexadiene). The reaction kinetics was monitored by the H<sub>2</sub> consume. Samples were taken from the reaction mixture at regular intervals, and the conversion and selectivity was corroborated by GC-analysis of the reaction samples using *n*-heptane as internal standard. After the desired reaction time, the reactor was cooled to room temperature and then depressurized. GC analyses were run with an Agilent Technologies GC System 6820 using a DB-17 column. GC conditions are: injector and detector (FID) temperature of 260 °C; N<sub>2</sub> as carrier (1 mL min<sup>-1</sup>), column head pressure of 10 psi and temperature program from 40 °C (10 min) to 250 °C at a heating rate of 10 °C min<sup>-1</sup>.

## 5.3 Results and Discussion

In continuation of the synthesis of transition metal nanoparticles by sputtering deposition method, our recent efforts brought a series of size controlled well-distributed Pd/C-supported **1-5**, and Pd/TiO<sub>2</sub> NPs (Table 5.1). The generated Pd-NPs (1-5) were found to possess an average size of 3,6-3.7 nm in diameter having different concentrations of Pd<sup>0</sup> (0.15 - 2.36 Wt. %) with supporting material. Further significant properties, and characterization of sputtered Pd-NPs 1-5 have been summarized in the Table 5.1. The modified sputtering chamber has the advantage of mixing the generated Pd-NPs for the uniform deposited in the solid supports. Our research group has successfully reported several well-distributed sputtered transitional M-NPs by using the same sputtering method. Specially, IL-modified Al<sub>2</sub>O<sub>3</sub>, and SiO<sub>2</sub> supported Pd, Ru-NPs for the selective hydrogenation of 1,3-cyclohexadienes, and partial reduction of benzene under liquid-phase condition by using solvents. [24-26]

This series of well-distributed Pd/C-1 to Pd/C-5 NPs have been revealed super hydrogenation activities of model substrate nitrobenzene and cyclohexene by using of H<sub>2</sub> (4 bar). And also revealed the simultaneous dehydrogenation-hydrogenation activities so called disproportion of 1,3-cyclohexadiene and cyclohexene under reaction conditions.

Further, comparatively investigated the activity of sputtered Pd/C-supported NPs with Pd/TiO<sub>2</sub>, Pd/SBA-15 supported NPs (synthesized by same sputtering deposition method), and also used commercially available Pd/C-Degussa (5 wt%) catalysts. The Pd/C-supported **1-5** NPs comparatively indicated super activities than the commercial one and other reported active catalysts under solvent-free liquid-phase condition.

### 5.3.1 Sputtering deposition and characterization of Pd-NPs

**Table 5.1** Pd-nanocatalysts supported onto activated carbon (Pd-NPs/**Cat.1** to Pd-NPs/**Cat.5**) prepared by magnetron sputtering.

Entry <sup>[a]</sup>	Sample	Time / min	Metal / wt. % <sup>[b]</sup>	Ø / nm <sup>[c]</sup>	Metal dispersion / % <sup>[d]</sup>
1	Pd/C-1	0.50	0.15±0.01	3.74±1.69	-
2	Pd/C-2	2.50	0.73±0.01	3.66±1.50	25.3
3	Pd/C-3	5.00	1.31±0.01	3.77±1.88	22.6
4	Pd/C-4	7.50	1.94±0.01	3.71±1.82	20.4
5	Pd/C-5	12.00	2.36±0.01	3.88±1.90	14.6
6	Pd/TiO <sub>2</sub>	0.50	0.15±0.01	3.73±1.49	-
7	Pd/TiO <sub>2</sub>	2.50	0.73±0.01	3.72±1.79	-

[a] Sputtering-deposition conditions: 100 mg of solid support, 50 W of power, 23 Hz of vibration frequency, 4x10<sup>-7</sup> mbar vacuum, 4x10<sup>-3</sup> mbar Ar (Ar 5.0), and room temperature (298 K); [b] Metal content (wt. %) determined by ICP-OES; [c] Mean diameter and size distributions determined by TEM analysis; [d] Metal dispersion determined by H<sub>2</sub>-chemisorption.

A series of Pd-nanocatalyst supported onto charcoal (Pd-NPs/C-1 to Pd-NPs/C-5) were synthesized by the magnetron sputtering of Pd-targets at 50 W of voltage and using the sputtering chamber described with a frequency of 23 Hz for the vibration of the flask. The sputtered Pd-NPs were well distributed and deposited on solid supports (carbon, TiO<sub>2</sub>) by using a modified sputtering chamber (Figure 5.1) involving constant mixing of the solid supports during the sputtering of Pd-NPs. Sputtering deposition of Pd-NPs were mainly performed by placing the solid support materials (1.0 g) in a conical Al flask inside a vacuum chamber (Figure 5.1). The vacuum chamber was then placed under a sputtering working at a pressure of 4 mbar by adding Ar flow. Size of the Pd-NPs was controlled applying an appropriate tuning for the sputtering-depositions.

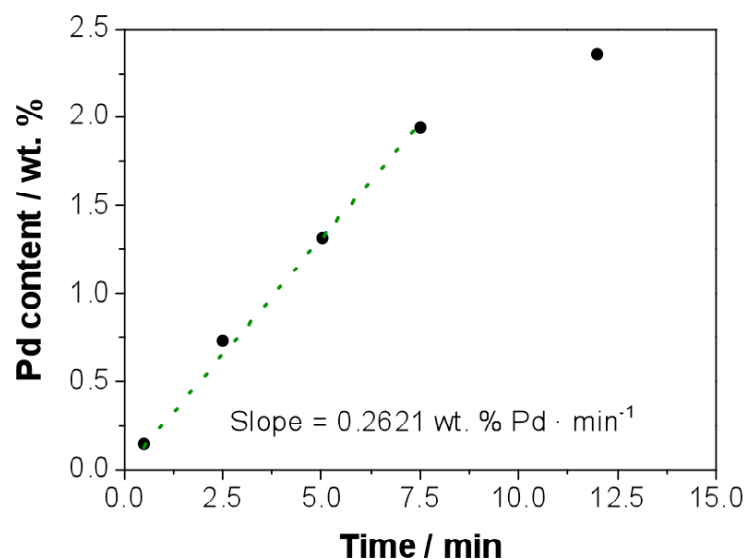


**Figure 5.2a** Deposition of Pd(0)-*fcc* nanoparticles on carbon using the magnetron-sputtering chamber developed by our group. Palladium content (wt. %) vs. deposition time (min).

Samples Pd-NPs/C-1 to Pd-NPs/C-5 were obtained by after five different deposition times (i.e., 0.50 min, 2.50 min, 5.00 min, 7.50 min and 12.00, see Table 5.1). ICP-OES analysis revealed that the Pd content was increased with the deposition time. This ratio between the deposition time and the Pd content is linear between 0.50 min and 7.50 min with an increase of the Pd content in the support of 0.2621 wt.% min<sup>-1</sup> (See Table 5.1 and Figure 5.2a). The sample obtained by using a

deposition time of 12.00 min displayed a decrease in the deposition tax after 7.50 min.

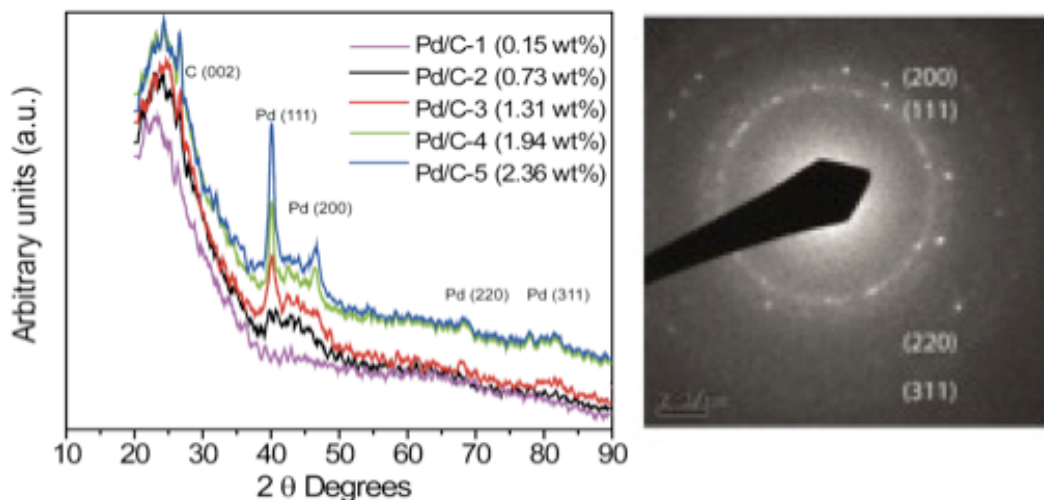


**Figure 5.2b** XRD pattern of Pd<sup>0</sup>/C-1 to 5 (Pd<sup>0</sup> = 0.15, 0.73, 1.31, 1.94, and 2.36 Wt%) deposited by sputtering on carbon(C 002) support.

Additionally performed the XRD analysis for the supplementary justification showed characteristic Pd-lattice peak Pd (111), (220, 311) intensities, which increases with increasing Pd concentration in the Pd/C-1 to 5 catalysts (Figure 5.2b). Furthermore, TEM analysis for the Pd/C-1 to Pd/C-5 catalysts indicated the formation of very similar small Pd-nanoparticles (i.e., mean diameter between 3.6 and 3.9 nm) with narrow size distributions (Figure 5.3a).

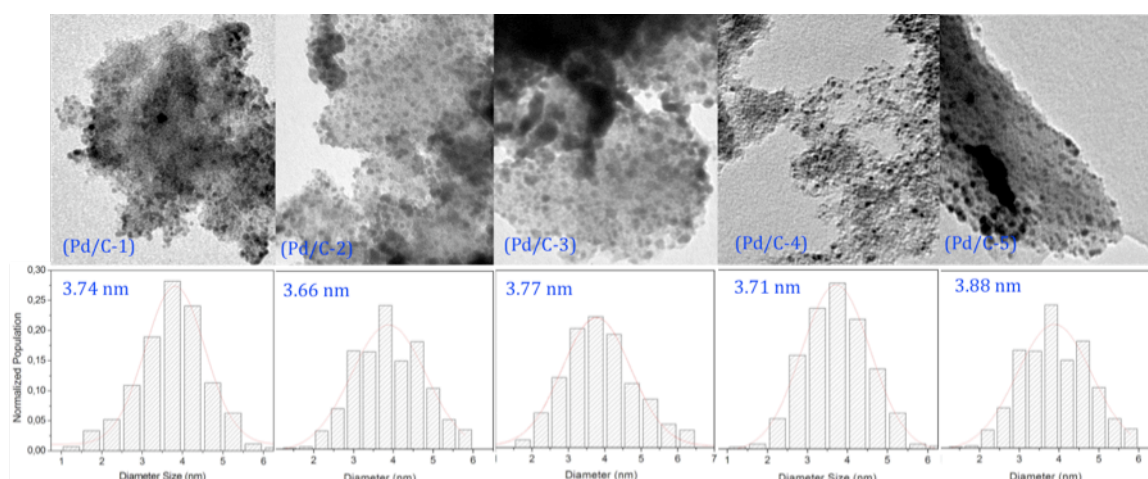


**Figure 5.3a** TEM images of Pd/C-1 Pd/C-5 NPs narrow distributed and deposited onto solid supports active carbon.

The dispersion, and surface properties of these Pd/C-supported NPs were deliberated by H<sub>2</sub>-chemisorptions analysis summarized in tabl-5.1, Figure 5.3b. The chemisorptions analysis indicated the % metal distribution is constantly decreased as the concentration of Pd increases from Pd/C-1-to-5 NPs. Among them, the Pd/C-2 (0.73 wt %) NPs showed highest metal distribution %, metallic.

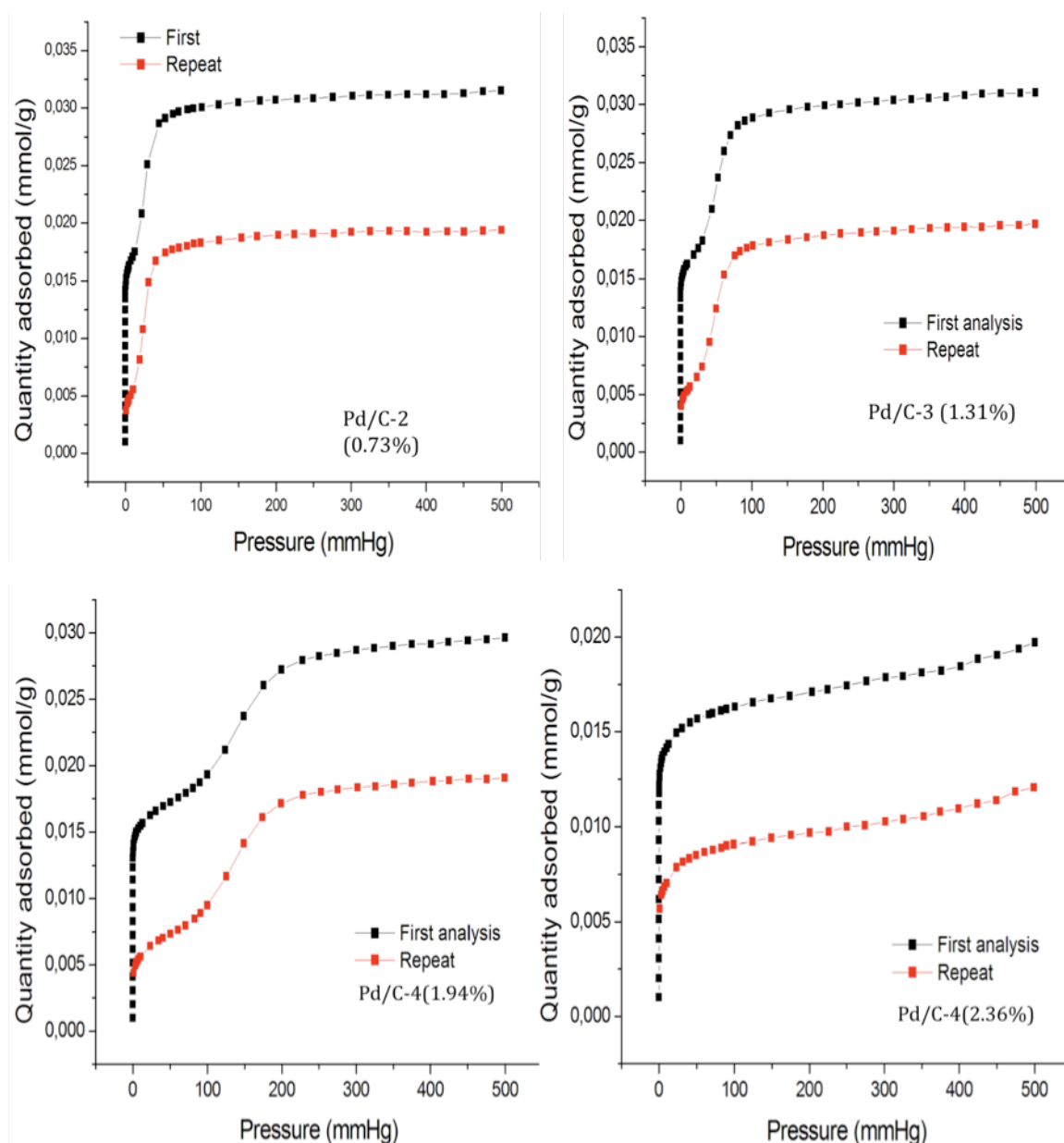


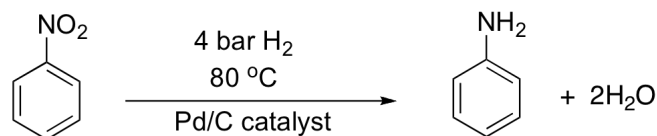
**Figure 5.3b** H<sub>2</sub>-chemisorptions analysis of Pd/C-2 Pd/C-5 NPs deposited onto solid supports active carbon.

## 5.3.2 Catalytic activities

### 5.3.2.1 Catalytic activity of Pd/C-1 to Pd/C-5 for hydrogenation reactions

The catalytic performance of the Pd-nanocatalyst supported onto activated charcoal (Pd-NPs/C-1 to Pd-NPs/C-5) prepared by magnetron sputtering was evaluated and compared with the catalytic performance of commercially available Pd/C-D catalyst (in the hydrogenation of model substrates (i.e., nitrobenzene and cyclohexene). The reactions were performed under solvent-less conditions under constant pressure of 4 bar of H<sub>2</sub>. The reaction kinetics were monitored by the quantification of the consumption of H<sub>2</sub>. Substrate conversions and selectivities were also determined by GC-analysis of reaction sample aliquots.

**Table 5.2** Hydrogenation of aniline catalysed by Pd-nanocatalyst supported onto activated charcoal (Pd-NPs/C-1 to Pd-NPs/C-5) prepared by magnetron sputtering. <sup>a</sup>



E	Catalyst	Pd con./ % wt	Ph-NO <sub>2</sub> / Pd ratio	Conv./% <sup>b</sup>	TON <sup>c</sup>	TOF (min <sup>-1</sup> ) <sup>c</sup>
1	Pd/C-0	5.00	4113	>99.9	4113	35.5
2	Pd/C-1	0.15	64717	2.0	1314	2.1
3	Pd/C-2	0.73	13298	>99.9	13298	141.7
4	Pd/C-3	1.31	7410	>99.9	7410	64.8
5	Pd/C-4	1.94	5004	>99.9	5004	52.9
6	Pd/C-5	2.36	4113	>99.9	4113	55.8

[a] Selective-hydrogenation of Ph-NO<sub>2</sub> (1.123 g) into aniline catalyzed by Pd/C-1 to 5 (10 mg) catalysts reaction condition: 4 bar H<sub>2</sub>, 80°C, [b] % Conv. calculated by GC- analysis by using *n*-heptane as an internal standard, [c] TOF (min<sup>-1</sup>), TON of reactions.



Kinetics expressions between conversion Vs time, and TOF ( $\text{min}^{-1}$ ) Vs TON relationship of reactions (Figures 5.4-5.5) catalyzed by Pd/C-1 to 5 and Pd/C-D catalysts generally indicated the best activity at high TON, and selectively produced aniline at >99.9% conversion of nitrobenzene. But Pd/C-2 (0.73 Wt%) catalyst (3.6 nm) having higher metallic dispersion revealed highest TOF values with highest TON in both cases comparatively others Pd/C-1, Pd/C-3-5, Pd/C-D, and Pd/SAB catalysts (Figures 5.4-5.5). However, the catalysts activities of Pd/C-1 to 5 for the hydrogenation of nitrobenzene and cyclohexene evidenced that on decreasing the metallic dispersion and surface area of Pd-NPs, ultimately decreases the activity.

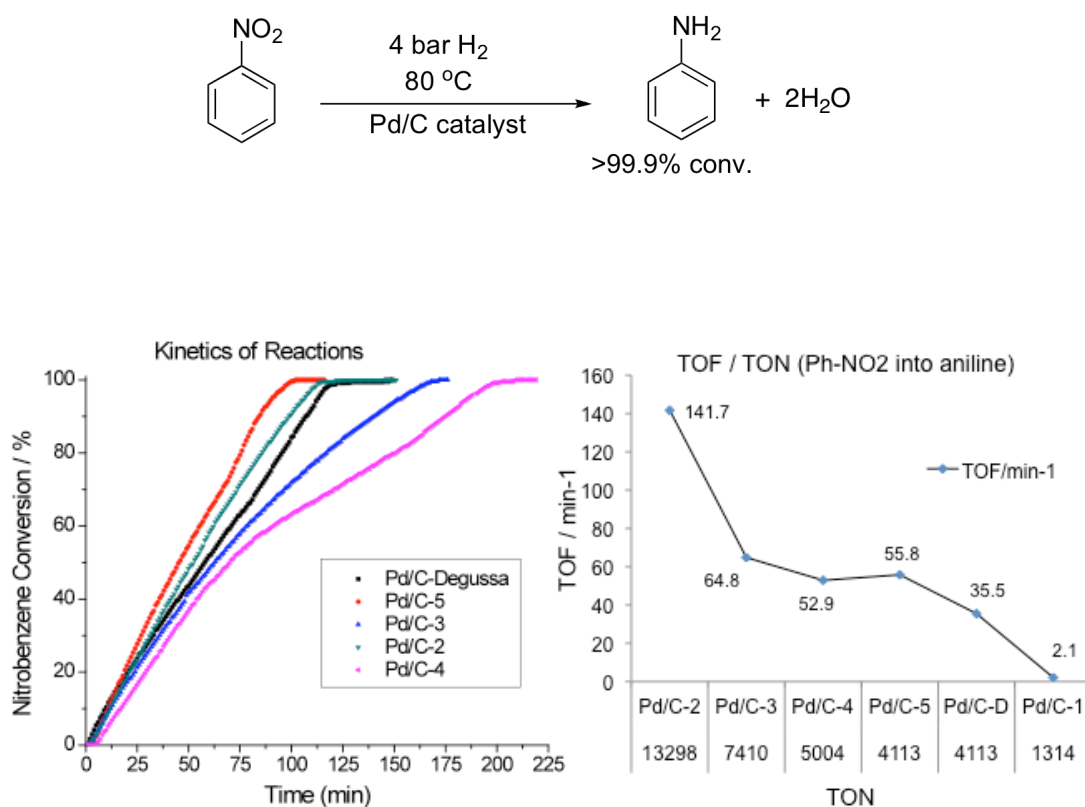


**Figure-5.4** Kinetic expression between % Conv. Vs Time (min), and TOF Vs TON relationship for the selective hydrogenation of nitrobenzene into aniline catalyzed by sputtered Pd/C-1 to Pd/C-5 catalysts, and Pd/C-D under solvent-free liquid-phase condition.

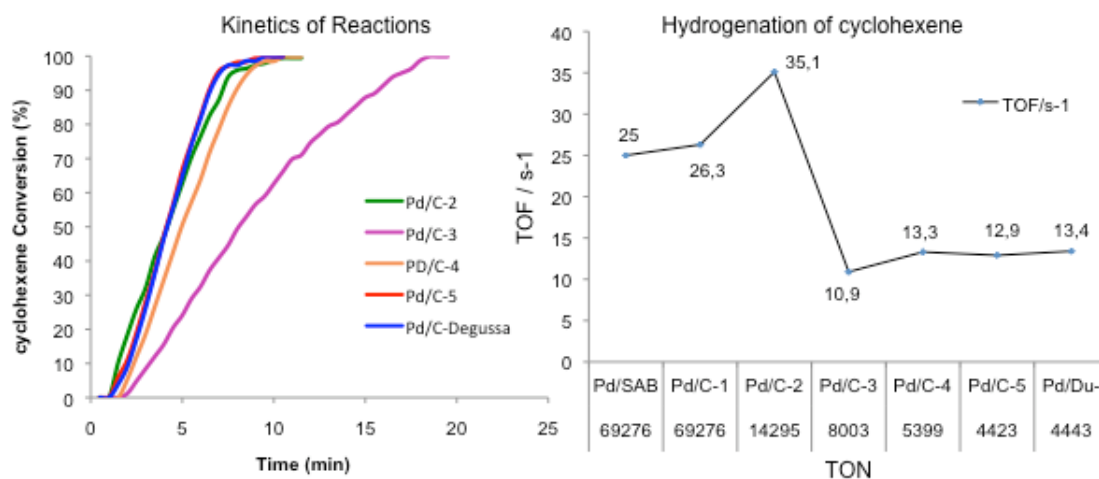
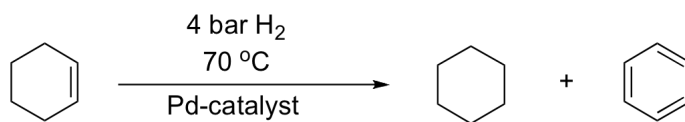
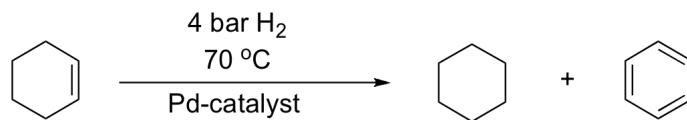


**Figure 5.5** Kinetic between % Conv. Vs Time (min), and TOF Vs TON for the hydrogenation of cyclohexene catalyzed by sputtered Pd/C-1 to 5, Pd/SAB-15 and Pd/C-D, under solvent-free liquid-phase condition.

Similar trends were observed in the hydrogenation of aniline and cyclohexene catalyzed by Pd-catalysts. The commercial catalyst produced (Pd/C-D) similar TON and TOF than catalysts Pd/C-3 and Pd/C-4 (See Table 5.2-5.3, Figure 5.4, 5.5). The catalysts prepared by sputtering with lower metal loadings (Pd/C-2 and Pd/C-1) and higher metal dispersions produced higher activity and productivity than the catalyst with higher metal loadings (Pd/C-3 and Pd/C-4).

The difference relies in the fact that the Pd/C-1 displayed the highest activity and productivity in the hydrogenation of cyclohexene, whereas this same catalyst displayed very poor activity in the hydrogenation of aniline due to the deactivation in the initial stages. This behavior was ascribed to the deactivation of the catalyst by low content impurities present in the aniline. Similar behaviours were observed previously in processes involving compounds with impurities able to deactivate the catalyst.<sup>[28-30]</sup>

**Table 5.3** Hydrogenation of cyclohexene catalysed by Pd-nanocatalyst supported onto activated charcoal (Pd-NPs/ C-1 to Pd-NPs/ C-5) prepared by magnetron sputtering. a



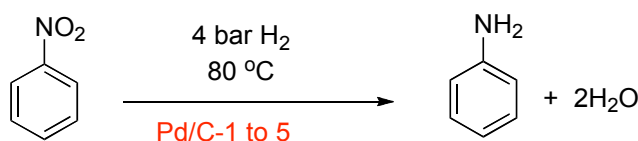
E	Catalysts	Pd/C wt %	C <sub>6</sub> H <sub>10</sub> / Pd	%Conv. /min	Yield C <sub>6</sub> H <sub>12</sub> %	Yield C <sub>6</sub> H <sub>6</sub> %	TON	TOF / s <sup>-1</sup>
1	Pd/SBA-15	0.15	69962	96.2 [126]	96.12	0.06	67248	25.8
2	Pd/C-1	0.15	69962	99.1 [111]	99.02	0.09	69276	26.3
3	Pd/C-2	0.73	14375	99.3 [10.0]	99.13	0.14	14295	35.1
4	Pd/C-3	1.31	8011	100 [19.5]	99.90	0.10	8003	10.9
5	Pd/C-4	1.94	5409	100 [10.5]	99.81	0.19	5399	13.3
6	Pd/C-5	2.36	4446	100 [9.5]	99.47	0.53	4423	12.9
7	Pd/C-0	5.00	4446	100 [9.5]	99.90	0.10	4443	13.4

[a] Pd/C catalyzed hydrogenation of cyclohexene (810 mg) into cyclohexane; reaction condition: 4 bar H<sub>2</sub>, 70 °C, (b) conversion, and yields of products calculated by GC-FID analysis using *n*-heptane as an internal standard, (c) TON, TOF/min<sup>-1</sup> or S<sup>-1</sup> values of catalysts.

### 5.3.2.2 Activity of Pd/C-1 NPs on decreasing Ph-NO<sub>2</sub>/Pd ratio

The activity of Pd/C-1 NPs were further investigated on decreasing the Ph-NO<sub>2</sub>/Pd ratios of: 13298 > 7410 > 5004 > 4325 and 3555, indicating same ratios which used for Pd/C-2 to 5 catalyzed reactions under sane reaction condition. All reactions revealed >99.9% conversion under the same reaction conditions. In general, the activity of catalysts Pd/C-1 increases with decreasing the Ph-NO<sub>2</sub>/Pd ratio (Table 5.4, Entries 1-4).

**Table 5.4** Hydrogenation of aniline catalysed by Pd-NPs/ C-1 prepared by magnetron sputtering.<sup>a</sup>



E	Catalyst	Pd con./ % wt	Ph-NO <sub>2</sub> / Pd ratio	Conv./% <sup>b</sup>	TON <sup>c</sup>	TOF (min <sup>-1</sup> ) <sup>c</sup>
1	Pd/C-1	0.15	13298	>99.9	13298	71.4
2	Pd/C-1	0.15	7410	>99.9	7410	165.5
3	Pd/C-1	0.15	5004	>99.9	5004	154.9
3	Pd/C-1	0.15	4323	>99.9	4323	139.5
4	Pd/C-1	0.15	3555	>99.9	3555	142.2

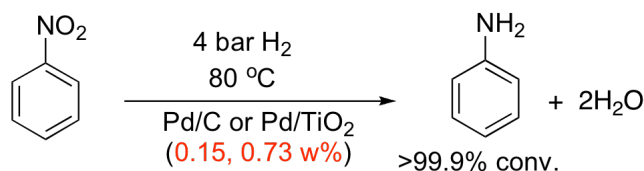
[a] Selective conversion of Ph-NO<sub>2</sub> into aniline using Pd/C-1 NPs under the same solvent free liquid-phase reaction condition: 4 bar H<sub>2</sub>, 80°C, [b] % Conv. calculated by GC- analysis, (c) TOF (min<sup>-1</sup>), TON of reaction.

### 5.3.2.3 Catalytic activity of Pd/C, and Pd/TiO<sub>2</sub> supported NPs

Further comparatively investigated the activity of sputtered Pd/C-1, 2 NPs with Pd/TiO<sub>2</sub>-supported NPs containing same Pd<sup>0</sup> concentration (0.15, 0.73 wt %) by using Ph-NO<sub>2</sub>/Pd ratio (13298, 7410, and 5004, at 4 bar H<sub>2</sub>, 80°C). The kinetic expression between conversion of nitrobenzene Vs reaction time (Figure 5.6), and TOF/min<sup>-1</sup> values (Table 5.5, Entry 1-8) indicated that Pd/TiO<sub>2</sub> supported catalysts are slightly more active initially with the starting of reactions then Pd/C-supported catalysts. While in the case of Pd/C, and Pd/TiO<sub>2</sub> supported (0.15 wt %) NPs catalyzed by using of Ph-NO<sub>2</sub>/Pd ratios of: 13298, 7410, and 5004 (Conv. > 99.9%) Pd/C-1 (0.15 wt %) indicated high TOF values then Pd/ TiO<sub>2</sub> supported NPs. Kinetic representation (Figure-5.6), TON, and TOF/min<sup>-1</sup> values (Table-5.5, Entries 7-8) indicated slight differences in the activities of Pd-NPs deposited on active carbon and TiO<sub>2</sub> supports. Bu the Pd/C-supported catalysts always showed

linearity in all cases, it is representing that the Pd/C supported NPs are better recyclable catalyst than Pd/TiO<sub>2</sub> supported NPs (Figure 5.6).

**Table 5.5** Comparative study between Pd/C-0.15, 0.73 wt%, and Pd/TiO<sub>2</sub>-0.15, 0.73 wt% NPs <sup>a</sup>



E	Catalyst	Pd/ Wt%	Ph-NO <sub>2</sub> / Pd ratio	Conv./ % <sup>b</sup>	TON <sup>c</sup>	TOF (min <sup>-1</sup> ) <sup>c</sup>
1	Pd/C-1	0.15	13298	>99.9	13298	71.4
2	Pd/ TiO <sub>2</sub>	0.15	13298	>84.57	11246	69.4
3	Pd/C-1	0.15	7410	>99.9	7410	154.9
4	Pd/ TiO <sub>2</sub>	0.15	7410	>99.9	7410	133.1
5	Pd/C-1	0.15	5004	>99.9	5004	165.5
6	Pd/ TiO <sub>2</sub>	0.15	5004	>99.9	5004	142.7
7	Pd/C-2	0.73	13298	>99.9	13298	141.7
8	Pd/ TiO <sub>2</sub>	0.73	13298	>99.9	13298	142.8

[a] Selective conversion of Ph-NO<sub>2</sub> into aniline using Pd/C, TiO<sub>2</sub> supported NPs under the same solvent free liquid-phase reaction condition: 4 bar H<sub>2</sub>, 80°C, [b] % Conv. calculated by GC- analysis, (b) TOF (min<sup>-1</sup>), TON of reaction.

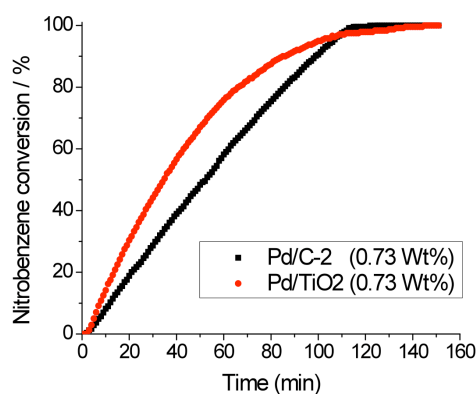


**Figure 5.6** Kinetic expression between 0.73 Wt% Pd/C or TiO<sub>2</sub> supported NPs by using same Ph-NO<sub>2</sub>/ Pd ratio of 13298.

### 5.3.2.4 Pd-catalyzed disproportionation of 1,3-cyclohexadiene

The Pd/C-supported NPs **1-5** were further investigated for the selective hydrogenation or dehydrogenation of the 1,3-cyclohexadiene under solvent-free liquid-phase condition. Initially, Reaction was optimized for the selective hydrogenation of 1,3-cyclohexadiene into cyclohexene by controlling the reaction time using H<sub>2</sub> (4 bar) as reducing agent. Experiments were probed with Pd/C-2 catalyst (0.73 wt %, 10 mg), by using 1,3-cyclohexadiene (790 mg), under solvent-free liquid-phase condition: at 70 °C temperature. Samples of reactions were collected after each 1-2 min, and measured the % conversion of substrate and % selectivity of products (**1-3**) by GC-MS, GC- FID analysis using *n*-heptane as an internal standard (Figure 5.7).

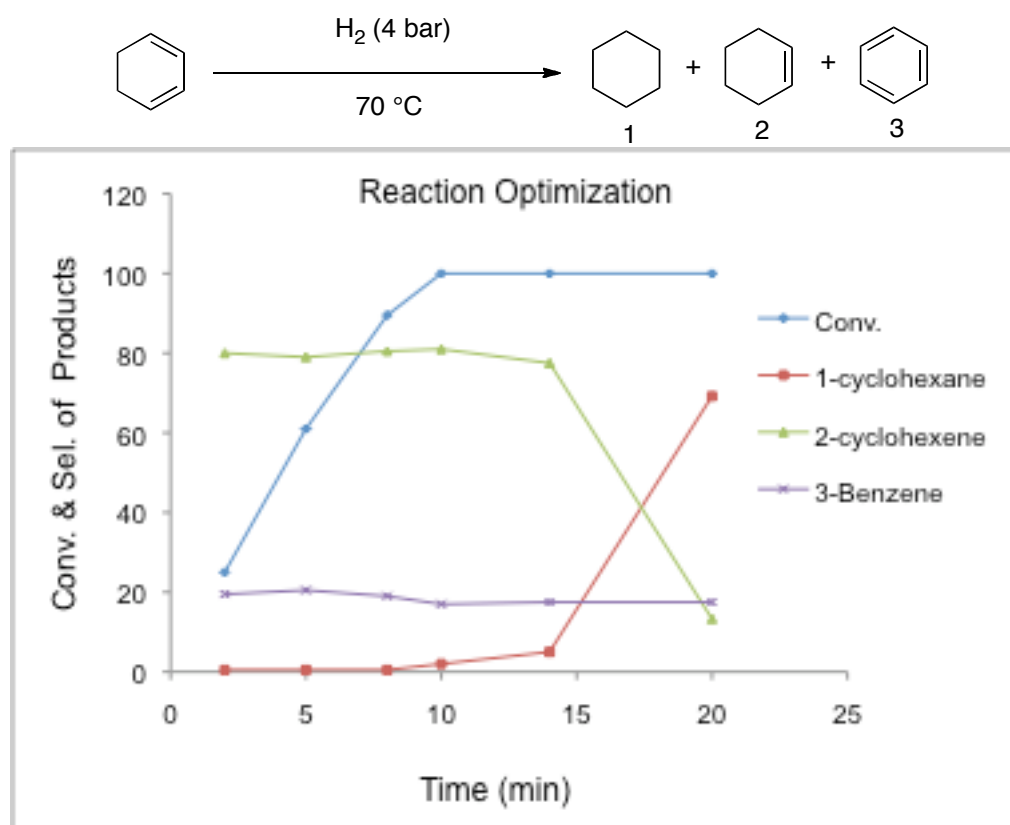
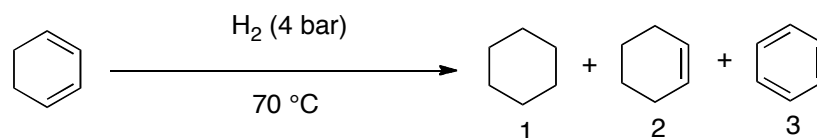


**Figure 5.7** Pd/C-2 catalyzed reaction optimization for the disproportionation of 1,3-cyclohexadiene by controlling the reaction time.

The reaction optimization (Figure 5.7) revealed highest selectivity of cyclohexene (Sel. = 81-82%), with benzene (Sel. = 17%), and cyclohexane as side product (Sel. < 1%), at > 99 % conversion of 1,3-cyclohexadiene within 9-10 mins. Instead of using H<sub>2</sub> (4 bar), it was observed that, 1,3-cyclohexadiene easily dehydrogenated into benzene. In contrast, these catalysts were completely inactive for the hydrogenation of benzene under the same reaction condition. In the same way, further Pd/C-3 to 5 catalysts were also investigated for the disproportionation of 1,3-cyclohexadiene (Table 5.6, Entry 3-5).

**Table 5.6** Pd-catalyzed catalyzed disproportionation of 1,3-cyclohexadiene activities by using 4 bar H<sub>2</sub> condition.<sup>a</sup>



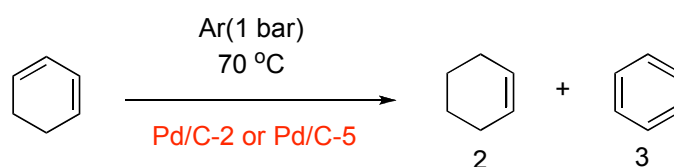
E	Catlysts	1,3- CHD/Pd	Time /min <sup>-1</sup>	Conv. % <sup>b</sup>	Sel. 1% <sup>b</sup>	Sel. 2% <sup>b</sup>	Sel. 3% <sup>b</sup>
1	Pd/C-2	14375	8	89.5	0,5	80.5	19.0
2	Pd/C-2	14375	10	100	2.0	81.0	17.0
3	Pd/C-3	14375	11	100	1.5	81.0	17.5
4	Pd/C-4	14375	12	99.5	1.5	81.5	17.0
5	Pd/C-5	8011	12	100	1.0	82.0	17.0

[a] Selective hydrogenation of 1,3-cyclohexadiene (790 mg), Pd/C-2 to 5 NPs (10 mg), reaction condition: H<sub>2</sub> 4 bar, 70 °C, (b) conversion, and selectivity calculated by GC-MS, and GC- analysis by using *n*-heptane as internal standard.

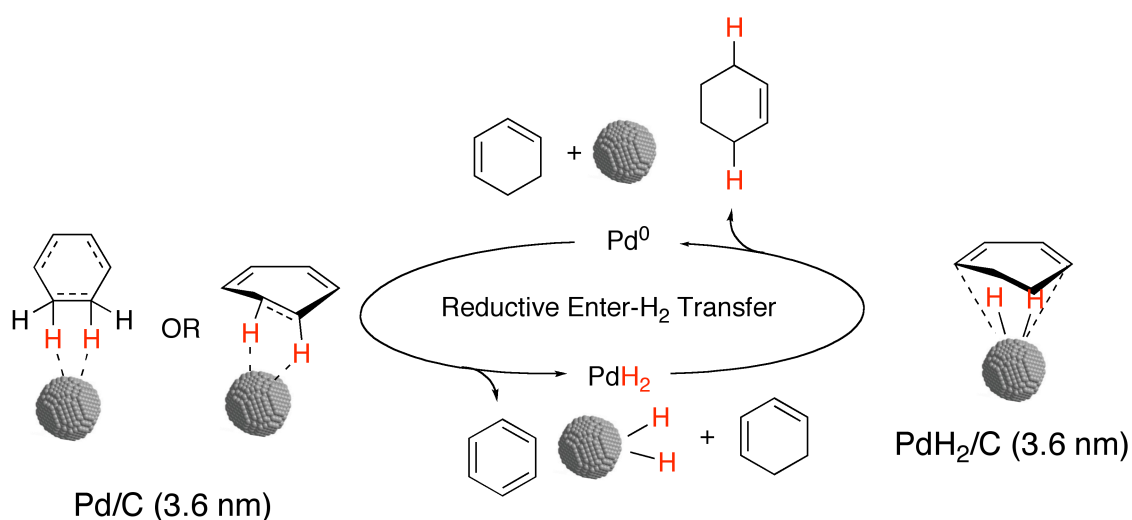
The heterogeneous nature of this system was confirmed by their activity to the disproportionation of 1,3-cyclohexadiene into benzene and cyclohexene, a reaction typically catalysed by metal surfaces/nanoparticles (See scheme 1).<sup>[31]</sup> The Pd-catalyst supported onto activated charcoal displayed slightly lower activities in the hydrogantion of 1,3-cyclohexadiene (24.0 s<sup>-1</sup>) than in the hydrogenation of cyclohexene (35.1 s<sup>-1</sup>). In contrast, Pd-NPs also synthesized by sputtering but supported onto SiO<sub>2</sub> and Al<sub>2</sub>O<sub>3</sub> displayed much higher activity in the hydrogenation

of cyclohexadiene than in the hydrogenation of cyclohexene.<sup>[24-26]</sup> This behavior was attributed to a support effect and it was also related with the higher cyclohexene selectivity (ca. 95-98 %) and lower benzene (ca. 2-5 %) production reported by the Pd-NPs supported onto SiO<sub>2</sub> and Al<sub>2</sub>O<sub>3</sub>.

**Table 5.7** Pd-catalyzed catalyzed disproportionation of 1,3-cyclohexadiene activities under Ar condition.



E	Catlysts	1,3-CHD/Pd	Time /min <sup>-1</sup>	Conv. % <sup>b</sup>	Sel. 2% <sup>b</sup>	Sel. 3% <sup>b</sup>
1	Pd/C- 2	14375	30	40	49.5	50.5
2	Pd/C- 2	14375	60	75.5	49	51
3	Pd/C- 2	14375	105	100	49	51
4	Pd/C-5	8011	120	100	49	51



**Scheme 5.1** Pd/C-2, Pd/C-5 catalyzed disproportionation of 1,3-cyclohexadiene by reductive enter hydrogen transfer mechanism.



Further Pd/C-2, Pd/C-5 catalysts investigated for the disproportion of 1,3-cyclohexadiene without using H<sub>2</sub> under Ar (1 bar) atmosphere. The reaction showed simultaneous dehydrogenation-by the reductive H<sub>2</sub> transfer (RHT) mechanism. The reactions revealed 49% cyclohexene, and 51% benzene at >99% conversion (Table 5.7). Proposed a mechanistic approach for the Pd-catalyzed simultaneous dehydrogenation-hydrogenation of 1,3-cyclohexadiene by reductive enter-H<sub>2</sub> transfer mechanism (Scheme 5.1) indicated the modification of Pd/C surface into PdH<sub>2</sub>/C NPs during reaction. The PdH<sub>2</sub>/C-NPs are strongly active for the hydrogenation, which simultaneously hydrogenated 1,3-cyclohexadiene into cyclohexene during the reaction.

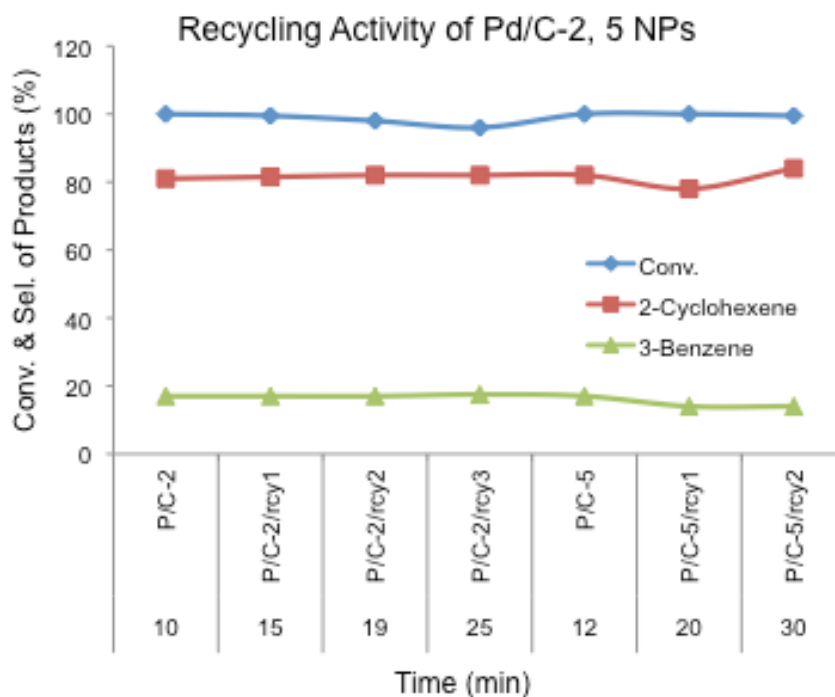


**Figure 5.8** Recycling activities of the Pd/C-2, Pd/C-5 for the disproportion of 1,3-cyclohexadiene.

Furthermore Pd/C-2, and Pd/C-5 catalysts were tested 3-4-time for the estimation of the recycling activities for the disproportion of 1,3-cyclohexadiene. So the recycled catalysts revealed almost same selectivity of products, cyclohexene

(Sel. = 82-84 %) benzene (Sel. = 14-17%), at > 99 % conversion, under the optimized condition. But the rate of reactions catalyzed by recycling catalysts was slightly decreased, gradually taking more time for >99 % conversion of 1,3-cyclohexadiene (Figure 5.8).

### 5.3 Conclusions

The magnetron-sputtering approach was used for the deposition of palladium nanoparticles onto commercially available activated charcoal (AC). The study of the effect of the deposition time revealed the linear dependence of the deposition time with the final metal content and the formation of small (ca. 3.7 nm) and uniformly distributed Pd-NPs onto the solid supports. H<sub>2</sub>-chemisorption measurement revealed a decrease of the metal dispersion (ca. metallic surface area) with the deposition time. The Pd-NPs catalytic performances were evaluated in the reduction of model of model substrates (i.e., nitrobenzene, 1,3-cyclohexadiene and cyclohexene) at 70 – 80 °C under 4 bar dihydrogen (H<sub>2</sub>). The catalytic results revealed improved efficiencies in terms of activity and selectivity to those displayed by commercially available catalyst. Disproportion of 1,3-cyclohexadiene and cyclohexene were revealed also as active processes under reaction conditions.

### 5.5- References:

- [1] Nishihata, Y.; Mizuki, J.; Akao, T.; Tanaka, H.; Uenishi, M.; Kimura, M.; Okamoto, T.; Hamada, N. *Nature* **2002**, *418*, 164-167.
- [2] Kim, S. W.; Kim, M.; Lee, W. Y.; Hyeon, T. *J. Am. Chem. Soc.* **2002**, *124*, 7642-7643.
- [3] Jin, M. S.; Zhang, H.; Xie, Z. X.; Xia, Y. N. *Angew. Chem. Int. Ed.* **2011**, *123*, 7996-8000.
- [4] Jin, M. S.; Zhang, H.; Xie, Z. X.; Xia, Y. N. *Angew. Chem. Int. Ed.* **2011**, *50*, 7850-7854.
- [5] Xiong, Y. J.; Xia, Y. N. *Adv. Mater.* **2007**, *19*, 3385-3391.
- [6] Balanta, A.; Godard, C.; Claver, C. *Chem. Soc. Rev.* **2011**, *40*, 4973-4985.

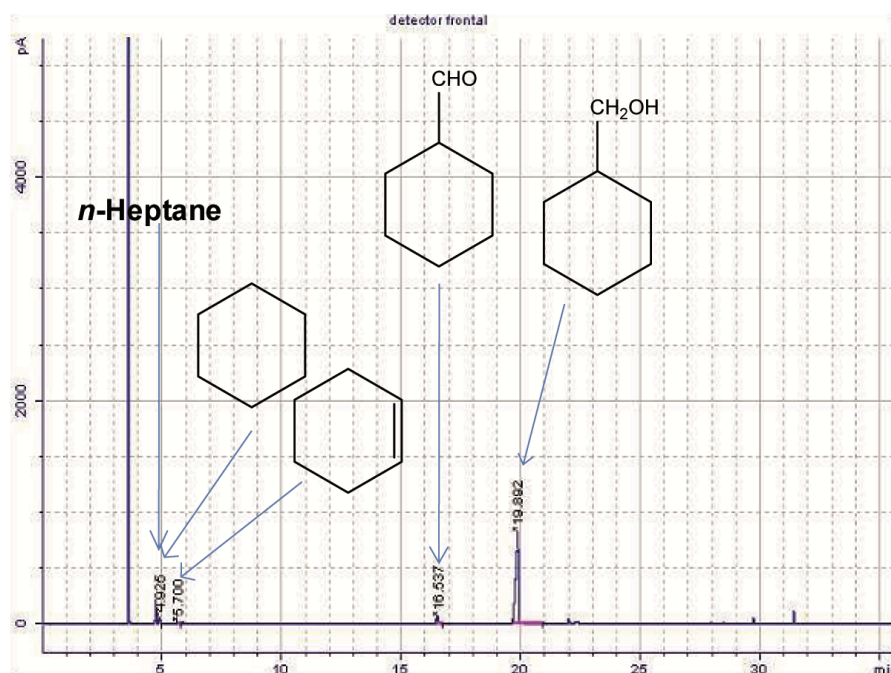
- [7] Martins, D. d. L.; Alvarez, H. M.; Aguiar, L. C. S. *Tetrahedron Lett.* **2010**, *51*, 6814.
- [8] Albiter, M. A.; Morales, R.; Zaera, F. *Appl. Catal., A* **2011**, *391*, 386.
- [9] Pallavicini, P.; Chirico, G.; Collini, M.; Dacarro, G.; Dona, A.; D'Alfonso, L.; Falqui, A.; Diaz-Fernandez, Y.; Freddi, S.; Garofalo, B.; Genovese, A.; Sironi, L.; Taglietti, A. *Chem. Commun.* **2011**, *47*, 1315.
- [10] Scholten, J. D.; Leal, B. C.; Dupont, J. *ACS Catal.* **2012**, *2*, 184-200.
- [11] Kuwabata, S.; Tsuda, T.; Torimoto, T. *J. Phys. Chem. Lett.* **2010**, *1*, 3177-3188.
- [12] Meyer, C.; Hager, V.; Schwieger, W.; Wasserscheid, P. *J. Catal.* **2014**, *292*, 157-165.
- [13] Wender, H.; Andrezza, M. L.; Correia, R. R. B.; Teixeira, S. R.; Dupont, J. *Nanoscale* **2011**, *3*, 1240-1245.
- [14] Richter, K.; Birkner, A.; Mudring, A.-V. *Angew. Chem. Int. Ed.* **2010**, *49*, 2431-2435.
- [15] Bussamara, R.; Eberhardt, D.; Feil, A. F.; Migowski, P.; Wender, H.; Moraes, D. P. d.; Machado, G.; Papale'ó, R. M.; Teixeira, S. R.; Dupont, J. *Chem. Commun.* **2013**, *49*, 1273-1275.
- [16] Wender, H.; Oliveira, L. F. d.; Migowski, P.; Feil, A. F.; Lissner, E.; Pechtl, M. H. G.; Teixeira, S. R.; Dupont, J. *J. Phys. Chem. C*, **2010**, *114*, 11764-11768.
- [17] Wender, H.; Migowski, P.; Feil, A. F.; Teixeira, S. R.; Dupont, J. *Coord. Chem. Rev.* **2013**, *257*, 2468-2483.
- [18] Wender, H.; Gonçalves, R. V.; Feil, A. F.; Migowski, P.; Poletto, F. S.; Pohlmann, A. R.; Dupont, J.; Teixeira, S. R. *J. Phys. Chem. C*, **2011**, *115*, 16362-16367.
- [19] Kauling, A.; Ebeling, G.; Morais, J.; Pádua, A.; T. Grehl; Brongersma, H. H.; Dupont, J. *Langmuir* **2013**, *29*, 14301-14306.
- [20] Luza, L.; Gual, A.; Eberhardt, D.; Teixeira, S. R.; Chiaro, S. S. X.; Dupont, J. *ChemCatChem* **2013**, *5*, 2471-2478.
- [21] Abe, T.; Tanizawa, M.; Watanabe, K.; Taguchi, A. *Energy Environ. Sci.* **2009**, *2*, 315-321.
- [22] Liu, B.; Wen, L.; Zhao, X. *Sol. Energy Mater. Sol. Cells* **2008**, *92*, 1-10.
- [23] Kashin, A. S.; Ananikov, V. P. *Russ. Chem. Bull. Int. Ed.* **2007**, *60*, 2602-2607.

- [24] Foppa, L.; Luza, L.; Gual, A.; Weibel, D. E.; Eberhardt, D.; Teixeira, S. R.; Dupont, J. Sputtering-deposition of Ru nanoparticles onto Al<sub>2</sub>O<sub>3</sub> modified with imidazolium ionic liquids: synthesis, characterisation and catalysis. *Dalton Transactions* **2015**.
- [25] Luza, L.; Gual, A.; Eberhardt, D.; Teixeira, S. R.; Chiaro, S. S. X.; Dupont, J. "Imprinting" Catalytically Active Pd Nanoparticles onto Ionic-Liquid-Modified Al<sub>2</sub>O<sub>3</sub> Supports. *ChemCatChem* **2013**, *5*, 2471-2478.
- [26] Luza, L.; Gual, A.; Rambor, C. P.; Eberhardt, D.; Teixeira, S. R.; Bernardi, F.; Baptista, D. L.; Dupont, J. Hydrophobic effects on supported ionic liquid phase Pd nanoparticle hydrogenation catalysts. *Physical Chemistry Chemical Physics* **2014**.
- [27] Koenigsmann, C.; Santulli, A. C.; Gong, K.; Vukmirovic, M. B.; Zhou, W.-p.; Sutter, E.; Wong, S. S.; Adzic, R. R. Enhanced Electrocatalytic Performance of Processed, Ultrathin, Supported Pd–Pt Core–Shell Nanowire Catalysts for the Oxygen Reduction Reaction. *Journal of the American Chemical Society* **2011**, *133*, 9783-9795.
- [28] Pope, D.; Walker, D. S.; Moss, R. L. The structure and activity of supported metal catalysts. *Journal of Catalysis* **1973**, *28*, 46-53.
- [29] Turáková, M.; Králik, M.; Lehocký, P.; Pikna, L.; Smrčová, M.; Remeteiová, D.; Hudák, A. Influence of preparation method and palladium content on Pd/C catalysts activity in the liquid phase hydrogenation of nitrobenzene to aniline. *Applied Catalysis A: General* **2014**, *476*, 103-112.
- [30] Cárdenas-Lizana, F.; Hao, Y.; Crespo-Quesada, M.; Yuranov, I.; Wang, X.; Keane, M. A.; Kiwi-Minsker, L. Selective Gas Phase Hydrogenation of p-Chloronitrobenzene over Pd Catalysts: Role of the Support. *ACS Catalysis* **2013**, *3*, 1386-1396.
- [31] Luza, L.; Gual, A.; Dupont, J. The Partial Hydrogenation of 1,3-Dienes Catalysed by Soluble Transition-Metal Nanoparticles. *ChemCatChem* **2014**, *6*, 702-710.
- [32] W. L. F. Armarego; Perrin, D. D.: *Purification of Laboratory Chemicals, Oxford (UK)*; 4th ed.; Butterworth-Heineman, 1997.

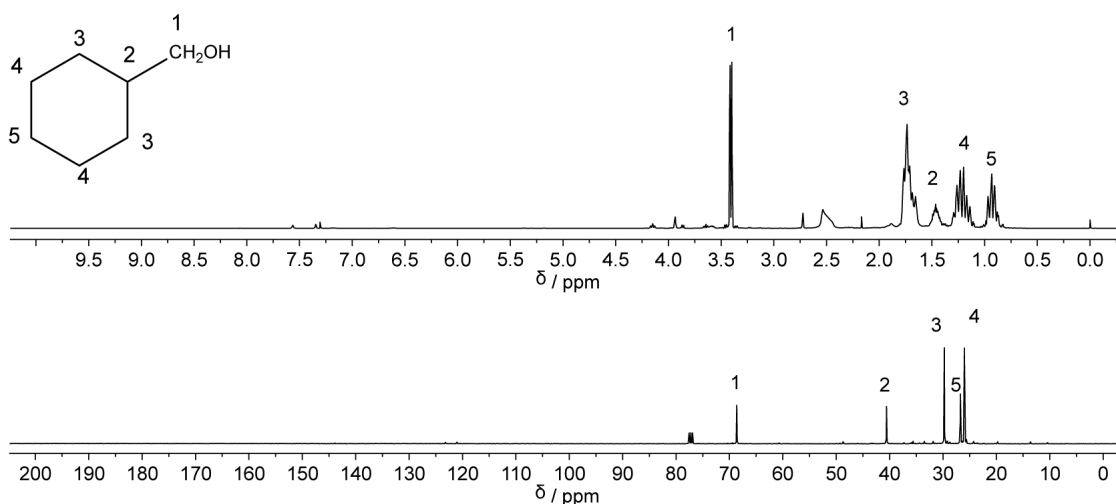
## **CHAPTER-6**

### **“GC-analysis, NMR Spectras of Compounds, And Reactions Mixtures”**

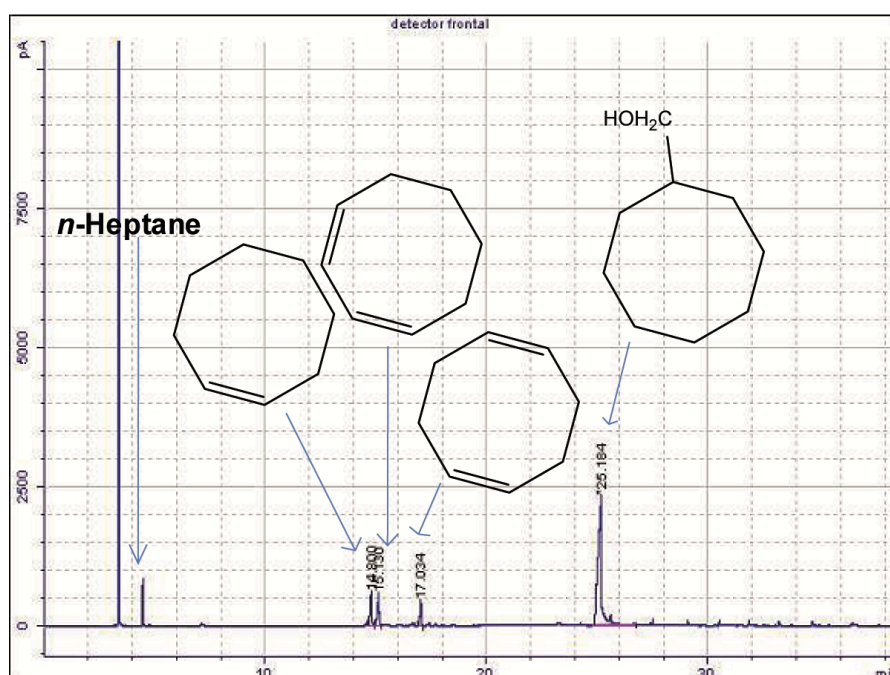
## 6.1 GC analysis and NMR spectras for hydroformylation of alkenes by using CO<sub>2</sub> as CO source.



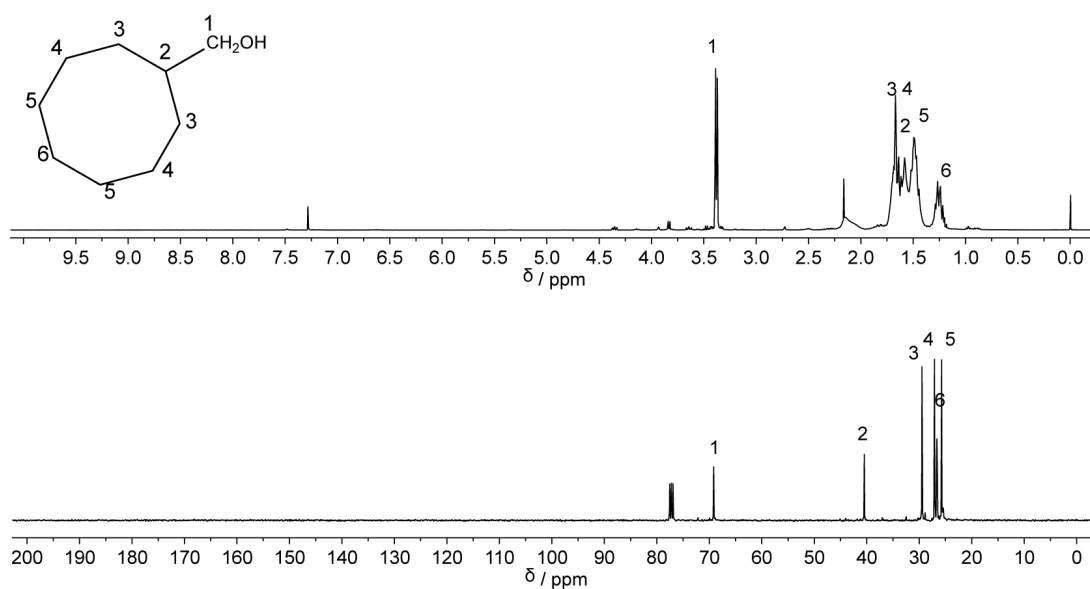
**Figure 6.1** GC analysis of the crude reaction mixture obtained from the Ru- catalysed hydroformylation of cyclohexene using CO<sub>2</sub> as a CO source.



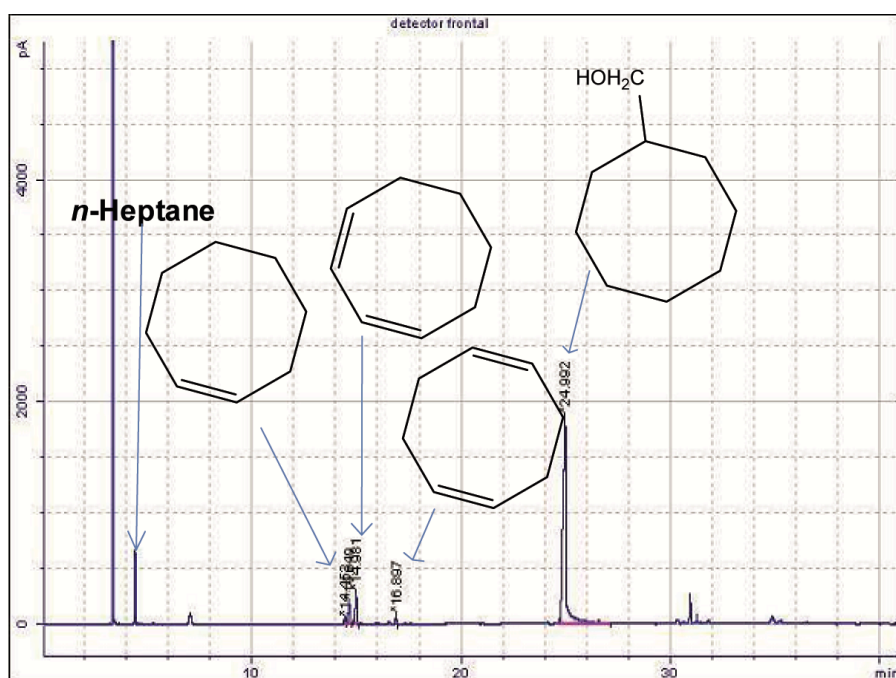
**Figure 6.2** <sup>1</sup>H (400 MHz, CDCl<sub>3</sub>) and <sup>13</sup>C {<sup>1</sup>H} (100 MHz, CDCl<sub>3</sub>) NMR analysis of the reaction mixture after vacuum drying obtained from the Ru-catalysed hydroformylation of cyclohexene using CO<sub>2</sub> as a CO source.



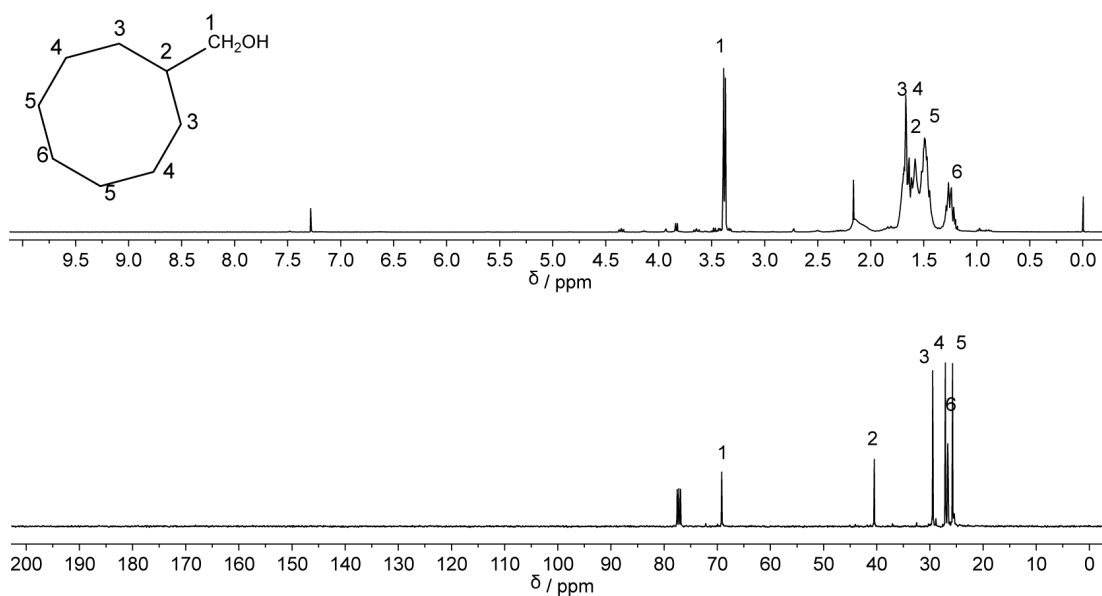
**Figure 6.3** GC analysis of the crude reaction mixture obtained from the Ru-catalysed hydroformylation of cyclooctene using CO<sub>2</sub> as a CO source.



**Figure 6.4** <sup>1</sup>H (400 MHz, CDCl<sub>3</sub>) and <sup>13</sup>C {<sup>1</sup>H} (100 MHz, CDCl<sub>3</sub>) NMR analysis of the reaction mixture after vacuum drying obtained from the Ru-catalysed hydroformylation of cyclooctene using CO<sub>2</sub> as a CO source.

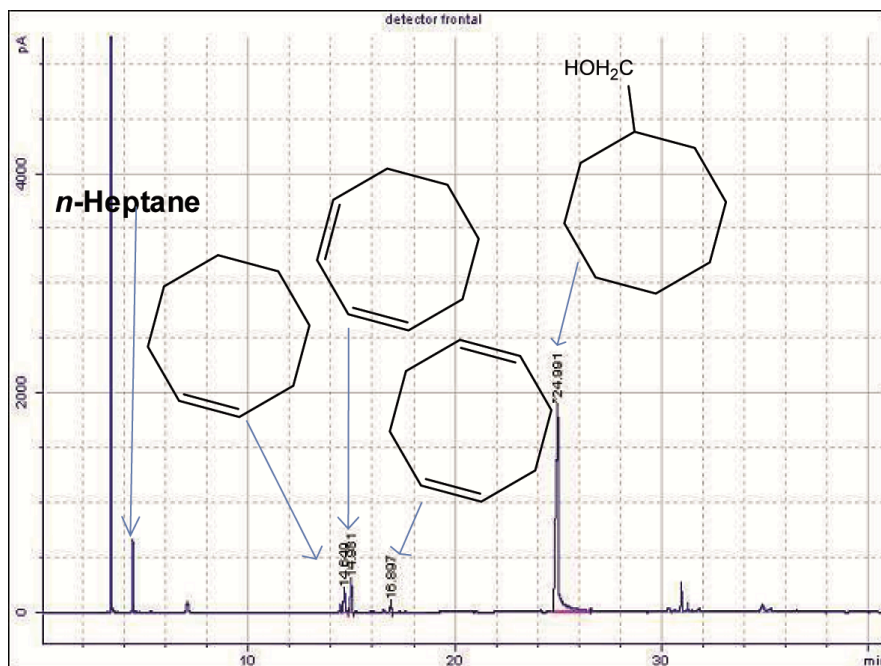


**Figure 6.5** GC analysis of the crude reaction mixture obtained from the Ru-catalysed hydroformylation of 1,5-cyclooctadiene using  $\text{CO}_2$  as a CO source.

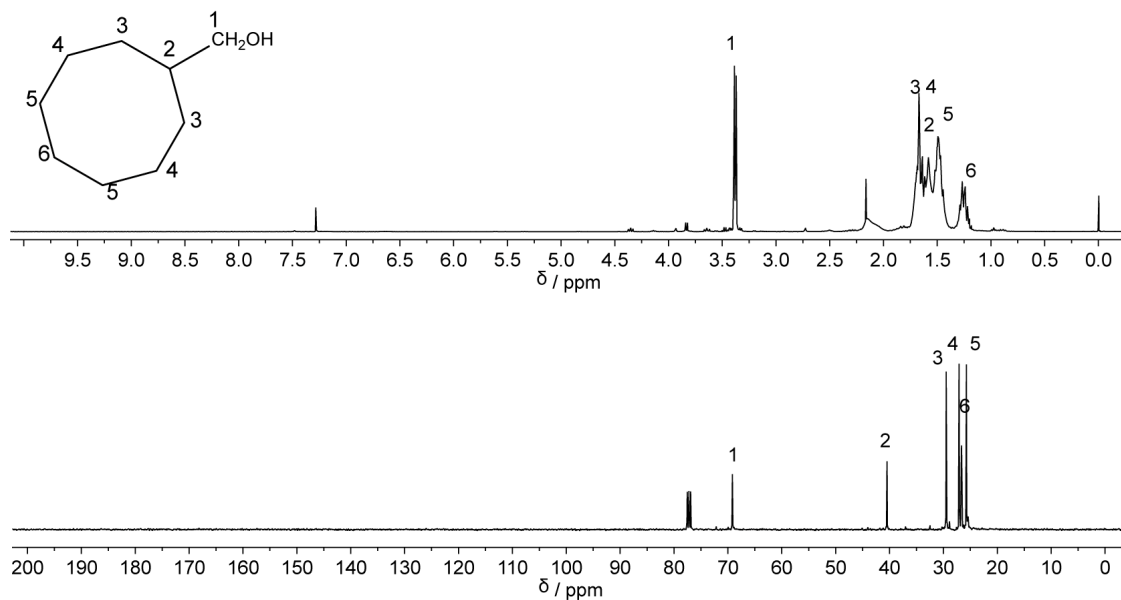


**Figure 6.6**  $^1\text{H}$  (400 MHz,  $\text{CDCl}_3$ ) and  $^{13}\text{C}$   $\{^1\text{H}\}$  (100 MHz,  $\text{CDCl}_3$ ) NMR analysis of the reaction mixture after vacuum drying obtained from the Ru-catalysed hydroformylation of 1,5-cyclooctadiene using  $\text{CO}_2$  as a CO source.

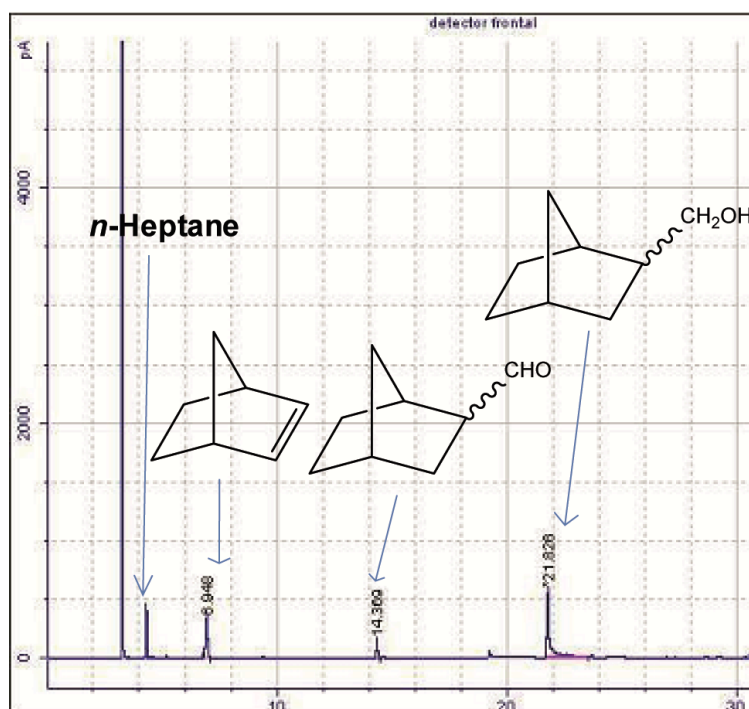




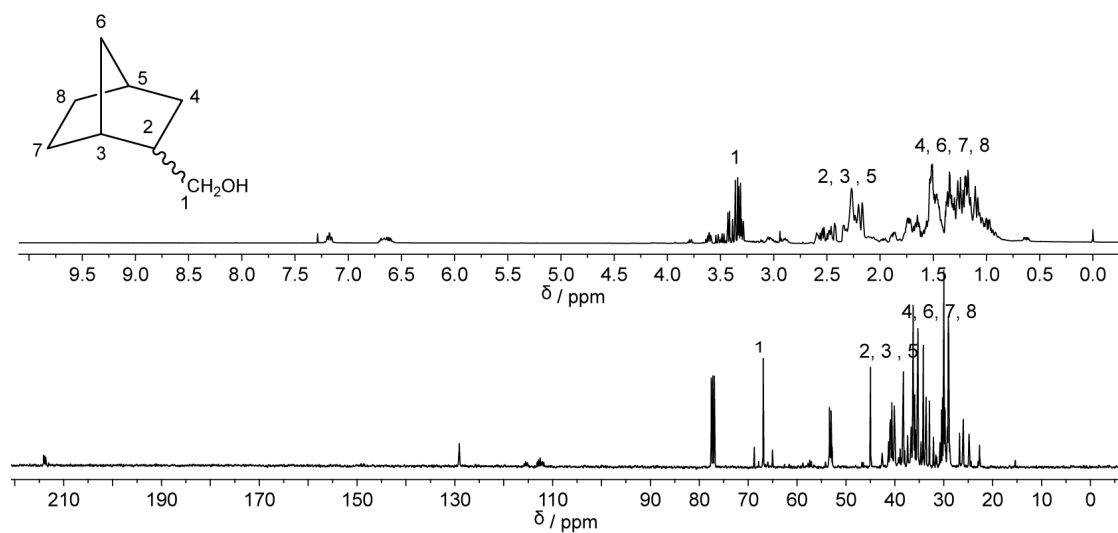
**Figure 6.7** GC analysis of the crude reaction mixture obtained from the Ru-catalysed hydroformylation of 1,3-cyclooctadiene using  $\text{CO}_2$  as a CO source.



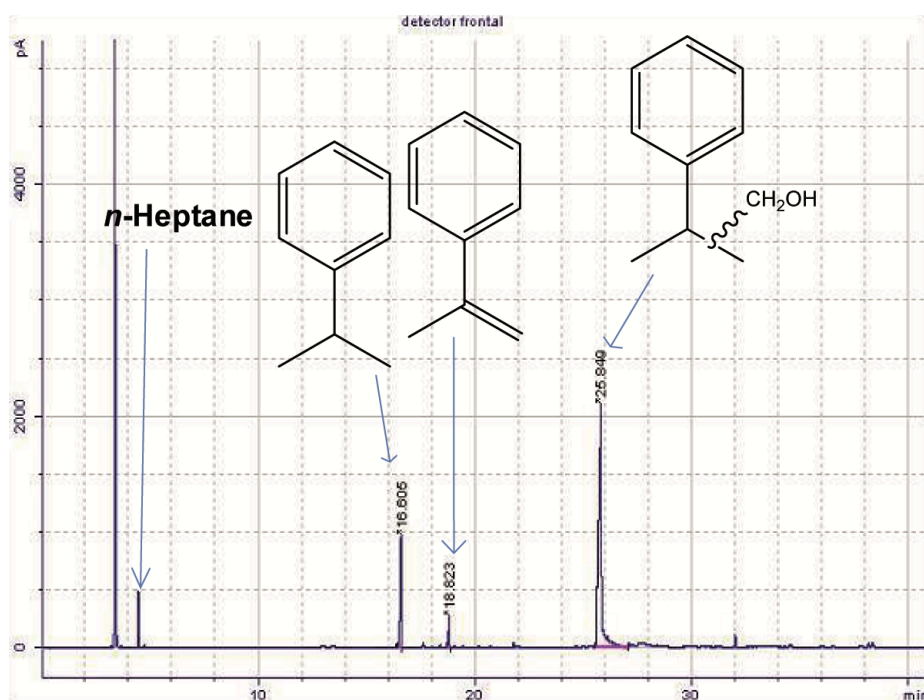
**Figure 6.8**  $^1\text{H}$  (400 MHz,  $\text{CDCl}_3$ ) and  $^{13}\text{C}$   $\{^1\text{H}\}$  (100 MHz,  $\text{CDCl}_3$ ) NMR analysis of the reaction mixture after vacuum drying obtained from the Ru-catalysed hydroformylation of 1,3-cyclooctadiene using  $\text{CO}_2$  as a CO source.



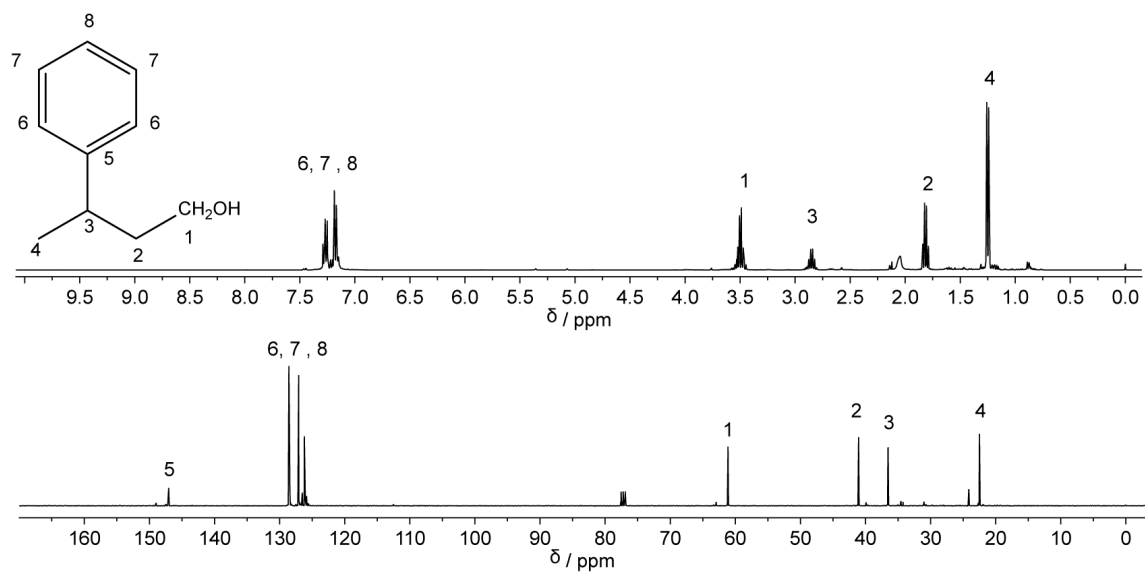
**Figure 6.9** GC analysis of the crude reaction mixture obtained from the Ru-catalysed hydroformylation of norbornene using  $\text{CO}_2$  as a CO source.



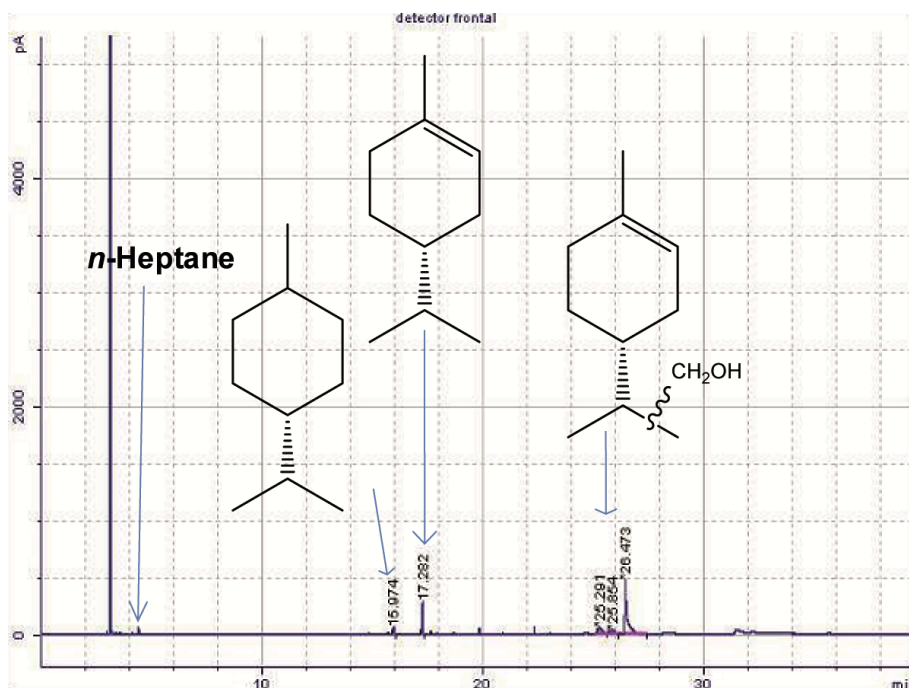
**Figure 6.10**  $^1\text{H}$  (400 MHz,  $\text{CDCl}_3$ ) and  $^{13}\text{C}$   $\{^1\text{H}\}$  (100 MHz,  $\text{CDCl}_3$ ) NMR analysis of the reaction mixture after vacuum drying obtained from the Ru-catalysed hydroformylation of norbornene using  $\text{CO}_2$  as a CO source.



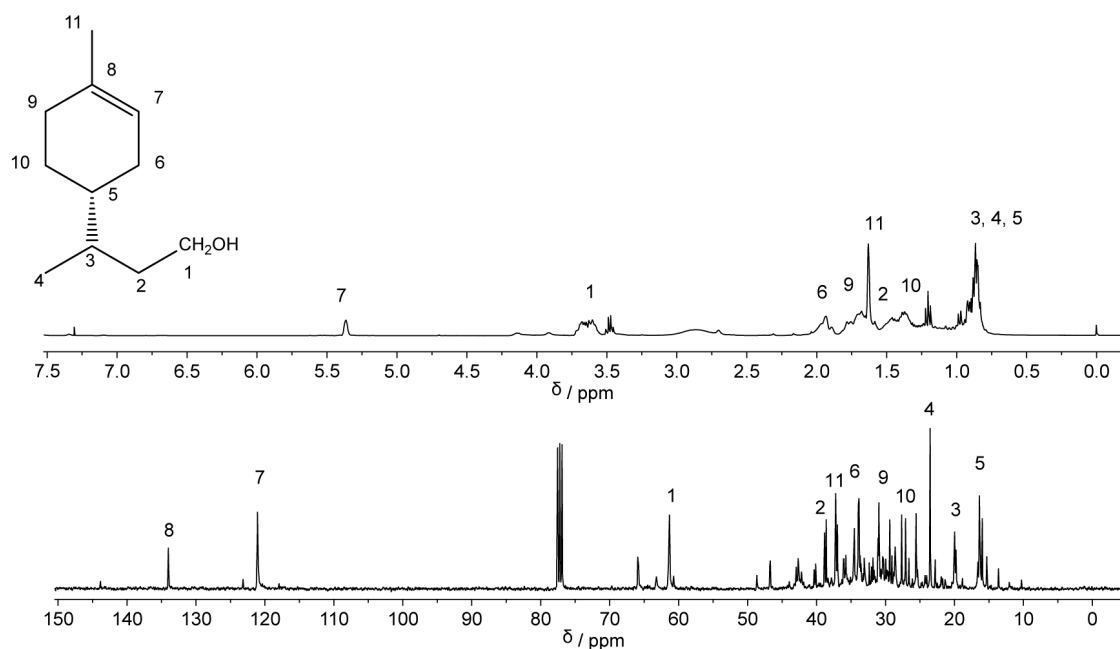
**Figure 6.11** GC analysis of the crude reaction mixture obtained from the Ru-catalysed hydroformylation of 1,1'-methylstyrene using  $\text{CO}_2$  as a CO source.



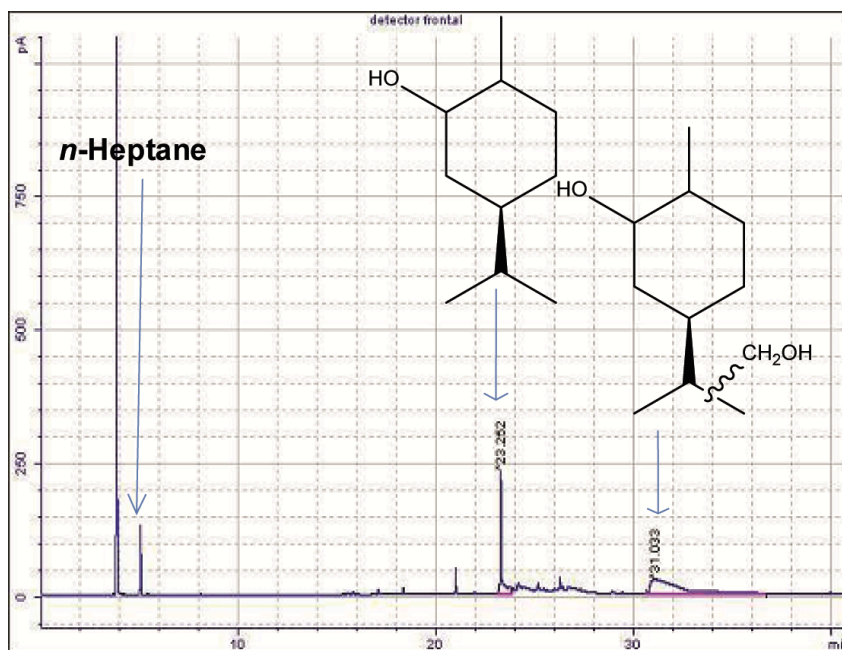
**Figure 6.12**  $^1\text{H}$  (400 MHz,  $\text{CDCl}_3$ ) and  $^{13}\text{C}$   $\{^1\text{H}\}$  (100 MHz,  $\text{CDCl}_3$ ) NMR analysis of the reaction mixture after vacuum drying obtained from the Ru-catalysed hydroformylation of 1,1'-methylstyrene using  $\text{CO}_2$  as a CO source.



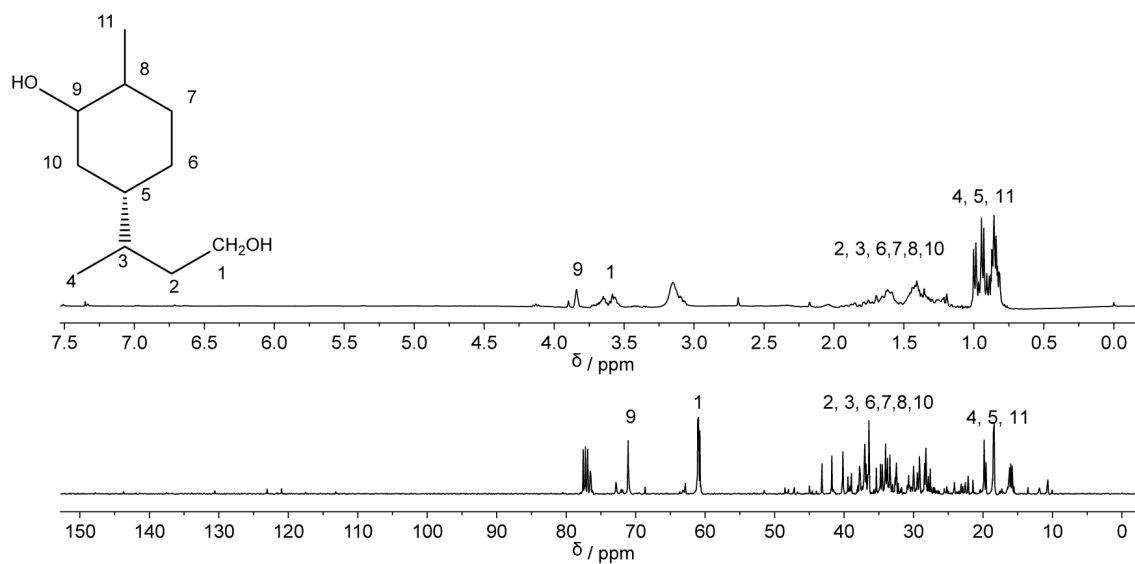
**Figure 6.13** GC analysis of the crude reaction mixture obtained from the Ru-catalysed hydroformylation of (R)-(+)-limonene using CO<sub>2</sub> as a CO source.



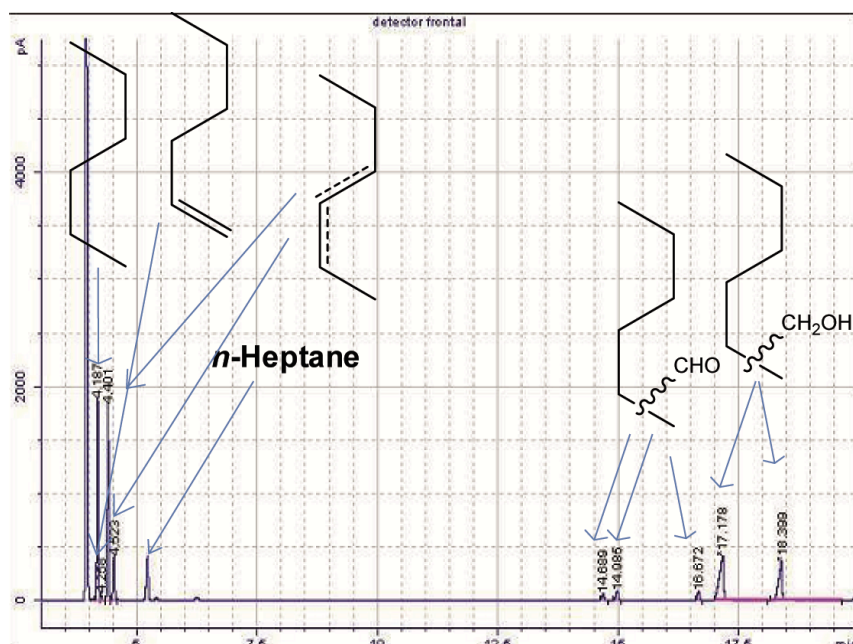
**Figure 6.14** <sup>1</sup>H (400 MHz, CDCl<sub>3</sub>) and <sup>13</sup>C {<sup>1</sup>H} (100 MHz, CDCl<sub>3</sub>) NMR analysis of the reaction mixture after vacuum drying obtained from the Ru-catalysed hydroformylation of limonene using CO<sub>2</sub> as a CO source.



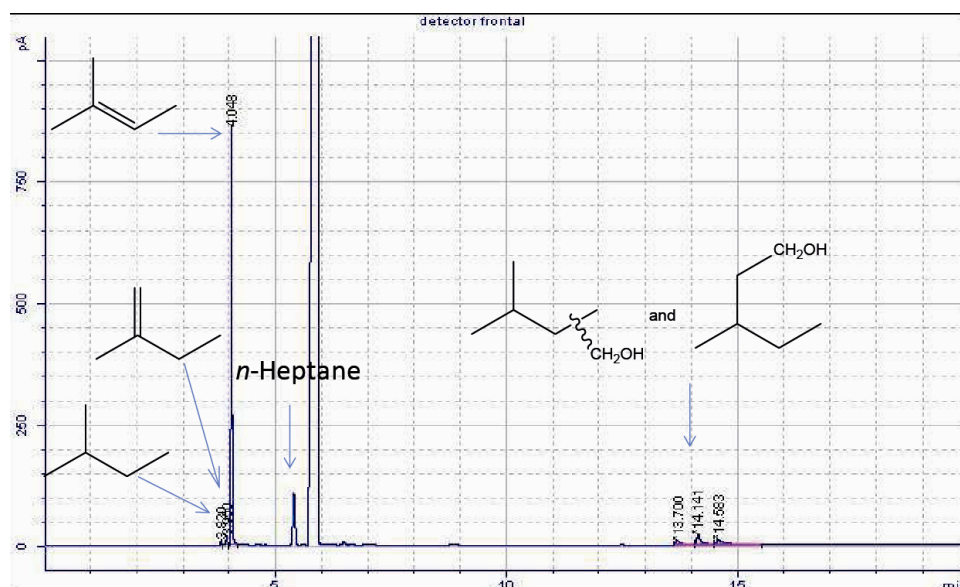
**Figure 6.15** GC analysis of the crude reaction mixture obtained from the Ru-catalysed hydroformylation of carvone using CO<sub>2</sub> as a CO source.



**Figure 6.16** <sup>1</sup>H (400 MHz, CDCl<sub>3</sub>) and <sup>13</sup>C {<sup>1</sup>H} (100 MHz, CDCl<sub>3</sub>) NMR analysis of the reaction mixture after vacuum drying obtained from the Ru-catalysed hydroformylation of carvone using CO<sub>2</sub> as a CO source.

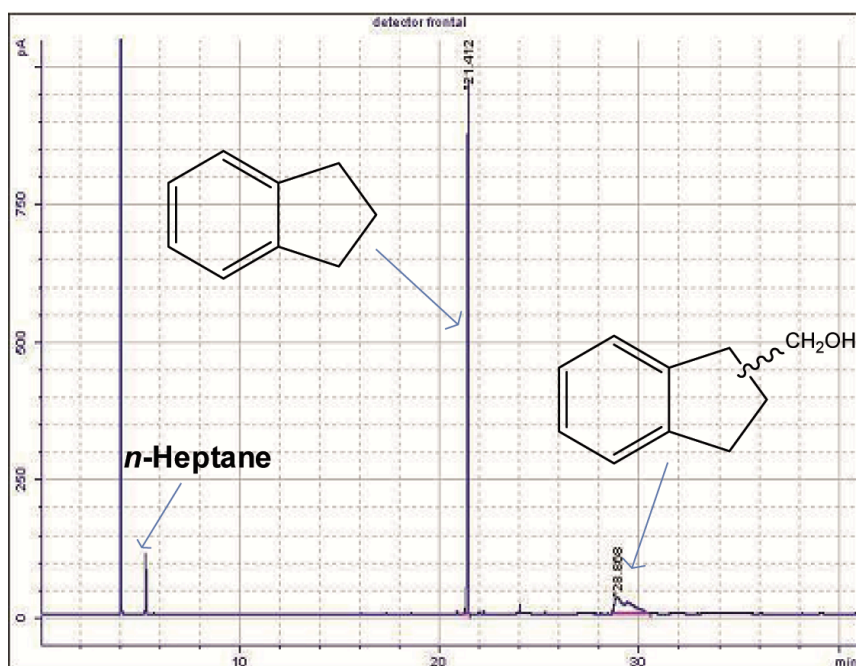


**Figure 6.17** GC analysis of the crude reaction mixture obtained from the Ru-catalysed hydroformylation of 1-hexene using  $\text{CO}_2$  as a CO source.

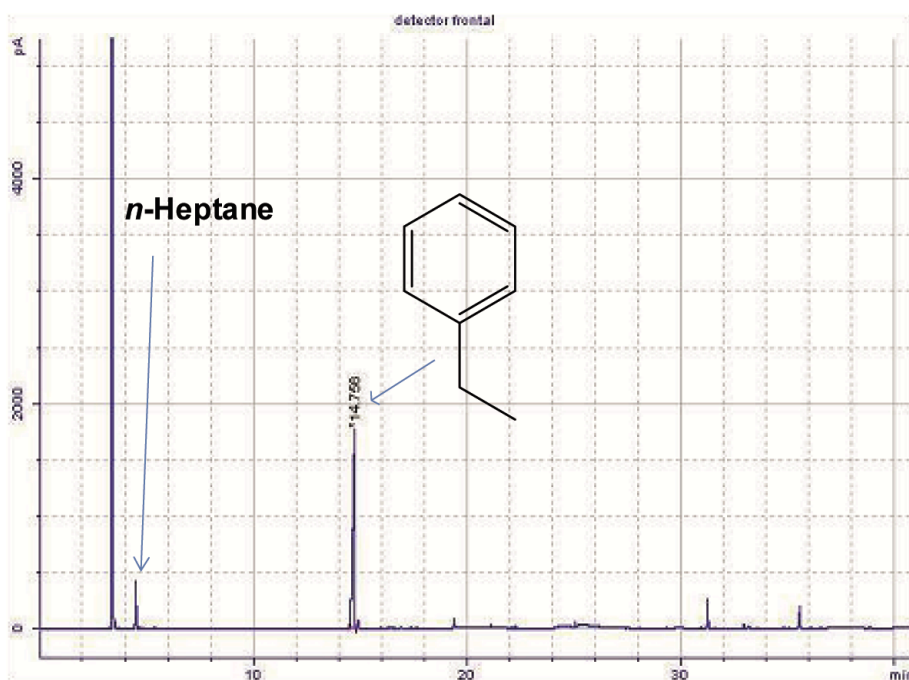


**Figure 6.18** GC analysis of the crude reaction mixture obtained from the Ru-catalysed hydroformylation of 2-methyl-2-butene using  $\text{CO}_2$  as a CO source.



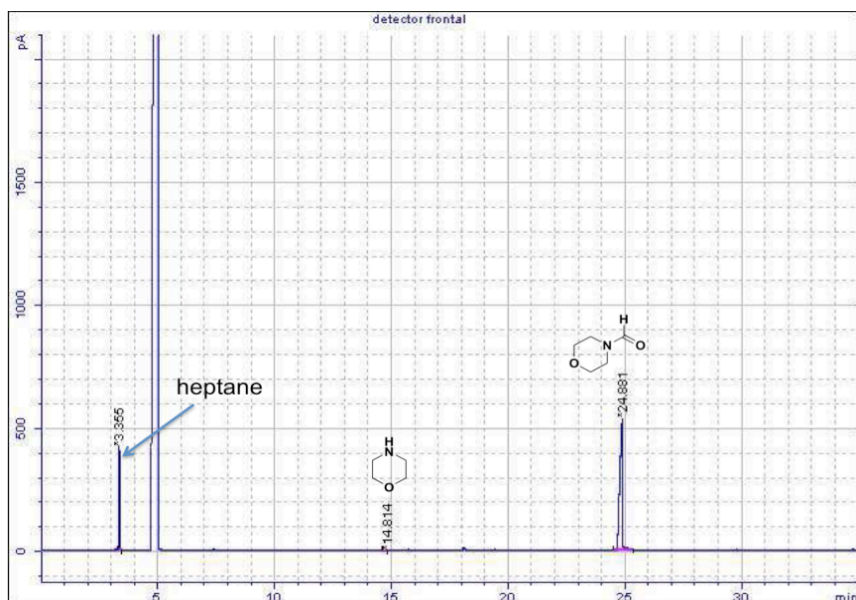


**Figure 6.19** GC analysis of the crude reaction mixture obtained from the Ru-catalysed hydroformylation of indene using CO<sub>2</sub> as a CO source.

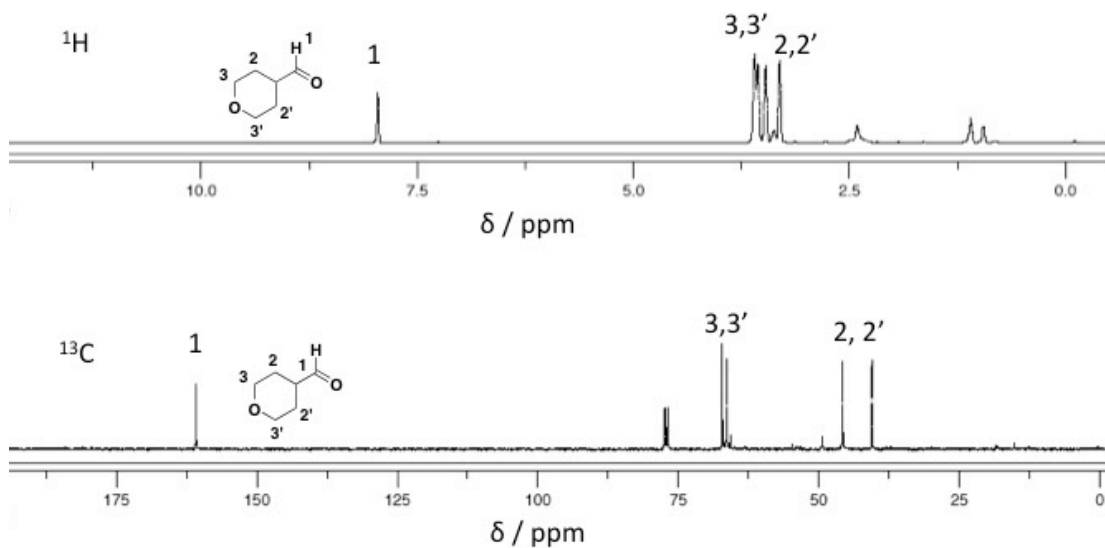


**Figure 6.20** GC analysis of the crude reaction mixture obtained from the Ru-catalysed hydroformylation of styrene using CO<sub>2</sub> as a CO source.

## 6.2 GC, NMR Spectras for Ru-catalysed *N*-formylation of amines using CO<sub>2</sub> as a CO source

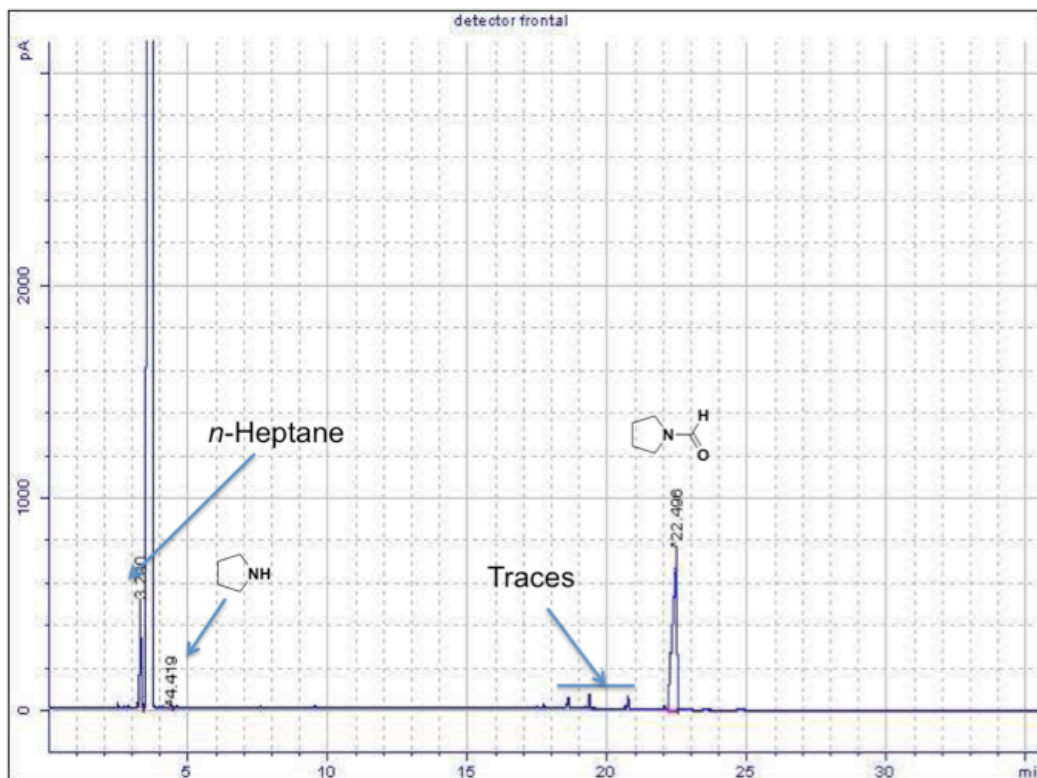


**Figure 6.21** GC analysis of the Ru-catalysed *N*-formylation of morpholine crude reaction mixture.

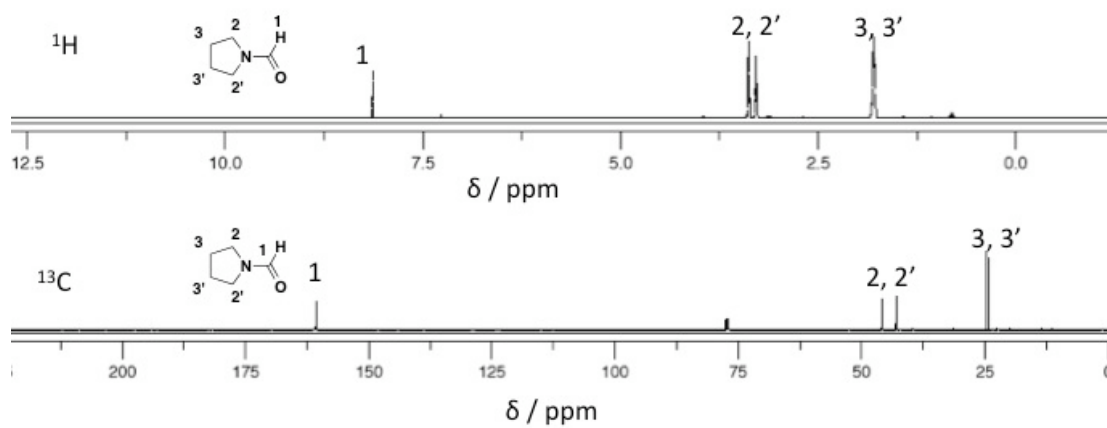


**Figure 6.22** <sup>1</sup>H (400 MHz, CDCl<sub>3</sub>) and <sup>13</sup>C {<sup>1</sup>H} (100 MHz, CDCl<sub>3</sub>) NMR analysis of the Ru-catalysed *N*-formylation of morpholine crude reaction mixture.

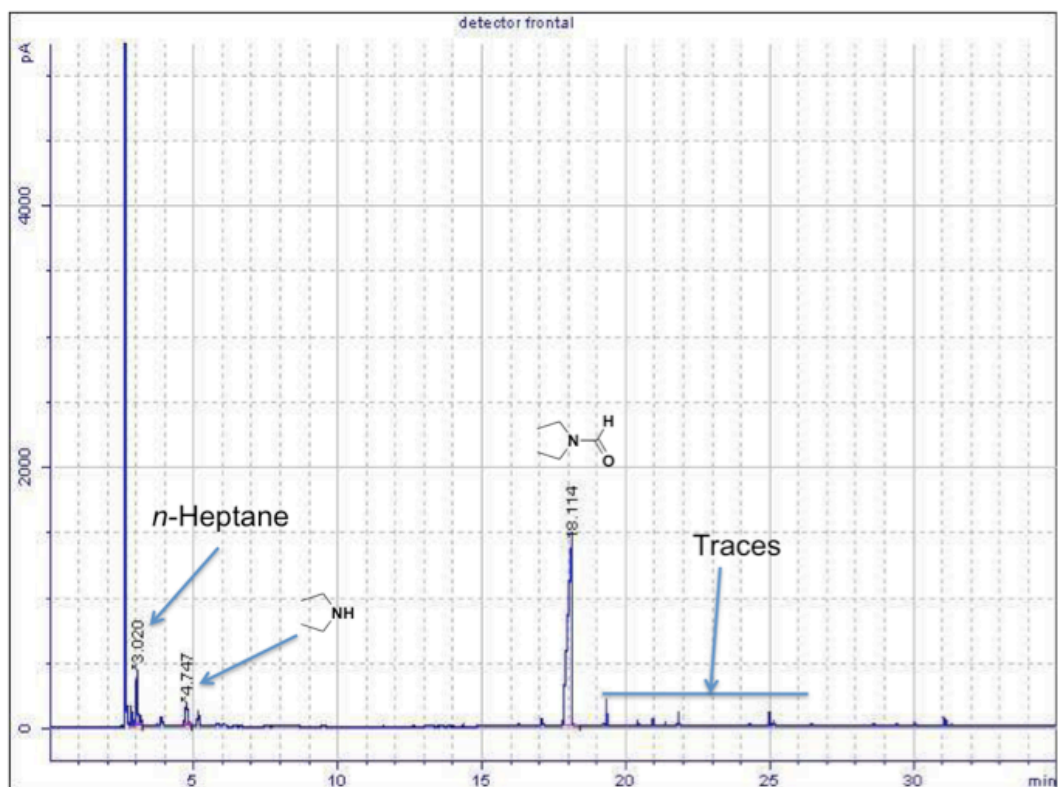




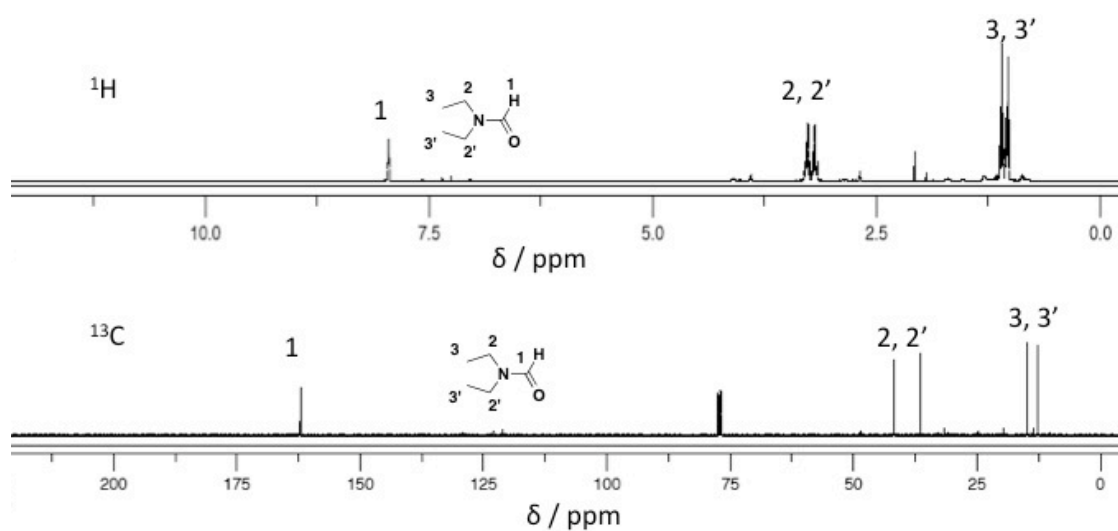
**Figure 6.23** GC analysis of the Ru-catalysed *N*-formylation of pyrrolidine crude reaction mixture.



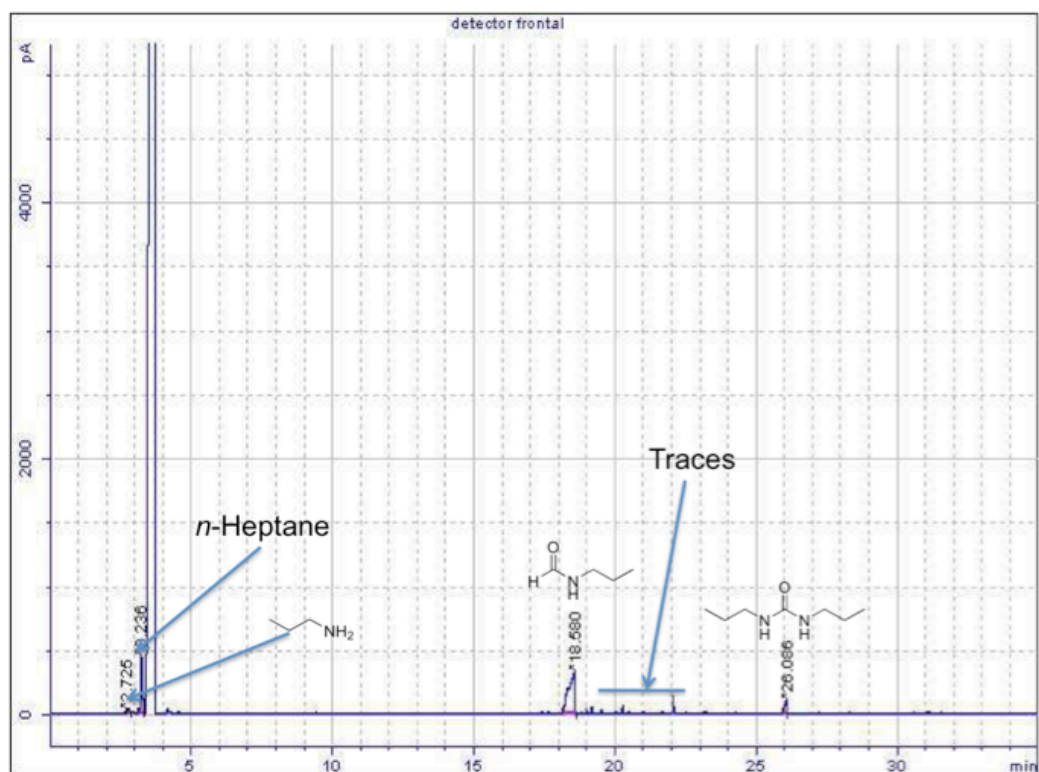
**Figure 6.24**  $^1\text{H}$  (400 MHz,  $\text{CDCl}_3$ ) and  $^{13}\text{C}$   $\{^1\text{H}\}$  (100 MHz,  $\text{CDCl}_3$ ) NMR analysis of the Ru-catalysed *N*-formylation of pyrrolidine crude reaction mixture.



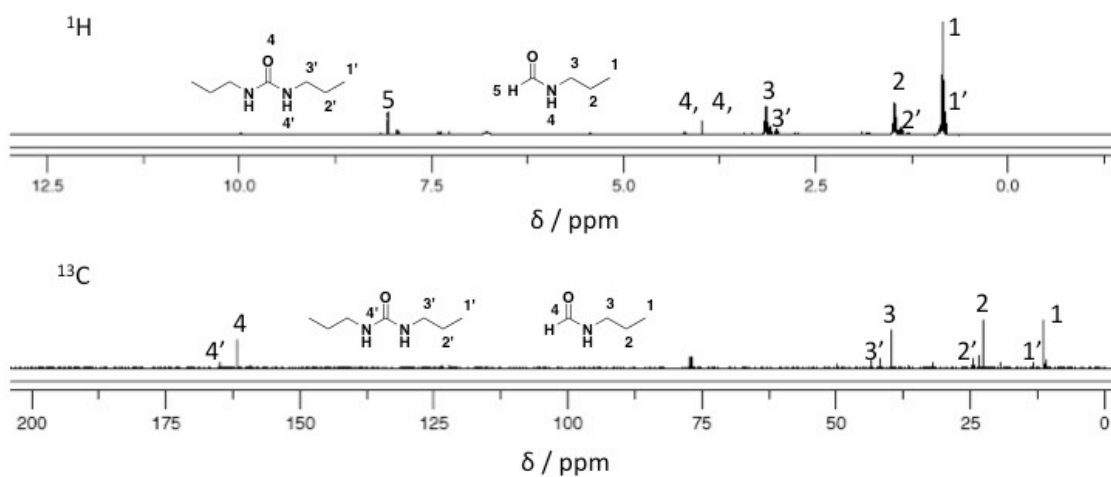
**Figure 6.25** GC analysis of the Ru-catalysed *N*-formylation of diethylamine crude reaction mixture.



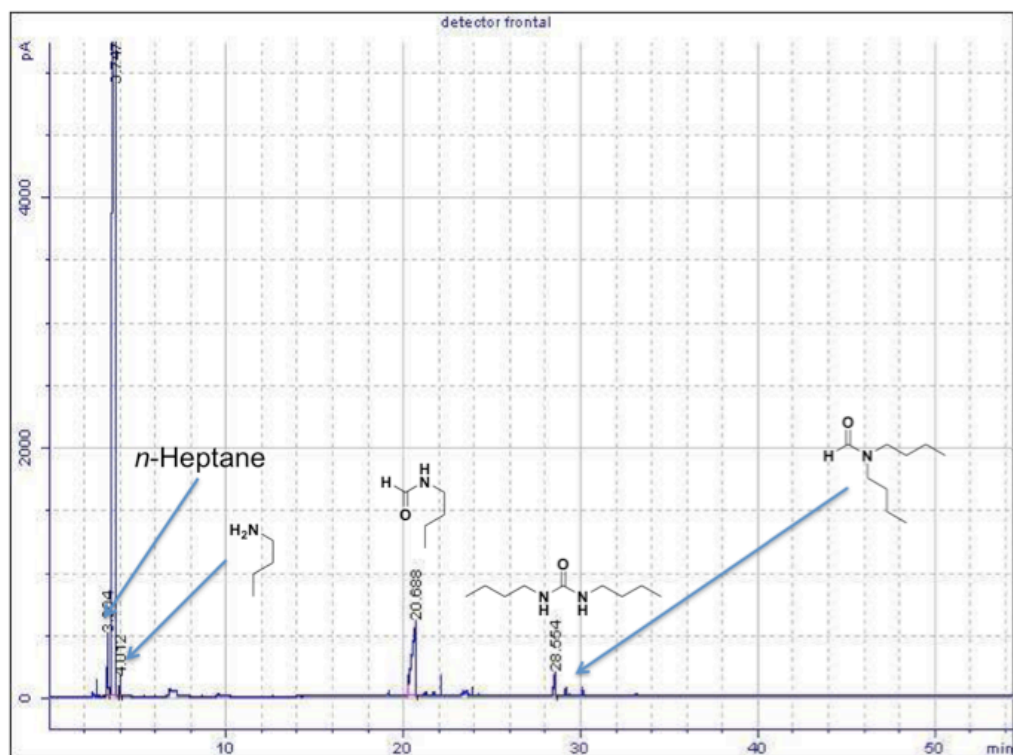
**Figure 6.26**  $^1\text{H}$  (400 MHz,  $\text{CDCl}_3$ ) and  $^{13}\text{C}$   $\{^1\text{H}\}$  (100 MHz,  $\text{CDCl}_3$ ) NMR analysis of the Ru-catalysed *N*-formylation of diethylamine crude reaction mixture.



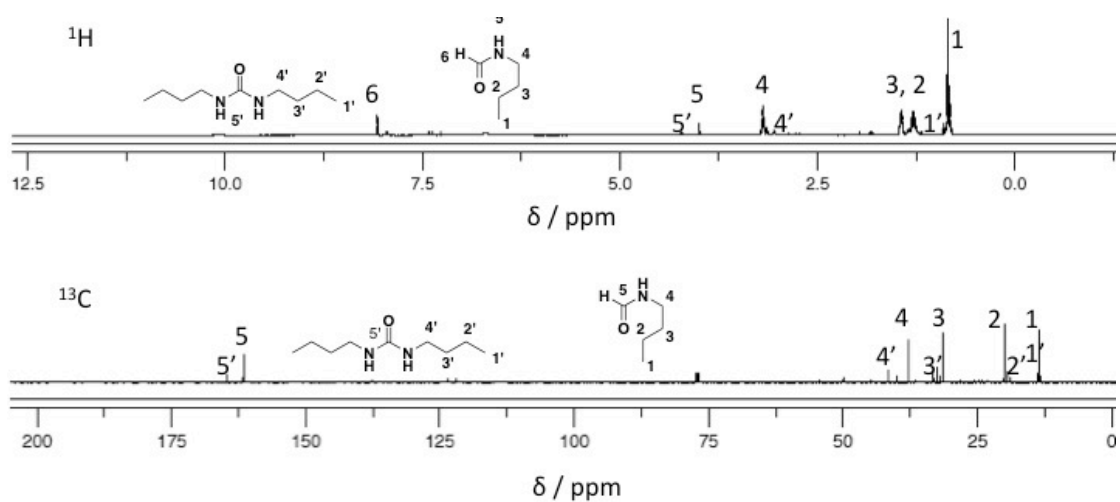
**Figure 6.27** GC analysis of the Ru-catalysed *N*-formylation of *n*-propylamine crude reaction mixture.



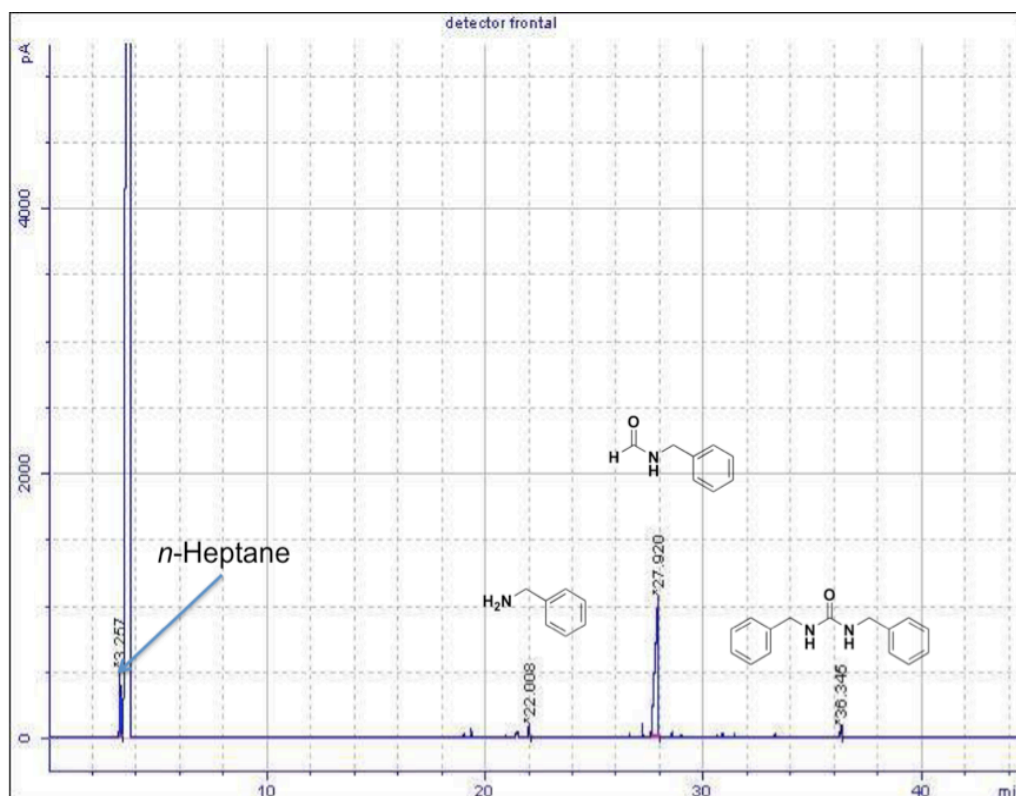
**Figure 6.28**  $^1\text{H}$  (400 MHz,  $\text{CDCl}_3$ ) and  $^{13}\text{C}$   $\{^1\text{H}\}$  (100 MHz,  $\text{CDCl}_3$ ) NMR analysis of the Ru-catalysed *N*-formylation of *n*-propylamine crude reaction mixture.



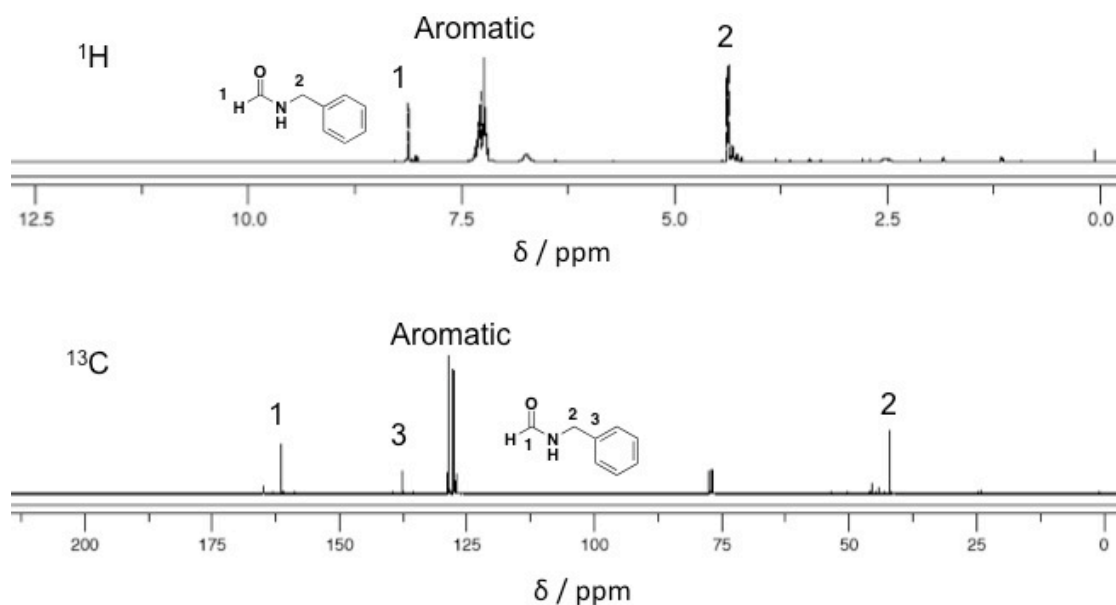
**Figure 6.29** GC analysis of the Ru-catalysed *N*-formylation of *n*-butylamine the crude reaction mixture.



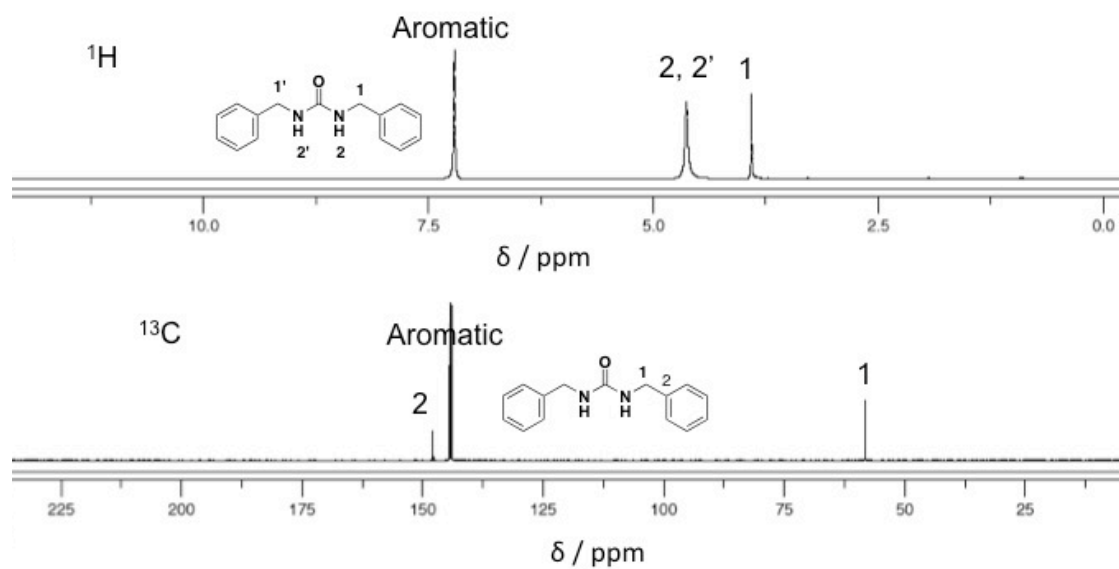
**Figure 6.30**  $^1\text{H}$  (400 MHz,  $\text{CDCl}_3$ ) and  $^{13}\text{C}$   $\{^1\text{H}\}$  (100 MHz,  $\text{CDCl}_3$ ) NMR analysis of the Ru-catalysed *N*-formylation of *n*-butylamine the crude reaction mixture.



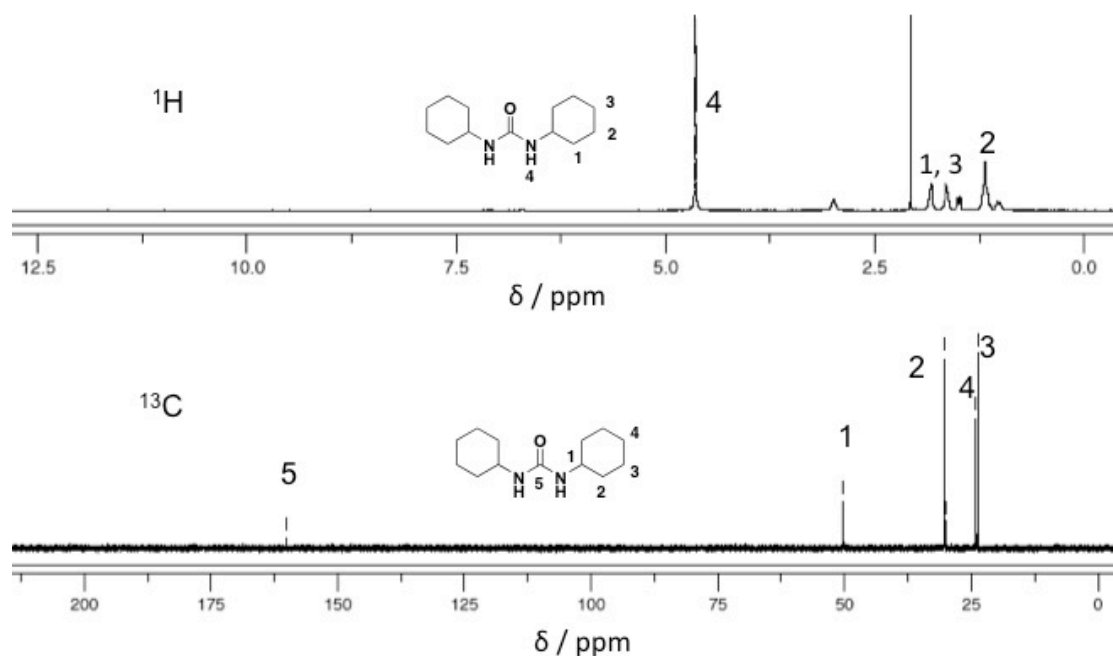
**Figure 6.31** GC analysis of the Ru-catalysed *N*-formylation of benzylamine crude reaction mixture.



**Figure 6.32**  $^1\text{H}$  (400 MHz,  $\text{CDCl}_3$ ) and  $^{13}\text{C}$   $\{^1\text{H}\}$  (100 MHz,  $\text{CDCl}_3$ ) NMR analysis of the Ru-catalysed *N*-formylation of benzylamine crude reaction mixture.



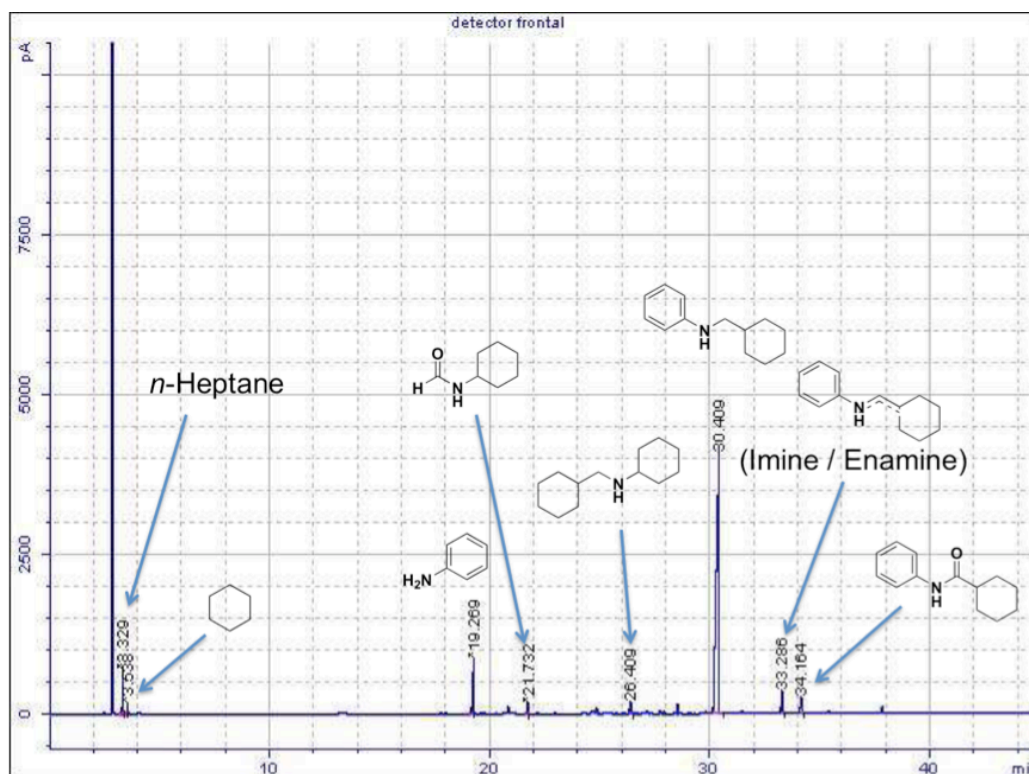
**Figure 6.33**  $^1\text{H}$  (400 MHz,  $\text{CDCl}_3$ ) and  $^{13}\text{C}$   $\{^1\text{H}\}$  (100 MHz,  $\text{D}_2\text{O}$ ) NMR analysis of the solid product obtained in the the Ru-catalysed N-formylation of benzylamine.



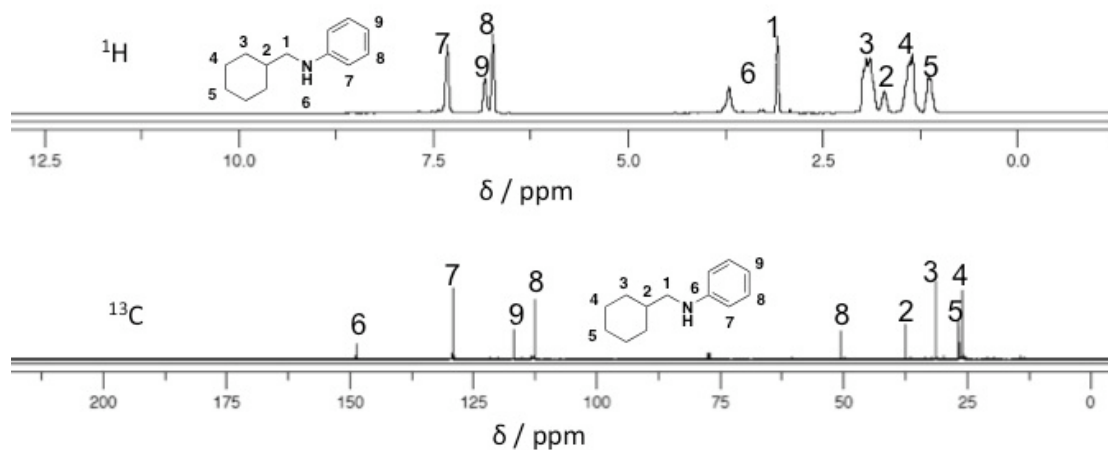
**Figure 6.34**  $^1\text{H}$  (400 MHz,  $\text{CDCl}_3$ ) and  $^{13}\text{C}$   $\{^1\text{H}\}$  (100 MHz,  $\text{D}_2\text{O}$ ) NMR analysis of the solid product obtained in the the Ru-catalysed N-formylation of aniline.



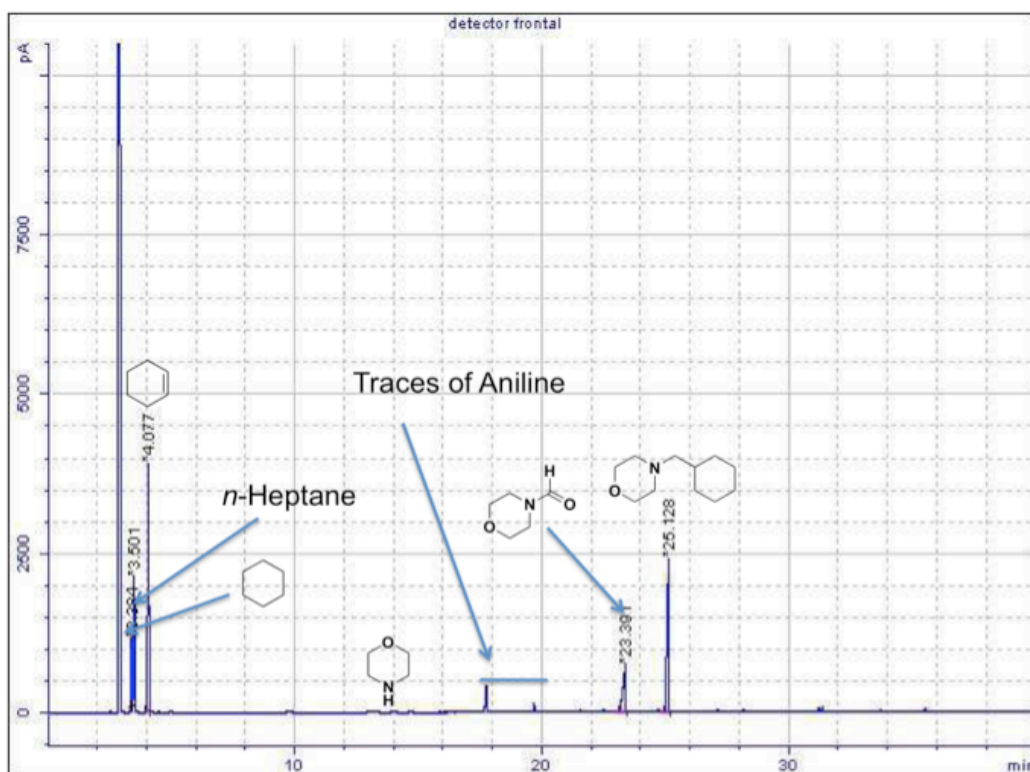
6.3 GC, NMR spectras for Ru-catalysed hydroaminomethylation of alkenes using CO<sub>2</sub> as CO source.



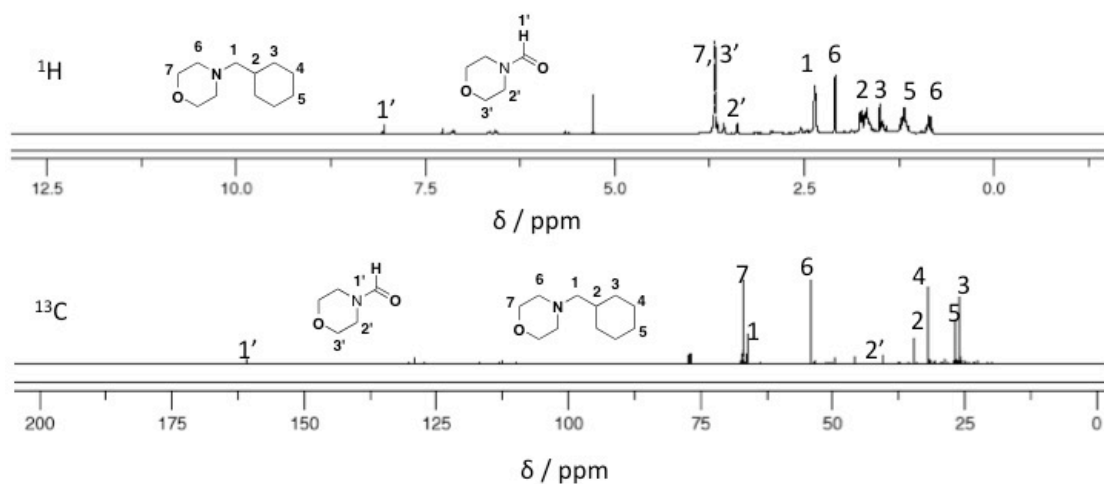
**Figure 6.35** GC analysis of the Ru-catalysed selective hydroaminomethylation of cyclohexene with aniline crude reaction mixture.



**Figure 6.36** <sup>1</sup>H (400 MHz, CDCl<sub>3</sub>) and <sup>13</sup>C {<sup>1</sup>H} (100 MHz, CDCl<sub>3</sub>) NMR analysis of the Ru-catalysed selective hydroaminomethylation of cyclohexene with aniline crude reaction mixture.

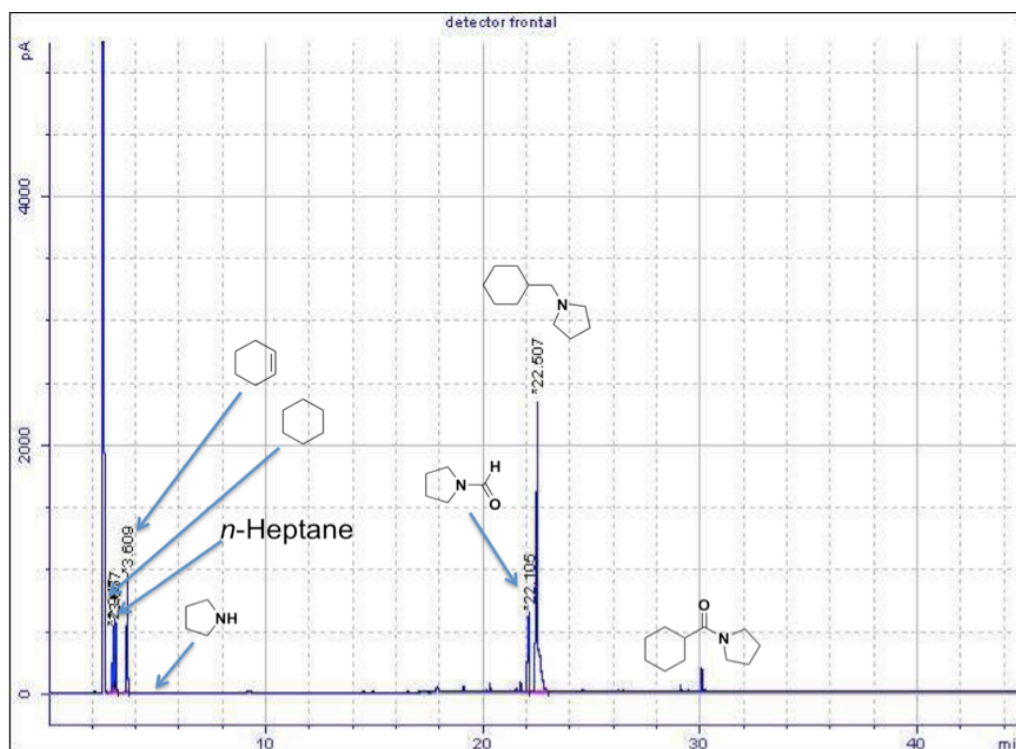


**Figure 6.37** GC analysis of the Ru-catalysed selective hydroaminomethylation of cyclohexene with morpholine crude reaction mixture.

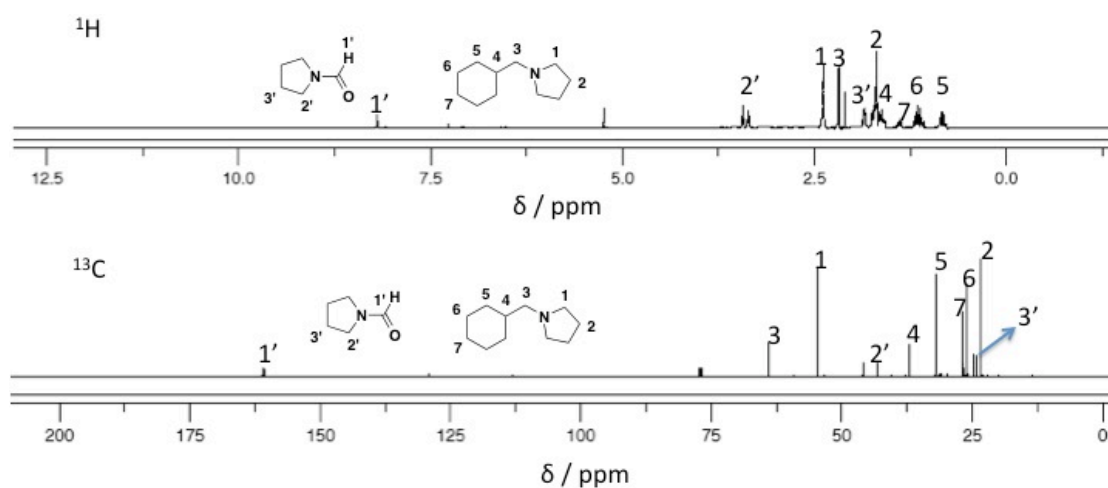


**Figure 6.38**  $^1\text{H}$  (400 MHz,  $\text{CDCl}_3$ ) and  $^{13}\text{C}$   $\{^1\text{H}\}$  (100 MHz,  $\text{CDCl}_3$ ) NMR analysis of the Ru-catalysed selective hydroaminomethylation of cyclohexene with morpholine crude reaction mixture.

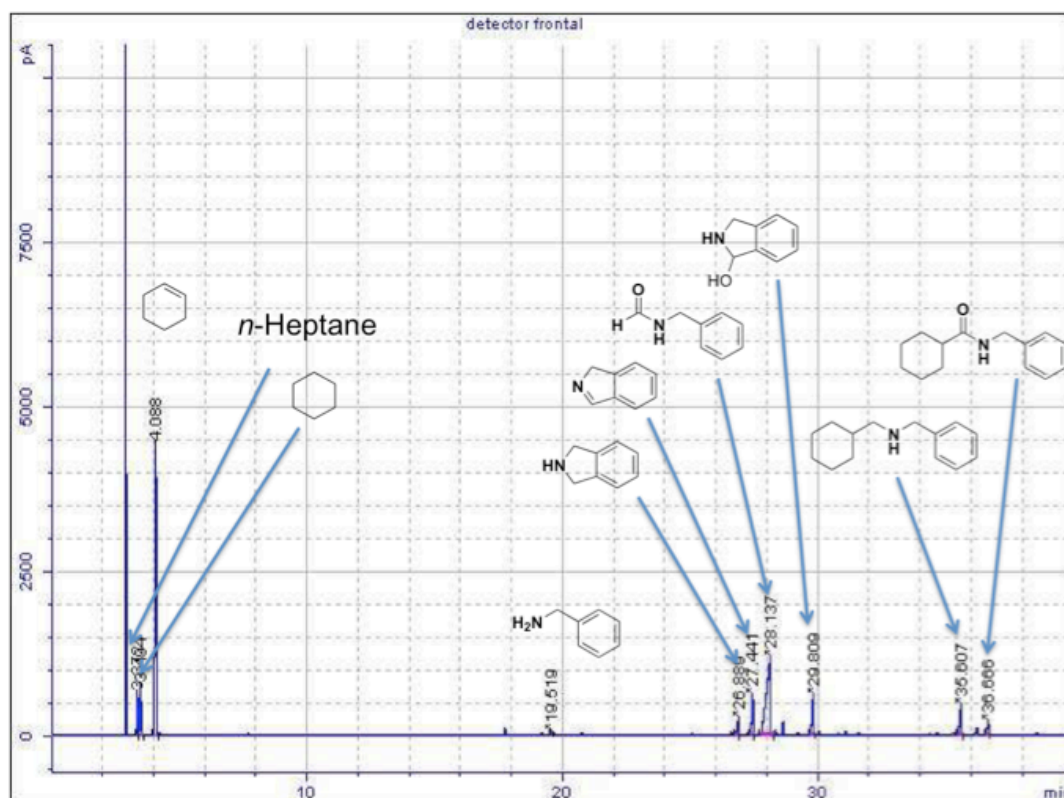




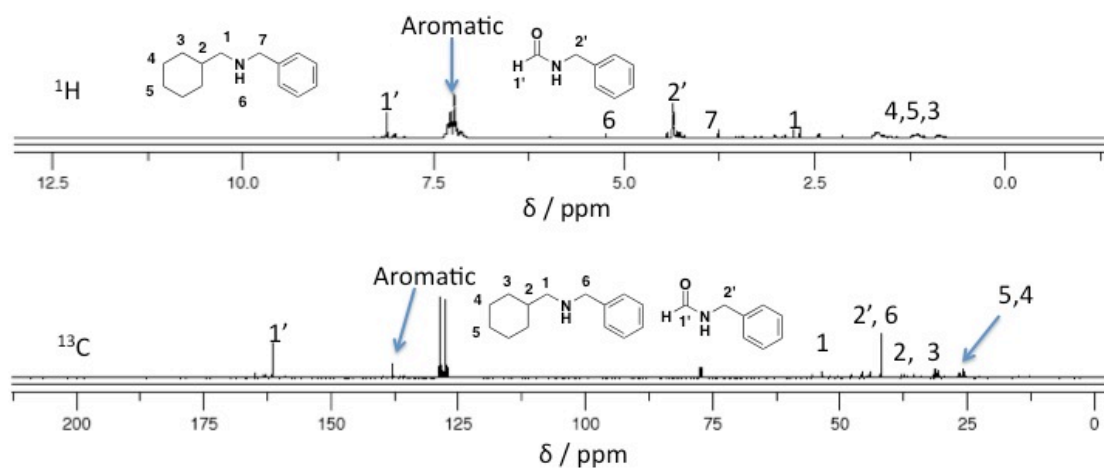
**Figure 6.39** GC analysis of the Ru-catalysed selective hydroaminomethylation of cyclohexene with pyrrolidine crude reaction mixture.



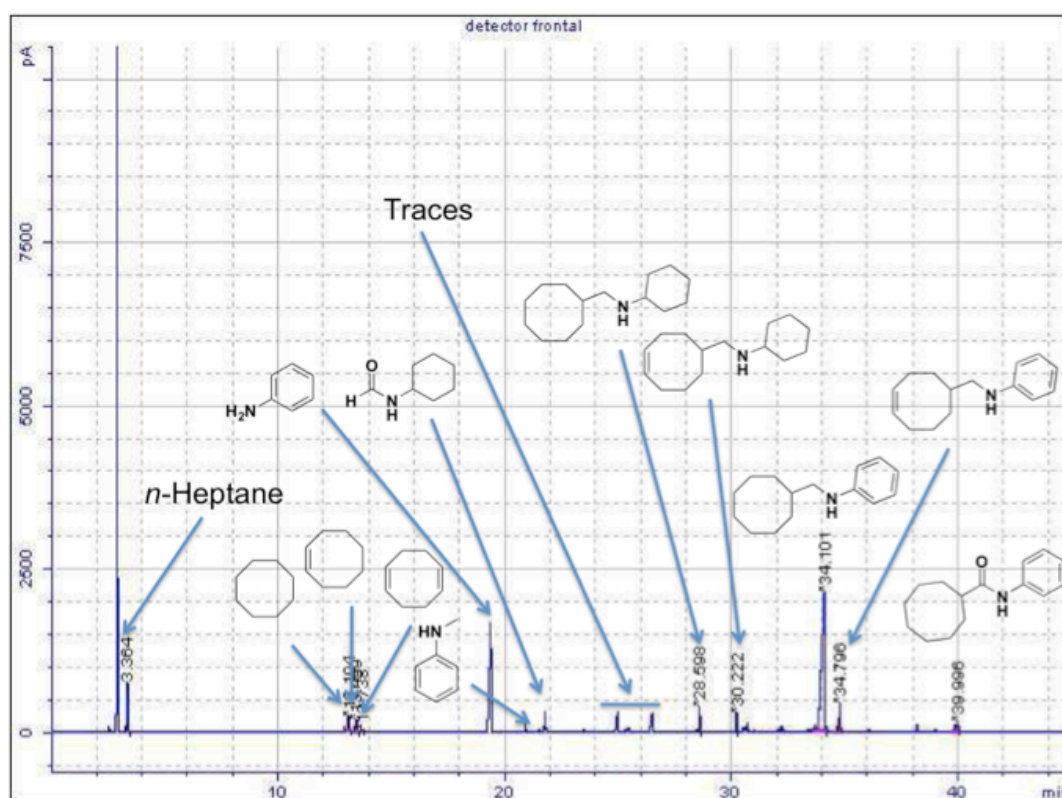
**Figure 6.40** <sup>1</sup>H (400 MHz, CDCl<sub>3</sub>) and <sup>13</sup>C {<sup>1</sup>H} (100 MHz, CDCl<sub>3</sub>) NMR analysis of the Ru-catalysed selective hydroaminomethylation of cyclohexene with pyrrolidine crude reaction mixture.



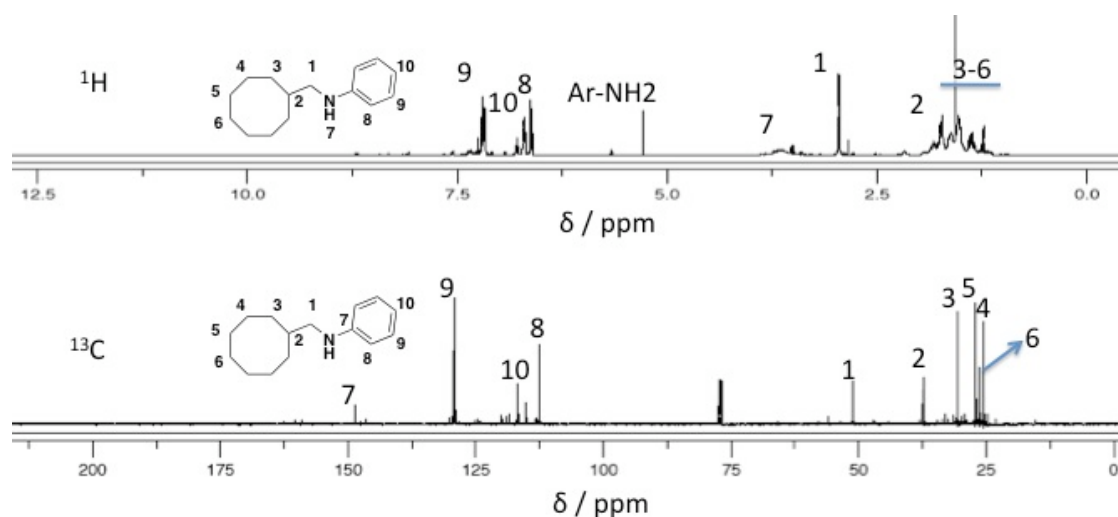
**Figure 6.41** GC analysis of the Ru-catalysed selective hydroaminomethylation of cyclohexene with benzylamine crude reaction mixture.



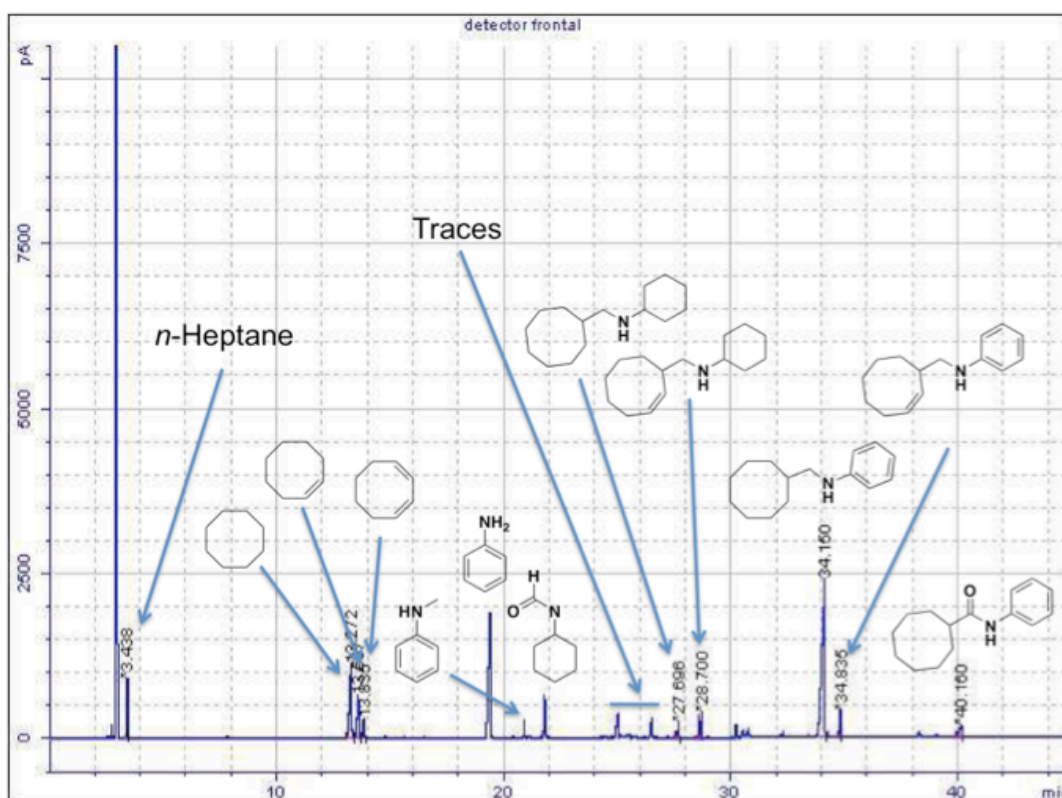
**Figure 6.42**  $^1\text{H}$  (400 MHz,  $\text{CDCl}_3$ ) and  $^{13}\text{C}$   $\{^1\text{H}\}$  (100 MHz,  $\text{CDCl}_3$ ) NMR analysis of the Ru-catalysed selective hydroaminomethylation of cyclohexene with pyrrolidine crude reaction mixture.



**Figure 6.43** GC analysis of the Ru-catalysed selective hydroaminomethylation of 1,5-cyclooctadiene with aniline crude reaction mixture.



**Figure 6.44**  $^1\text{H}$  (400 MHz,  $\text{CDCl}_3$ ) and  $^{13}\text{C}$   $\{^1\text{H}\}$  (100 MHz,  $\text{CDCl}_3$ ) NMR analysis of the Ru-catalysed selective hydroaminomethylation of 1,5-cyclooctadiene with aniline crude reaction mixture.



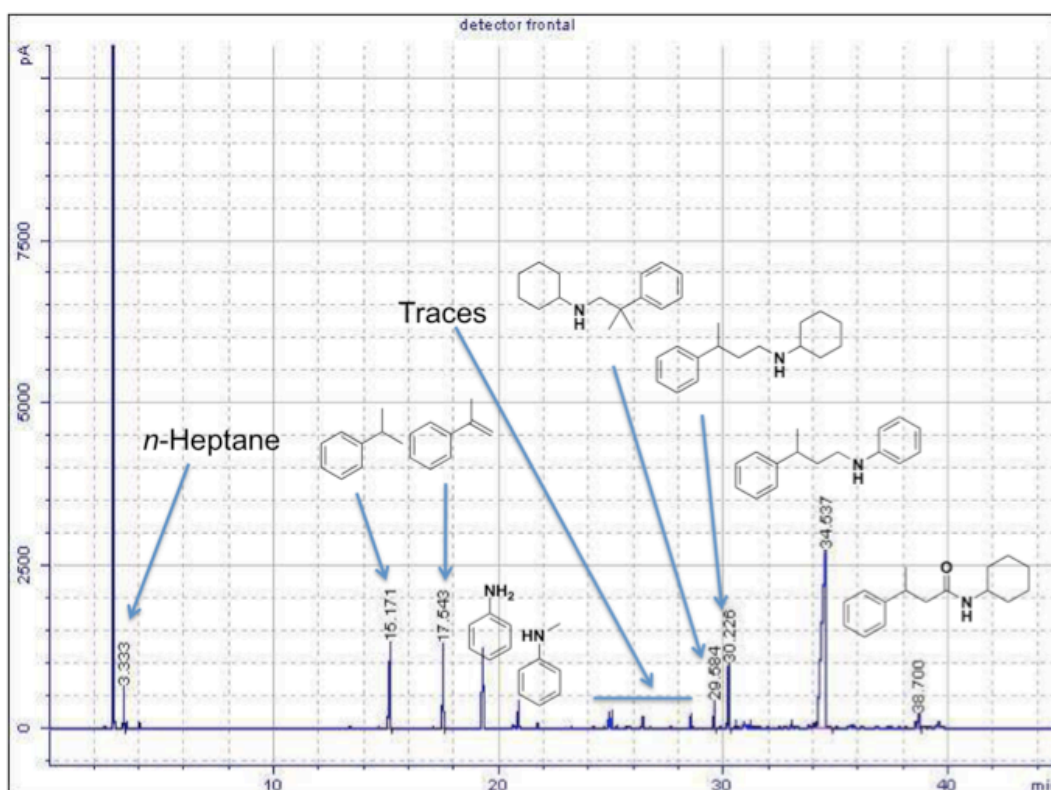


**Figure 6.47** GC analysis of the Ru-catalysed selective hydroaminomethylation of  $\alpha$ -methylstyrene with aniline crude reaction mixture.

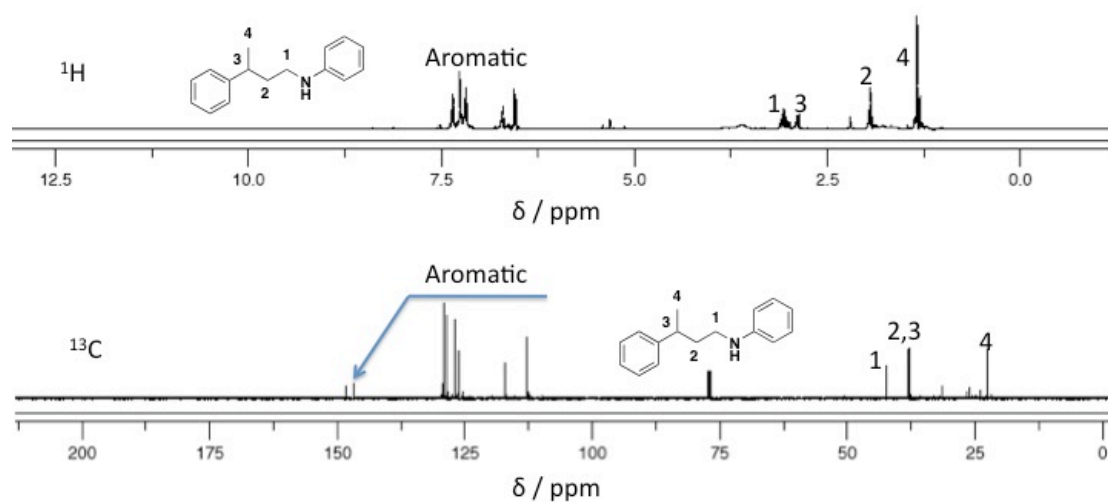


**Figure 6.48**  $^1\text{H}$  (400 MHz,  $\text{CDCl}_3$ ) and  $^{13}\text{C}$   $\{^1\text{H}\}$  (100 MHz,  $\text{CDCl}_3$ ) NMR analysis of the Ru-catalysed selective hydroaminomethylation of  $\alpha$ -methylstyrene with aniline crude reaction mixture.



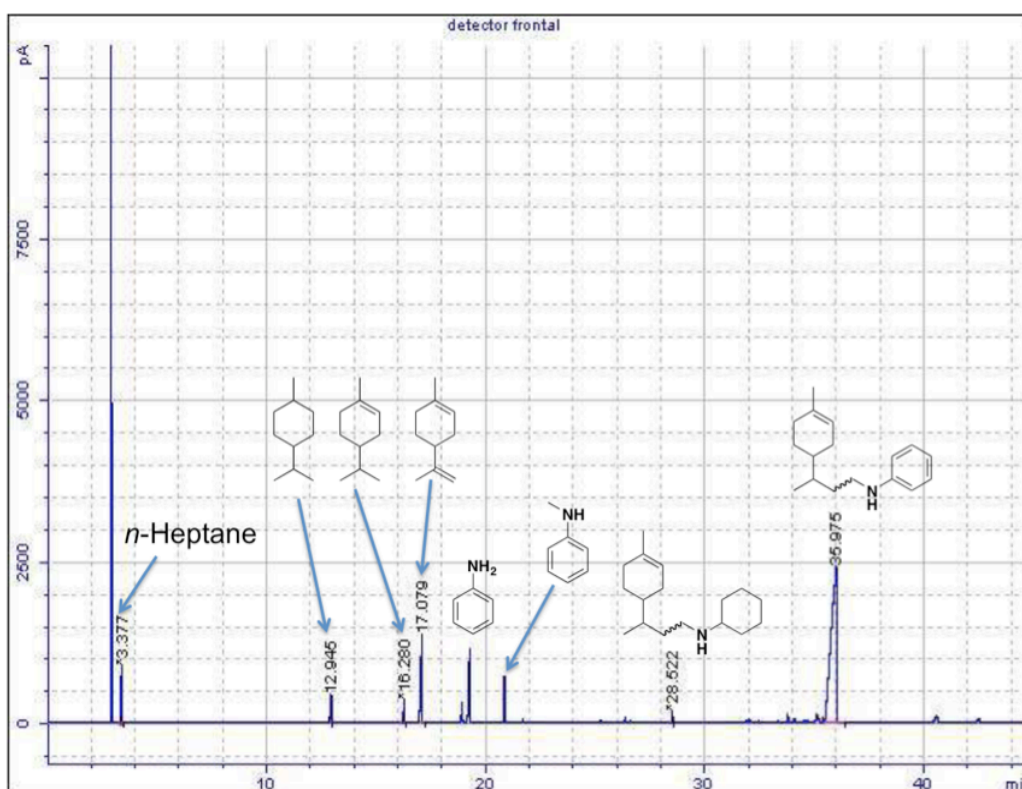


**Figure 6.49** GC analysis of the Ru-catalysed selective hydroaminomethylation of limonene with aniline crude reaction mixture.

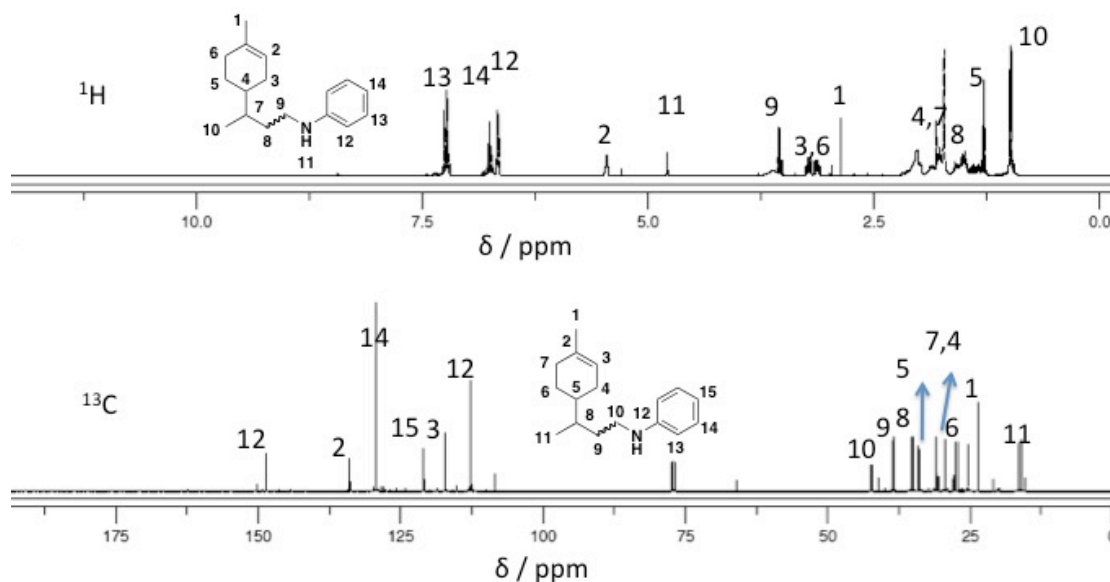


**Figure 6.50**  $^1\text{H}$  (400 MHz,  $\text{CDCl}_3$ ) and  $^{13}\text{C}$   $\{^1\text{H}\}$  (100 MHz,  $\text{CDCl}_3$ ) NMR analysis of GC analysis of the Ru-catalysed selective hydroaminomethylation of limonene with aniline crude reaction mixture.

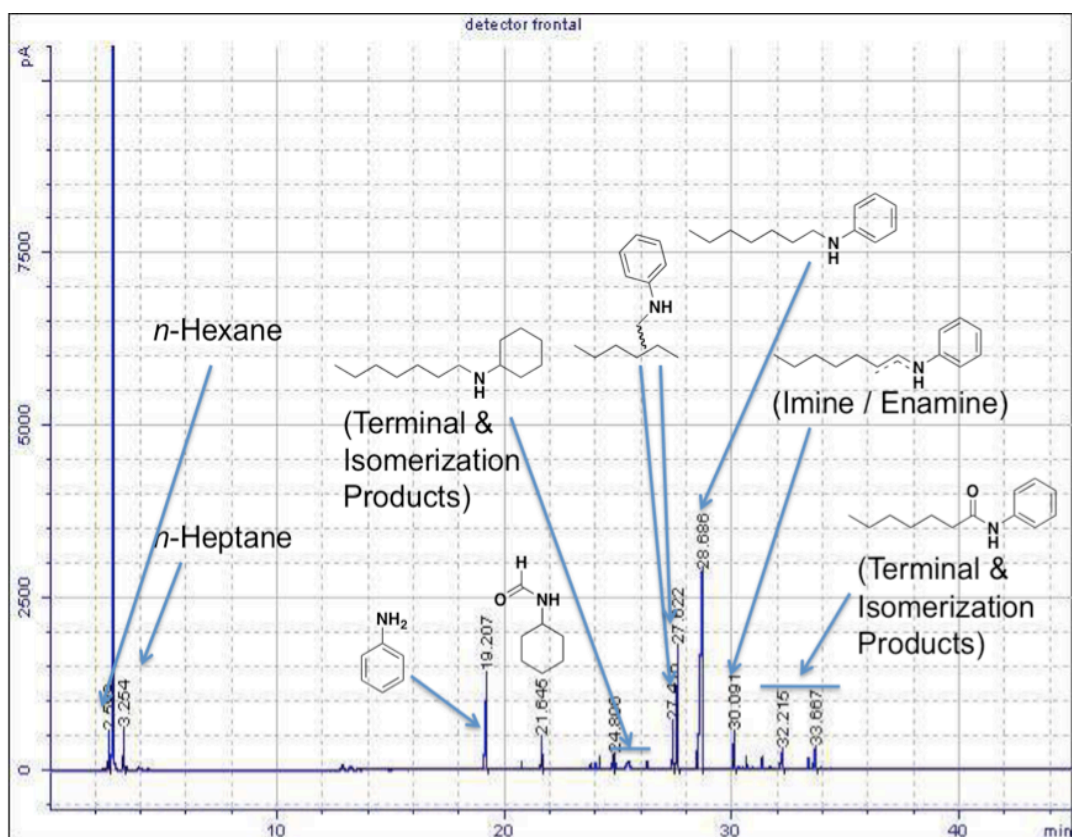


**Figure 6.51** GC analysis of the Ru-catalysed selective hydroaminomethylation of 1-hexene with aniline crude reaction mixture.

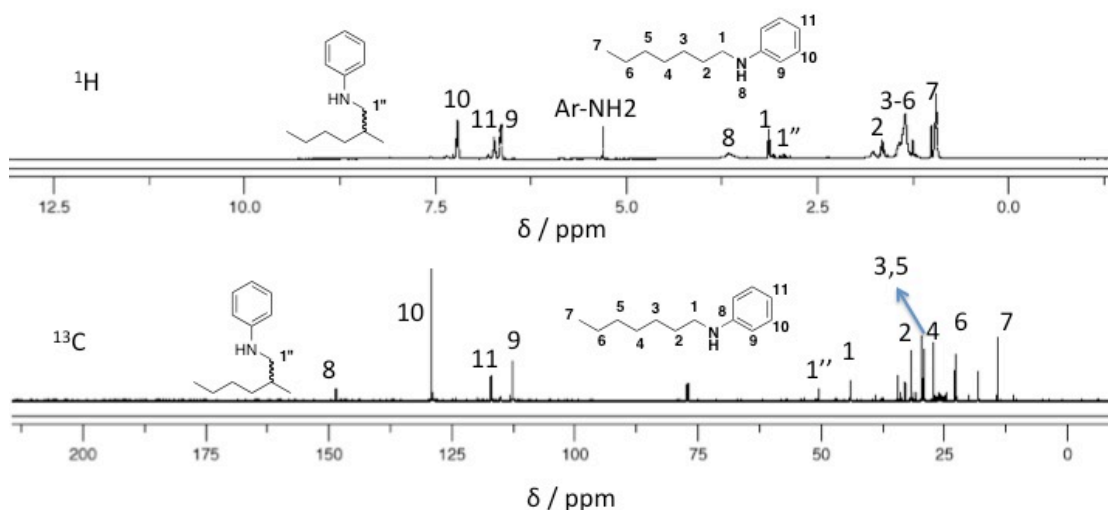


**Figure 6.52**  $^1\text{H}$  (400 MHz,  $\text{CDCl}_3$ ) and  $^{13}\text{C}$   $\{^1\text{H}\}$  (100 MHz,  $\text{CDCl}_3$ ) NMR analysis of the Ru-catalysed selective hydroaminomethylation of 1-hexene with aniline crude reaction mixture.

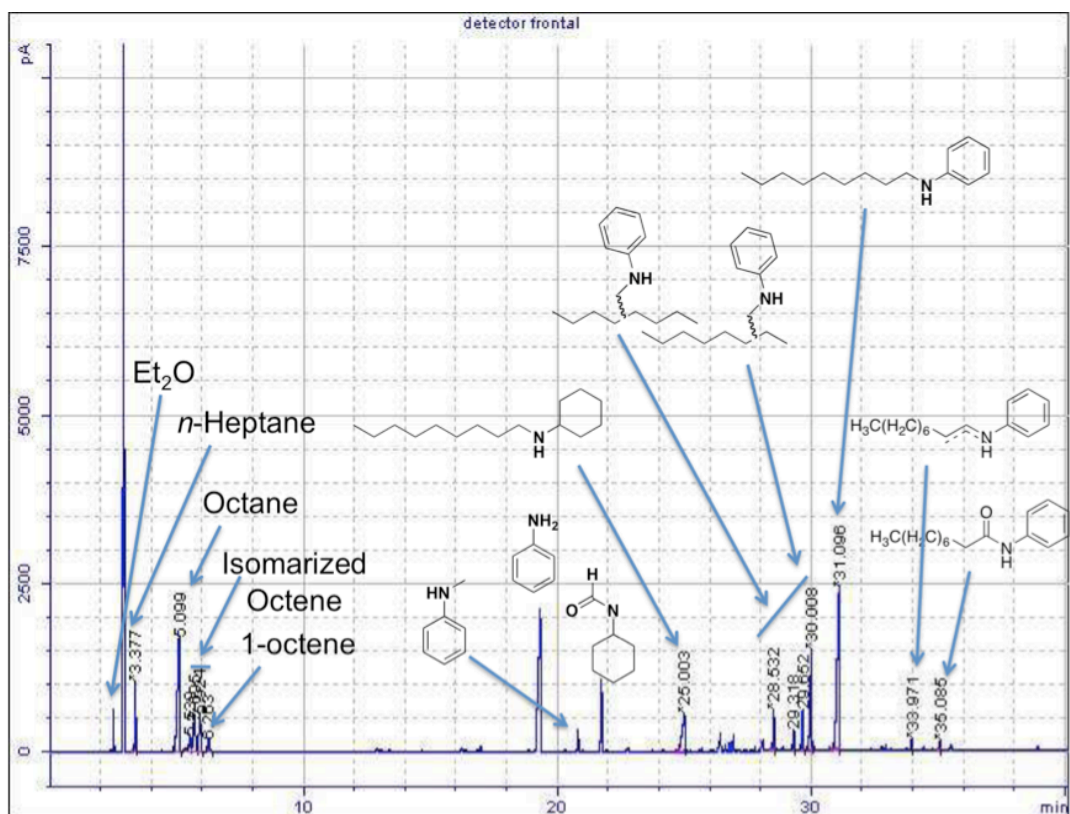


**Figure 6.53** GC analysis of the Ru-catalysed selective hydroaminomethylation of 1-octene with aniline crude reaction mixture.

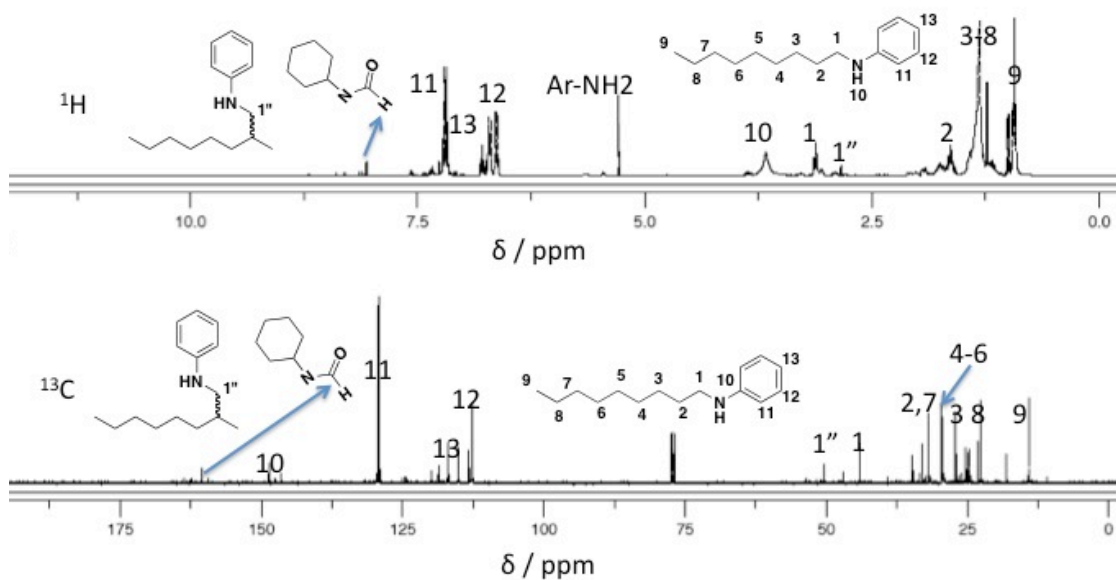


**Figure 6.54**  $^1\text{H}$  (400 MHz,  $\text{CDCl}_3$ ) and  $^{13}\text{C}$   $\{^1\text{H}\}$  (100 MHz,  $\text{CDCl}_3$ ) NMR analysis of the Ru-catalysed selective hydroaminomethylation of 1-octene with aniline crude reaction mixture.



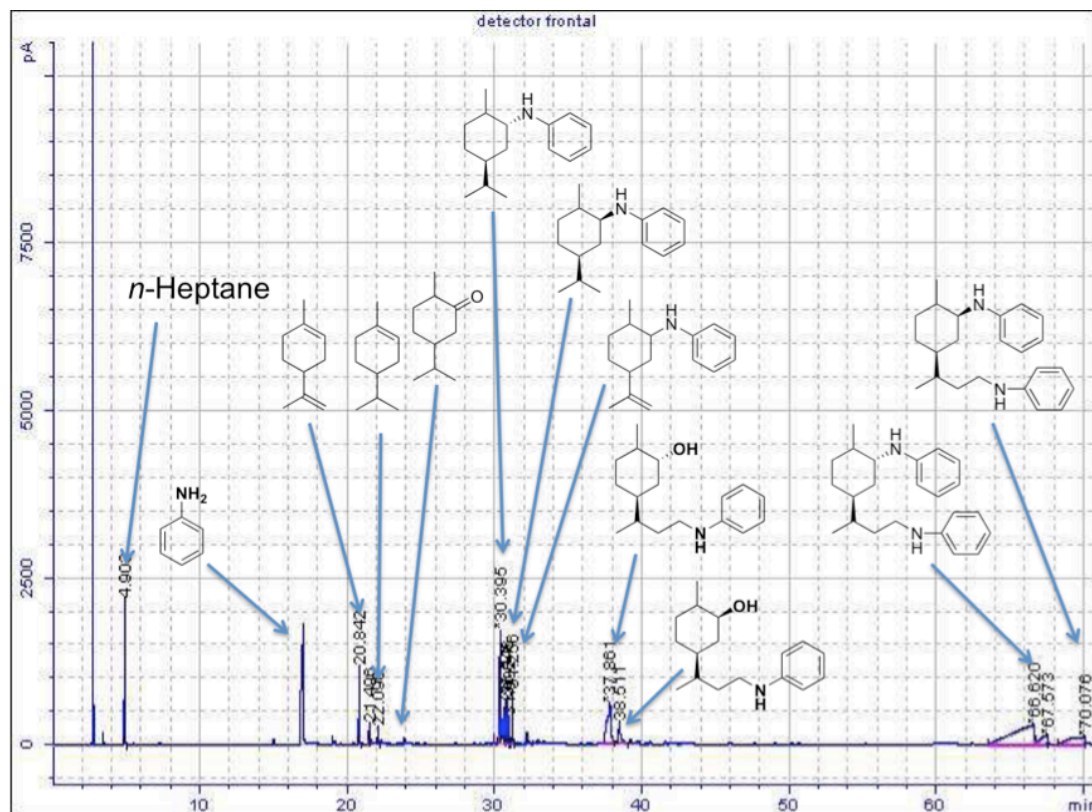


**Figure 6.55** GC analysis of the Ru-catalysed selective hydroaminomethylation of carvone with aniline crude reaction mixture.

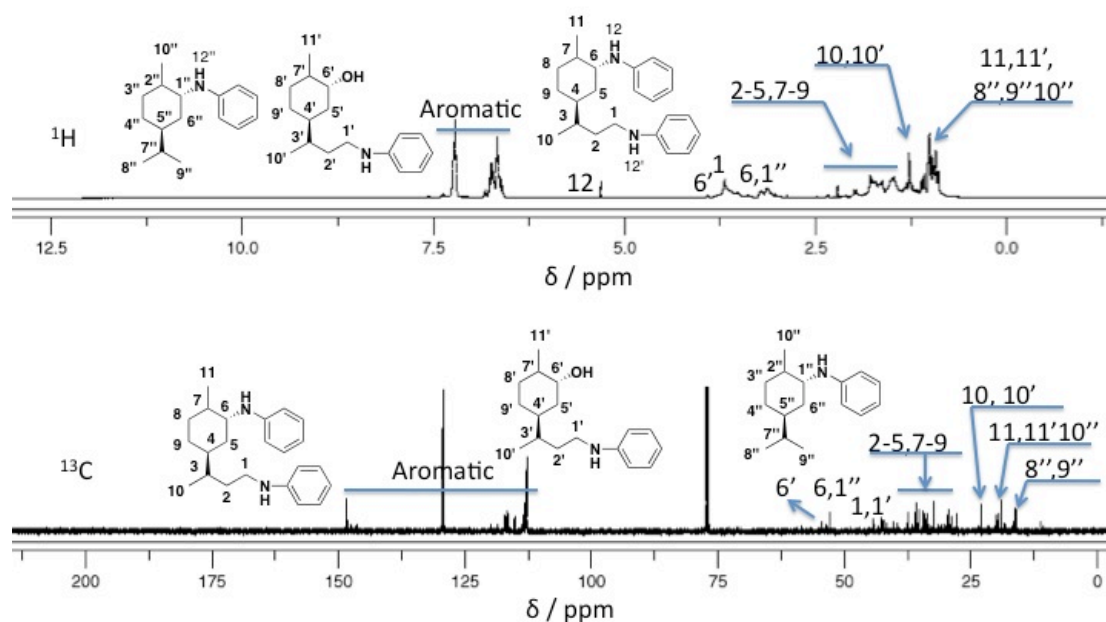


**Figure 6.56**  $^1\text{H}$  (400 MHz,  $\text{CDCl}_3$ ) and  $^{13}\text{C}$   $\{^1\text{H}\}$  (100 MHz,  $\text{CDCl}_3$ ) NMR analysis of the Ru-catalysed selective hydroaminomethylation of carvone with aniline crude reaction mixture.

#### 6.4 GC, NMR spectras for Ru-catalysed reductive amination.

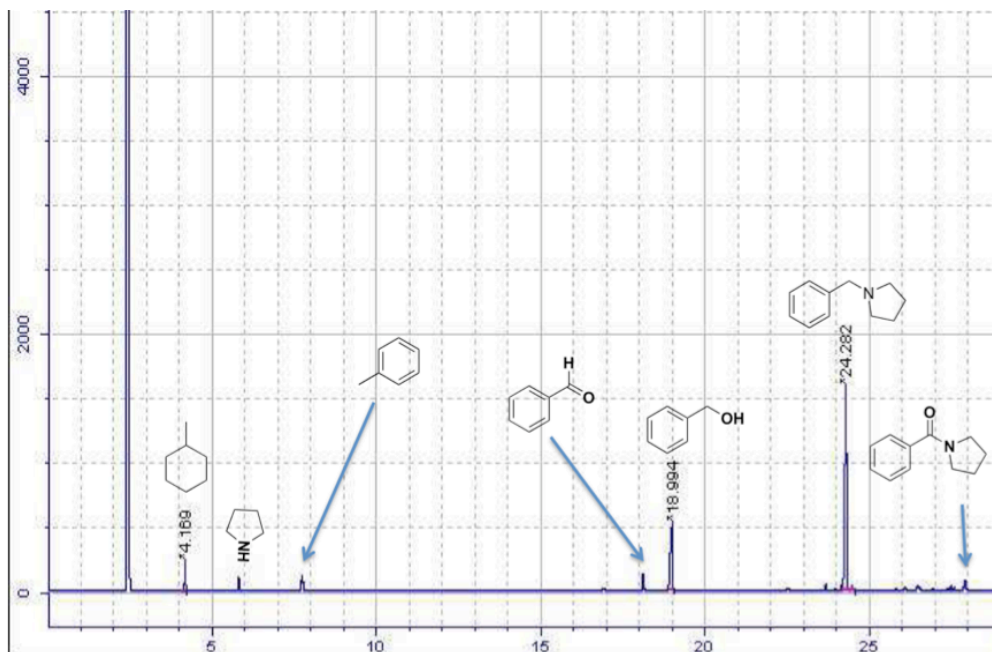


**Figure 6.57** GC analysis of the Ru-catalysed selective reductive amination of benzaldehyde with pyrrolidine by using H<sub>2</sub> (20 bar) crude reaction mixture.

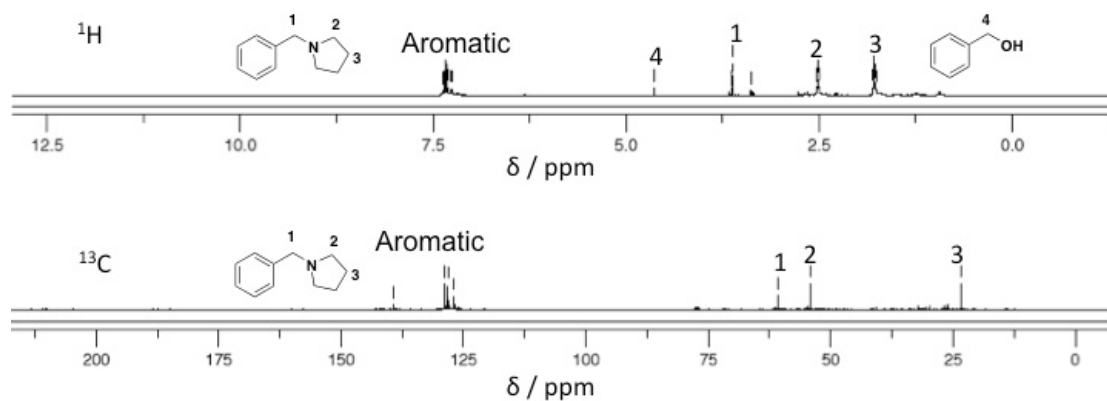


**Figure 6.58** <sup>1</sup>H (400 MHz, CDCl<sub>3</sub>) and <sup>13</sup>C {<sup>1</sup>H} (100 MHz, CDCl<sub>3</sub>) NMR analysis of the Ru-catalysed selective reductive amination of benzaldehyde with pyrrolidine crude reaction mixture.

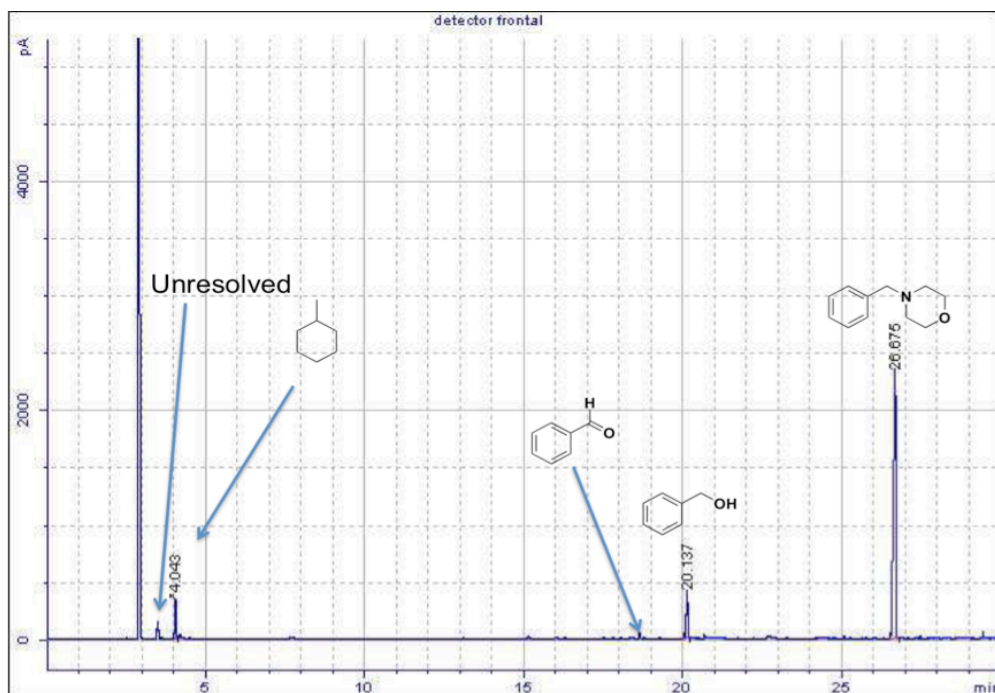


**Figure 6.59** GC analysis of the Ru-catalysed selective reductive amination of benzaldehyde with morpholine by using the mixture of CO<sub>2</sub>/H<sub>2</sub> (1:1, 60 bar) crude reaction mixture.

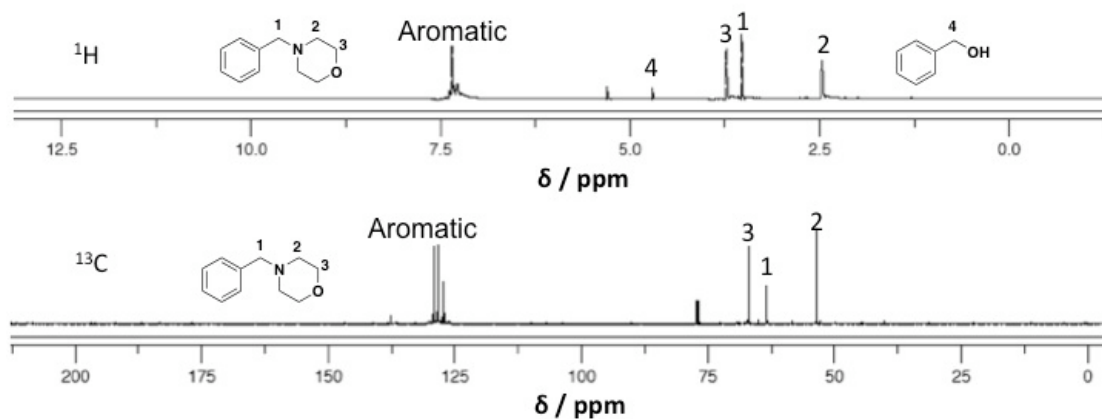


**Figure 6.60** <sup>1</sup>H (400 MHz, CDCl<sub>3</sub>) and <sup>13</sup>C {<sup>1</sup>H} (100 MHz, CDCl<sub>3</sub>) NMR analysis of the Ru-catalysed selective reductive amination of benzaldehyde with morpholine crude reaction mixture.

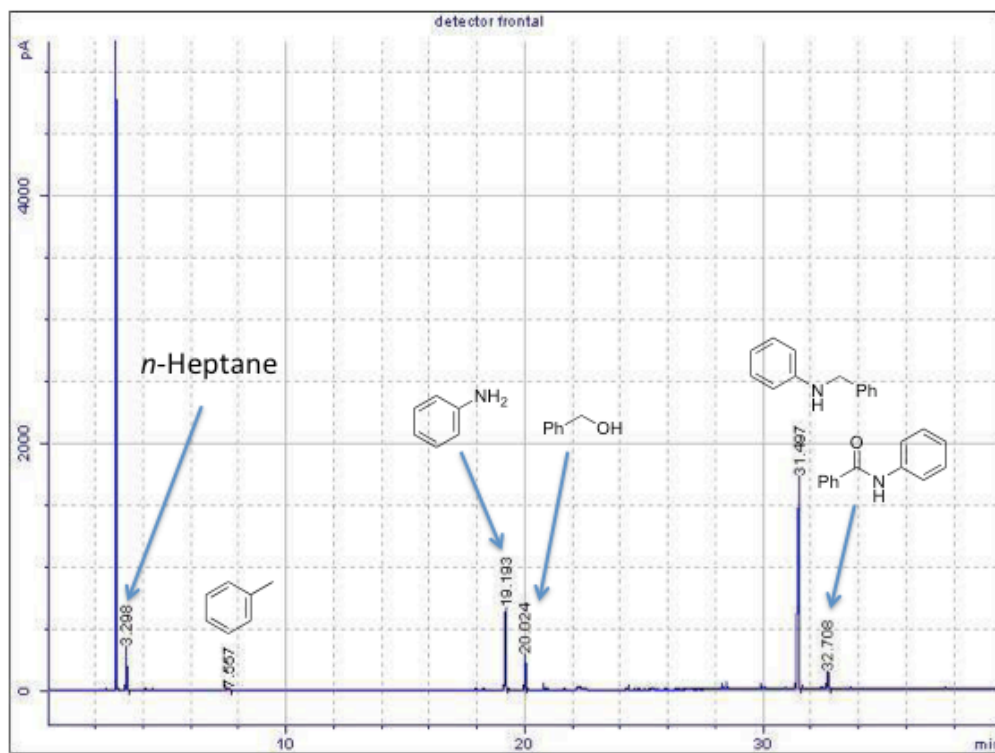


**Figure 6.61** GC analysis of the Ru-catalysed selective reductive amination of benzaldehyde with aniline by using the mixture of CO<sub>2</sub>/H<sub>2</sub> (1:1, 60 bar) crude reaction mixture.

6.5 GC analysis for Pd-NPs catalyzed selective hydrogenation of 1,3-cyclohexadiene into cyclohexene.

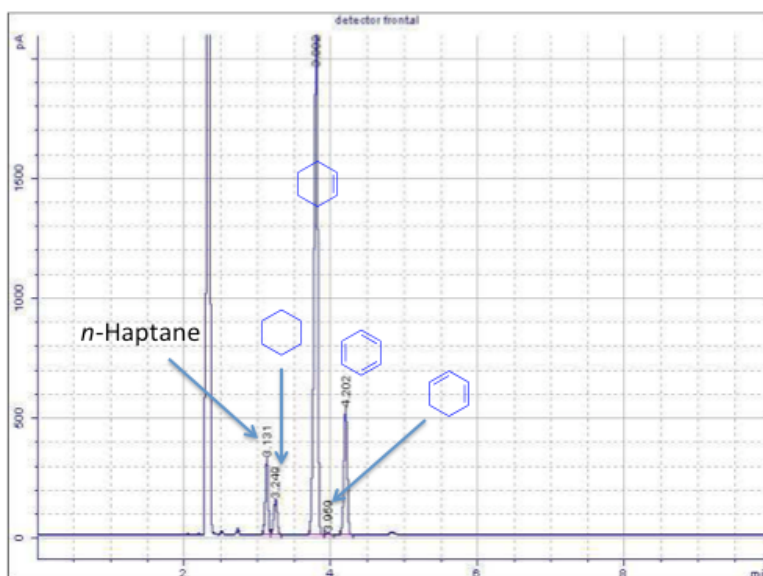


**Figure 6.62** Pd/C-0.73 wt % catalyzed liquid phase selective reduction of 1,3-cyclohexadiene in to cyclohexene (10 min).

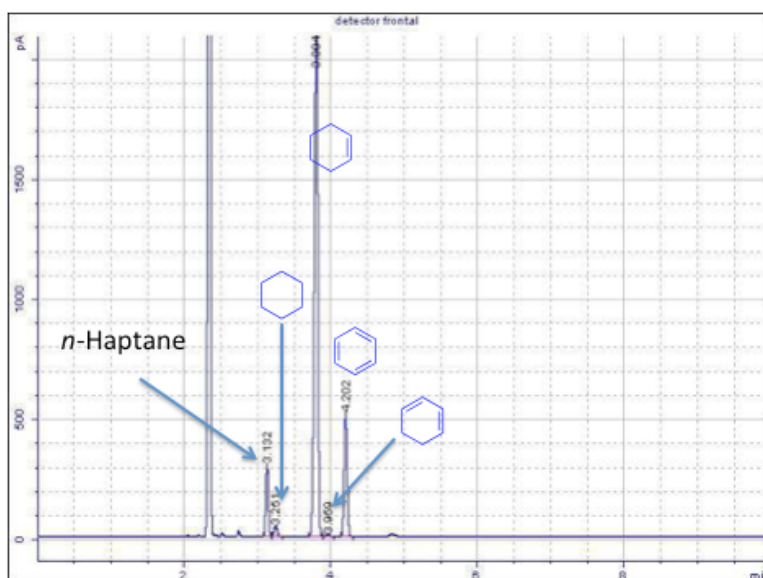


**Figure 6.63** 2<sup>nd</sup> time recycling test for the Pd/C-0.73 wt % catalyzed liquid phase selective reduction of 1,3-cyclohexadiene into cyclohexene (15 min).



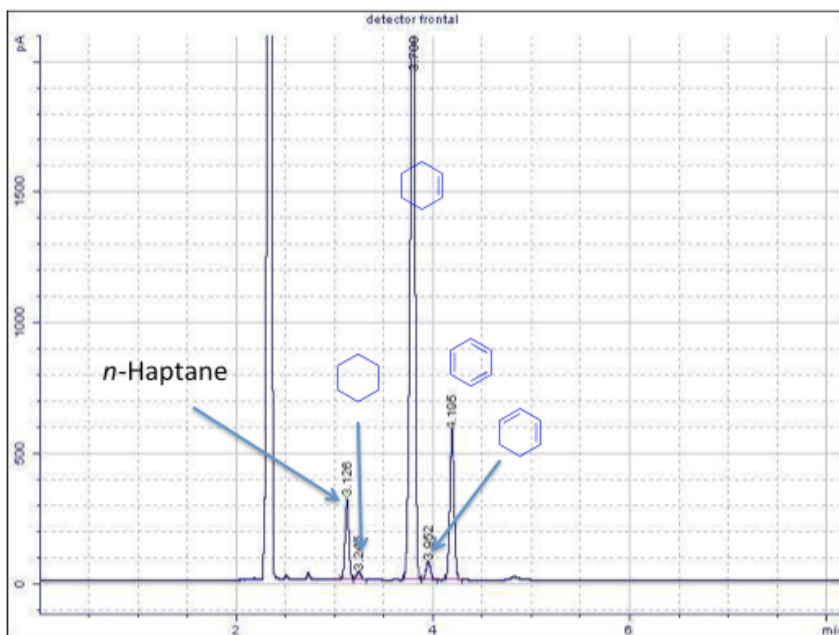


**Figure 6.64** 3<sup>rd</sup> time recycling test for the Pd/C-0.73 wt % catalyzed liquid phase selective reduction of 1,3-cyclohexadiene into cyclohexene (19 min).

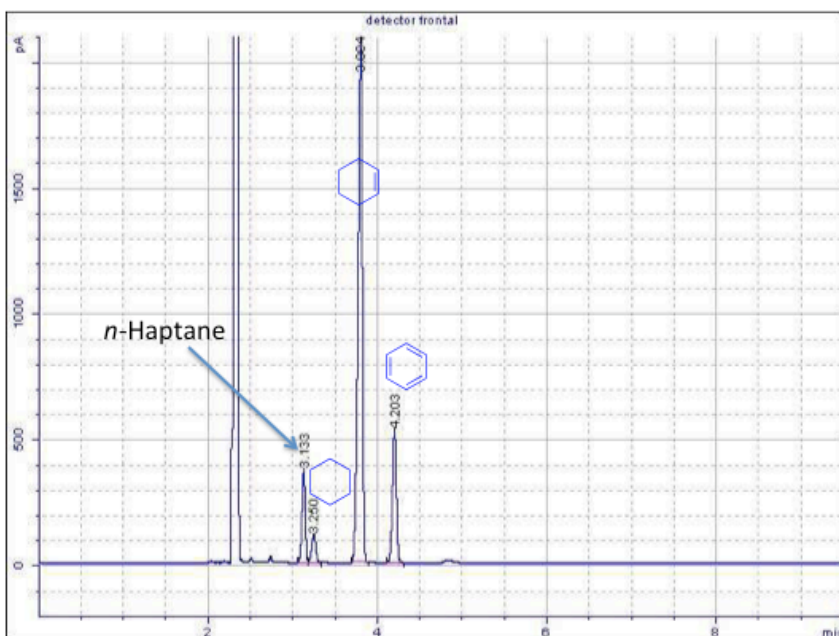


**Figure 6.65** Pd/C-2.36 wt % catalyzed liquid phase selective reduction of 1,3-cyclohexadiene into cyclohexene (12 min).

6.6 GC analysis for Pd-NPs catalyzed dehydrogenation-hydrogenation of 1,3-cyclohexadiene by enter-H<sub>2</sub> transfer mechanism.

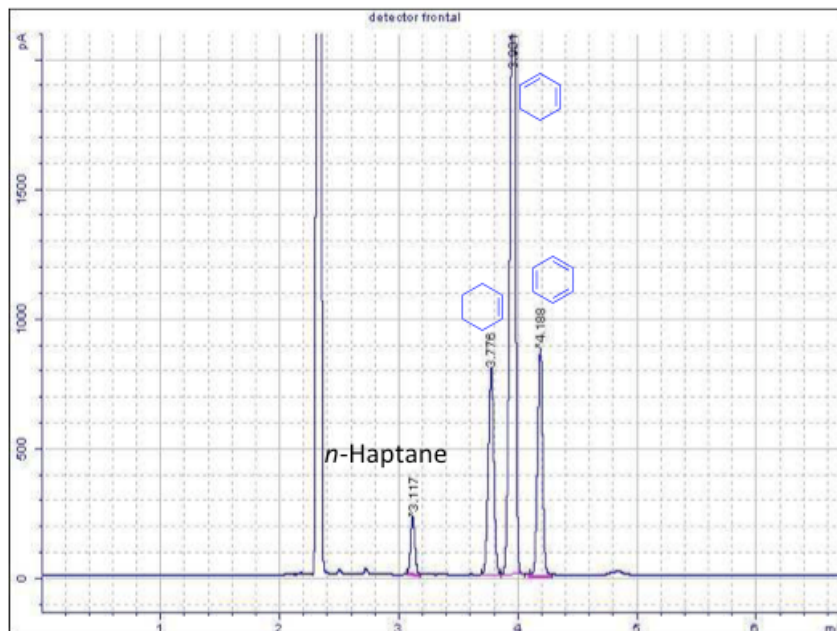


Figure 6.66 Pd/C-0.73 wt % catalyzed liquid phase dehydrogenation-hydrogenation of 1,3-cyclohexadiene by reductive enter-H<sub>2</sub> transfer-mechanism (30 min).

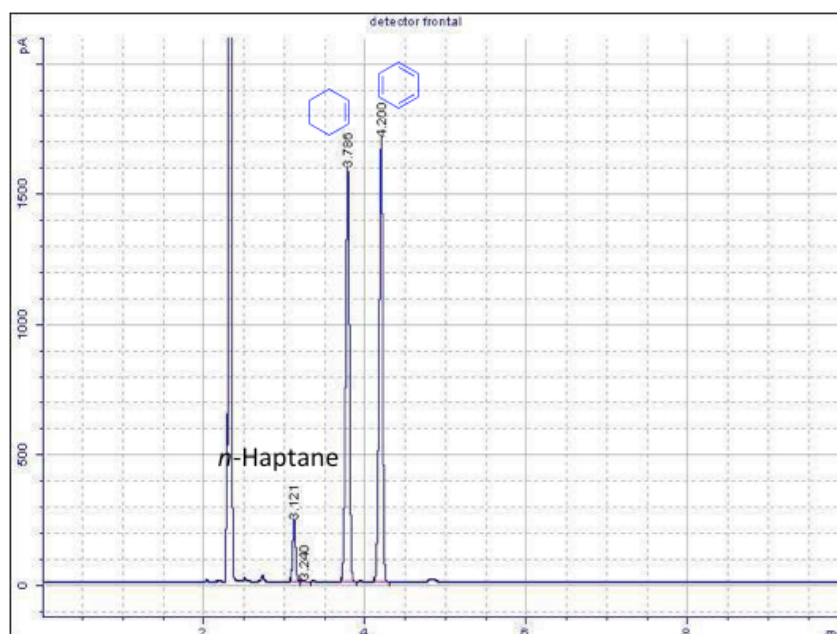


Figure 6.67 Pd/C-0.73 wt % catalyzed liquid phase dehydrogenation-hydrogenation of 1,3-cyclohexadiene by reductive enter-H<sub>2</sub> transfer-mechanism (105 min)